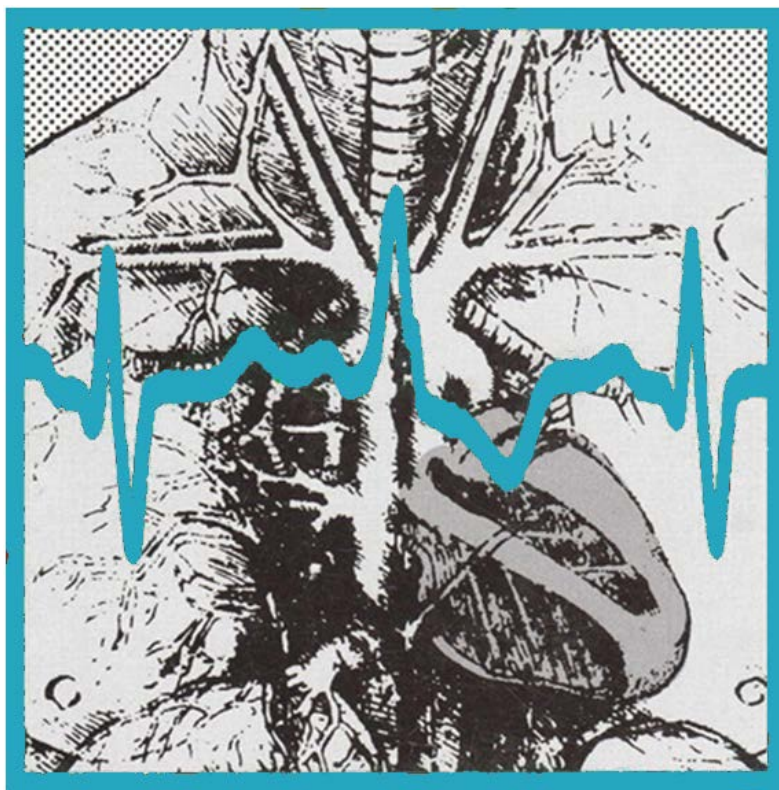


COMPUTING IN CARDIOLOGY

September 6-9, 2015

Nice, France





Welcome to Nice!

Bienvenue à Nice !

Table of Contents

Sponsors.....	iv
About Next Year’s Conference, CinC 2016.....	v
CinC Affiliation with IEEE/EMBS.....	vi
Letter from the President	vii
Board of Directors.....	ix
Program Committee & Session Chairs	xi
Welcome to Nice.....	xiii
Map of Nice.....	xv
Map of the Campus Saint Jean d’Angely (SJA).....	xvi
Meeting Site.....	xvii
Transportation	xvii
Directions to Monday Gala Diner and Tuesday Reception	xviii
Hotel & Practical Information	xx
Accommodations	xx
Climate.....	xxi
Business Hours.....	xxi
Money/currency	xxi
Emergency phone numbers.....	xxi
Calling to and from France.....	xxi
Tips for a pleasant trouble-free stay.....	xxii
Things to Do in and Near Nice	xxii
Internet Access	xxiii
Meals.....	xxiii
Accompanying Persons (Guests).....	xxiii
Monday Social Program.....	xxiv
Tuesday Evening Reception	xxiv
Wednesday Farewell Snack	xxv
Sunday Symposium.....	xxv
For Authors and Speakers.....	xxvi
Rosanna Degani Young Investigator Award	xxvii
PhysioNet/Computing in Cardiology Challenge 2015	xxvii
Manuscripts	xxvii
Scientific Sessions Program Overview	xxix
Scientific Program	xxx
Abstracts	1

Sponsors

We would like to thank our sponsors and those who have made generous donations:



VILLE DE NICE
www.nice.fr



Région
Provence
Alpes
Côte d'Azur





SIMON FRASER
UNIVERSITY
ENGAGING THE WORLD



COMPUTING
IN
CARDIOLOGY



Vancouver, September 11-14, 2016

About Next Year's Conference, CinC 2016

The 2016 Computing in Cardiology Conference will be held in the beautiful city of Vancouver, Canada from Sept 11th to Sept 14th. The meeting is affiliated with Simon Fraser University and will be held at the Marriott Pinnacle located in downtown Vancouver overlooking picturesque Burrard inlet and the North Shore Mountains. Consistently ranked one of the top 10 most livable cities in the world and the best place to live in North America, Vancouver boasts a global fusion of cultural and culinary delights. The conference is at the tail end of summer when the weather is normally very mild making it possible for participants to enjoy the natural beauties of British Columbia and in particular Vancouver.

Located at the mouth of the Fraser River and at the edge of the Mountains, the city boasts a rich First Nations history. Approximately 8000 years ago salmon were harvested in the Fraser Canyon and for over 3000 years the indigenous peoples of the Pacific Northwest Coast settled and lived off the resources of what is now Vancouver. With the arrival of Spanish and British explorers (it is named after Captain George Vancouver) immigration has shaped it into a vibrant multicultural cosmopolitan city. Vancouver has an endless supply of attractions and things to see and do. It doesn't matter what time of day or what time of year - whether you want to be indoors or out, active or a spectator, spend a lot of money or none at all - Vancouver has it all.

The Social program will include visits to local attractions and the world famous Stanley Park. While in Vancouver you are never far from nature, with an abundance of wildlife; it is not uncommon to view deer, coyotes, eagles and bears and in recent years Orca have been seen in the harbor.

Vancouver is easy to reach by plane with direct flights from major cities in Europe, North America and Asia and is less than a three-hour drive from Seattle USA.

Before or after or the CINC meeting participants will have the opportunity to take in the natural beauty of the surrounding region: Hop on a ferry and visit Vancouver Island and Victoria; take a cruise in the inside passage or to Alaska; or tour the Canadian Rockies by train. For further details, please refer to: www.cinc2016.org

CinC Affiliation with IEEE/EMBS



The Engineering in Medicine and Biology Society of the IEEE advances the application of engineering sciences and technology to medicine and biology, promotes the profession, and provides global leadership for the benefit of its members and humanity by disseminating knowledge, setting standards, fostering professional development, and recognizing excellence.

The field of interest of the IEEE Engineering in Medicine and Biology Society is the application of the concepts and methods of the physical and engineering sciences in biology and medicine. This covers a very broad spectrum ranging from formalized mathematical theory through experimental science and technological development to practical clinical applications. It includes support of scientific, technological and educational activities.

Engineering in Medicine and Biology Society

445 Hoes Lane
Piscataway, New Jersey, USA 08854
Telephone: +1 732 981 3433
Facsimile: +1 732 465 6435
E-mail: emb-exec@ieee.org, www.embs.org

PUBLICATIONS

IEEE PULSE
Transactions on Biomedical Engineering/Transactions on Biomedical Engineering Letters
Transactions on Information Technology in Biomedicine
Transactions on Neural Systems and Rehabilitation Engineering
Transactions on Medical Imaging
Transactions on NanoBioscience
Transactions on Computational Biology and Bioinformatics
Transactions on Biomedical Circuits and Systems
Reviews on Biomedical Engineering

ELECTRONIC PRODUCTS

EMBS Electronic Resource

CONFERENCES

Annual International Conference of the IEEE Engineering in Medicine and Biology Society (EMBC)
IEEE EMBS Special Topic Conference on Neural Engineering (NER)
International Symposium on Biomedical Imaging (ISBI)
International Conference on Biomedical Robotics and Biomechatronics (BIOROB)
International Conference on Rehabilitation Robotics (ICORR) AMA/IEEE-EMBS Medical Technology Conference (MedTech)
Grand Challenges Conference Series (GCBE)

SUMMER SCHOOLS Sponsored by EMBS

International Summer School on Biomedical Imaging
International Summer School on Biomedical Signal Processing
International Summer School on Biocomplexity
International Summer School on Medical Devices and Biosensors
International Summer School on Information Technology in Biomedicine



Letter from the President

Dear Participant,

Welcome to the 42nd Computing in Cardiology conference. This is just the second time, after Lyon 2005, that the Computing in Cardiology community is meeting in France, a country with a long tradition of engineering applied to cardiology. The Board of Directors was delighted when Olivier Meste and his colleagues from University of Nice Sophia Antipolis volunteered to host this year's meeting. They have prepared an excellent meeting and social program, and a very high number of abstracts have been submitted.

This is the first time that I am writing this letter as CinC President. I would like to take this opportunity to thank the board members for nominating me for this responsibility. At the same time, I would like to reaffirm my commitment to do my best for guiding the steps of our organization in the coming years. Research by itself is extraordinarily dynamic and the conference should reflect this fact and promote, support and be at the forefront of efforts to adapt and synergize the constant evolution of the field. We, as members of the Board of Directors, are committed to this vision and goal, and for that we remain open to, and we encourage initiatives, or any other input, from you the Computing in Cardiology community.

For the first time, we have introduced a theme that we hope will promote and support better connection between the clinical and engineering aspects involved at Computing in Cardiology. Specifically, we have commissioned two talks that we hope will provide a platform for the clinical experts to air their views on the engineering challenges for the future in cardiology. These talks are entitled "Engineering Issues in Clinical Electrocardiography" and "Technological challenges of computing in cardiology in AF management", and appear in the program in sessions S51 and SA1. We encourage you to attend these talks and join in helping to build this important link.

Looking to the future, we also encourage any of you who would be considering hosting a Computing in Cardiology conference to contact us. Advanced planning is definitely encouraged so please do step forward now. We should stress that we welcome all potential hosts and particularly encourage interest from regions/countries that have not yet hosted a Computing in Cardiology conference.

Here I want to make special mention of the Board members during the past years. Firstly, Peter Macfarlane is to be thanked and acknowledged for his eminent work as President of Computing in Cardiology during the term 2008–2014. Many thanks, Peter! In addition I must mention Pim Dassen and Harold Ostrow who departed from the Board in 2014. Pim was responsible for organizing the YIA competition and Harold has served both as President and Past President. Many thanks to Pim and Harold! I am also grateful to all the

other members of the Board of Directors for their work and commitment; they will continue for another three-year term.

I hope you will have a scientifically stimulating meeting that will enable you to continue your work, raising new ideas and projects, and which will inspire you to submit an abstract for presentation at next year's meeting in Vancouver, Canada from 11th -14th, September, 2016. Let me take this opportunity to thank Olivier Meste and all of the Local Organizing Committee for the work they have done in preparing Computing in Cardiology 2015. I am sure it will be a great success.

Best wishes

Pablo Laguna

President, Computing in Cardiology

Board of Directors

President

Pablo Laguna, PhD
University of Zaragoza
Zaragoza, Spain

Secretary

Leif Sörnmo, DSc
Lund University
Lund, Sweden

Treasurer

Victor Mor-Avi, PhD, FASE
University of Chicago
Chicago, IL, USA

Cristiana Corsi, PhD
University of Bologna
Bologna, Italy

Olaf Doessel, PhD
Karlsruhe Institute of Technology (KIT)
Karlsruhe, Germany

Dewar Finlay, PhD
University of Ulster
Belfast, UK

Paul Kligfield, MD, FACC
Weill Cornell Medical School
New York, NY, USA

Rob MacLeod, PhD
SCI Institute, University of Utah
Salt Lake City, Utah, USA

Ex-Officio

Chair of the ESC Working Group on e-Cardiology:
Goran Krstacic, MD, PhD, FESC
Director of the Institute for Cardiovascular
Prevention and Rehabilitation
Zagreb, Croatia

Past President

Peter Macfarlane, DSc
University of Glasgow, UK

Non-Elected:

Editor, Proceedings
Alan Murray, PhD Freeman Hospital
Newcastle upon Tyne, UK

Director of Information Services:

Sheryl Prucka, MSEE
Prucka Engineering, Inc
Park City, UT, USA

Physionet Challenge Coordinator:

George Moody
Massachusetts Institute of Technology
Cambridge, MA, USA

2015 Organizing Committee

Olivier Meste, PhD, Chair
Aline Cabasson, PhD, Co-chair
Guillaume Allibert, PhD
Gregory Blain, PhD
Gabriel Latcu, MD
Marianna Meo, PhD
Hervé Rix, PhD
Nadir Saoudi, MD
Vicente Zarzoso, PhD

Secretariat Address

Corinne Julien
CinC2015 Secretariat
Laboratoire d'Informatique, Signaux et
Systèmes de Sophia-Antipolis
I3S - UMR7271 - UNS CNRS
2000, route des Lucioles
Les Algorithmes - bât. Euclide B
06900 Sophia Antipolis – France

2015 CinC Physionet Challenge responsibilities:

Gari Clifford, PhD
Emory University
Atlanta, GA USA

Ikaro Silva
Massachusetts Institute of Technology
Cambridge, MA USA

Program Committee & Session Chairs

The CinC Board would like to offer our sincere gratitude to the Local Organizing Committee and also to the many individuals who helped review abstracts in order to build an outstanding program for CinC 2015. In Addition, we would like to thank those that are serving as session chairs during the meeting.

Program Committee

The Program Committee is made of all of the members of the CinC Board of Directors and all of the Local Organizing Committee (who are listed elsewhere). In addition, the following individuals generously donated their time and expertise to reviewing abstracts and in some cases, manuscripts, for helping determine the program.

Oleg Aslanidi	Ary Goldberger	Esther Pueyo
Piotr Augustyniak	Claus Graff	Hervé Rix
Riccardo Barbieri	Richard Gregg	Paul Rubel
Joachim Behar	Daniel Guldenring	Frank Sachse
Omer Berenfeld	Weichih Hu	Javier Saiz
Andrew Blaber	Alistair Johnson	Frida Sandberg
Raymond Bond	Nadjia Kachenoura	Roberto Sassi
Giovanni Bortolan	Gabriel Latcu	Rafa Sebastian
Dana Brooks	Francesco Maffessanti	Gunnar Seemann
Nico Bruining	Luca Mainardi	Maxime Sermesant
Aline Cabasson	Hagen Malberg	Ikaro Silva
Enrico Caiani	Juan Pablo Martinez	Vito Starc
Gari Clifford	James McLaughlin	Kees Swenne
Jaume Coll-Font	Olivier Meste	Peter Van Dam
Valentina Corino	Jose Millet	Jean-Marc Vesin
Madalena Costa	Violeta Monasterio	Ed Vigmond
Johan DeBie	Bjorn Fredrik Nielsen	John Wang
Omar Escalona	Julien Oster	Urban Wiklund
Jocelyne Fayn	Olle Pahlm	Vicente Zarzoso
Sergio Furuie	Gernot Plank	Henggui Zhang
Eduardo Gil	Danila Potyagaylo	Dingchang Zheng

Session Chairs

Thanks to all of individuals who have graciously agreed to serve as session chairs during CinC 2015.

Rute Almeida	Dana Brooks	Catherine Chronaki
Riccardo Barbieri	Nico Bruining	Elaine Clark
Andrew Blaber	Laura Burattini	Gari Clifford
Raymond Bond	Enrico Caiani	Jean-Philip Couderc
Pietro Bonizzi	Guy Carrault	Pim Dassen
Giovanni Bortolan	Paolo Castiglioni	Johan De Bie

Olaf Doessel
Trygve Eftestøl
Jocelyn Fayn
Dewar Finlay
Eduardo Gil
Daniel Guldenring
Nadjia Kacheneura
Eliasz Kantoch
Alan Kennedy
Paul Kligfield
Pablo Laguna
Claudio Lamberti
Philip Langley
Peter Macfarlane
Francesco Maffesanti
Luca Mainardi
Roger Mark

Marianna Meo
Olivier Meste
Jose Millet
Victor Mor-Avi
Alan Murray
Giandomenico Nollo
Michele Orini
Julien Oster
Ivo Provaznik
Flavia Ravelli
Jeremy Rice
Jose Felix Rodriguez-Matas
Paul Rubel
Javier Saiz
Frida Sandberg
Roberto Sassi

Stefano Severi
Ikaro Silva
Leif Sornmo
Vito Starc
Johannes Struijk
Cees Swenne
Kouhyar Tavakolian
Carolina Varon
Ceisar Veiga
Jean-Marc Vesin
John Wang
Linwei Wang
Ronald Wilders
Vicente Zarzoso
Henggui Zhang
Dingchang Zheng

Welcome to Nice

Dear Colleagues,

On behalf of the organizing committee, it is our pleasure to welcome you to the 42nd Annual Scientific Conference of Computing in Cardiology and to Nice, the heart of the French Riviera. September 6-9 is the perfect period to enjoy this welcoming city surrounded by the sea and the Alps.

The Nice area brings together a perfect combination of both scientific excellence and social festivity. At the heart of excellence is the Center for Scientific and Medical Research (CHU, CHPG), Sophia Antipolis Technology Park, University of Nice-Sophia Antipolis and the European Society of Cardiology Heart House. Plus you will discover that Nice is not only renowned for its beaches but also offers many recreational facilities, tasty regional cuisine, and a beautiful old town with narrow streets and full with culture.

Computing in Cardiology provides an international forum for scientists and professionals from the fields of medicine, physics, engineering and computer science, and has been held annually since 1974. Taking place in France for the second time, 10 years after Lyon, and following the MIT in Cambridge, we are tremendously proud to host Computing in Cardiology.

The local organizing committee aims to enhance the high-tech scientific sessions provided by the Computing in Cardiology conference by locating it in the typical architectural landmarks that make Nice city proud of its living past. The events will take place in the “Centre Universitaire Méditerranéen”, the “Musée des Beaux-Arts” and the “Negresco” Hotel and will overwhelm the attendees of this reminiscence.

The Conference will begin on Sunday afternoon 6th September at 1pm with a special symposium on invited talks related to the topic of Multiscale Computing in Cardiology. A reception at “Centre Universitaire Méditerranéen” will be offered at the end of the symposium. The scientific sessions include oral and poster presentations and will begin on Monday morning. Note that this year some sessions will be followed by open discussions on various topics aiming to strengthen the relationship between Clinicians and Engineers. A direct live ablation procedure will be also broadcasted during these sessions.

In the afternoon, the traditional social program will take place either with an active treasure hunt or with a more relaxed guided tour through the old city. This exploration will finish with a marvelous gala dinner in the famous Negresco Hotel that will delight your taste buds. Sessions will continue on Tuesday, ending with a reception at the « Musée de Beaux-Arts » offered by the city of

Nice, and the meeting will be concluded on Wednesday afternoon, followed by a farewell snack.

As the local organizer, Laboratory I3S of the University of Nice-Sophia Antipolis and CNRS has the pleasure and honor to be the host of Computing in Cardiology 2015. To continue the hospitality tradition of Nice we warmly welcome delegates from around the world and hope that you will enjoy your visit to Nice. The Local Organizing Committee will enjoy assisting you in meeting your requests.

We hope that you will be intellectually stimulated and challenged by the CinC2015 scientific program and that at the same time Nice will enchant you. We look forward to seeing you in Nice.

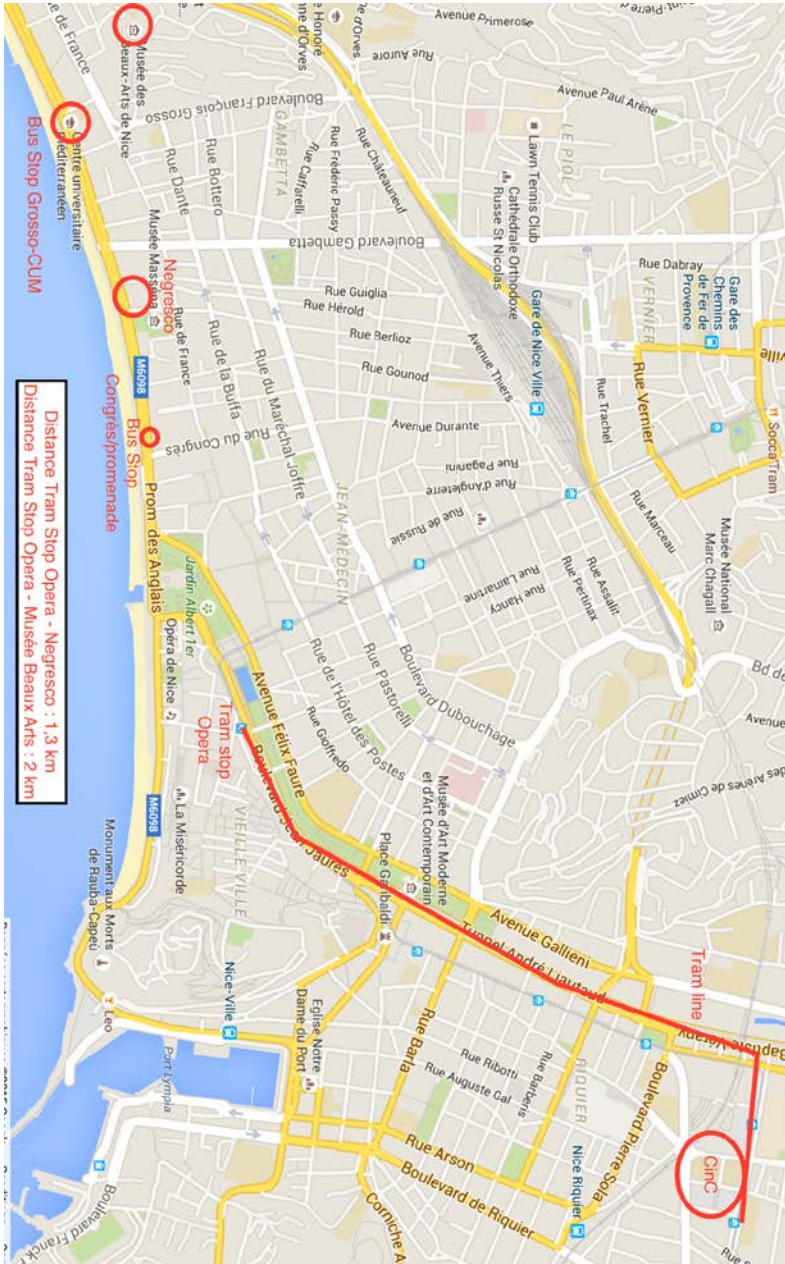


Olivier MESTE
Chair of the LOC



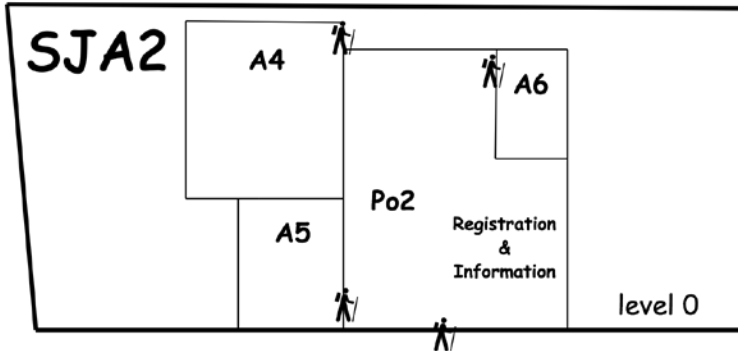
Aline CABASSON
Co-Chair of the LOC

General Map of Nice (Map G)

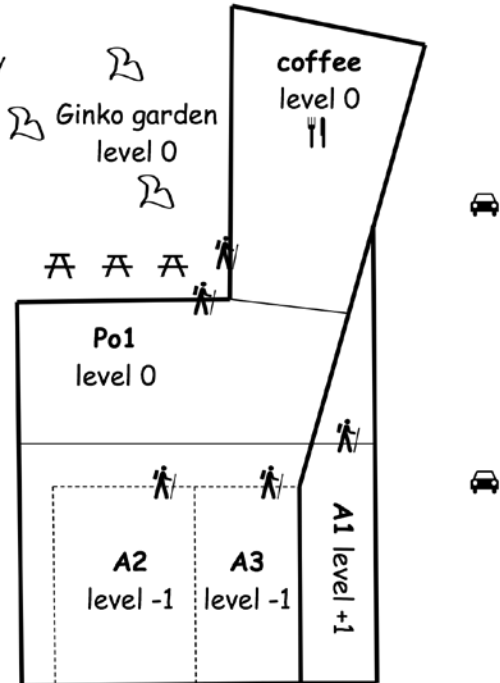


Map of the Campus Saint Jean d'Angely (SJA)

Tram line Tram line SJA stop



SJA=Saint-Jean D'Angely



Meeting Site

The 42nd annual international conference of Computing in Cardiology will meet at the Saint Jean d'Angely (SJA) Campus of the University of Nice-Sophia Antipolis, and Centre Universitaire Méditerranéen (CUM), from Sunday, September 6th through Wednesday, September 9th, 2015.

Computing in Cardiology 2015 will begin at 13:00 of Sunday 6th in the amphitheater of the Centre Universitaire Méditerranéen (CUM) with a special symposium of invited speakers. This historical place is by the seaside and conceals one of the most beautiful French amphitheatres. The address is: Centre Universitaire Méditerranéen, 65 Promenade des Anglais, 06000 Nice.

Scientific sessions, on Monday, Tuesday and Wednesday will take place in Saint Jean d'Angely (SJA) Campus. The place is easily reachable by tram (tram stop "Saint-Jean d'Angely-Université", see "General map" above). The conference is being held in lecture rooms as outlined:

- Opening and closing ceremonies Room **A1**
- Regular oral sessions Room **A1, A2, A3, A4, A5**
- Poster sessions **Po1, Po2**

Please refer to the map "Map of the Campus Saint Jean d'Angely" above for room localizations. The buildings and lecture rooms will be clearly marked with the Computing in Cardiology signs.

Transportation

Nice is popular for its ease of access: the Nice Côte d'Azur Airport is France's second-largest international airport. It is located 15 minutes driving from the old city centre. More than 50 airlines provide regular service to destinations throughout the world. An 80-minute flight links Nice to Paris, a connection that is offered 23 times a day. For more details, please visit

<http://en.nice.aeroport.fr>

For your transportation in Nice and around (Antibes, Monaco ...), the website <http://www.ceparou06.fr/index.asp> will help you select the best journey (bus/tramway/train ...).

Nice inaugurated the first line (T1) of its tramway on November 2007. The line runs for 8.7 km and stretches from the northern tip of Nice, Nice-Nord "Las Planas" near the Ray Stadium and the A8 motorway, all the way to "Pont Michel" in the Saint Roch neighborhood. The Conference Site tram stop is "Saint-Jean d'Angely-Université"

The main Nice train station "Gare Thiers SNCF" is located in the heart of the city and can be easily reached by tramway or bus: http://www.sncf.fr/en_EN/flash

Bus service is also an excellent way to get around Nice. The network is extensive and serves the entire city: www.lignedazur.com

Note that your welcome bag will include a 3-day (7-9 sept) bus/tram travel pass that will allow you to move around in Nice for free.

Directions to Monday Gala Diner and Tuesday Reception

Monday Gala Dinner: Hotel Negresco

37 Promenade des Anglais, Nice

Tuesday Reception : Musée des Beaux-Arts

33 ave des Baumettes, Nice

If you like walking exit tram at stop « Opera » and walk by the sea side (MapG).

If not:

1. First solution from the conference center or from “Masséna” place

- Tram (~15min) from Saint Jean d’Angely to Masséna
- Walk to bus stop “J. Médecin / Hôtel des Postes” (see MapA ~1min)
- Bus number : 3 - 9 -10 -22- 59- 70 (~9-15min) from J. Médecin / Hôtel des Postes → Grosso-CUM / Promenade (**Beaux-Arts** MapC) or Congrès/Promenade (**Negresco** MapD)

10 min walking to **Beaux-Arts** and 5 min to **Negresco**

2. Second solution from the conference center or from “Garibaldi” place

- Tram (~7min) from Saint Jean d’Angely to Garibaldi
- Walk to bus stop “Garibaldi” (see MapB ~1min)
- Bus number : 3 - 9 -10 (~15-20min) from J. Médecin / Hôtel des Postes → Grosso CUM / Promenade (**Beaux-Arts** MapC) or Congrès/Promenade (**Negresco** MapD)

10 min walking to **Beaux-Arts** and 5 min to **Negresco**

MapA



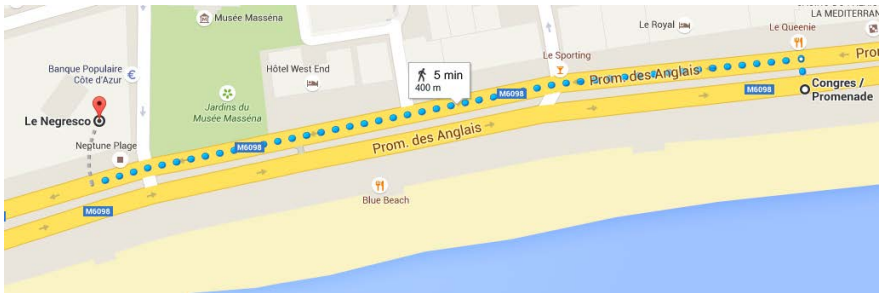
MapB



MapC



MapD



Hotel & Practical Information

Accommodations

For any budget: from 5-star luxury hotels to 1-star hotel as well as tourist residences, youth hostels... We recommend that you find a hotel close to the tram line (Tramway stop for conference site: Saint Jean d'Angely). Alternatively, there are many hotels on the seaside (around the Promenade des Anglais) with good bus connection with the tram line.

CinC2015 has two partners with negotiated prices:

* [Hi Park Residence Nice](#) - With a special Promotion code (CINC15), you will be able to book directly on their website

* [Hotel de Flore Nice](#) - Contact them and precise you are from Computing In Cardiology 2015 (CinC2015)

Climate

The French Riviera benefits from a Mediterranean-type climate, characterized by exceptional sunshine (almost 300 days per year) and mild temperatures all year round. The weather in Nice in September is usually warm and sunny with daily temperatures ranging from 15°C to 26°.

Business Hours

Shops are usually open from 9 am to 7 pm from Monday to Saturday. Department stores may stay open until 9 pm. Banks are open from 8.30 am to 12 noon and 2 pm to 4.30 pm, Tuesday to Friday, with some branches also opening on Saturday mornings. Most banks are closed on Monday.

Money/currency

Credit cards are accepted in many shops, hotels and restaurants (there is usually a minimum amount of between 7€ and 15€). You will find cash-points on just about every street corner (24 hours a day).

Bank branches, exchange offices and some post offices handle currency exchange transactions and traveller's cheques. Whatever you are buying, prices are net. A gratuity is however the custom in restaurants and for certain specific services (e.g., taxi cabs).

Emergency phone numbers

- Dial the following numbers (toll-free)
- SAMU (medical emergencies): 15
- Police emergency: 17
- Fire brigade: 18
- European emergency call: 112
- Local Committee: (+33) 6 84 75 72 58, (+33) 6 95 79 67 73

Calling to and from France

To call *France* in France: 0 + area number + number

To call France from abroad: 00 + 33 + number

To call abroad from France: 00 + country exchange number + number

Electric standards

220 Volts - 380 Volts / 50 Hertz

Tips for a pleasant trouble-free stay

- You are strongly recommended to respect smoking/no smoking signs in public places. By law, most bars and restaurants in France operate a non-smoking policy.
- It is always useful to have a little cash on you at all times for little out-of-pocket expenses like taxi fares to the airport, drinks, etc.
- A service charge is included in the price of each item on the menu in any cafe or restaurant as required by French law. In theory, no further tipping is expected.
- However, it is pretty common to leave something after a bite to eat or a drink. But it is never expected and it is only given for good or attentive service, or at a place where you are a frequent customer. Extra generosity will never hurt.
- If you are driving, park only where authorized and respect speed limits on highways and motorways.

Useful link

<http://www.frenchriviera-tourism.com/>

Things to Do in and Near Nice

Things to do in Nice

Culture and visits, shopping, gastronomy, night life, surroundings, sport activities.

- All details can be found on <http://en.nicetourisme.com/what-to-do>

Places to visit around Nice

Very close (< 30 km): Monaco, Antibes, Èze, Grasse, Cannes, Lérins Islands, ...

A little bit further away : Italy (Vintimille, San Remo, ...), Saint Tropez, Corsica, Hyères Islands (Porquerolles, Port Cros), Marseille, Aix-en-Provence, ...

The conference registration and information desk will be located on level 0 (ground floor) of SJA2 and CUM (only on Sunday) buildings. The registration desk will be labeled with the CinC sign and will be open during the following hours:

- | | |
|----------------------------|---------------|
| • Sunday, 6th September | 13:00 – 18:00 |
| • Monday, 7th September | 08:00 – 13:00 |
| • Tuesday, 8th September | 08:00 – 18:00 |
| • Wednesday, 9th September | 08:00 – 18:00 |

Internet Access

Within the conference rooms, wireless network will be available free of charge. The network name and password will be given at the registration desk. For those using **eduroam**, this network is available at the conference site. The only device you need is a WiFi-enabled laptop or smartphone. Should you need assistance in getting connected, please ask the nearest volunteer for help.

Meals

The delegates will not have to worry about meals. Just, in order to keep up the meeting timetable, the attendees are kindly asked to proceed quickly to the restaurants or buffet immediately after the session finishes.

- The **Sunday** symposium concludes with a **cocktail** at 19:00 in the splendid and unique "*Centre Universitaire Méditerranéen*" (see "Sunday Symposium" section below).
- **Monday lunch** box will be served in the University Restaurant of the Campus from 13:00 to 14:00
- **Monday** social event concludes with a **dinner** at 20:00 in the marvelous *Negresco* Hotel nearby the sea (see "General map" or "Access to Negresco" above). The location is in the city center.
- **Tuesday buffet lunch** will be provided on the Campus after the S5 sessions and overlapping the Poster session P6, from 12:00 to 14:00
- After **Tuesday** sessions, participants are invited to travel by their own to the "*Musée des Beaux Arts*" (just behind the "*Centre Universitaire Méditerranéen*" (see "General map" or "Access to Musée des Beaux-Arts" above) to enjoy a reception offered at 19:00 by the City Hall.
- **Wednesday** buffet **lunch** will be served in the University Restaurant of the Campus after the SA sessions and overlapping the Poster session PB, from 12:00 to 14:00. For the end of the conference a **Farewell snack** will be given after 17:00 on the Campus to taste some Nice specialties and refreshments.

Accompanying Persons (Guests)

The accompanying person (guest) registration allows the guest to attend

- The visit and reception on Sunday evening at the *Centre Universitaire Méditerranéen*" (see "Sunday Symposium" section below)
- The Monday social event starting at 13:00 with lunch, participation as an activist or passivist in the activities and in the gala dinner, to be held at 20:00 at the *Negresco Hotel* (see "General map" or "Access to Negresco" above).

- The Tuesday reception at the "*Musée des Beaux arts*" 19:00 (just behind the "*Centre Universitaire Méditerranéen*" (see "General map" or "Access to Musee des Beaux-Arts" above).
- The Wednesday farewell snack at 17:00 on the Campus (SJA).

Monday Social Program

Each year at CinC, Monday afternoon is set aside to facilitate a social event. This is an important part of the conference program as it allows attendees to network and relax in a more informal setting away from the scientific sessions. It is also the opportunity to uncover the history and treasures of Nice. Please consider the following remarks:

- All social program participants are required to wear their CinC badges
- As the social program starts immediately after the sessions, the participants may consider comfortable informal dress for the whole-day . However the dressing code for the Gala Dinner should **not** be streetwear style!

The social program will start at 13:00 on Monday with lunch at the **Conference Site (SJA)**. As it is traditional in the Computing in Cardiology Social Program, participants can choose between Activist or Passivist activities on the registration website.

The activist program will start at 14:00. At that time a briefing will be given at the Conference site (SJA) and participants will go by their own, using the tram (3 days free tickets are provided), toward old town (**Tram stop Opéra**) for a rich, competitive and "flavored" treasure hunt. Participants will have free time to enjoy the "Promenade des Anglais" to reach the *Negresco* Hotel (see "General map" or "Access to Negresco" above) where the Gala Dinner will take place at 20:00.

The passivist program will also start at 14:15. At that time, city guides will join us at the Conference site (SJA) and we will take the tram (3 days free tickets are provided), toward old town (**Tram stop Opéra**) for a relaxing and colorful walk accompanied by city guides. Participants will have free time to enjoy the "Promenade des Anglais" to reach the *Negresco* Hotel (see "General map" or "Access to Negresco" above) where the Gala Dinner will take place at 20:00.

Tuesday Evening Reception

The Nice City Hall will offer us a reception at the "*Musée des Beaux arts*" 19:00 (just behind the "*Centre Universitaire Méditerranéen*" (see "General map" or "Access to Negresco" above) to all conference participants, including accompanying persons. We will have the opportunity to visit the

"Musée des Beaux Arts" and its garden with some refreshments and "canapés".

Wednesday Farewell Snack

For those remaining in Nice and planning to take a bath in the Mediterranean sea in late afternoon, a friendly snack will be served at 17:00 on the Campus (SJA) with some Nice specialties, glass of "rosé" and other refreshments.

Sunday Symposium

For this new edition, the symposium will take place in one of the most beautiful French amphitheatres, located at the Centre Universitaire Méditerranéen (CUM), right on the world-famous Promenade des Anglais.

Address: Centre Universitaire Méditerranéen, 65 Promenade des Anglais, 06000 Nice

Bus lines: 3, 8, 9, 10, 12, 22, 23, 11 ("Grosso CUM Promenade" stop)
No tram is available for travel to the Sunday Symposium

The topic of this year's symposium will be "**Multiscale Computing in Cardiology**", where five exciting talks by renowned experts in the field will look at the heart from different perspectives, ranging from cell level to cardiac pathology and interaction with other organs.

- 13h00-13h45: Registration
- 13h45-14h00: Opening remarks
- 14h00-14h45: *Pr. J. Barhanin*, LP2M - CNRS-UNS, Faculty of Medicine, University of Nice Sophia Antipolis, France, "**Roles of cardiac potassium channels in repolarization and arrhythmia**"
- 14h45-15h30: *Dr. J. Jeremy Rice*, Computational Biology Center, IBM T.J. Watson Research Center, USA, "**Applications requiring high-resolution electrical and mechanical heart models**"
- 15h30-16h00: Coffee break
- 16h00-16h45: *Dr. G. Latcu*, Cardiology Service, Princess Grace Hospital Center, Monaco, "**How and when can we manage atrial fibrillation with catheter ablation techniques?**"
- 16h45-17h30: *Pr. M. Sermesant*, Asclepios Project, INRIA, France, "Integration of electrophysiology and imaging for patient-specific models and intervention planning"
- 17h30-18h15: *Pr. M. Amann*, Department of Internal Medicine, University of Utah, USA "Neural circulation control during exercise: impact of aging and heart failure"
- 18h15-18h45: Closing remarks and discussion
- 19h00-21h00: Reception at CUM.

For Authors and Speakers

Oral Presentations

The time allocated for each oral presentation is 10 minutes, followed by 5 minutes for discussion (except for Physionet Challenge sessions). Speakers are expected to adhere strictly to this schedule, which will be enforced by session chairpersons in order to finish sessions on time and to permit participants to move successfully from one parallel session to another.

- All conference rooms will be equipped with a computer projection system (LCD projector and PC with Windows 7, Powerpoint 2013, Windows Media Player and Adobe Acrobat Reader).
- Due to Powerpoint version issues, PDF format is probably the most reliable one.
- Some MacBooks will be also at disposal.

Speakers are required to allow adequate time prior to their sessions to load and check their presentations. In addition, speakers are required to meet with their session chairpersons in the scheduled conference room at least 10 minutes before the beginning of the session. It is a good idea to ensure that the chairperson knows how to correctly pronounce your name.

Poster Presentations

Poster sessions will take place in SJA1 and SJA2 location (Lobby of the two buildings SJA1 and SJA2), on Tuesday, 8th September from 12:30 , and on Wednesday, 9th September, from 12:30. Authors are required to be present at their posters during their assigned session in order to discuss their work with other conference attendees.

- Check in: Authors presenting posters must check in with the session chair in the exhibition centre during the 30 minutes prior to the poster sessions in which their presentations are scheduled
- Posters may be hung between 8:30 and 12:00 for the Tuesday and Wednesday sessions
- Posters stands (**grid stands**) and mounting material will be provided. Note that this year the posters stands are **90 cm (35") wide** and **180 cm (70 ") tall**
- Posters are grouped by subjects area, and each poster should be hung on the stand assigned to it (marked with a card corresponding to the page number of the abstract in the program book)

Posters must be removed immediately after the end of the sessions to allow the timely cleaning of the Exhibition room

Rosanna Degani Young Investigator Award

Computing in Cardiology runs an annual competition to encourage young investigators and to provide a living memorial to Rosanna Degani. The competition for the 2015 Rosanna Degani Young Investigator Award was open to persons under 36 years of age and in “training status” at the submission deadline of April 15th 2015. Finalists in the competition will present their work in session M1, at 8:45 on Monday, 7th September in room A1. The name of the winner will be announced during the closing plenary session on Wednesday.

PhysioNet/Computing in Cardiology Challenge 2015

Since 2000, Computing in Cardiology has annually issued a Physionet Challenge in cooperation with Physionet, part of the NIH sponsored Research Resource for Complex Physiologic Signals. The aim of this year’s challenge is “Reducing false arrhythmia alarms in the ICU”. The challenge sessions are on Tuesday, September 8th:

- Oral session S52 10:30 – 12:00
- Oral session S84 16:00 – 17:30

Challenge Session II is Wednesday, September 9th:

- Poster session PB9 12:30 – 14:30

Manuscripts

Computing in Cardiology will publish the conference proceedings containing the complete manuscripts of all presentations. The complete proceedings will be freely available via the CinC Web site (<http://www.cinc.org>). Also they will be published by IEEE at their IEEEXplore digital library. For any questions about manuscripts, consult the CinC web site <http://www.cinc.org> or contact via email Alan Murray, the Editor of the proceedings: Alan.Murray@ncl.ac.uk

Scientific Sessions Program Overview

Monday, September 7, 2015

8:30	Welcome to CinC 2015	A1
8:45	M1: Rosanna Degani Young Investigator Finals.....	A1
10:15	Coffee Break	
10:30	S21: Blood Pressure Analysis	A3
	S22: Atrial Fibrillation Classification	A1
	S23: Cardiac Electrophysiology.....	A4
	S24: Cardiac Chamber Quantification.....	A2
12:00	Break	
12:15	S31: Wearable Technology	A2
	S32: Fetal Signal Modelling and Analysis	A5
	S33: Repolarization and Potassium Channels.....	A4
	S34: Ambulatory ECG.....	A3
	S35: New Trends in Cardiac Imaging	A1
1:15	Social Event and Lunch	

Tuesday, September 8, 2015

8:30	S41: Databases and Web Technology.....	A5
	S42: ECG Interval Analysis.....	A2
	S43: ECG Imaging	A4
	S44: Blood Pressure Dynamics	A3
10:00	Coffee Break	
10:30	S51: Atrial Fibrillation Clinical Prediction	A2
	S52: Challenge I.....	A5
	S53: Cardiorespiratory Applications	A4
	S54: Excitation Contraction Coupling and Contraction	A3
12:00	Break (Pick up Lunch)	
12:30	P6: Poster Session with Lunch	Po1, Po2
	P61: Cardiovascular Imaging	Po2
	P62: Cardiovascular Models.....	Po1
	P63: Health Informatics: Technology	Po2
	P64: Tissue and Organ Modelling	Po1
	P65: Atrial Fibrillation	Po2
	P66: ECG-Arrhythmias.....	Po2
	P67: ECG Processing I	Po1
14:30	Break	
14:45	S71: Modelling of Causal Interactions	A2
	S72: Medical Informatics	A5
	S73: Reentry and Defibrillation	A4
	S74: ECG-Based Arrhythmia Diagnosis.....	A3
15:45	Coffee Break	
16:00	S81: ECG Signal Processing	A2
	S82: Ventricular Arrhythmias	A4
	S83: Vascular Imaging	A3
	S84: Challenge II.....	A5
19:00	Reception	Musée des Beaux-Arts

Wednesday, September 9, 2015

8:30	S91: Cardiac MRI Technological Challenges	A3
	S92: Heart Rate Variability	A2
	S93: ECG Miscellaneous	A5
	S94: Atrial Fibrillation - Clinical.....	A4
10:00	Coffee Break	
10:30	SA1: Clinical Electrocardiography	A3
	SA2: Atrial Modelling and Fibrillation	A2
	SA3: Automaticity and Markov Chains	A5
	SA4: Atrial Fibrillation Detection	A4
12:00	Break (Pick up Lunch)	
12:30	PB: Poster Session with Lunch	Po1, Po2
	PB1: Health Informatics: Algorithms	Po1
	PB2: ECG Imaging.....	Po2
	PB3: Cardiovascular Models.....	Po1
	PB4: Autonomic Nervous System	Po2
	PB5: Heartrate Variability	Po2
	PB6: Blood Pressure Measurement and Monitoring	Po1
	PB7: Membrane and Cellular Modelling	Po1
	PB8: ECG Processing II.....	Po1
	PB9: Challenge Posters	Po2
14:30	Break	
14:45	MD: Plenary	A1
16:15	Closing Ceremony	A1
16:45	Conference Closes and Farewell Snack	

Scientific Program

Monday, September 7, 2015, 08:45

M1: Rosanna Degani Young Investigator Finals

Room: A1

Chair(s): Pablo Laguna and Olaf Doessel

1-364 Rate-Adapted Dynamic-Clamp of the Funny Current in Sinoatrial Pacemaker Cells

Chiara Bartolucci*, Enrico Ravagli, Annalisa Bucchi, Mirko Baruscotti, Dario DiFrancesco, Stefano Severi

2-228 Left Atrium MRI 4D-flow in Atrial Fibrillation: Association with LA Function

Morgane Evin*, Fraser M Callaghan, Carine Defrance, Stuart M Grieve, Alain De Cesare, Philippe Cluzel, Alban Redheuil, Nadjia Kachenoura

3-318 Extraction of Morphological QRS-based Biomarkers in Hypertrophic Cardiomyopathy for Risk Stratification using L1 Regularized Logistic Regression

Aurore Lyon*, Ana Mincholé, Rina Ariga, Pablo Laguna, Stefan Neubauer, Hugh Watkins, Nando de Freitas, Blanca Rodríguez

4-187 Three-Dimensional Segmentation and Quantification of the Anatomic Regurgitant Orifice in Mitral Regurgitation using 3D Ultrasound Images

Miguel Sotaquira*, Mauro Pepi, Gloria Tamborini, Enrico Caiani

Monday, September 7, 2015, 10:30

S21: Blood Pressure Analysis

Room: A3

Chair(s): Eduardo Gil and Paolo Castiglioni

- 5-8 **Need for Re-validation of Automated Blood Pressure Devices for Use in Unstable Conditions**
Dingchang Zheng, Chengyu Liu*, John Amoore, Stephan Mieke, Alan Murray
- 6-11 **Beat-to-Beat Response Patterns of Spectral Sympathetic Estimators to the Cold Face Test and their Comparison to Those of the Orthostatic Stress Test**
Salvador Carrasco-Sosa, Alejandra Guillén-Mandujano*, Aldo R Mejía-Rodríguez
- 7-179 **Seismocardiograms Segmented Without ECG Return Valid Heart Rate Variability Indices**
Alexandre Laurin*, Kouhyar Tavakolian, Farzad Khosrow-Khavar, Andrew Blaber
- 8-260 **Heart Rate Estimation from Dual Pressure Sensors of a Dialysis Machine**
Mattias Holmer*, Frida Sandberg, Kristian Solem, Bo Olde, Leif Sörnmo
- 9-12 **Performance of the Low-Frequency Power of Pulse Pressure Variability as a Sympathetic Activity Measure During Supine, Controlled Breathing, Standing and Exercise**
Salvador Carrasco-Sosa, Alejandra Guillén-Mandujano*
- 10-383 **Pulse Transit Time Extraction from Seismocardiogram and its Relationship with Pulse Pressure**
Ajay Verma, Reza Fazel-Rezai, Kouhyar Tavakolian*

Monday, September 7, 2015, 10:30

S22: Atrial Fibrillation Classification

Room: A1

Chair(s): Frida Sandberg and Pietro Bonizzi

- 11-13 **Classification of Atrial Fibrillation Episodes by Means of Phase Variations of Time-Frequency Transforms**
Nuria Ortigosa*, Óscar Cano, Antonio Galbis, Carmen Fernández
- 12-247 **Adaptive Wavelets Applied to Automatic Local Activation Wave Detection in Fractionated Atrial Electrograms of Atrial Fibrillation**
Jorge Felix*, Raul Alcaraz, Jose J Rieta
- 13-250 **Study on the Trustability of Phase Mapping Methods to Represent Atrial Potentials in Atrial Fibrillation**
Jorge Felix*, Vincent Jacquemet, Raul Alcaraz, Jose J Rieta
- 14-173 **Unifying Automated Fractionated Atrial Electrograms Classification using Electroanatomical Mapping Systems in Persistent Atrial Fibrillation Studies**
Tiago P Almeida, Gavin S Chu, João L Salinet, Frederique J Vanheusden, Xin Li, Jiun H Tuan, Peter J Stafford, G André Ng, Fernando S Schlindwein*
- 15-176 **Combination of Frequency and Phase to Characterise the Spatiotemporal Behaviour of Cardiac Waves during Persistent Atrial Fibrillation in Humans**
Nawshin Dastagir*, Xin Li, Frederique J Vanheusden, Tiago P Almeida, João Salinet, Gavin S Chu, Peter J Stafford, G André Ng, Fernando S Schlindwein
- 16-153 **Recurrent High Dominant Frequency Spatial Patterns in Atrial Fibrillation**
Xin Li*, Gavin S Chu, Tiago P Almeida, Frederique J Vanheusden, Nawshin Dastagir, João L Salinet, Peter J Stafford, G André Ng, Fernando S Schlindwein

Monday, September 7, 2015, 10:30

S23: Cardiac Electrophysiology

Room: A4

Chair(s): Johannes Struijk and Alan Murray

17-412 using Electromechanical Signals Recorded from the Body for Respiratory Phase Detection and Respiratory Time Estimation: A Comparative Study

Nasim Alamdari, Kouhyar Tavakolian*, Reza Fazel-Rezai, Alireza Akhbardeh

18-208 Electrical Dyssynchrony on Noninvasive Electrocardiographic Mapping correlates with SAI QRST on surface ECG

Larisa Tereshchenko*, Elyar Ghafoori, Muammar Kabir, Markus Kowalsky

19-156 A Computational Model of Open-Irrigated Electrode for Endocardial RF Catheter Ablation

Ana González-Suárez*, Enrique Berjano, Jose M Guerra, Luca Gerardo-Giorda

20-83 An Additional Marker of ventricular Dyssynchrony

Pavel Jurak*, Josef Halamek, Filip Plesinger, Tereza Reichlova, Jolana Lipoldova, Miroslav Novak, Katerina Jurakova, Pavel Leinveber

21-249 Preliminary Comparison Study of Two Electro-Mechanical Cardiopulmonary Resuscitation Devices

Alejandro Mendoza Garcia*, Stefan Eichhorn, Annemarie Stroh, Marcin Polski, Alois Knoll

22-312 Analysis of the Spectrum of Cardiac Signals during Partially Correlated Spatiotemporal Dynamics: A Simulation Approach

Ferney A Beltrán-Molina, Lizet C Salgado, Luis J Martinez, Jesús Requena-Carrión*

Monday, September 7, 2015, 10:30

S24: Cardiac Chamber Quantification

Room: A2

Chair(s): Victor Mor-Avi and Trygve Eftestøl

- 23-201 **Right Ventricular Diastolic Function Evaluation in Magnetic Resonance Imaging**
Nadjia Kachenoura*, Emilie Bollache, Alban Redheuil, Stéphanie Clément-Guinaudeau, Ludivine Perdrix, Benoit Diebold, Magalie Ladouceur, Elie Mousseaux
- 24-217 **Automated Detection of Left Atrium Boundary in Intracardiac Echocardiography During Atrial Fibrillation Ablation**
Rachele Angeletti*, Corrado Tomasi, Matteo Zimmitti, Cristiana Corsi
- 25-220 **Quantification of Myocardial Viability in Late-Gadolinium Enhancement Cardiac MRI**
M Chiara Carminati, Cinzia Boniotti, Mauro Pepi, Enrico G Caiani*
- 26-50 **Model-based 3-D LV Shape Recovery in Biplane X-Ray Angiography: A-Priori Information Learned from CT**
Roland Swoboda*, Josef Scharinger, Clemens Steinwender
- 27-282 **Evaluation of Different Statistical Shape Models for Segmentation of the Left Ventricular Endocardium from Magnetic Resonance Images**
Concetta Piazzese*, M Chiara Carminati, Andrea Colombo, Rolf Krause, Mark Potse, Lynn Weinert, Gloria Tamborini, Mauro Pepi, Roberto M Lang, Enrico G Caiani
- 28-367 **A Nearly-Automated Approach for Left Ventricular Segmentation using Feature Asymmetry from Real-time 3D Echocardiography**
Claudio Fabbri*, Simone Pertutti, Cristiana Corsi

Monday, September 7, 2015, 12:15

S31: Wearable Technology

Room: A2

Chair(s): Alan Kennedy and Eliaz Kantoich

29-175 **BAN-Based Health Telemonitoring System for In-Home Care**

Eliaz Kańtoch*

30-15 **A Multi-Channel Electrode-Tissue Impedance Detection Approach for Motion Artifact Suppression in Ambulatory ECG**

Huanqian Zhang*, XiaoWei Du, Shulin Zhang, Qinghui Jin, Ruojie Tao, Qing Li, Jian Yang, Jianlong Zhao

31-254 **A Wearable Device for Physical and Emotional Health Monitoring**

Srinivasan Murali*, Francisco Rincon, David Atienza

32-372 **Wearable Monitoring: A Project for the Unobtrusive Investigation of Sleep Physiology Aboard the International Space Station**

Marco Di Rienzo, Emanuele Vaini, Prospero Lombardi*

Monday, September 7, 2015, 12:15

S32: Fetal Signal Modelling and Analysis

Room: A5

Chair(s): Julien Oster and Roberto Sassi

33-178 A Qualitative Dynamical Model for Cardiotocography Simulation

Alfredo Illanes, Michel Haritopoulos*, Felipe Robles,
Francisco Guerra

34-199 Fetal Heart Rate Complexity Measures to Detect Hypoxia

Óscar Barquero-Pérez*, Rebeca Goya-Esteban, Antonio
Caamaño, Carlos Martín-Caballero, José Luis Rojo-Álvarez

35-394 Mutual Information Estimates of CTG Synchronization

Philip A Warrick*, Emily F Hamilton

36-376 Fetal ECG Extraction using Hybrid BSS Techniques

Luis Omar Sarmiento Alvarez, Alberto Gonzalez Salvador,
Jose Millet Roig*

Monday, September 7, 2015, 12:15

S33: Repolarization and Potassium Channels

Room: A4

Chair(s): Olivier Meste and Ronald Wilders

- 37-77 **Quantification of the Ionic Current Contributions to Alterations in the Action Potential Repolarization by means of Piecewise-Linear Approximation**
Michelangelo Paci*, Jari Hyttinen, Stefano Severi
- 38-81 **Drug Toxicity on Cardiac Pacemaking: a Multi-Scale Modelling Study**
Xiangyun Bai*, Henggui Zhang, Kuanquan Wang, Yongfeng Yuan, Qince Li, Na Zhao
- 39-54 **Diabetes Affects the Temporal Dynamics of the Repolarization Properties of Cardiomyocytes**
Olivier Meste*, Marianna Meo, Sergio Signore, Marcello Rota
- 40-291 **Real-Time Simulation of IK1 in Cardiomyocytes Derived from Human Induced Pluripotent Stem Cells**
Rosalie ME Meijer van Putten, Isabella Mengarelli, Kaomei Guan, Jan G Zegers, Antoni CG van Ginneken, Arie O Verkerk, Ronald Wilders*

Monday, September 7, 2015, 12:15

S34: Ambulatory ECG

Room: A3

Chair(s): Laura Burattini and Luca Mainardi

- 41-255 **Real-Time Probabilistic Heart-Beat Classification and Correction for Embedded Systems**
Grégoire Surrel*, Francisco Rincón, Srinivasan Murali, David Atienza
- 42-411 **Evaluation of Short-term Individual Variability on the Contribution of Spectral-based Predictors to Cardiac Arrest Neurological Performance and Survival Outcomes**
Conrado J Calvo*, David Filgueiras-Rama, Santiago Jimenez-Serrano, Francisco Castells, Francisco J Chorro, José Millet
- 43-401 **On the Derivation of the Spatial QRS-T Angle from Mason–Likar Leads I, II, V2 and V5**
Daniel Guldenring*, Dewar Finlay, Raymond Bond, Alan Kennedy, James McLaughlin
- 44-100 **ECG-Derived Respiration for Ambulatory Monitoring**
Carolina Varon*, Sabine Van Huffel

Monday, September 7, 2015, 12:15

S35: New Trends in Cardiac Imaging

Room: A1

Chair(s): Claudio Lamberti and Nadjia Kacheneura

- 45-301 **Inter-study Repeatability of Left Ventricular Strain Measurement using Feature Tracking on MRI Cine Images**
Jérôme Lamy*, Gilles Soulat, Alban Redheuil, Morgane Evin, Elie Mousseaux, Nadjia Kachenoura
- 46-251 **Speckle Tracking Analysis for Early Detection of Cardiotoxicity in Breast Cancer Patients**
Cinzia Lorenzini*, Claudio Lamberti, Michele Aquilina
- 47-216 **Comparison of Novel Image Fusion Algorithms for Echocardiography and Cardiac Computed Tomography**
Tim Nordenfur*, Aleksandar Babic, Ivana Bulatovic, Anders Giesecke, Jonaz Ripsweden, Eigil Samset, Reidar Winter, Matilda Larsson
- 48-120 **Spectral Analysis of Electroanatomical Maps for Spatial Bandwidth Estimation as Support to Ablation**
Margarita Sanromán-Junquera*, Inmaculada Mora-Jiménez, Arcadio García-Alberola, José Luis Rojo-Álvarez

Tuesday, September 8, 2015, 08:30

S41: Databases and Web Technology

Room: A5

Chair(s): Raymond Bond and Catherine Chronaki

- 49-302 **Cardiology eHealth Messages Routing Policies Management Driven by Dynamic Bayesian Networks**
Nachoua Guizani*, Jocelyne Fayn
- 50-264 **Designing Reliable Cohorts of Cardiac Patients Across MIMIC II and eICU**
Catherine* Chronaki, Abdullah Chalin, Roger Mark
- 51-170 **Web Application for Data Exchange and Follow-up in Heart Rate Turbulence**
Cristina Soguero-Ruiz, Alfonso Sánchez-Caro, Inmaculada Mora-Jiménez, Luis Lechuga-Suárez, Arcadi García-Alberola, José Luis Rojo-Álvarez*
- 52-246 **A Context-Aware Approach for Wellness Monitoring of Cardiac Patient using Social Network Service Expansion**
Abdur Rahim Mohammad Forkan*, Ibrahim Khalil
- 53-140 **Interactive Progressive-based Approach to Aid the Human Interpretation of the 12-lead Electrocardiogram**
Andrew Cairns, Raymond Bond*, Dewar Finlay, Cathal Breen, Daniel Guldenring, Robert Gaffney, Patrick Henn, Aaron Peace

Tuesday, September 8, 2015, 08:30

S42: ECG Interval Analysis

Room: A2

Chair(s): Rute Almeida and Jean-Marc Vesin

54-287 Dynamic Coupling Between Ventricular Repolarization Duration and RR-Interval Phase-Rectification Analysis in Chagas Disease

Olivassé Nasario-Junior, Paulo Roberto Benchimol-Barbosa, Roberto Coury Pedrosa, Jurandir Nadal*

55-23 Optimizing the Short- and Long Term Regression for QRS Detection in Presence of Missing Data

Piotr Augustyniak*

56-211 Robustness of the Segmented-beat Modulation Method to Noise

Angela Agostinelli, Corrado Giuliani, Sandro Fioretti, Francesco Di Nardo, Laura Burattini*

57-184 Spectral Analysis of QT Interval Variability and Muscle Sympathetic Nerve Activity in Normal Subjects During Head-Up Tilt

Fatima El-Hamad, Elisabeth Lambert, Mathias Baumert*

58-114 A Noise Robust QRS Delineation Method Based on Path Simplification

Tomás Teijeiro*, Paulo Félix, Jesús Presedo

59-86 T-P Interval Estimation in Case of Overlapping Waves

Hervé Rix*, Aline Cabasson, Michal Kania, Olivier Meste

Tuesday, September 8, 2015, 08:30

S43: ECG Imaging

Room: A4

Chair(s): Linwei Wang and Dana Brooks

- 60-373 **Quantitative Comparison of Two Cardiac Electrical Imaging Methods to Localize Pacing Sites**
Jaume Coll-Font*, Petr Stovicek, Dana H Brooks, Peter M van Dam
- 61-71 **In-vivo Evaluation of Reduced-Lead-Systems in Noninvasive Reconstruction and Localization of Cardiac Electrical Activity**
Matthijs Cluitmans*, Joël Karel, Pietro Bonizzi, Monique de Jong, Paul Volders, Ralf Peeters, Ronald Westra
- 62-141 **Local Conduction Velocity Mapping for Electrocardiographic Imaging**
Corentin Dallet*, Mark Potse, Laura Bear, Josselin Duchateau, Nejib Zemzemi, Valentin Meillet, Yves Coudière, Rémi Dubois
- 63-303 **Inverse Localization of Ischemia in a 3D Realistic Geometry: A Level Set Approach**
Carlos E Chávez, Felipe Alonso-Atienza*, Nejib Zemzemi, Yves Cudière, Diego Álvarez
- 64-382 **Effect of the Torso Conductivity Heterogeneities on the ECGI Inverse Problem Solution**
Nejib Zemzemi*, Laura Bear, Mark Potse, Corentin Dallet, Yves Coudière, Remi Dubois, Josselin Duchateau
- 65-271 **Comparison of Temporal Dimensionality Reduction Methods for Constrained Inverse in Cardiac Electrical Imaging**
Jaume Coll-Font*, Danila Potyagaylo, Walther Schulze, Olaf Doessel, Dana H Brooks

Tuesday, September 8, 2015, 08:30

S44: Blood Pressure Dynamics

Room: A3

Chair(s): Dingchang Zheng and Vito Starc

66-284 Synchronization of Respiratory, Heartbeat and Blood Pressure Signals: 3D Plots and Indices

Efrosini Gatsori, George Manis*

67-112 Comparison of Methods to Measure Baroreflex Sensitivity in Brugada Syndrome

Mireia Calvo*, Virginie Le Rolle, Daniel Romero, Nathalie Béhar, Pedro Gomis, Philippe Mabo, Alfredo Hernández

68-1 Heart Failure, End-Systolic Pressure-Volume Relation

Rachad Shoucri*

69-321 Aortic-finger Pulse Transit Time vs R-derived Pulse Arrival Time: a Beat-to-Beat Assessment

Emanuele Vaini*, Prospero Lombardi, Marco Di Rienzo

70-168 Changes of Pulse Wave Velocity in Lower Limbs in Hypertensive Patients

Magdalena Matejkova*, Vlastimil Vondra, Ladislav Soukup, Filip Plesinger, Ivo Viscor, Josef Halamek, Pavel Jurak

71-56 Computational Study of Altered Pressure induced Arterial Remodeling

Linxia Gu*, Shijia Zhao, Abdullah Ibrahim

Tuesday, September 8, 2015, 10:30

S51: Atrial Fibrillation Clinical Prediction

Room: A2

Chair(s): Philip Langley and Marianna Meo

- 72-138 **Automated Home Monitoring of Atrial Fibrillation in Heart Failure Patients**
Silviu Dovancescu*, Saeed Babaeizadeh
- 73-195 **A Novel Model of Atrial Fibrillation: Episode Recurrence and Disease Progression in a Virtual Patient Population**
Eugene TY Chang*, Yen Ting Lin, Julie Eatock, Kanwal K Bhatia, Tobias Galla, Richard H Clayton
- 74-279 **Drifting Rotors Prevalence Is Associated with Dominant Frequency Reduction after Persistent Atrial Fibrillation Ablation**
João Salinet*, Maria S Guillem, Tiago Almeida, Xin Li, Gustavo Goroso, Gavin Chu, G André Ng, Fernando Schlindwein
- 75-337 **Spectral Variation in Intracardiac Impedance as a Predictive Marker During Internal Cardioversion of Atrial Fibrillation**
Philip Walsh*, Omar Escalona, Vivek Kodoth, David McEneaney, Ganesh Manoharan
- 76-418 **Technological Challenges of Computing in Cardiology in AF Management**
Nadir Saoudi*

Tuesday, September 8, 2015, 10:30

S52: Challenge I

Room: A5

Chair(s): Ikaro Silva and Gari Clifford

- 77-43 **The PhysioNet/Computing in Cardiology Challenge 2015: Reducing False Arrhythmia Alarms in the ICU**
Gari Clifford*, Ikaro Silva, Benjamin Moody, Qiao Li, Danesh Kella, Abdullah Shahin, Tristan Kooistra, Diane Perry, Roger Mark
- 78-75 **A Multimodal Approach to Reduce False Arrhythmia Alarms in the Intensive Care Unit**
Sibylle Fallet*, Sasan Yazdani, Jean-Marc Vesin
- 79-78 **False Alarms in Intensive Care Unit Monitors: Detection of Life-threatening Arrhythmias using Elementary Algebra, Descriptive Statistics and Fuzzy Logic**
Filip Plesinger*, Petr Klimes, Josef Halamek, Pavel Jurak
- 80-22 **Reducing False Arrhythmia Alarms using Robust Interval Estimation and Machine Learning**
Christoph Hoog Antink*, Steffen Leonhardt
- 81-174 **Reduction of False Critical ECG Alarms using Waveform Features of Arterial Blood Pressure and/or Photoplethysmogram Signals**
Wei Zong*
- 82-129 **Decreasing the False Alarm Rate of Arrhythmias in Intensive Care using a Machine Learning Approach**
Linda M Eerikäinen*, Joaquin Vanschoren, Michael J Rooijackers, Rik Vullings, Ronald M Aarts

Tuesday, September 8, 2015, 10:30

S53: Cardiorespiratory Applications

Room: A4

Chair(s): Guy Carrault and Kouhyar Tavakolian

- 83-102 **A Robust Detection Algorithm to Identify Breathing Peaks in Respiration Signals from Spontaneously Breathing Subjects**
Chathuri Daluwatte*, Christopher G Scully, George C Kramer, David G Strauss
- 84-225 **A Comparison of Obstructive Sleep Apnoea Detection using Three Different ECG Derived Respiration Algorithms**
Nadi Sadr*, Philip de Chazal
- 85-358 **Identification of Respiratory Phases using Seismocardiogram: A Machine Learning Approach**
Vahid Zakeri, Kouhyar Tavakolian*
- 86-180 **Sleep Apnea Detection Directly from Unprocessed ECG through Singular Spectrum Decomposition**
Pietro Bonizzi*, Joel Karel, Stef Zeemering, Ralf Peeters
- 87-239 **Ballistocardiogram Amplitude Modulation Induced by Respiration: a Wavelet Approach**
Quentin Delière*, Jens Tank, Irina Funtova, Elena Luchitskaya, David Gall, Philippe Van de Borne, Pierre-François Migeotte
- 88-67 **Real-Time Detection of Sleep Respiratory Disorders**
Delphine Feuerstein*, Laurence Graindorge, Amel Amblard, Aziz Tatar, Gustavo Guerrero, Sylvain Christofle-Boulard, Corinne Loidice, Alfredo Hernandez, Jean-Louis Pepin

Tuesday, September 8, 2015, 10:30

S54: Excitation Contraction Coupling and Contraction

Room: A3

Chair(s): Ivo Provaznik and Jeremy Rice

- 89-48 **Mathematical Modeling of the Role of Cooperativity Between Contractile and Regulatory Proteins in the Mechano-Calcium Feedbacks in Myocardium**
Elena Shikhaleva, Tatiana Sulman, Arseniy Dokuchaev, Larisa Nikitina, Leonid B Katsnelson*
- 90-298 **From Microscopic Calcium Sparks to the ECG: Model Reduction Approaches for Multi-scale Cardiac Simulation**
Michael Alan Colman*, César Parra-Rojas, Erick Andres Perez Alday
- 91-117 **Calcium Alternans is a Global Order-Disorder Phase Transition: Robustness on RyR2 Release Dynamics**
Enrique Alvarez-Lacalle*, Angelina Peñaranda, Inmaculada R Cantalapiedra, Blas Echebarria, Yohannes Shiferaw
- 92-375 **Papillary Muscles Contraction Does Not Change Ventricular Wall Mechanics**
Jeremy Rice*, Slava Gurev

Tuesday, September 8, 2015, 12:30

P61: Cardiovascular Imaging

Room: Po2

- 93-26 **Customizing the Bull's-Eye to Improve the Clinician's Diagnostic Intuition**
Ezio-Maria Ferdeghini*, Vincenzo Positano, Gianluca Di Bella, Alessandro Pingitore, Daniele Rovai
- 94-326 **Fetal Magnetic Resonance Image Denoising Based on Homogeneity Testing and Non Local Means**
Kostas Haris, George Kantasis, Nicos Maglaveras, Anthony Aletras*
- 95-308 **MRI Simulation-based Evaluation of ECV Calculation using MOLLI T1 Maps**
Christos Xanthis, Anthony Aletras*
- 96-150 **Framework to Quantify the Metabolic Rate in the Heart using Monte Carlo Simulation and Compartmental Modeling**
Edward Florez Pacheco*, Henrique da Fonseca, Vani Vijayakumar, Sergio Shiguemi Furuie
- 97-63 **Left Ventricle Functional Geometry in Different Cardiac Pathology**
Tatiana Chumarnaya*, Olga Solovyova, Yulia Alueva, Sergey P Mikhailov, Valentina V Kochmasheva, Vladimir S Markhasin
- 98-266 **Detection of Fibrosis in LGE-Cardiac MRI using Kernel DL-based Clustering**
Juan Mantilla*, José Luis Paredes, Jean-Jacques Bellanger, Julian Betancur, Frédéric Schnell, Christophe Leclercq, Mireille Garreau
- 99-7 **Effect of Interpolation on Electroanatomical Mapping**
Margarita Sanromán-Junquera*, Raquel Díaz-Valencia, Arcadio García-Alberola, José Luis Rojo-Álvarez, Inmaculada Mora-Jiménez

Tuesday, September 8, 2015, 12:30

100-399 Classification of Doppler Ultrasound Signal Quality for the Application of Fetal Valve Motion Identification

Faezeh Marzbanrad*, Yoshitaka Kimura, Miyuki Endo,
Marimuthu Palaniswami, Ahsan H Khandoker

Tuesday, September 8, 2015, 12:30

P62: Cardiovascular Models

Room: Po1

- 101-49 **Classifying Lung Congestion in Congestive Heart Failure using Electrical Impedance - A 3D Model**
Noam Omer*, Shimon Abboud, Marina Arad
- 102-304 **Causality in the Cardio-Postural Interactions During Quiet Stance**
Ajay Verma, Amanmeet Garg, Andrew Blaber*, Reza Fazel-Rezai, Kouhyar Tavakolian
- 103-404 **Influence of Psychological Stress on Systolic-Diastolic Interval (SDI) Interaction Measured from Surface Electrocardiogram (ECG)**
Chandan Karmakar*, Mohammad Hasan Imam, Peng Li, Marimuthu Palaniswami
- 104-191 **Radial Artery Pressure Wave-Derived Systolic and Diastolic Duration in Healthy Adults: Relation to Heart Rate and Age**
Peng Li, Chandan Karmakar*, Chengyu Liu, Changchun Liu
- 105-143 **Calculation of the Pulse Wave Velocity from Waveform of the Central Aortic Pressure Pulse in Young Adults**
Jana Hruskova*, Eva Zavodna, Jiri Moudr

Tuesday, September 8, 2015, 12:30

P63: Health Informatics: Technology

Room: Po2

- 106-320 **A Low-Cost Solution to follow the Evolution of Arrhythmic Patients**
Rene Ivan Gonzalez-Fernandez*, Margarita Mulet-Cartaya, Juan Dayron Lopez-Cardona, Alejandro Lopez Reyez, Rolando Lopez-Rodriguez, Rolando Emilio Lopez-Creagh, Eyglis Ledesma-Valdes
- 107-324 **A Mobile Application for Cardiac Rhythm Study**
Rene Ivan Gonzalez-Fernandez*, Margarita Mulet-Cartaya, Juan Dayron Lopez-Cardona, Rolando Lopez-Rodriguez
- 108-262 **Continuous Vital Monitoring and Automated Alert Message Generation for Motorbike Riders**
Björn Schmitz*, Christian Hofmann, Rafael Maestre, Andres Bleda, Vivien Melcher, Jos van Gent, Andreas Tobola
- 109-161 **Training-Induced Gene Expression Plasticity in Cardiac Function and Neural Regulation for Ultra-Trail Runners**
María Maqueda*, Emma Roca, Daniel Brotons, J Manuel Soria, Alexandre Perera
- 110-121 **Future Directions of Power Sources for Ambulatory ECG Monitors**
Philip A Catherwood, David Branagh, Dewar D Finlay*, James AD McLaughlin
- 111-365 **A Usability Evaluation of ECGSim: A Simulation Tool to Aid Learning in Electrocardiology**
Raymond Bond*, Eelco van Dam, Peter van Dam, Dewar Finlay, Daniel Guldenring
- 112-128 **Cardiac Monitoring in Head Area for Motorcycle Applications**
Andres L Bleda*, Rafael Maestre, Björn Schmitz, Christian Hofmann, Jose M Nacenta, Guadalupe Santa, Soledad Pellicer, Vivien Melcher

Tuesday, September 8, 2015, 12:30

113-231 Human Authentication Implemented for Mobile Applications Based on ECG-Data Acquired from Sensorized Garments

Daniel Tantinger*, Markus Zrenner, Nadine Lang, Heike Leutheuser, Bjoern Eskofier, Christian Weigand, Matthias Struck

114-139 VitalSimML: A Well-Formed Data Structure to Capture Patient Monitoring Scenarios to Facilitate the Training of Nurses via Computer-Based Simulation

Jonathan Currie*, Raymond Bond, Paul McCullagh, Pauline Black, Dewar Finlay

Tuesday, September 8, 2015, 12:30

P64: Tissue and Organ Modelling

Room: Po1

115-294 Microscopic Modelling of the Non-Linear Gap Junction Channels

Andjela Davidovic*, Yves Coudiere, Thomas Desplantez, Clair Poignard

116-226 Adaptation of Rabbit Ventricular Cell Model to Reproduce Action Potentials in Isolated Papillary Muscles

Ask Schou Jensen*, Cristian Pablo Pennisi, Cristian Sevcencu, Jørn Bolstad Christensen, Jette Elisabeth Kristiansen, Johannes Jan Struijk

117-223 T-wave Morphology Depends on Transmural Heterogeneity in a High-Resolution Human Left-Ventricular Wedge Model

Massimo W Rivolta*, Graham H Bevan, Viatcheslav Gurev, John J Rice, Coeli M Lopes, Jean-Philippe Couderc

118-222 Influence of Gap Junction Dynamics on the Stability of Reentrant Waves in Cardiac Tissue

Claudia Hawks*, Jorge Elorza, Jean Bragard, Inma R Cantalapiedra, Angelina Penaranda, Blas Echebarria

119-194 Parameter Sensitivity from Single Atrial Cell to Tissue: How Much does it Matter? A Simulation and Multivariate Regression Study

Eugene TY Chang*, Richard H Clayton

120-59 Effects of Enhanced Sodium Currents in Mathematical Model of Heterogeneous Myocardium

Nathalie Vikulova*, Anastasia Khokhlova, Olga Solovyova, Leonid Katsnelson

Tuesday, September 8, 2015, 12:30

- 121-214 **Influence of Right and Left Atrial Tissue Heterogeneity on Atrial Fibrillation Perpetuation**
Adrian Luca*, Vincent Jacquemet, Nathalie Virag, Jean-Marc Vesin
- 122-245 **Computer Analysis of Isolated Cardiomyocyte Contraction Process via Advanced Image Processing Techniques**
Jan Odstrcilik*, Vratislav Cmiel, Radim Kolar, Marina Ronzhina, Larisa Baiazitova, Martin Pesl, Jan Pribyl, Ivo Provaznik
- 123-405 **Voltage Sensitive Dye di-4-ANNEPS Prolongs Impulse Conduction Through Ventricles, but not Through AV Node in Isolated Rabbit Heart**
Veronika Olejnickova*, Marina Ronzhina, Oto Janousek, Jana Kolarova, Katerina Fialova, Ivo Provaznik, Marie Novakova
- 124-280 **Quantification of the Effects of Electrical Remodelling due to Hypertrophic Cardiomyopathy on Human Ventricular Electromechanical Activity and Energetics**
Gareth M Jones*, Michael A Colman, Ismail Adeniran, Henggui Zhang
- 125-393 **Robust Framework for Quantitative Analysis of Optical Mapping Signal without Filtering**
Ilija Uzelac*, Flavio Fenton
- 126-181 **3-D Modeling of the Thorax for Seismocardiography**
Alexandre Laurin*, Kouhyar Tavakolian, Andrew Blaber, Sébastien Imperial, Philippe Moireau, Dominique Chapelle
- 127-300 **Massively Parallel CUDA Simulations of Cardiac and Embryonic MRI on a Cloud-based Cluster**
George Kantasis, Christos Xanthis, Anthony Aletras*

Tuesday, September 8, 2015, 12:30

P65: Atrial Fibrillation

Room: Po2

- 128-232 **Robust Statistical Modeling of the Atrioventricular Node during Atrial Fibrillation**
Mikael Henriksson*, Valentina DA Corino, Leif Sörnmo, Frida Sandberg
- 129-229 **Characterization of AV-nodal Properties during Atrial Fibrillation using a Multilevel Modelling Approach**
Mikael Wallman*, Frida Sandberg
- 130-80 **Influence of Left Atrial Geometry on Rotor Core Trajectories in a Model of Atrial Fibrillation**
Konstantinos N Tzortzis*, Caroline H Roney, Norman A Qureshi, Fu Siong Ng, Phang Boon Lim, Spencer J Sherwin, Nicholas S Peters, Chris D Cantwell
- 131-403 **Methods for Analyzing Signal Characteristics of Stable and Unstable Rotors in a Realistic Heart Model**
Markus Rottmann*, Laura Unger, Gunnar Seemann, Amir Jadidi, Thomas Arentz
- 132-297 **Surface ECG Spectral Analysis to Predict Atrial Fibrillation Catheter Ablation Long-term Outcome**
Raul Alcaraz*, Fernando Hornero, Lorenzo Facila, Jose Joaquin Rieta
- 133-293 **The Lagged Central Tendency Measure Applied to Assess P-wave Duration Variability Improves Paroxysmal Atrial Fibrillation Onset Prediction**
Raul Alcaraz*, Arturo Martinez, Jose Joaquin Rieta

Tuesday, September 8, 2015, 12:30

- 134-335 **Far-Field Effect in Unipolar Electrograms Recorded from Epicardial and Endocardial Surface: Quantification of Epi-Endo Dissociation During Atrial Fibrillation in Humans**
Piotr Podziemski, Stef Zeemering*, Elham Bidar, Pawel Kuklik, Arne van Hunnik, Ulrich Schotten
- 135-124 **Towards Application of Complexity Measures of Atrial Electrograms to Predict Outcome of the Ablation Procedure**
Katarzyna Kořna*, Piotr Podziemski, Paweł Kuklik, Daniel Steven, Jan J Źebrowski, Stephan Willems
- 136-221 **F-wave Amplitude Stability on Multiple Electrocardiogram Leads in Atrial Fibrillation**
Marianna Meo*, Antonio R Hidalgo-Muñoz, Vicente Zarzoso, Olivier Meste, Decebal G Latcu, Nadir Saoudi
- 137-380 **Teager Energy Based Approach to Detect Atrial Peaks to Predict Atrial Fibrillation Recurrence**
Raquel Cervigón*, Javier Moreno, José Millet, Francisco Castells

Tuesday, September 8, 2015, 12:30

P66: ECG-Arrhythmias

Room: Po2

138-278 Dynamic Coupling Between Atrio-Ventricular Duration and RR-Interval Histogram Phase-Rectification Analysis in Chronic Chagas Disease

Paulo Roberto Benchimol-Barbosa, Olivassé Nasario-Junior, Roberto Coury Pedrosa, Jurandir Nadal*

139-307 Comparison of Electric and Magnetic Cardiograms Produced by Myocardial Ischemia in Models of the Human Ventricle and Torso

Erick Andres Perez Alday*, Chen Zhang, Michael Alan Colman, Haibo Ni, Zizhao Gan, Henggui Zhang

140-149 The Effect of Voltage Sensitive Dye di-4-ANEPPS on the RT/RR Coupling in Rabbit Isolated Heart

Petr Veselý*, Marina Ronzhina, Kateřina Fialová, Jana Kolářová, Josef Halánek, Marie Nováková

141-273 A Novel Method for Automatic Standardization of Digital Electrocardiographs

Eduardo Freitas*, João Salinet, Tiago Almeida, Henrique Oliveira

142-406 Comparison of Intensity-based B-splines and Point-to-Pixel Tracking Techniques for Motion Reduction in Optical Mapping

Jaime Yagüe-Mayans, Conrado J Calvo*, Antonio Cebrián, Francisco J Chorro, José Millet

143-130 Cardiac Resynchronization Efficiency Estimation by New Ultra-High-Frequency ECG Dyssynchrony Descriptor

Tereza Reichlova*, Pavel Jurak, Josef Halamek, Filip Plesinger, Jolana Lipoldova, Miroslav Novak, Pavel Leinveber

Tuesday, September 8, 2015, 12:30

- 144-95 **Feasibility of Compression Depth Estimation from the Acceleration Signal during Cardiopulmonary Resuscitation in Long-Distance Trains**
Digna M González-Otero*, Sofía Ruiz de Gauna, Jesús Ruiz, Beatriz Chicote, Sandra Plaza
- 145-276 **In Silico Investigation of the Pro-arrhythmogenic Effect of KCNQ1-G269S Mutation in Human Ventricles**
Haibo Ni*, Wei Wang, Erick Andres Perez Alday, Henggui Zhang
- 146-243 **Electrocardiographic Detection And Monitoring of Pulmonary Hypertension**
Marjolein C de Jongh*, Vivian P Kamphuis, Sumche Man, Arie C Maan, Hubert W Vliegen, Cees A Swenne
- 147-332 **Reliability of APD-Restitution Slope Measurement: Quantification and Methodological Comparison**
Michele Orini*, Neil Srinivasan, Peter Taggart, Pier Lambiase
- 148-206 **Role of Mechanics in Rhythm Disturbances in 1D Mathematical Model of Myocardial Tissue with Local Ca²⁺-Overload**
Alexander Kursanov*, Olga Solovyova, Leonid Katsnelson, Vladimir Markhasin
- 149-68 **Pulse Annotation of Automatic External Defibrillators Recordings during Out of Hospital Cardiac Arrest**
Clément Neyton*, Sarah Ménétré, Daniel Jost, Fabielle Angel, Bernard Gény, Vincent Lanoë, Jean-Philippe Didon
- 150-148 **Sample Entropy as a Shock Outcome Predictor during Basic Life Support**
Beatriz Chicote*, Unai Irusta, Elisabete Aramendi, Daniel Alonso, Carlos Jover, Carlos Corcuera

Tuesday, September 8, 2015, 12:30

151-87 Alternatives to Estimate the Compression Depth from the Acceleration Signal during Cardiopulmonary Resuscitation

Sofía Ruiz de Gauna*, Digna M González-Otero, Jesús Ruiz, Beatriz Chicote, Noelia Vidales

Tuesday, September 8, 2015, 12:30

P67: ECG Processing I

Room: Po1

- 152-24 **A Wavelet-Based High-Frequency Analysis of Fragmented QRS Complexes in Patients with Myocardial Infarction**
Chun-Cheng Lin*, Weichih Hu, Yu-Wei Lin
- 153-127 **Robust detection of ECG waves**
Anna Wojdeł*, Vicent J Ribas Ripoll, Miguel Teixidó-Roman, Pablo Ramos, Josep Brugada
- 154-258 **Detection of Irregular Heartbeats using Tensors**
Griet Goovaerts*, Ofelie De Wel, Bert Vandenberg, Rik Willems, Sabine Van Huffel
- 155-386 **ECG Baseline Wander Removal with Recovery of the Isoelectric Level**
Antonio Fasano, Valeria Villani*
- 156-109 **Low-Delay Estimation of the Real-Time Respiratory Rate from the ECG using a Bank of Notch Filters**
Leila Mirmohamadsadeghi*, Jean-Marc Vesin
- 157-347 **Causality Analysis of Atrial Fibrillation Electrograms**
David Luengo*, Gonzalo Rios-Muñoz, Victor Elvira
- 158-261 **Neural Network Approach for T-wave End Detection: a Comparison of Architectures**
Alexander Alexeis Suárez León*, Danelia Matos Molina, Griet Goovaerts, Carlos Vázquez Seisdedos, Steven Vandeput, Sabine Van Huffel
- 159-218 **A Comparison of Three Methodologies for the Computation of V-index**
Ebadollah Kheirati Roonizi*, Massimo W Rivolta, Luca T Mainardi, Roberto Sassi

Tuesday, September 8, 2015, 12:30

- 160-333 **Fractal Pattern of Heart Rate Variability Revealing Unknown Very Low Frequency Properties**
Dorota Kokosińska*, Jan Gierałtowski, Jan Żebrowski
- 161-204 **Angular Velocity Transition Along the QRS Loop Aid in the Detection of the QRS Complex End and Detection of Acute Myocardial Infarction**
Vito Starc*, Todd T Schlegel
- 162-164 **A LightWAVE Plug-in for Semi-automatic Annotation of Heart Beats from ECG Time Series**
Luca Citi*, Claudia Olariu, Riccardo Barbieri
- 163-98 **Novel Algorithm for Estimation ST-Segment Parameters**
Vadim Konuhov, Sergey Akulov, Anna Akulova*
- 164-183 **A Robust, Simple and Reliable Measure of Heart Rate Variability using Relative RR Intervals**
Marcus Vollmer*
- 165-407 **Assessment of Autonomic Nerve Activity by Circadian Rhythm at Different Stages after Acute Myocardial Infarction Based on Holter Data**
Hongduoer Liu*, Ping Zhan, Zhigang Wang, Yi Peng

Tuesday, September 8, 2015, 14:45

S71: Modelling of Causal Interactions

Room: A2

Chair(s): Giandomenico Nollo and Michele Orini

- 166-363 **Causal Relationships in Cardiovascular System Revealed by Transfer Entropy**
Dorota Wejer*, Luca Faes, Danuta Makowiec, Beata Graff
- 167-263 **Parameter Estimation of a Mathematical Model Describing the Cardiovascular-Respiratory Interaction**
Layli S Goldoozian, Antonio R Hidalgo-Muñoz, Vicente Zarzoso*, Edmond Zahedi
- 168-357 **Investigation of Causal Interactions Between Ventricular Action Potential Duration, Blood Pressure and Respiration**
Stefan Van Duijvenboden*, Michele Orini, Nick Child, Jaswinder S Gill, Peter Taggart, Ben Hanson
- 169-57 **Information-Theoretic Assessment of Cardiovascular-Brain Networks during Sleep**
Luca Faes*, Daniele Marinazzo, Giandomenico Nollo

Tuesday, September 8, 2015, 14:45

S72: Medical Informatics

Room: A5

Chair(s): Daniel Guldenring and Giovanni Bortolan

- 170-369 **Visualizing Evolving Clinical Sentiment using Vector Representations of Clinical Notes and Distributed Stochastic Neighbor Embedding**
Mohammad Mahdi Ghassemi*, Roger Mark, Shamim Nemati
- 171-159 **Heart Rate Estimation in Photoplethysmogram Signals using Nonlinear Model-Based Signal Processing**
Federico Wadehn*, Yue Zhao, Hans-Andrea Loeliger
- 172-359 **Comparison of Four Smartphone Compatible Blood Pressure Monitors**
Roderick Treskes*, Enno van der Velde, Daniëlle Eindhoven, Martin J Schalij
- 173-58 **A Novel Algorithm for Estimating Beat-to-Beat Systolic and Diastolic Blood Pressure using Chest Based ECG and Photoplethysmography**
*Xinhui Yang, Kevin Xu, Gang Chen, Shiping Li, Jordan Davis (Xuelin Xu)

Tuesday, September 8, 2015, 14:45

S73: Reentry and Defibrillation

Room: A4

Chair(s): Jose Felix Rodriguez Matas and Jean-Philip Couderc

- 174-92 **Self-Terminating Re-Entrant Cardiac Arrhythmias: Quantitative Characterization**
Alan P Benson, Barrie Hayes-Gill, Arun V Holden*, Rosa Matthews, Aneela Naz, Stephen Page, Eleftheria Pervolaraki, Muzahir Tayebjee
- 175-133 **Sustained Re-entry in a 3D Regionally Ischemic Human Heart: A Simulation Study**
Andres Mena-Tobar, Jose M Ferrero, Jose F Rodriguez-Matas*
- 176-344 **Multiple Virtual Electrodes Widen the Unpinning Interval**
Sebastian Berg*, T K Shajahan, Tariq Baig, Valentin Krinsky, Stefan Luther
- 177-396 **A New Low-Energy, Far-Field Defibrillation Mechanism**
Niels Otani*, Valentin Krinski, Stefan Luther

Tuesday, September 8, 2015, 14:45

S74: ECG-Based Arrhythmia Diagnosis

Room: A3

Chair(s): Dewar Finlay and Paul Rubel

- 178-19 **Classification of Cardiac Arrhythmia In Vitro Based on Multivariate Complexity Analysis**
Binbin Xu, Sabir Jacquir, Stéphane Binczak*, Hussein Yahai, Rémi Dubois
- 179-84 **Logistic Regression to Enhance Risk Assessment by Left Ventricular Ejection Fraction and f99**
Corrado Giuliani, Cees A Swenne, Sumche Man, Angela Agostinelli*, Sandro Fioretti, Francesco Di Nardo, Laura Burattini
- 180-288 **Big-Data Analytics for Arrhythmia Classification using Data Compression and Kernel Methods**
José María Lillo Castellano*, Inmaculada Mora Jiménez, Rafael Moreno-González, María Monserrat-García-de-Pablo, Arcadi García-Alberola, José Luis Rojo Álvarez
- 181-163 **Automatic Diagnosis of Complete Left Bundle Branch Block from Standard 12-lead Electrocardiogram**
Xiaojuan Xia*, Anne-Christine Ruwald, Martin Ruwald, Nene Ugoeke, Barbara Szepletowska, Valentina Kutyifa, Mehmet Aktas, Poul Erik Bloch Thomsen, Wojciech Zareba, Arthur Moss, Jean-Philippe Couderc

Tuesday, September 8, 2015, 16:00

S81: ECG Signal Processing

Room: A2

Chair(s): Vicente Zarzoso and Jocelyn Fayn

- 182-281 **Orthogonal Component Analysis to Remove Ventricular Far Field in Non Periodic Sustained Atrial Flutter**
Gustavo Lenis, Tobias Oesterlein, Dan-Timon Rudolph, Olaf Dössel*
- 183-327 **Validation of the V-index as a Metric of Ventricular Heterogeneity in Endocavitary Recordings**
Michele Orini, Claudio Blasi, Malcom Finlay, Ben Hanson, Pier Lambiasi, Roberto Sassi, Luca Mainardi*
- 184-61 **Determining the Connection between Capacitively Coupled Electrocardiography Data and the Ground Truth**
Anna Böhm*, Christoph Hoog Antink, Steffen Leonhardt, Daniel Teichmann
- 185-155 **A Principal Component Analysis Approach for Heart Rate Turbulence Assessment in Chagas Disease**
Alex C Alberto*, Gabriel A Limeira, Jurandir Nadal
- 186-186 **Algorithm for Real-time Prediction of Neurally Mediated Syncope Integrating Indexes of Autonomic Modulation**
Ricardo Couceiro*, Paulo Carvalho, Rui Pedro Paiva, Jens Muehlsteff, Jorge Henriques, Christian Eickholt, Christoph Brinkmeyer, Malte Kelm, Christian Meyer
- 187-296 **Reliability Loss with Sampling Rate Reduction**
Paulo Sousa, Rute Almeida*, Marta João Silva, Ana Paula Rocha

Tuesday, September 8, 2015, 16:00

S82: Ventricular Arrhythmias

Room: A4

Chair(s): Jose Millet and Cees Swenne

- 188-110 **The Origin of Diastolic Micro-Signals Observed in Defibrillator Recipients Might Be Qualitatively Explained by a Simple Computational Model**
Aldo Casaleggio*, Paolo Rossi, Michele Migliore
- 189-62 **Investigation of the Functional Effects of KCNJ2-linked Short QT Syndrome on Electrical Conduction at Purkinje-Ventricle Junction at Low- and High-Frequency**
Cunjin Luo*, Kuanquan Wang, Qingjie Wang, Yongfeng Yuan, Zhili Li, Ming Yuan, Henggui Zhang
- 190-299 **Epicardial-Limited Electrophysiological Heterogeneities do not Facilitate Ventricular Arrhythmia Induction: An Experimental Study**
Antonio Guill, Alvaro Tormos, Conrado J Calvo, Eduardo J Roses, Antonio Cebrian, Luis Such-Miquel, Luis Such, Manuel Zarzoso, Francisco J Chorro, Jose Millet*
- 191-269 **Control of Ventricular Tachycardia under Myocardial Ischemic Conditions and Infarction**
Edda Boccia*, Stefan Luther
- 192-20 **Effects of Early Afterdepolarizations on Ventricular Tachycardia in Human Heart**
Jieyun Bai, Kuanquan Wang*, Yinghui Li, Henggui Zhang

Tuesday, September 8, 2015, 16:00

S83: Vascular Imaging

Room: A3

Chair(s): Ceisar Veiga and Nico Bruining

193-311 Left Ventricular–Aortic Coupling in Sickle Cell Disease Underlies Diastolic Dysfunction

Emilie Bollache*, Nadjia Kachenoura, Roberto Lang, Victor Mor-Avi, Amit Patel

194-314 Phase Contrast MRI: Development of a User-Friendly Platform for Fast-Automated Segmentation and Fluid-Dynamic Post-Processing

Selene Pirola, Filippo Piatti*, Francesco Sturla, Emiliano Votta, Igor Nesteruk, Massimo Lombardi, Alessandro Della Corte, Malenka Bissell, Alberto Redaelli, Enrico Caiani

195-346 Design of Anthropomorphic Atherosclerotic Carotid Artery Flow Phantoms for Ultrasound Images

Francesca Galluzzo*, Filippo Leonardo, Alessandro Ceruti, Luca De Marchi, Cristiana Corsi

196-202 Aortic Pulse Wave Velocity using Wavelet Analysis in Magnetic Resonance Imaging

Ioannis Bargiotas*, Elie Mousseaux, Wen-Chung Yu, Bharath Ambale Venkatesh, Emilie Bollache, Alain De Cesare, Joao A C Lima, Alban Redheuil, Nadjia Kachenoura

197-41 A Fully Automated Approach to Aortic Distensibility Quantification from Fetal Ultrasound Images

Giacomo Tarroni*, Silvia Visentin, Erich Cosmi, Enrico Grisan

198-30 Measurement of IMT with Fuzzy Segmentation in Carotid Ultrasound Images

Nader Jafarnia Dabanloo*, Faezeh Foolad, Gholamreza Attarodi, Emad Fatemizadeh

Tuesday, September 8, 2015, 16:00

S84: Challenge II

Room: A5

Chair(s): Gari Clifford and Ikaro Silva

- 199-415 **The PhysioNet/Computing in Cardiology Challenge 2015: Reducing False Arrhythmia Alarms in the ICU**
Gari Clifford*, Ikaro Silva, Benjamin Moody, Qiao Li, Danesh Kella, Abdullah Shahin, Tristan Kooistra, Diane Perry, Roger Mark
- 200-189 **Enhancing Accuracy of Arrhythmia Classification by Combining Logical and Machine Learning Techniques**
Vignesh Kalidas*, Lakshman Tamil
- 201-21 **Validation of Arrhythmia Detection Library on Bedside Monitor Data for Triggering Alarms in Intensive Care**
Vessela Krasteva, Irena Jekova, Remo Leber, Ramun Schmid, Roger Abaecherli*
- 202-36 **Reduction of False Alarms in Intensive Care Unit using Multi-feature Fusion Method**
Chengyu Liu*, Hong Tang, Lina Zhao
- 203-42 **Heart Beat Fusion Algorithm to Reduce False Alarms for Arrhythmias**
Chathuri Daluwatte*, Lars Johannesen, Jose Vicente, Christopher G Scully, Lorian Galeotti, David G Strauss
- 204-32 **Suppression of False Arrhythmia Alarms using ECG and Pulsatile Waveforms**
Paula Couto, Ruben Ramalho, Rui Rodrigues*

Wednesday, September 9, 2015, 08:30

S91: Cardiac MRI Technological Challenges

Room: A3

Chair(s): Enrico Caiani and Francesco Maffesanti

- 205-64 **Automatic Generation of Surface Meshes for Right Ventricle with 1-to-1 Vertex Correspondence from Cine-MR Images**
Yi Su*, May-Ling Tan, Soo-Kng Teo, Liang Zhong, Ru-San Tan
- 206-213 **Automatic Detection of Microvascular Obstruction in Patients with Myocardial Infarction**
Trygve Eftestøl*, Erlend Singsaas, Kjersti Engan, Leik Woie, Stein Ørn
- 207-277 **Feasibility of Variable Step Size Least Mean Squares for intra-MRI ECG Artefact Reduction**
André Guillou*, Sarah Ménétré, Grégory Petitmangin, Jacques Felblinger, Laurent Bonnemains
- 208-190 **Temporary Cardiac Pacing Leads Safety in MRI**
Qi Zeng*, Qinyan Wang, Ji Chen
- 209-374 **Comparison of Measurement and Calculation of the Electric Field Transfer Function for an Active Implant Lead in Different Media**
John Nyenhuis, John Jallal, Xiaoyi Min, Shiloh Sison*, Gabriel Mouchawar
- 210-316 **Lead Heating of a MRI Conditionally Safe Pacemaker System**
Gabriel Mouchawar, Shiloh Sison*, Shawn Chen, Xiaoyi Min, Ji Chen, John Nyenhuis, Richard Williamson

Wednesday, September 9, 2015, 08:30

S92: Heart Rate Variability

Room: A2

Chair(s): Carolina Varon and Riccardo Barbieri

211-111 Spectral and Fractal Structures of Heart Rate Variability in Coronary Artery Disease Patients without Myocardial Infarction

Paolo Castiglioni*, Marco Di Rienzo, Alberto Radaelli

212-207 On Modelling RR Tails in Heart Rate Variability Studies: An Extreme Value Analysis

Sónia Gouveia*, Manuel G Scotto

213-377 Heart Rate Variability Analysis of Normal and Intrauterine Growth Restricted Children using Sample Entropy

Taher Biala*, J Alexandre Lobo M, Michael Wailoo, Fernando Schlindwein

214-165 Instantaneous Bispectral Analysis of Heartbeat Dynamics for the Assessment of Major Depression

Ronald G Garcia*, Gaetano Valenza, Carlos Tomaz, Riccardo Barbieri

215-286 Autonomic Nervous System Assessment in Critically Ill Patients Undergoing a Cognitive Rehabilitation Therapy

David Hernando*, Marc Turon, Raquel Bailón, Sol Fernandez-Gonzalo, Jesús Lázaro, Gemma Gomà, Eduardo Gil, Jaume Montanyà, Josefina López, Candelaria De Haro, Pablo Laguna, Lluís Blanch

216-142 Heart Rate Variability Associated with Walking Zen Meditation Kinhin: towards 'Contemplatio Actione'

Masaki Hoshiyama*, Asagi Hoshiyama

Wednesday, September 9, 2015, 08:30

S93: ECG Miscellaneous

Room: A5

Chair(s): John Wang and Elaine Clark

- 217-352 **Impact of Mental Stress on Heart Rate Asymmetry**
Saman Parvaneh*, Nima Toosizadeh, Sadaf Moharreri
- 218-290 **Heart Morphology Differences Induced by Intrauterine Growth Restriction Measured on the ECG in Teenagers**
Nuria Ortigosa*, Fátima Crispi, Raquel Bailón, Mérida Rodríguez, Eduard Gratacós, Sebastián Savari, Marta Sitges, Bart Bijmens, Pablo Laguna
- 219-96 **Superiority of the Automated 5-Minute Summary ECG to Cardiologist Over-read Triplicate ECGs in Detection of QTc Change**
Jay W Mason*, Shaun Szot, Brock Heinz
- 220-88 **Predicting Mood Changes in Bipolar Disorder through Heartbeat Nonlinear Dynamics: a Preliminary Study**
Gaetano Valenza*, Mimma Nardelli, Gilles Bertschy, Claudio Gentili, Antonio Lanata, Enzo Pasquale Scilingo
- 221-132 **Repolarization Parameters of Heart Transplant Subjects**
Josef Halamek*, Pavel Jurak, Tereza Reichlova, Petr Vesely, Pavel Leinveber
- 222-185 **Assessment of Joint Interactions between Respiration and Baroreflex Activity using Joint Symbolic Dynamics in Heart Failure Patients**
Muammar Kabir*, Elyar Ghafoori, Larisa Tereshchenko

Wednesday, September 9, 2015, 08:30

S94: Atrial Fibrillation - Clinical

Room: A4

Chair(s): Johan De Bie and Pim Dassen

- 223-157 Electrogram Coupling as a Measure of Local Conduction during Atrial Fibrillation**
Stef Zeemering*, Piotr Podziemski, Arne van Hunnik, Bart Maesen, Pietro Bonizzi, Ulrich Schotten
- 224-224 Diagnosis of Atrial Fibrillation by means of Implantable Devices: The Role of Remote Monitoring**
Eugenio Cervesato*, Eugenia Bruschetta, Denis Fantin, Francesca Loro, Delia Zadnik, Marco Brieda, Ermanno Dametto, Federica Del Bianco, Sara Zardo, Edda Pollesel, Catya Zorzi, Matteo Cassin
- 225-289 Assessment of QT-RR Intervals Relation in Patients with Atrial Fibrillation**
Luca Iozzia*, Luca T Mainardi, Federico Lombardi, Valentina D A Corino
- 226-113 A High-Density Activation Map Estimation During Atrial Fibrillation**
Alejandro Alcaine*, Natasja MS de Groot, Pablo Laguna, Juan Pablo Martínez, Richard PM Houben
- 227-234 Automatic Detection of Atrial Fibrillation using a MEMS Accelerometer**
Tero Koivisto*, Mikko Pänkäälä, Tero Hurnanen, Tuija Vasankari, Tuomas Kiviniemi, Antti Saraste, Juhani Airaksinen
- 228-306 The U Wave in Atrial Fibrillation**
Philip Langley*, John Bourke, Alan Murray

Wednesday, September 9, 2015, 10:30

SA1: Clinical Electrocardiography

Room: A3

Chair(s): Paul Kligfield and Peter Macfarlane

229-334 STEMI Classification in Acute Ischemia: Dependence on the Position of the ST-Deviation Measurement Relative to the J Point

Sumche Man*, C Cato Ter Haar, Arie C Maan, Martin J Schalij, Cees A Swenne

230-79 Long Term Follow Up of the Early Repolarization Pattern in Participants in the West of Scotland Coronary Prevention Study

Elaine Clark*, Ian Ford, Peter Macfarlane

231-330 Circadian Modulation on T-wave Alternans Activity in Chronic Heart Failure Patients

Alba Martín-Yebra*, Enrico G Caiani, Pablo Laguna, Violeta Monasterio, Juan Pablo Martínez

232-235 Validation of the Vessel-Specific Leads (VSLs) for Acute Ischemia Detection on a Dataset with Non-Ischemic ST-Segment Deviation

John Wang*, Olle Pahlm, Galen Wagner, James Warren, Milan Horacek

233-371 A Fundamental Relationship between Intraventricular Conduction and Heart Rate

Jay W Mason*, Robert L Lux, Benhur Aysin, Thomas E Moon, Martino Vaglio, Fabio Badilini, Brock Heinz

234-419 Engineering Issues in Clinical Electrocardiography

JW Mason*

Wednesday, September 9, 2015, 10:30

SA2: Atrial Modelling and Fibrillation

Room: A2

Chair(s): Flavia Ravelli and Javier Saiz

235-295 In Silico Investigation of Short QT Syndrome-Linked Potassium Channel Mutations on Electro-Mechanical Function of Human Atrial Cells

Dominic G Whittaker*, Michael A Colman, Haibo Ni, Jules C Hancox, Henggui Zhang

236-193 Uncertainty and Sensitivity Analysis of the Courtemanche-Ramirez-Nattel Human Atrial Cell mMdel using Gaussian Process Emulators

Eugene TY Chang*, Richard H Clayton

237-188 Sensitivity Analysis of Ectopic Electrical Activity in Pulmonary Vein Myocardium

Hitomi Sano*, Yuichiro Tanaka, Yasuhiro Naito, Masaru Tomita

238-259 Are Multi-electrode Arrays Able to Differentiate Anatomical from Functional Reentries in an Excitable Sheet?

Laura Martínez*, José Jalife, Omer Berenfeld, Javier Saiz

Wednesday, September 9, 2015, 10:30

SA3: Automaticity and Markov Chains

Room: A5

Chair(s): Henggui Zhang and Stefano Severi

- 239-135 **Simulation of the Pacemaker Created from the Cardiomyocytes by Reducing Inward-Rectifier K⁺ Current**
Yue Zhang, Kuanquan Wang*, Henggui Zhang, Qince Li, Yongfeng Yuan
- 240-55 **The Role of Purkinje Automaticity as an Arrhythmia Mechanism in Hyperkalaemia**
Violeta Monasterio*, Jesús Carro, Esther Pueyo, José Félix Rodríguez
- 241-362 **A Novel Computational Model of the Human Sinoatrial Action Potential**
Alan Fabbri*, Matteo Fantini, Ronald Wilders, Stefano Severi
- 242-123 **Development of a Novel Markov Chain Model for Oxidative-dependent CaMKII δ Activation**
Shanzhuo Zhang, Qince Li, Kuanquan Wang*, Henggui Zhang
- 243-267 **Evaluating Exponential Integrators for Markov Chain Ion Channel Models**
Tomas Stary*, Vadim Biktashev
- 244-94 **Applying Novel Identification Protocols to Markov Models of INa**
Michael Clerx*, Pieter Collins, Paul GA Volders

Wednesday, September 9, 2015, 10:30

SA4: Atrial Fibrillation Detection

Room: A4

Chair(s): Roger Mark and Leif Sornmo

245-400 The Accuracy of Beat-Interval Based Algorithms for Detecting Atrial Fibrillation

Alan Kennedy*, Dewar Finlay, Daniel Guldenring, Raymond Bond, James McLaughlin

246-85 Analyzing the Atrial Depolarization Wavefront Triggered from Sinus Node and Coronary Sinus for Identification of the Arrhythmogenic Substrate

Bhawna Verma*, Tobias Oesterlein, Armin Luik, Claus Schmitt, Olaf Dössel

247-18 Atrial Fibrillation Detection Evaluation - Performance Measures

Sándor Hargittai*

248-323 Improved Detection of Activation Timings in Endoatrial Electrograms Through a Modified Sinusoidal Recomposition Method

Maddalena Valinoti*, Graziano Vito Lozupone, Paolo Sabbatani, Roberto Mantovan, Stefano Severi, Cristiana Corsi

249-125 Causality in Atrial Fibrillation Determined by Transfer Entropy

Katarzyna Kośna*, Daniel Steven, Stephan Willems, Jan J Żebrowski, Paweł Kuklik

250-116 Extracting Atrial Activations from Intracardiac Signals during Atrial Fibrillation using Adaptive Mathematical Morphology

Sasan Yazdani*, Andrea Buttu, Etienne Pruvot, Jean-Marc Vesin, Patrizio Pascale

Wednesday, September 9, 2015, 12:30

PB1: Health Informatics: Algorithms

Room: Po1

- 251-230 **Novel Filter Technique to Improve R-Peak Detection for ECG Data with Motion Artefacts from Wearable Systems**
Nadine Lang*, Erik Haßlmeyer, Daniel Tantinger, Matthias Brischwein, Axel Heinrich, Heike Leutheuser, Stefan Gradl, Christian Weigand, Bjoern Eskofier, Matthias Struck
- 252-34 **Assessment of the Potential of Morphological ECG Features for Person Identification**
Irena Jekova*, Ivaylo Christov, Vessela Krasteva, Giovanni Bortolan, Mikhail Matveev
- 253-90 **Adaptive Frequency Tracking for Robust Heart Rate Estimation using Wrist-Type Photoplethysmographic Signals during Physical Exercise**
Sibylle Fallet*, Jean-Marc Vesin
- 254-167 **Studying Heart Rate Variability from Ballistocardiography Acquired by Force Platform: Comparison with Conventional ECG**
Alba Martín-Yebra*, Federica Landreani, Claudia Casellato, Esteban Pavan, Carlo Frigo, Pierre-François Migeotte, Enrico G Caiani
- 255-270 **Cardiac Arrhythmia Recognition with Robust Discrete Wavelet-Based Feature Extraction via Classifier Synthesis of MLP-BP and PNN Neural Networks**
Farhad Asadi*, Mohammad Javad Mollakazemi, Seyyed Abbas Atyabi, Ali Ghaffari, Dena Mafi
- 256-268 **Fusion Visualization for Cardiac Anatomical and Ischemic Models with Depth Weighted Optic Radiation Function**
Fei Yang, Weigang Lu*, Lei Zhang, Wangmeng Zuo, Kuanquan Wang, Henggui Zhang

Wednesday, September 9, 2015, 12:30

PB2: ECG Imaging

Room: Po2

- 257-200 **Accuracy of Lead Removal Versus Linear Interpolation in Noninvasive Electrocardiographic Imaging (ECGI)**
Laura Bear*, Mark Potse, Josselin Duchateau, Nejib Zemzemi, Rémi Dubois
- 258-265 **Exercise Induced Depolarization Changes in BSPMs for Assessment of Ischemic Heart Disease**
Michał Kania*, Roman Maniewski, Rajmund Zaczek, Małgorzata Kobylecka, Grzegorz Opolski, Leszek Królicki
- 259-315 **Virtual Normal Bipolar and Laplacian Electrodes for Activation Map Construction in ECGi**
Josselin Duchateau*, Yves Coudière, Mélèze Hocini, Michel Haïssaguerre, Rémi Dubois
- 260-160 **Generation of Combined-Modality Tetrahedral Meshes**
Karli Gillette*, Jess Tate, Peter Van Dam, Eugene Kholmovski, Rob MacLeod
- 261-356 **Evaluation of 2-norm versus Sparsity Regularization in Spline-Based Joint Reconstruction of Epicardial and Endocardial Potentials from Body-Surface Measurements**
Jaume Coll-Font*, Jingjia Xu, Petr Stovicek, Dana H Brooks, Linwei Wang

Wednesday, September 9, 2015, 12:30

PB3: Cardiovascular Models

Room: Po1

- 262-366 **Method for Adult Cardiomyocytes Long-Term Viability Monitoring using Confocal Microscopy Techniques**
Vratislav Cmiel*, Jan Odstrcilik, Ondrej Svoboda, Larisa Baiazitova, Ivo Provaznik
- 263-205 **Load-Dependency in Mechanical Properties of Sub-Epicardial and Sub-Endocardial Cardiomyocytes**
Anastasia Khokhlova*, Gentaro Iribe, Olga Solovyova
- 264-233 **Effects of Cardiac Structural Remodelling During Heart Failure on Cardiac Excitation – Insights from a Heterogeneous 3D Model of the Rabbit Atria**
Petros Kottas, Michael Colman*, Robert Stephenson, Simon Castro, Mark Boyett, Jonathan Jarvis, Henggui Zhang
- 265-166 **Silicon Heart: An Easy to Use Interactive Real-Time Baroreflex Simulator**
Michael Menzel*, Christopher Schölzel, Gernot Ernst, Andreas Dominik

Wednesday, September 9, 2015, 12:30

PB4: Autonomic Nervous System

Room: Po2

- 266-285 **Estimation of the Maximal Heart Rate to Improve Online Tonic-Clonic Seizure Detection using ECG**
Thomas De Cooman*, Anouk Van de Vel, Berten Ceulemans, Lieven Lagae, Wim Van Paesschen, Bart Vanrumste, Sabine Van Huffel
- 267-354 **Entropy in Description of Vasovagal Syndrome Mechanism**
Katarzyna Buszko*, Agnieszka Piątkowska, Edward Koźluk
- 268-182 **Is a Short Re-Feeding Program Effective in Reducing Adverse Cardiac Events in Eating Disorder Patients?**
Herbert F Jelinek*, Mika P Tarvainen, David J Cornforth, Ian Spence, Jan Russell
- 269-203 **Heart Rate Turbulence Modeling using Boosted Regression Trees**
Óscar Barquero-Pérez*, Rebeca Goya-Esteban, Arcadi García-Alberola, José Luis Rojo-Álvarez
- 270-253 **Evaluation of Vital Parameter Response to Load Changes using an Ergometer System in a Group of Healthy Subjects**
Alejandro Mendoza Garcia*, Ulrich Schreiber, Alois Knoll
- 271-33 **Validation of Fetal Autonomic Brain Age Score**
Dirk Hoyer*, Uwe Schneider, Dietrich Grönemeyer, Peter van Leeuwen
- 272-89 **Changes in Instantaneous Complex Dynamics during Exercise in Chronic Mountain Sickness**
Gaetano Valenza*, Francesco Faita, Lorenza Pratali, Nicola Vanello, Antonio Lanata, Riccardo Barbieri, Enzo Pasquale Scilingo

Wednesday, September 9, 2015, 12:30

- 273-144 **A Method to Measure Ventilation Rate during Cardiopulmonary Resuscitation using the Capnogram**
Andoni Elola*, Beatriz Chicote, Elisabete Aramendi, Erik Alonso, Unai Irusta, Mohamud Daya, James K Russell
- 274-305 **Changes in Respiration During Emotional Stress**
Alberto Hernando*, Jesús Lázaro, Adriana Arza, Jorge Mario Garzón, Eduardo Gil, Jordi Aguiló, Raquel Bailón
- 275-10 **Cost-efficient Accurate Monitoring of Respiration Rate using ECG**
Saeed Babaeizadeh*
- 276-169 **New Indices for Sleep Apnea Detection in Long-Time ECG Recordings**
Agata Pietrzak, Gerard Cybulski*
- 277-272 **Accelerations versus Decelerations of the Heart Rhythm Differentiate Vasovagal Sensitive Humans**
Danuta Makowiec*, Wieslaw Miklaszewski, Zbigniew Struzik

Wednesday, September 9, 2015, 12:30

PB5: Heartrate Variability

Room: Po2

- 278-39 **Visualization of Autonomic Drive on the Heart Rhythm by Network Representation of RR Increments**
Danuta Makowiec*, Zbigniew R Struzik
- 279-196 **Endurance Exercise Improves Heart Rate Complexity in the Presence of Vagal Withdrawal in Young Adults**
Steven Perkins, Herbert Jelinek*, Beverlie de Jong, David Cornforth, Mika Tarvainen, Hayder Al-Aubaidy
- 280-322 **Mental Stress Measurement- A Comparison Between HRV based and Respiration Based Technique**
Shreyans Gandhi*, Maryam Shojaei Baghini, Soumyo Mukherji
- 281-351 **Evolution of the Heart Rate Variability Complexity during Kangchenjunga Climbing**
Óscar Barquero-Pérez, Rebeca Goya-Esteban*, Antonio Caamaño, Elena Sarabia-Cachadiña, Carlos Martínez-García, José Luis Rojo-Álvarez
- 282-97 **Lower Instantaneous Entropy of Heartbeat Dynamics during Seizures in Untreated Temporal Lobe Epilepsy**
Riccardo Barbieri*, Gaetano Valenza, Luca Citi, Fabio Placidi, Francesca Izzi, Maria Albanese, Maria Grazia Marciani, Maria Guerrisi, Andrea Romigi, Nicola Toschi
- 283-4 **Early Prediction of Ventricular Tachyarrhythmias based on Heart Rate Variability Analysis**
Hyojeong Lee*, Myeongsook Seo, Segyeong Joo
- 284-275 **The Development of LF/HF Ratio and its Dependence on the Mean Heart Rate in Children and Adolescents**
Eva Zavodna*, Jana Hruskova, Ksenia Budinskaya, Zuzana Novakova, Hana Hrstkova, Ludmila Brazdova, Natasa Honzikova

Wednesday, September 9, 2015, 12:30

285-118 **The Effect of Voltage-Sensitive Dye di-4-ANEPPS on Heart Rate Variability in Langendorff-Perfused Isolated Rabbit Heart**

Oto Janoušek*, Marina Ronzhina, Jakub Hejč, Veronika Olejníčková, Tibor Stračina, Kateřina Fialová, Marie Nováková, Ivo Provazník, Jana Kolářová

286-398 **Changes in Heart Rate Circadian Rhythm following Exercise in Middle-Aged Men**

Herbert F Jelinek*, Chandan Karmakar, Antti M Kiviniemi, Mikko P Tulppo, Timo H Mäkikallio, Arto J Hautala, Heikki V Huikuri, Ahsan H Khandoker, Marimuthu Palaniswami

287-360 **Evaluating Valence level of Pictures Stimuli in Heart Rate Variability Respons**

Shahab Rezaei*, Sadaf Moharreri, Nader Jafarnia Dabanloo

288-158 **Reduced Variability in Pulse Wave Velocity and Heart Rate in Depressed Patients with Suicidal Ideation**

Ahsan Habib Khandoker*, Veena Luthra, Yousef Abou Allaban, Raqibul Mostafa, Nayeefa Chowdhury, Khawza I Ahmed, Simanto Saha, Herbert Jelinek

Wednesday, September 9, 2015, 12:30

PB6: Blood Pressure Measurement and Monitoring

Room: Po1

289-395 **Discovering Prototypical Vital Signs Dynamic Behaviors within a Patient Cohort for Physiological Monitoring**

Li-Wei Lehman*, Roger Mark

290-392 **Patient Prognosis from Vital Sign Time Series: Combining Convolutional Neural Networks with a Dynamical Systems Approach**

Li-Wei Lehman*, Mohammad Ghassemi, Jasper Snoek, Shamim Nemati

291-53 **Comparison of Repeatability of Blood Pressure Measurements between Oscillometric and Auscultatory Methods**

Chengyu Liu*, Dingchang Zheng, Clive Griffiths, Alan Murray

292-378 **Aging Changes in the Regularity of Hemodynamic Parameters during Six-Minute Walk Test**

Marcos Hortelano, Richard Reilly, Raquel Cervigón*

293-325 **A Novel Method for Arterial Blood Pressure Pulse Detection Based on a New Coupling Strategy and Discrete Wavelet Transform**

Farhad Asadi*, Mohammad Javad Mollakazemi, Seyyed Ali Akbar Moosavian, Dena Mafi

Wednesday, September 9, 2015, 12:30

PB7: Membrane and Cellular Modelling

Room: Po1

- 294-37 **Investigation of the Pro-arrhythmic Effects of Domperidone by a Simulation Study**
Jing Zhou, Yongfeng Yuan, Qince Li, Kuanquan Wang*, Zhili Li, Henggui Zhang
- 295-227 **Model-based Analysis of the Effects of Thioridazine Enantiomers on the Rabbit Papillary Action Potential**
Ask Schou Jensen*, Cristian Pablo Pennisi, Cristian Sevcencu, Jørn Bolstad Christensen, Jette Elisabeth Kristiansen, Johannes Jan Struijk
- 296-65 **Effects of Amiodarone on Ventricular Excitation Associated with the KCNJ2-Linked Short QT Syndrome: Insights from a Modelling Study**
Cunjin Luo*, Kuanquan Wang, Ming Yuan, Zhili Li, Qingjie Wang, Yongfeng Yuan, Henggui Zhang
- 297-46 **Modeling and Simulation of Developmental Changes in Contractile Apparatus of Ventricular Cells**
Mao Takiguchi*, Tamami Toki, Hitomi Sano, Yasuhiro Naito, Masaru Tomita
- 298-147 **Investigation of The Mechanisms Underlying Cardiac Alternans – insights from a Computational Study**
Wei Wang*, Haibo Ni, Henggui Zhang
- 299-212 **Simulation of Effects of Inward-Rectifier K⁺ Current on the Automaticity of Human Ventricular Tissue**
Yue Zhang, Kuanquan Wang*, Henggui Zhang, Qince Li, Yongfeng Yuan
- 300-76 **Calcium Leak Induced Sinus Bradycardia**
Qingjie Wang*, Sanjay Kharche, Gareth Jones, Cunjin Luo, Chengchun Tang, Henggui Zhang

Wednesday, September 9, 2015, 12:30

PB8: ECG Processing II

Room: Po1

- 301-248 **Estimation of the Extent of Tissue Damage by Multi-resolution Analysis of the Electrocardiogram and Arterial Blood Pressure**
Seyyed Abbas Atyabi*, Mohammad Javad Mollakazemi, Farhad Asadi, Hamid Ebrahimi Orimi, Ali Ghaffari, Dena Mafie
- 302-409 **Time-Course of T-wave Flattening and P-R Prolongation under β -Adrenergic Challenge are Associated with Short-Term Biphasic Poincaré Shift in Mice**
Conrado J Calvo*, David Filgueiras, Francisco J Chorro, José Millet
- 303-313 **A Comparison Study Between Fainter and Non-fainter Subjects During Head-Up Tilt Test using Reconstructed Phase Space**
Nadine Khodor*, Guy Carrault, David Matelot, Nathalie Ville, François Carre, Alfredo Hernandez
- 304-329 **The Effect of Heart Orientation on High Frequency QRS Components in Multiple Bandwidths**
Jakub Hejč*, Marina Ronzhina, Oto Janoušek, Veronika Olejníčková, Marie Nováková, Jana Kolářová
- 305-210 **Ischemic ST Deviation Episodes Recognition via ECG using Extreme Learning Machine and Kernel Density Estimation**
Dena Mafie*, Seyyed Abbas Atyabi, Ali Ghaffari
- 306-343 **Characterisation of Cells Migration Through Cardiac Tissue using Advanced Microscopy Techniques and Matlab Simulation**
Larisa Baiazitova*, Josef Skopalík, Vratislav Čmiel, Ondřej Svoboda, Ivo Provazník, Zdenka Fohlerová, Jaromír Hubálek

Wednesday, September 9, 2015, 12:30

307-3 **Changes in the Electrocardiogram Induced by Coronary Artery Bypass Grafting**

Dimiter Simov, Ivaylo Christov*, Giovanni Bortolan, Mikhail Matveev, Ivo Petrov, Vessela Krasteva

308-9 **Hemodialysis-Induced ST-Segment Deviation**

Iana Simova, Ivaylo Christov*, Giovanni Bortolan, Roger Abächerli, Liliana Kambova, Irena Jekova

309-126 **Classification of Ventricular Premature and Ischemic Beats in Animal Electrograms**

Marina Ronzhina*, Lucie Maršánová, Radovan Smíšek, Veronika Olejníčková, Oto Janoušek, Petr Veselý, Jana Kolářová, Marie Nováková, Ivo Provazník

310-368 **The Frequency Changes in Electrograms During Ischemia Experiments – Analysis by Matching Pursuit Decomposition**

Jana Kolářová*, Petr Doležal, Marie Nováková, Ivo Provazník

311-292 **Magnetocardiography did not Uncover Electrically Silent Ischemia in an In-Silico Study Case**

Danila Potyagaylo*, Gunnar Seemann, Walther Schulze, Olaf Dössel

312-35 **Detection of Electrode Interchange in Right Precordial and Posterior ECG Leads**

Irena Jekova*, Vessela Krasteva, Remo Leber, Ramun Schmid, Roger Abächerli

313-197 **Distribution Entropy for short-term QT Interval Variability Analysis: A Comparison between the Heart Failure and Normal Control Groups**

Yang Li, Peng Li, Chandan Karmakar*, Changchun Liu

Wednesday, September 9, 2015, 12:30

314-397 A Novel Technique for Analysing Beat-to-Beat Dynamical Changes of QT-RR Distribution for Arrhythmia Prediction

Mohammad Hasan Imam, Chandan Karmakar*, Ahsan Khandoker, Marimuthu Palaniswami

315-385 The Effects of Electrode Placement on an Automated Algorithm for Detecting ST Segment Changes on the 12-Lead ECG

Dewar Finlay*, Raymond Bond, Alan Kennedy, Daniel Guldenring, James McLaughlin

Wednesday, September 9, 2015, 12:30

PB9: Challenge Posters

Room: Po2

- 316-106 **Reduction of False Cardiac Arrhythmia Alarms Through the Use of Machine Learning Techniques**
Miguel Caballero, Grace Mirsky*
- 317-171 **Signal Quality-Based Approach to False Arrhythmia Alarms Reduction**
Adam Mahdi*, Dragana Nikolic
- 318-115 **Reducing False Arrhythmia Alarms in the ICU**
Nadi Sadr*, Doan Trang Nguyen, Chandan Kalra, Alistair McEwan, Philip de Chazal
- 319-238 **False Alarm Reduction in ICU by Fusion of Neuro-SVM Classifiers and Heartbeat Detection from Multimodal Data: Geometrical and Multi-resolution Analysis**
Mohammad Javad Mollakazemi*, Seyyed Abbas Atyabi, Farhad Asadi, Ali Ghaffari, Dena Mafi
- 320-66 **Reducing False Arrhythmia Alarms in the ICU**
Soo-Kng Teo, Jian Cheng Wong, Bo Yang, Feng Yang, Tian You Zhang, Ling Feng, Toon Wei Lim, Yi Su*
- 321-387 **Multi-modal Integrated Approach towards Reducing False Arrhythmia Alarms During Continuous Patient Monitoring; PhysioNet/Computing in Cardiology Challenge 2015**
Sardar Ansari*, Ashwin Belle, Kayvan Najarian
- 322-60 **Reliability of Clinical Alarm Detection in Intensive Care Units**
Charalampos Tsimenidis, Alan Murray*

Wednesday, September 9, 2015, 12:30

- 323-52 **Reducing False Arrhythmia Alarms in the ICU using Novel Signal Quality Indices Assessment Method**
Runnan He*, Henggui Zhang, Kuanquan Wang, Yongfeng Yuan, Qince Li, Jiabin Pan, Zhiqiang Sheng, Na Zhao
- 324-136 **Reducing False Arrhythmia Alarms by Means of Beat Clustering**
Tilo Himmelsbach*
- 325-219 **Identification of ECG Signal Pattern Changes to Reduce the Incidence of Ventricular Tachycardia False Alarms**
Vytautas Abromavičius*, Artūras Serackis, Andrius Gudiškis
- 326-390 **Reducing False Arrhythmia Alarm by Quality Assessment of Multimodal Physiological Signals using Cepstrum Analysis**
Yongwei Zhu*
- 327-93 **Case-Based Reasoning and Multimodal Data Classification using Exponential Similarity and Signal Quality Indices**
Haiyan Yu*, Jiang Shen, Man Xu
- 328-119 **Algorithm for Life-Threatening Arrhythmias Detection with Reduced False Alarms Ratio**
Iga Grzegorzczuk*, Kamil Ciuchciński, Jan Gierałtowski, Katarzyna Kośna, Piotr Podziemski, Mateusz Soliński

Wednesday, September 9, 2015, 14:45

MD: Plenary

Room: A1

Chair(s): Olivier Meste and Andrew Blaber

- 329-70 **T-Wave Alternans Hysteresis on Heart Rate**
Laura Burattini*, Sumche Man, Sandro Fioretti, Francesco Di Nardo, Cees A Swenne
- 330-338 **Three-Dimensional Echocardiography Based Evaluation of Right Ventricular Remodeling in Patients with Pressure Overload**
Francesco Maffessanti*, Karima Addetia, Megan Yamat, Lynn Weinert, Roberto Lang, Victor Mor-Avi
- 331-6 **A Study of Early Afterdepolarizations in Human Ventricular Tissue**
Nele Vandersickel, Alexander V Panfilov*
- 332-237 **Computer Simulations of Three-dimensional Coronary Blood Flow After CABG and Simulated PCI Procedures**
Jun-Mei Zhang*, Tong Luo, Jia Lin Soon, Ning Kang, Kenny Yoong Kong Sin, Swee Yaw Tan, Teing Ee Tan, Chong Hee Lim, Mathew Jose Chakaramakkil, Adrian Seng Wae Ooi, Aileen Mae Lomarda, Ru San Tan, Liang Zhong

Abstracts

Rate-Adapted Dynamic-Clamp of the Funny Current in Sinoatrial Pacemaker Cells

Chiara Bartolucci*, Enrico Ravagli, Annalisa Bucchi, Mirko Baruscotti, Dario DiFrancesco, Stefano Severi

University of Bologna
Cesena, Italy

A typical feature of sinoatrial node (SAN) pacemaker cells is the presence of the ‘funny current’, I_f , that activates upon hyperpolarization. The aims of this work were to: 1) test the impact of I_f different mathematical models in real cells by using the Dynamic Clamp (DC) technique; 2) implement a DC protocol to adequately simulate a shift of the I_f activation curve in real SAN cells. Experiments were performed using the real-time biological experimentation system RTX1. The I_f time course was dynamically reconstructed from the experimentally recorded action potentials of a single isolated rabbit SAN cell according to the mathematical models, Maltsev-Lakatta (ML) and Severi-DiFrancesco (SDiF). Two different protocols were implemented: i) selective I_f block by Ivabradine and substitution with the “synthetic” I_f ; ii) virtual negative shift of the I_f activation curve by the injection of a compensatory outward current using DC. The pacemaking rate was significantly reduced by Ivabradine (2.77 ± 0.13 to 2.20 ± 0.06 Hz, $p < 0.05$). The SDiF model allowed the restoration of control rate (2.70 ± 0.09 , N.S. vs Control) while the injection of ML synthetic current doesn’t show significant alterations (2.39 ± 0.10 , N.S. vs ivabradine). Early results on the virtual shift forced us to adapt the DC; it was necessary to tune the current amplitude based on the cell spontaneous firing rate to avoid injection of extremely high or low delta current. The Ivabradine protocol was then repeated with this adjustment and the results were fully consistent with those previously obtained (Ctrl: 2.89 ± 0.16 vs SDiF injection: 2.79 ± 0.15 Hz, N.S). Results suggest that SDiF formulation is closer to the current contribution in real myocytes, whereas the ML one is quantitatively insufficient. The “cell-specific” adaptation of the DC protocol succeeded in reproducing the effects of a negative activation-shift and will allow the use of DC to investigate the effects of autonomic modulation of I_f .

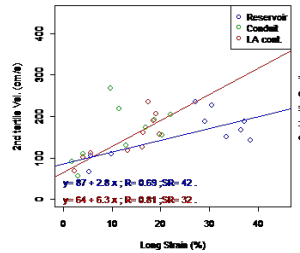
Left atrium MRI 4D-flow in atrial fibrillation: association with LA function

Morgane Evin*, Fraser M. Callaghan, Carine Defrance, Stuart M. Grieve, Alain De Cesare, Philippe Cluzel, Alban Redhueil, Nadjia Kachenoura

Sorbonne Universites, UPMC Univ Paris 06, INSERM UMRS 1146, CNRSUMR 7371, Laboratoire d'Imagerie Biomedicale, Paris, France
 University of Sydney, Heart Research Institute, Sydney, Australia

Left atrium (LA) is the principal site of thrombus formation and LA low flow velocities have been reported to be highly associated with thromboembolic events. Recent developments in MRI 4D flow velocities enable a non-invasive visualization of LA flow patterns.

Our main objective was to identify modification of LA flow organization using velocity and vorticity indices in regards to LA function modifications in 4 patients (55.8±9.9y.) with atrial fibrillation (AF) and 6 healthy volunteers (24.7±2.4y.). Vorticity threshold and Q-criterion ($Q = \frac{1}{2}(\|S^2\| + \|\Omega^2\|) > 0$) were computed from the centered vorticity calculation on filtered velocity images from the Jacobian matrix J ($S = \frac{1}{2}(J + J^T)$ and $\Omega = \frac{1}{2}(J - J^T)$). Phasic LA longitudinal strains were computed from cine MRI images using LA feature tracking algorithm.



Flow-function correlation in LA.

Phasic mean vorticity (s^{-1}); R: reservoir, C: conduit, A: LA contraction phases

	Healthy sub.	AF Patients
R Vor.	25 038± 8 240	21 919± 10 224
C Vor.	7 131± 1 850	6 699± 2 895
A Vor.	17 793± 3 699	12 927± 7 001
R Q-crit.	4 342e6± 3 480e6	4 016e6± 3 584e6
C Q-crit.	188.9e6± 123.6e6	303.7e6± 383.8e6
A Q-crit.	23.7e6± 18.8e6	77.4e6± 99.9e6

Along with the expected LA dilation in AF patients, a substantial reduction in LA strain values was found. Best correlations between LA flow and function were found for associations between velocity index and reservoir and LA

contraction longitudinal strains ($r=0.69$ and $r=0.81$, $p<0.03$). Besides a good correlation was found between LA contraction longitudinal strains and Q-criterion index during LA contraction phase ($r=0.52$).

Vorticity criteria provided additional information regarding LA flow modifications in AF and its interplay with LA functional alterations revealed the potential role of LA contraction in the development of vortices and stasis.

Extraction of Morphological QRS-based Biomarkers in Hypertrophic Cardiomyopathy for Risk Stratification using L1 Regularized Logistic Regression

Aurore Lyon*, Ana Mincholé, Rina Ariga, Pablo Laguna, Stefan Neubauer, Hugh Watkins, Nando de Freitas, Blanca Rodríguez

University of Oxford
Oxford, United Kingdom

Hypertrophic cardiomyopathy (HCM) is a genetic disease characterized by the thickening of the heart ventricles. It affects 1 in 500 people in the UK but no reliable biomarkers have been presented so far and standard biomarkers have low sensitivity to current risk factors. Our goal is to identify new ECG-based biomarkers that detect electrophysiological abnormalities and classify HCM patients compared to healthy volunteers. HCM patients suffer from structural myocardial abnormalities such as wall thickening and fibre disarray that affect the conduction properties of the heart, and, in turn, the QRS complex. Therefore, our work will focus on extracting morphological features of the QRS complex to highlight any abnormality related to the activation sequence in HCM. 50 12-lead Holter recordings were analysed (29 HCM patients and 21 control patients) and morphological biomarkers such as QRS amplitude, QRS width or slopes, were extracted. Additionally, biomarkers based on the Hermite transform of the QRS complex such as the first four coefficients and the root mean square error of the QRS fitting were also computed in order to exploit the ability of this transform to describe the morphology of the QRS complex. Feature selection and classification were then performed using the L1 regularized logistic regression. The classification reached 95.7% of accuracy, 94.96% of sensitivity and 96.90% of specificity for HCM by making use of only two biomarkers with the highest discriminative power: the percentage of negative regions with respect to the isoelectric level and the 3rd coefficient of the Hermite transform in V3. Additionally, these two features showed p -values $< 1e-6$ in most of the leads, especially V3 and V4. These findings are in agreement with the common existence of structural remodelling in the septum and left ventricle in HCM patients, and they highlight the importance of abnormalities in the QRS morphology in HCM patients.

Three-dimensional Segmentation and Quantification of the Anatomic Regurgitant Orifice in Mitral Regurgitation Using 3D Ultrasound Images

Miguel Sotaquira^{*1,3}, Mauro Pepi², Gloria Tamborini², Enrico Caiani³

¹Universidad de San Buenaventura, Bogota, Colombia

²Centro Cardiologico Monzino IRCCS, Milan, Italy

³Politecnico di Milano, Dipartimento di Elettronica, Informazione e Bioingegneria, Milan, Italy

Aims. Current guidelines for the assessment of mitral regurgitation (MR) recommend the use of 2D color-Doppler imaging. However, as the anatomic regurgitant orifice (ARO) has a 3D not circular shape, it cannot be accurately represented by 2D parameters (vena contracta, effective regurgitant orifice area). Our aims were: 1) to develop a novel semi-automated procedure for 3D ARO surface detection and quantification from 3D transesophageal echocardiographic (TEE) grayscale datasets; 2) to validate 2D ARO parameters vs manual planimetry; 3) to characterize the ARO morphology both in patients with prolapse (MVP) and functional MR (FMR).

Methods. 25 patients with mild to severe MR (12 FMR, 13 MVP) were studied. Following semi-automated active contour segmentation of blood in a TEE image portion surrounding the regurgitant valve, the 3D contour of its narrowest section, corresponding to the ARO surface, was found by max-flow/min-cut algorithm driven by shape diameter function and average geodesic distance. From it, several parameters were defined: 3D and 2D areas, planarity index, and circularity index (CI).

Results. ARO 2D area and CI in the combined groups correlated well with planimetry ($r^2=0.77$ and 0.90 , respectively). However, ARO 2D projected area was underestimating 3D area in both groups (by 43% in MVP and by 8% in FMR). In 19/25 pts, ARO planarity was <0.9 (range $0.5-0.94$ a.u.), confirming its 3D morphology, with more planar ARO in FMR than in MVP. Both groups showed elongated AROs: only 1/25 pts exhibited an almost circular ARO (CI 0.92), while 24/25 pts had more elongated AROs (CI <0.8).

Conclusions. We proposed and preliminary validated a novel method for 3D ARO quantification from 3D TEE images in patients with MR. This approach appears able to overcome the strong assumptions about ARO planarity and circularity that currently affect the 2D color-Doppler assessment of MR severity.

Need for Re-validation of Automated Blood Pressure Devices for Use in Unstable Conditions

Dingchang Zheng, Chengyu Liu*, John Amooore, Stephan Mieke, Alan Murray

Newcastle University
United Kingdom

S21

Non-invasive blood pressure (NIBP) devices are widely used by the general public. Device validation required by the international standards is performed under resting condition. However, NIBPs are often used without giving much consideration about the measurement conditions. This study aimed to provide scientific data on the use of BP devices in unstable conditions. BP measurements were performed on 20 healthy subjects under both resting and regular deep breathing conditions. During the measurement the oscillometric cuff pressure waveforms were recorded digitally at a recommended deflation rate of 2-3 mmHg/s. They were then regenerated by a specially designed BP simulator and presented to two clinically validated hospital grade automatic NIBP devices to obtain automated BPs. Automated SBP and DBP from both resting and regular deep breathing conditions were finally compared between the two devices. Under resting condition, there was no significant difference in both automated SBP and DBP between the two devices (mean±SD: 119.1±10.1 vs 118.9±10.6 mmHg for SBP; 72.2±8.5 vs 71.2±8.8 mmHg for DBP). However, under regular deep breathing condition, significant SBP and DBP differences were observed between the two devices (both $P < 0.01$; mean±SD: 118.8±10.6 vs 115.1±11.6 mmHg for SBP; 68.5±8.6 vs 65.3±8.9 mmHg for DBP). For the effect of deep breathing with each device, a significant SBP decrease was observed with only device 2 ($P < 0.01$, with a mean ±SD of 3.8±6.2 mmHg), indicating inconsistent measurements between the two devices under unstable conditions. Our results provide scientific evidence that automated BP devices can be used only under the condition for which the validation was performed, and also confirm that a separate validation should be performed for the devices to be used under different conditions.

Beat-to-Beat Response Patterns of Spectral Sympathetic Estimators to the Cold Face Test and their Comparison to Those of the Orthostatic Stress Test

S21

Salvador Carrasco-Sosa, Alejandra Guillén-Mandujano*, Aldo R Mejía-Rodríguez

Universidad Autónoma Metropolitana-I
Mexico City, Mexico

We recently proposed that the low-frequency power of the maximal amplitude of the arterial pressure first derivative (LFdmAP) is a suitable sympathetic marker. To further support its estimation capability and to establish the instantaneous time course of sympathetic activity spectral indexes during the cold face test (CFT), which has not been reported, we: a) assessed the effects of CFT and active orthostatic stress (OST) on the instantaneous dynamics of LFdmAP and of low-frequency power of systolic pressure (LFSP), and b) compared their performance as sympathetic markers as well as the magnitude of the sympathetic response evoked by each maneuver. Twenty-five healthy volunteers underwent 1-min control, 1-min maneuver (CFT, OST) and 2-min recovery stages. From ECG, arterial pressure (AP), first derivative of AP and tidal volume (TV) recorded during the maneuvers, RR intervals (RR), systolic pressure (SP), maximal amplitude of the first derivative of AP and TV time series were computed. Time-frequency spectra of the series were estimated using the smoothed pseudo-Wigner-Ville distribution to obtain the instantaneous dynamics of LFSP, LFdmAP and high-frequency power of RR (HFRR). LFdmAP, LFSP and mean SP displayed distinct instantaneous response patterns to each maneuver: while during CFT they increased to a plateau, during OST they presented overshoots at the beginning of both maneuver and recovery stages. Mean values of LFdmAP in the maneuver stage of CFT (2166 ± 2005 mmHg 2 /s 2) were smaller ($p < 0.001$) than those during OST (8344 ± 3926 mmHg 2 /s 2). LFdmAP-LFSP and LFdmAP-mean RR correlations were 0.83 ± 0.17 and -0.68 ± 0.17 respectively. Supported by their similar instantaneous response patterns, their ability to adequately indicate the sympathetic increases evoked by CFT and OST, and their very strong correlation, LFSP and LFdmAP powers exhibit similar performance as sympathetic measures. Moreover, our results show that the sympathetic activation evoked by CFT is 6 times smaller than the one produced by OST.

Seismocardiograms Segmented Without ECG Return Valid Heart Rate Variability Indices

Alexandre Laurin*, Kouhyar Tavakolian, Farzad Khosrow-Khavar, Andrew Blaber

Simon Fraser University
Vancouver, Canada

S21

Seismocardiography (SCG) is the measurement of sternum acceleration caused by the beating heart. SCG provides mechanical information that would otherwise be unavailable, such as systolic time intervals. Previous SCG segmentation algorithms have relied on concurrent ECG measurements. The purpose of this research was to design an algorithm capable of self-segmenting SCG and eliminate the need for the collection of other signals. Eighteen participants were exposed to graded LBNP levels 0, -10, -20, -30, -40, and -50 mm Hg at 5 minutes per level. RR intervals were obtained from ECG with the Pan Tompkins algorithm. The SCG signal was manually annotated using R waves to identify isovolumic moments (IM). In parallel, we developed an algorithm to identify IM without ECG as a reference. IM locations obtained by the algorithm were compared to those obtained by manual annotation for levels 0 (baseline) and -40 mmHg. For all participants, at baseline, the algorithm was 98% accurate, with 12 participants having 100% accuracy. At -40 mmHg, accuracy was reduced to 59%, with 7 participants having 100% accuracy. From the baseline and -40 mmHg time series the normalized high frequency power of beat intervals was computed using the R waves as well as the IM points obtained with and without ECG as a reference. Sets of IM-obtained indices were compared to those obtained from R waves. For manual-annotated IM points mean difference at baseline was $-0.2\% \pm 1\%$ (standard error); whereas at -40 mmHg the mean difference was $-1.4\% \pm 1\%$. For the algorithm annotated IM points, mean difference at baseline was $1.2\% \pm 0.9\%$, and at -40 mmHg the mean difference was $4.7\% \pm 2.5\%$. In conclusion, self-segmentation of SCG was accurate under at-rest conditions. Since the misidentification of IM in certain subjects was systematic, the HRV indices obtained under any condition were accurate.

Heart Rate Estimation from Dual Pressure Sensors of a Dialysis Machine

Mattias Holmer*, Frida Sandberg, Kristian Solem, Bo Olde, Leif Sörnmo

Lund University
Lund, Sweden

Introduction: Dialysis patients often suffer from cardiovascular diseases, motivating the use of continuous monitoring of cardiac activity in clinical routine. Cardiac pressure pulses propagate through the vascular system and enter the extracorporeal blood circuit, where the pulses are captured by pressure sensors. The cardiac pulses are obscured by the much stronger pressure pulses, which originate from the peristaltic blood pump. We have previously shown that a cardiac signal can be extracted from the venous pressure signal during periods of constant blood flow. However, that method has been found to perform less well at very low cardiac amplitudes. In the present study, we propose a novel method which addresses this issue, and compare its performance to that of the previous method.

Methods: Both methods are based on an iterative procedure, which estimates the cardiac signal by subtracting an iteratively refined blood pump signal from the pressure signal. However, in contrast to the previous method the new method utilizes both the arterial and the venous pressure when modeling the pump signal and estimating the cardiac signal. Heart rate was estimated from the extracted cardiac signal and compared to the heart rate estimated from a reference pulse oximeter.

Results: The results show that at very low cardiac signal amplitudes of 0.1 mmHg, the heart rate can be estimated with median absolute error of 5.9 bpm when both arterial and venous pressure are used, whereas the corresponding error was 42.0 bpm when only venous pressure was used.

Conclusions: Heart rate can be estimated from pressure signals with lower cardiac signal amplitude when both arterial and venous pressure is used.

Performance of the Low-Frequency Power of Pulse Pressure Variability as a Sympathetic Activity Measure During Supine, Controlled Breathing, Standing and Exercise

S21

Salvador Carrasco-Sosa, Alejandra Guillén-Mandujano*

División de Ciencias Biológicas y de la Salud, Universidad Autónoma Metropolitana-I
Mexico City, Mexico

It is still unclear if maneuvers that modify autonomic and respiratory activities affect the spectral powers of diastolic pressure variability (DPV) similarly to those of the systolic pressure variability (SPV). Considering that pulse pressure variability (PPV) is obtained from the differences between SPV and DPV, we examined: a) the effects of four maneuvers that elicit different sympathetic activity levels on the spectral powers of PPV, SPV and DPV, and b) the relations between them and with the spectral measures of heart rate variability. RR intervals, SPV, DPV, PPV and respiration (Resp) time series were computed from ECG, arterial pressure and respiratory movements recorded from 28 healthy subjects during 5-min supposedly steady-state conditions: supine rest (SR), controlled breathing (CB), standing (S) and exercise (E). Time-frequency spectra of the series were estimated with the smoothed pseudo-Wigner-Ville distribution to compute the instantaneous dynamics of their low-frequency (LFRR, LFSP, LFDP and LFPP) and high-frequency powers (HFRR, HFSP, HFDP, HFPP and HFResp). With respect to SR condition, except for LFDP in CB, LFPP, LFDP and LFSP increased progressively in CB ($p < 0.001$), S ($p < 0.001$) and E ($p < 0.001$), being the increments of LFSP larger than those of LFDP ($p < 0.001$). LFPP presented strong correlations with HFRR (-0.76 ± 0.09), mean RR (-0.77 ± 0.09), LFSP (0.95 ± 0.07) and LFDP (0.89 ± 0.11). LFDP-LFSP and HFDP-HFSP correlations were 0.97 ± 0.02 and 0.56 ± 0.17 respectively. Mean HFSP (21 ± 4 mmHg²) and HFDP (4 ± 1 mmHg²) in S showed the greatest difference. The progressive sympathetic increase evoked by the maneuvers, estimated by HFRR and mean RR, are adequately marked by LFPP, which rises proportionally, mainly due to the LFSP increase. LFDP cannot discriminate the subtle sympathetic increase in CB, and HFDP is six times smaller than HFSP in S condition. Thus, the maneuvers provoke distinct effects on the spectral powers of SPV and DPV, being those associated to respiration the most prominent.

Pulse Transit Time Extraction from Seismocardiogram and its Relationship with Pulse Pressure

Ajay Verma, Reza Fazel-Rezai, Kouhyar Tavakolian*

University of North dakota
United States

Background Pulse Transit Time (PTT) is defined as the time it takes a pulse wave to travel between two arterial sites. It is determined as a difference between the timing of the pulse between the distal and proximal sides of the artery. In a lot of works, ECG's R peak has been used as the start of PTT and the rise point in PPG signal is used as the end of it. Using R peak for timing the distal waveform causes an error in blood pressure estimation as it includes isovolumic contraction period in it. Method In this research we explored Seismocardiogram (SCG) as a method for timing the start of PTT. SCG is low frequency chest acceleration recorded using accelerometers. SCG has a point corresponding to the aortic valve opening; we used this point as reference for the starting time of PTT. Thus, PTT was computed as a time difference between aortic-valve opening (AO) point in a Seismocardiogram (SCG) signal and the rise point in a finger Pulse-plethysmogram (PPG) signal. Data from ten subjects were recorded under rest and different stages of lower body negative pressure (LBNP). Systolic and diastolic blood pressure values were also recorded for reference. Pulse blood pressure was computed as a difference between systolic and diastolic blood pressures. PTT was estimated for all the subjects under each stages of LBNP using both SCG and ECG as the proximal pulse. Results It was found that pulse pressure values correlated with the PTTs. The average correlation coefficient for ten subjects was found to be 0.81 ± 0.19 , using ECG as the proximal pulse, we got 0.68 ± 0.31 . Thus, the results achieved by SCG were superior to ECG. Thus, we imagine a simple non-invasive blood pressure estimation system including an accelerometer on the chest and a pulse sensor on the finger for continuous blood pressure monitoring. Such a system will need to be calibrated for very individual subject.

Classification of Atrial Fibrillation Episodes by means of Phase Variations of Rime-frequency Transforms

Nuria Ortigosa¹, Óscar Cano², Antonio Galbis³, Carmen Fernández³

¹ I.U. Matemática Pura y Aplicada, Universitat Politècnica de València, Spain

² Hospital Universitari i Politècnic La Fe, Servicio de Cardiología, IIS-La Fe, Valencia, Spain

³ Univ. Valencia, Dept. Math. Analysis, Burjassot, Spain

S22

Aims: This study aimed to assess an early classification of paroxysmal and persistent atrial fibrillation episodes by means of the surface ECG, which would allow electrophysiologists to prescribe the most suitable treatment to lower recurrence and stop the natural progression of the arrhythmia.

Methods: 129 consecutive unselected patients suffering from an atrial fibrillation episode conformed the study population (23 paroxysmal and 106 persistent). They belong to a heterogeneous cohort of patients (in terms of antiarrhythmic treatment and state of evolution of the arrhythmia) similar to the context that clinicians find at tertiary centres in their daily work. Modulus and phase features extracted from several time-frequency transforms of the ECG were studied, and it was phase variations which arose as determinant providing the best classification results using a Linear Discriminant Analysis classifier trained with 20 signals.

Results: The test dataset consisted of 109 patients (14 paroxysmal and 95 persistent), 91 of which were correctly classified (11 paroxysmal and 80 persistent). Obtained performances were: Accuracy = 83.5% (total correct classifications), Sensitivity = 78.6% (paroxysmal AF episodes correctly classified), Specificity = 84.2% (persistent subjects properly classified).

Conclusion: Using a widely available technique as the surface ECG, atrial fibrillation episodes from a heterogeneous cohort of patients are mostly correctly classified when using phase information from time-frequency transforms. Thus, phase variations arise as discriminant features able to address the problem of paroxysmal and persistent atrial fibrillation differentiation in general scenarios.

Adaptive Wavelets Applied to Automatic Local Activation Wave Detection in Fractionated Atrial Electrograms of Atrial Fibrillation

J Felix^{1,2}, R Alcaraz², JJ Rieta¹

¹Biomedical Synergy, Electronic Engineering Department, Universidad Politécnica de Valencia, Gandia, Spain

²Research Group in Electronic, Biomedical and Telecommunication Engineering, University of Castilla-La Mancha, Cuenca, Spain

Atrial fibrillation (AF) is the most common cardiac arrhythmia, thus leading to a significant development of signal analysis methods in recent years. The wavelet decomposition has proven to be a powerful tool in the analysis of fractionated AF Electrogram (EGM) recordings in invasive studies, where the accurate detection of the Activation Point (AP) in every Local Activation Wave (LAW) is a key first step which becomes critical for later methodologies, like cardiac mapping or ablation guiding. This task is commonly done manually by clinicians in order to avoid false detections that would dramatically alter the results. But trustable automated methods would be desirable in order to provide real-time support for any other computational methodology relying on LAW detection. This work introduces a novel application of wavelet decomposition to precisely locate AP times in fractionated EGMs of AF.

A set of 21 AF endocardial recordings of 10 seconds in length were selected during an AF ablation procedure from different patients. Then, the five most representative LAWs were automatically extracted from each EGM following amplitude and morphological criteria. Next, every LAW was correlated with the whole recording in order to select the one providing the highest average correlation, which was set later as the pattern defining the tailored mother wavelet to be applied on the recording. This wavelet was used to perform a 16 scales continuous wavelet transform of the EGM, thus providing a clear peak wherever an AP was present in the EGM under analysis. Finally, these automatically detected APs were assessed with the manual annotations performed by two expert clinicians on the same EGM.

The developed LAW detector yielded only 3 False Positive (FP) and 8 False Negative (FN) AP detections from a total of 970 in the database. Thus, its sensitivity was $99.18\% \pm 1.35\%$, the positive predictive $99.69\% \pm 0.66\%$ and the Accuracy $98.9\% \pm 1.51\%$. Furthermore, the application of limited cross-correlation operations together with the wavelet transform has provided a very computationally efficient algorithm suitable for robust real-time environments evaluating LAWs in AF EGMs, such as electroanatomical mapping systems.

Study on the Trustability of Phase Mapping Methods to Represent Atrial Potentials in Atrial Fibrillation

J Felix^{1,2}, V Jacquemet³, R Alcaraz², JJ Rieta¹

¹Biomedical Synergy, Electronic Engineering Department, Universidad Politécnica de Valencia, Gandia, Spain

²Research Group in Electronic, Biomedical and Telecommunication Engineering, University of Castilla-La Mancha, Cuenca, Spain

³Department of Molecular and Integrative Physiology, University of Montreal, Montreal, Canada

S22

Phase Mapping (PhM) is a recent alternative to map atrial fibrillation (AF) and guide catheter ablation by applying the Hilbert transform (HT) to electrogram potential maps (PM). These methods apply preprocessing steps with the aim to improve the reentrant activity plot as well as to get clearer and long-standing rotors. However, some studies have demonstrated the impossibility of getting stable rotors when high density maps are recorded in the fibrillating atria. The present work studies how PhMs may distort the initial PM due to preprocessing, interpolation as well as the application of the HT itself.

A biophysical full 3D model with 1.04 million cubic elements at a resolution of 0.33 mm and geometry based on magnetic resonance images of the human atria was used. A 3.5 seconds simulated AF recording was generated with 5.594 electrograms sampled at 1kHz and three different kinds of PhMs were computed. Firstly, a high-density PhM was obtained by direct application of the HT. Secondly, a 64 poles basket catheter was reproduced by selecting the corresponding electrograms that were interpolated up to 512 recording points to compute the interpolated PhM. The third PhM was obtained by the same interpolation and including as preprocessing linear detrending, low-pass filtering at 30 Hz and 2 Hz band-pass filtering centered on the dominant atrial frequency. 135 PhMs of 256×256 pixels from 45 time instants and places of the atrial model were generated and compared with the corresponding PMs through the Earth Mover's Distance algorithm, able to assess the concordance between two images by computing the lowest cost to transform one into another.

An average concordance of $89.26\% \pm 6.24\%$ between the first set of PhMs and the original PMs was obtained, lowering down to $72.26\% \pm 11.24\%$ for the interpolated set of PhMs and being even lower when interpolation and preprocessing were added yielding $34.43\% \pm 7.81\%$. Hence, PhMs as well as their preprocessing and interpolation have to be managed with caution because they may notably transform real PMs, thus creating fibrillatory activity or long-standing rotors that may not be observed in high-density potential maps.

Unifying Automated Fractionated Atrial Electrogram Classification using Electroanatomical Mapping Systems in Persistent Atrial Fibrillation Studies

S22

Tiago P Almeida*, Gavin S Chu, João L Salinet, Frederique J Vanheusden, Xin Li, Jiun H Tuan, Peter J Stafford, G André Ng, Fernando S Schlindwein

University of Leicester
Leicester, UK

Background: Complex fractionated atrial electrograms (CFAE) ablation for treating persistent atrial fibrillation (persAF) has shown conflicting results. Differences in automated algorithms embedded in NavX (St Jude Medical) and CARTO (Biosense Webster) might influence CFAE target identification for ablation, potentially affecting ablation outcomes.

Methods: To evaluate this effect, 797 bipolar electrograms, with their respective CFE-Mean and CFE-StdDev, were collected from 18 persAF patients undergoing ablation guided by NavX, prior to CFAE ablation. The Interval Confidence Level (ICL), Average Complex Interval (ACI) and Shortest Complex Interval (SCI), as defined by CARTO, were calculated offline with a validated MATLAB algorithm. CFAE classification was performed by NavX and CARTO using their default threshold (CFE-Mean \leq 120 ms; ICL \geq 7). Primary (CFE-Mean, ICL) and complementary (CFE-StdDev, ACI, SCI) metrics from each system were optimized to reduce the differences in CFAE classification between the two systems using receiver operating characteristic (ROC) curves. The relative agreement between both systems was assessed using Cohen's kappa (κ).

Results: Using the default thresholds (Figure 1), NavX classified 69 \pm 5% of the electrograms as CFAEs, while CARTO detected 35 \pm 5% ($\kappa\approx$ 0.3, $P<$ 0.0001). Using the revised thresholds optimized from the ROC curves (NavX: CFE-Mean \leq 84 ms, CFE-StdDev \leq 47 ms; CARTO: ICL \geq 4, ACI \leq 82 ms, SCI \leq 58 ms; area under the ROC curves

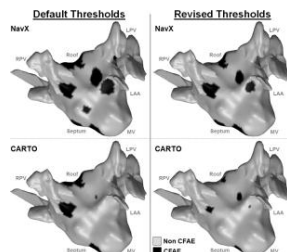


Figure 1. CFAE maps by NavX & CARTO

using default and revised thresholds, and CARTO detected 42 \pm 5% ($\kappa\approx$ 0.5, $P<$ 0.0001).

Conclusion: CFAE target identification is dependent on the system used during the procedure. We suggest customized thresholds that reduce differences in CFAE classification between commercial systems. This would facilitate direct comparisons of persAF CFAE-guided ablation outcome guided by NavX or CARTO and would help to improve the current understanding of the real significance of CFAE in the underlying mechanisms of persAF.

Combination of Frequency and Phase to Characterise the Spatiotemporal Behaviour of Cardiac Waves during Persistent Atrial Fibrillation in Humans

Nawshin Dastagir*, Xin Li, Frederique J Vanheusden, Tiago P Almeida, João Salinet, Gavin S Chu, Peter J Stafford, G André Ng, Fernando S Schlindwein

University of Leicester
Leicester, United Kingdom

S22

Dominant frequency and phase mapping have been used to characterise atrial fibrillation (AF) during electrophysiological studies. We hypothesize that during AF, phase singularity points (PS) are located around high dominant frequency (HDF) regions and also that HDF passes between two PS of opposite chirality. For 7 patients undergoing left-atrial persistent AF (persAF) ablation, 2048 noncontact virtual unipolar electrograms (EGMs) were simultaneously collected using a balloon array (Ensite Velocity, St. Jude Medical, resampled at 512Hz). After QRST subtraction, Fourier transform was used to detect DF on each atrial EGM (range 4Hz-10Hz; 4s time window; 87.5% overlap; HDF, $DF \pm 0.25\text{Hz}$; up to 30seconds/patient). Phases were computed using Hilbert-transform and PS are detected by finding the curl of spatial phase gradient. HDF along with phase and PS were plotted for each window and behaviour of the trajectory of HDF 'clouds' was inspected via semi-automatic algorithm. Figure-1 with subplots (a-b) illustrates the spatial distributions of phase, the corresponding PS and HDF of 2 persAF patients. The areas of interest are HDF regions (black colour), grey circles are anticlockwise rotors and white circles are clockwise. We frequently observed the transit of HDF 'cloud' between rotors of two opposite chirality and also that PS points tend to be located around the boundary of the HDF areas rather than within them. PS of opposite chirality was observed for 77 windows and out of those we observed HDF 'clouds' going through them in 61 windows(79.2%). This type of activity was observed for all patients. PS points tend to locate around the border of HDF regions. Generating and analysing these spatiotemporal maps may prove helpful in assimilating the spatial and temporal changes during fibrillation and tracking the activation patterns dynamically. We hypothesise that an interesting ablation strategy might be to ablate a line connecting pairs of PS with opposite chirality.

Recurrent High Dominant Frequency Spatial Patterns in Atrial Fibrillation

S22

Xin Li*, Gavin S Chu, Tiago P Almeida, Frederique J Vanheusden, Nawshin Dastagir, João L Salinet, Peter J Stafford, G André Ng, Fernando S Schindwein

University of Leicester
Leicester, UK

Introduction: Atrial regions hosting high dominant frequency (DF) may represent potential drivers of persistent atrial fibrillation (persAF). Previous work showed that DF can exhibit cyclic behavior. This study aims to better understand the spatiotemporal behaviors of persAF over longer time periods.

Method: 9 patients undergoing persAF ablation targeted at DF were included. Left atrial (LA) non-contact virtual electrograms (EGMs, Ensité Array, St Jude Medical) were collected for up to 5 min pre-/post- ablation. After QRST sub-traction, Fast Fourier transform was performed to estimate the power spectrum. DF was identified as the peak from 4-10 Hz, in 4 s windows (50% overlap). In each window, a high DF (HDF) map was created by the top 10% of the LA area hosting the highest DF. An automated pattern recognition algorithm was applied to look for recurring HDF spatial patterns within each patient.

Results: Recurring HDF patterns were found in all patients. Patients 4 and 5 were in atrial flutter post-DF ablation, and each demonstrated a corresponding single dominant pattern (DP) accounting for up to 94.8% (patient 5) and 68.1% (patient 4) of the recorded time period, consistent with the higher level of regularity during flutter. Ablation regularized AF demonstrated by increased DP recurrence after ablation. The time interval (median [IQR]) of DP recurrence for the patients still in AF after ablation (7 patients) decreased from 21.1 s [11.8~49.7 s] to 16.1 s [11.8~22.7s].

Conclusion: Recurrent spatial HDF patterns were observed in the LA during persAF. The proposed method quantifies HDF spatiotemporal regularity over long time periods and may offer a more comprehensive dynamic overview of persAF behavior and the impact of ablation.

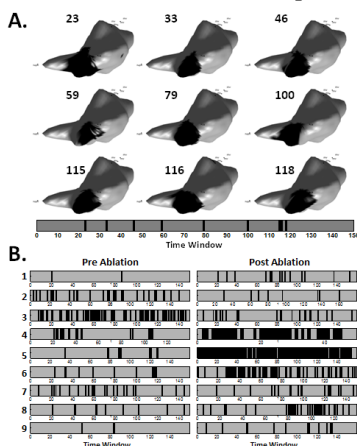


Figure 1 A. DP of patient 6 on 3D LA maps with the time occurrences. B. Time occurrence of the DP for all patients pre-/post-ablation

Using Electromechanical Signals Recorded from the Body for Respiratory Phase Detection and Respiratory Time Estimation: A Comparative Study

Nasim Alamdari, Kouhyar Tavakolian*, Reza Fazel-Rezai, Alireza Akhbardeh

United States

S23

Background: Electrocardiogram derived respiratory (EDR) is a non-invasive techniques for estimating the respiratory signal. In addition to EDR, recently there is a trend towards using accelerometer derived respiration techniques (ADR). This is achieved by placing an accelerometer on the chest and these accelerometers simultaneously record cardiac related signals also called Seimocardiogram (SCG). The aim of this study is to compare the efficacy of ADR to EDR in detecting the respiration phases and also the possibility of estimating the timings of inhale and exhale phases in both methods.

Methods: Acceleration signal, single lead electrocardiogram and respiration signal were recorded from 10 subjects. All measurements of healthy individuals were performed for ten minutes at Aalto University School of Electrical Engineering, Espoo, Finland. Common methods of EDR and ADR extractions were implemented such as linear and nonlinear principle component analysis (PCA), and envelope detection method. Upper envelope function of the data is calculated based on moving time window secant method. Then, IIR band pass filter was applied to the signal. The original respiration signal has been used as a reference in order to compare start inspiration and expiration points founded from ADR or EDR with their corresponding points in the reference signal. The data were manually annotated for finding initial points of inhale end exhale phases.

Conclusions: According to the achieved results ADR method (back to front direction) outperform the EDR. By taking advantage of ADR, about 75% of the respiration phases were correctly detected and more than 50% of the detected phases timings could be correctly estimated. Thus, they can be used for further processing such as discriminating which heart cycles are associate with inhale phase and which with exhale phase. The relevant cycles for each respiratory phase can be averaged separately.

Electrical Dyssynchrony on Noninvasive Electrocardiographic Mapping correlates with SAI QRST on ECG.

Larisa G. Tereshchenko, Elyar Ghafoori, Muammar M. Kabir, Markus Kowalsky.

Oregon Health & Science University, Knight Cardiovascular Institute. Portland, OR, USA

Introduction: Noninvasive electrocardiographic mapping is a gold standard for personalized assessment of electrical dyssynchrony in candidates for cardiac resynchronization therapy (CRT). However, correlations between mapped electrical dyssynchrony and traditional clinical and ECG predictors of CRT response have not been sufficiently studied. The goal of this study was to compare associations between clinical, ECG, and cardiac MRI predictors of CRT response with electrical dyssynchrony.

Methods: Body-surface potentials were recorded using 120-lead system in 4 patients (age 62 ± 12 y, left ventricular ejection fraction (LVEF) 29 ± 5 %; QRS duration 154 ± 19 ms) with post-myocardial infarction scar and left bundle branch block before CRT implantation. A patient-specific heart-torso model derived from MRI with 291 heart-surface nodes was developed. An electrical dyssynchrony index (EDI) was computed as the standard deviation of activation times on the epicardium. Uncoupling index (UI) was measured as the difference between the activation times.

Results: QRS duration correlated with mean activation time ($r = 0.977$; $P = 0.023$), but did not correlate with EDI or UI. LVEF inversely correlated with activation time at the lowest 20th percentile ($r = -0.960$; $P = 0.040$) and trended towards correlation with an area, occupied by delayed activation (> 80 th percentile). Out of all clinical predictors of CRT response only sum absolute QRST integral (SAI QRST), measured on orthogonal XYZ ECG, correlated with EUI ($r = 0.955$; $P = 0.045$), and characterized conduction block.

Conclusion: SAI QRST is a measure of electrical dyssynchrony on ECG.

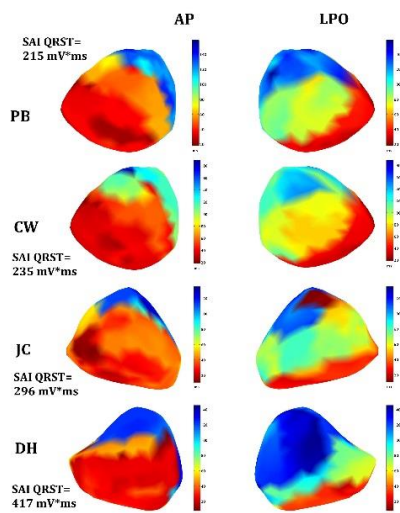


Figure. Epicardial maps of activation in the left anterior-posterior (AP) and left posterior oblique (LPO) views in 4 CRT patients.

A Computational Model of Open-Irrigated Electrode for Endocardial RF Catheter Ablation

Ana González-Suárez*, Enrique Berjano, Jose M Guerra, Luca Gerardo-Giorda

BCAM- Basque Center for Applied Mathematics
Bilbao, Spain

S23

Introduction: Radiofrequency (RF) catheter ablation (RFCA) is an important curative treatment for cardiac arrhythmias. During RFCA thrombus formation can occur when the electrode-tissue interface temperature exceeds 80°C. Open-irrigated electrodes have been developed to reduce the risk of thrombus formation by cooling the electrode-tissue interface, which also allows higher RF power delivery and the creation of larger lesions. No computer model of open-irrigated catheter for endocardial RF ablation accounting for both the effect of saline irrigation flow and the blood flow motion in the cardiac chamber has been proposed so far. Our aim was to build a computer model including the interaction of both effects.

Methods: The three-dimensional model considers two designs of open-irrigated electrodes. The effect of different irrigation flow rates, power settings, and two catheter-tissue orientations (perpendicular and parallel) on the blood temperature distribution around the ablating electrode and the lesion size are studied.

Results: Lesion size was greater with parallel catheter contact. Smaller surface widths and lower blood temperatures were obtained with higher irrigation flow rates, regardless of catheter tip design and catheter-tissue orientation. The lesion depth was not affected by changing the irrigation flow rate. The increase of RF power caused larger lesions (both surface width and depth) and higher blood temperatures, an effect more evident with parallel orientation. Surface width and blood temperature were affected by catheter tip design.

Conclusions: Our findings allowed to evaluate under which circumstances the blood temperature reaches the critical value of 80°C and when is possible to create thermal lesions with a minimum surface width without affecting the lesion depth. This indicates a reduction of the overheating at the electrode-tissue interface and thus guarantees a lower incidence of thrombus formation. The computational results are also in close agreement with experimental results from previous studies.

An Additional Marker of Ventricular Dyssynchrony

P. Jurak, J. Halamek, F. Plesinger, T. Reichlova, J. Lipoldova, M. Novak, K. Jurakova, P. Leinveber.

Institute of Scientific Instruments, ASCR, CZ
International Clinical Research Center, Brno, CZ

Patients suffering from left bundle branch block (LBBB) can be treated by resynchronization therapy (CRT). The QRS duration (QRSd) and QRS morphology are the main selection criteria. Unfortunately, approximately one-third of CRT patients are non-responders. Here we present an additional new marker capable of distinguishing ventricular dyssynchrony more accurately.

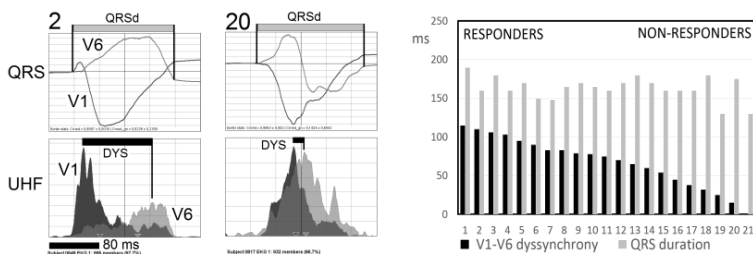


Fig. 1 V1, V6 averaged QRS and UHF envelopes. Patient 2 – DYS 110 ms, patient 20 – DYS 15 ms

Fig. 2 V1-V6 dyssynchrony (DYS, black) and QRS duration (QRSd, gray), 21 CRT indicated patients.

Methods: Ultra-high-frequency (UHF, sampling 25kHz) 12-lead ECG, 15-minute resting supine position, was measured. We analyzed 21 LBBB patients selected for CRT, the QRSd min/mean/max was 130/163/190 ms. Amplitude envelopes in the 500-1000 Hz passband were computed and averaged with R-wave trigger for each patient in V1 and V6 leads. V1-V6 dyssynchrony (DYS) was computed as the time difference between UHF amplitude maximums in the V1 and V6 QRS complex region (Fig. 1).

Results: Fig. 2 shows QRSd (gray bar) and V1-V6 dyssynchrony (DYS, black bar) parameters; patients are sorted in descending order from left to right according to the value of V1-V6 dyssynchrony parameter. Patient 1 (left) maximal V1-V6 dyssynchrony (115 ms) and patient 21 (right) minimal V1-V6 dyssynchrony (1 ms). While V1-V6 dyssynchrony parameters decrease, QRSd remains nearly the same. Patients with a small value of the V1-V6 dyssynchrony parameter, in spite of the QRS duration meet CRT criteria (>120 ms), are not expected CRT responders. The V1-V6 dyssynchrony parameter clearly indicates ventricular dyssynchrony and can potentially increase the percentage of CRT responders.

Preliminary Comparison Study of Two Electro-Mechanical Cardiopulmonary Resuscitation Devices

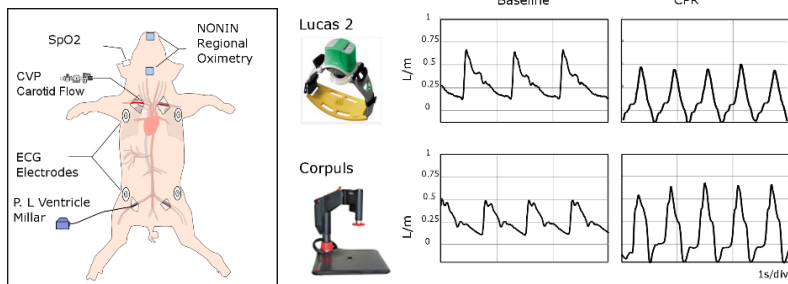
Alejandro Mendoza García, Stefan Eichhorn, Annemarie Stroh, Marcin Polski, Alois Knoll
Technical University Munich
Munich, Germany

Introduction: Over the past years several electro-mechanical devices have become available to the market, enabling paramedics to transport patients with cardiogenic shock to hospitals, while maintaining constant perfusion. These devices however have various mechanical structures and compression mechanisms that can affect the body perfusion. The presented paper shows the preliminary results of the comparison of two of such CPR devices using a pig model: the Lucas 2 and the Corpuls CPR.

Methods: Two middle sized domestic pigs weighing 30+-5 kg were used for this study. They were properly pre-medicated and given general anesthesia.

As preparation several sensors were placed to obtain vital parameters and blood flow during CPR. A normal oximeter was placed in the ear, and two regional oximetry sensors were placed at the level of the neck and on the tongue. Additionally the pressure at the left ventricle was captured using a Millar tip. The ECG and CO₂ were obtained using the Corpuls 3 monitoring system. After preparations were finished and before CPR all the parameters were recorded as a baseline. Afterwards the heart was stopped for 5 minutes and afterwards the CPR device was activated.

Results: The results obtained show that during the capturing of baseline parameters the mean carotid flow was of 0,31mL/min for the pig prepared for the Lucas 2 device and 230mL/min for the Corpuls device. After 3 minutes of CPR compressions the Lucas device generated 25% of the mean carotid flow, while the Corpuls device generated 76% of the carotid mean flow.



Analysis of the Spectrum of Cardiac Signals during Partially Correlated Spatiotemporal Dynamics: A Simulation Approach

S23

Ferney A Beltrán-Molina, Lizet C Salgado, Luis J Martinez, Jesús Requena-Carrión*

ECCI University
Bogotá, Colombia

Cardiac spectrum has been previously analyzed to characterize the spatiotemporal characteristics of complex arrhythmias such as fibrillation. Nevertheless, it is still unclear how the spatiotemporal characteristics of cardiac activity manifest on the spectrum of cardiac signals. Theoretical and simulation studies have shown that when cardiac activity is highly correlated, the bandwidth (BW) of cardiac signals is inversely related to the lead equivalent volume (LEV) of the electrode system. The analysis of partially correlated cardiac activity has however remained elusive. Partially correlated cardiac activity is of interest, since it might be appropriate to model complex cardiac arrhythmias. In this study, we analyze the spectrum of cardiac signals induced by partially correlated cardiac activity. We developed a 2D simulation environment that enabled us to control the degree of spatiotemporal correlation of the simulated activity. This simulation environment consists of a sheet of cardiac tissue that is randomly stimulated by an array of $N \times N$ electrodes. By setting N to increasing values we were able to shorten the correlation area of the simulated activity. We synthesized the cardiac signals measured by unipolar electrodes placed at increasing distances to the center of the tissue sample, allowing us to increase the LEV of the electrodes. The BW of synthesized cardiac signals was compared against the LEV of the corresponding electrode for different degrees of spatiotemporal correlation. For low LEV values, the BW was inversely related to the LEV. However, for higher LEV values, the BW saturated. We observed that the saturation LEV value was lower for low degrees of spatiotemporal correlation. The spectrum of cardiac signals depends both on the spatiotemporal characteristics of the underlying cardiac activity and on the characteristics of the electrode system. Our results have implications for the interpretation of cardiac spectrum in terms of the spatiotemporal characteristics of cardiac arrhythmias.

Right Ventricular Diastolic Function Evaluation in Magnetic Resonance Imaging

Nadjia Kachenoura*, Emilie Bollache, Alban Redheuil, Stéphanie Clément-Guinaudeau, Ludivine Perdrix, Benoit Diebold, Magalie Ladouceur, Elie Mousseaux

INSERM, UPMC Univ Paris 6
France

S24

Background: Although few studies demonstrated the ability of MRI dynamic anatomical sequences to assess right ventricular (RV) diastolic function no data are available for phase contrast MRI (PC-MRI), despite their demonstrated usefulness on the left ventricle (LV). Accordingly, our aim was to assess the ability of PC-MRI data to evaluate RV diastolic function compared to reference Doppler echocardiography.

Methods: We studied 90 healthy individuals (52 men, age: 40 ± 14 years) who underwent RV Doppler echocardiography and PC-MRI, on the same day. Dynamic MRI data were used to position a retrospectively ECG-gated PC pulse sequence (encoding velocity=150cm/s), in a plane perpendicular to the tricuspid inflow at the level of the tips of the opened leaflets. PC-MRI images were analyzed using an automated custom software, providing: early peak velocity (E,cm/s) and flow-rate (Ef,ml/s), atrial peak velocity (A,cm/s) and flow-rate (Af,ml/s) as well as E/A and Ef/Af ratios. Same velocity parameters were extracted from Doppler echocardiography (E,A,E/A).

Results: Despite the fair associations between echocardiographic E/A ratio and PC-MRI early to late peak flow-rate (Ef/Af) and velocity (E/A) ratios ($r > 0.36$; $p < 0.001$), the strongest correlation with age was obtained for the PC-MRI flow-rate ratio Ef/Af ($r = -0.65$, $p < 0.001$). Associations with age for velocity ratios (E/A) were equivalent between MRI ($r = -0.41$, $p < 0.001$) and echocardiography ($r = -0.36$, $p < 0.001$).

Conclusions: Automatically extracted PC-MRI tricuspid inflow parameters were strongly related to age. These associations were comparable to echocardiography for maximal velocities ratio and were stronger when considering peak flow-rate ratio, this index being less sensitive to changes in tricuspid flow orientation during the cardiac cycle. These findings highlight the consistency of PC-MRI for RV diastolic function assessment and its potential usefulness for clinical RV function evaluation, particularly in congenital disease.

Automated Detection of Left Atrium Boundary in Intracardiac Echocardiography During Atrial Fibrillation Ablation

S24

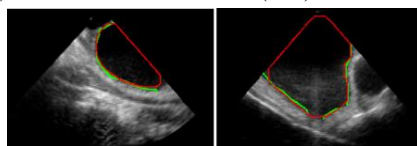
Rachele Angeletti, Corrado Tomasi, Matteo Zimmitti, Cristiana Corsi

DEI, Cesena Campus, University of Bologna, Bologna, Italy
AUSL della Romagna, Ravenna, Italy

Introduction: Intracardiac echocardiography (ICE) is used during radiofrequency ablation (RFA) of atrial fibrillation to visualize real-time left atrium (LA) anatomy and intracardiac catheters, as well as to monitor potential complications, including esophageal injuries. However, esophagus' dynamic interface with LA posterior wall (LAPW) can be only roughly depicted by any echo-based method. In clinical practice, the exact position of the LAPW is manually traced (MT) on ICE images by the cardiologist. This procedure is cumbersome and time-consuming. Accordingly, the present study aimed to automatically detect LAPW position by ICE during RFA, as a first step to track real-time esophageal-atrial spatial relationship.

Methods: The first step was the identification of LA cavity in the ICE sequence by exploiting LA shape and position knowledge. Due to the presence of noise and artifacts, two different algorithms were developed for LA detection: the first one relied on pixel clustering (CL) and it was applied to noisy images; the second one was based on a region-based level-set Chan-Vese model (CV). Output boundary was then refined using morphological operators and shape analysis. Algorithms were tested on 9 ICE acquisitions, for a total of 2048 frames. Two series of LA boundaries, obtained applying CV and CL method respectively, were compared with manually traced LA boundaries by an experienced cardiologist by linear regression, Bland-Altman analysis, Dice coefficient (D) and Hausdorff distance (HD).

Results: Analysis time was 0.6 and 1.5 sec/frame for CL and CV, respectively. Detected contours were in good agreement with MT (see figure and table).



Conclusion: The developed technique allows automated and accurate detection of LAPW and may represent the preliminary step for additional analyses including dynamic quantification of esophagus real-time position and its distance from the LAPW to prevent esophagus injuries.

Comparison between manually traced (green) and automatically detected (red) LA boundaries by applying the CV (left) and CL (right) method.

	Linear regression	Correlation coefficient	Bias (pixels (%))	SD (pixels)	D (mean±SD)	HD (pixels)
CL	$y=1.0x-1654$	0.92	-1159 (0.73)	1011	0.95 ± 0.029	4.5 ± 0.7
CV	$y=0.9x-153$	0.99	-827 (0.57)	376	0.94 ± 0.018	4.0 ± 0.6

Quantification of Myocardial Viability in Late-Gadolinium Enhancement Cardiac MRI

M Chiara Carminati, Cinzia Boniotti, Mauro Pepi, Enrico G Caiani*

Centro Cardiologico Monzino, IRCCS, Milano, Italy
Italy

S24

Late Gadolinium enhancement (LGE-CMR) is the standard technique for evaluation of left ventricular (LV) myocardial scar hyper-enhanced tissue (HET). Its identification is based on subjective experience-dependent and time-consuming analysis on multiple short-axis (SA) planes. Our aim was to develop an automated method for 3D LV HET detection, and to validate it against gold standard (GS) manual tracings.

Materials and Methods: LGE-CMR images from 10 patients with ischemic cardiomyopathy were analyzed by an experienced cardiologist to obtain (GS) HET borders, and corresponding scar mass. After myocardial borders manual delineation on each image, the myocardium was automatically classified into healthy or HET, by applying a mixture-model approach in which the myocardial pixel intensities were fitted by Gaussian distributions, and their intersection used as intensity threshold value for segmentation. This process was repeated considering: 1) each SA image separately (single-slice approach, SSA); 2) the entire SA image stack (global approach, GA). After classification, dedicated post-processing was implemented to minimize possible segmentation errors. Results were summarized in a modified bull's eye model (BEM) constituted by 144 sectors, each 2.5° wide, for all SA slices, to be compared with the corresponding GS.

Results: GS tracings resulted in 106 scars, with mass ranging from 0.4 g to 4.5 g. When compared with GS, SSA and GA resulted in 93.1% and 93.8% accuracy, respectively, with 81.2% and 88.6% sensitivity, 98.3% and 96.1% specificity. Linear correlation and Bland-Altman analyses vs GS scar mass resulted in good correlation, in particular for GA ($r^2=0.8$, SSA: $r^2=0.54$), with non-significant bias and narrow limits of agreement (GA: ± 0.22 g; SSA: ± 1.14 g).

Conclusions: The mixture model with GA resulted in better performance compared to SAA, with accurate detection of LV HET in SAX LGE-CMR images, leading to fast, objective and reliable measurements of scar volume and its extension, when compared to GS manual tracing.

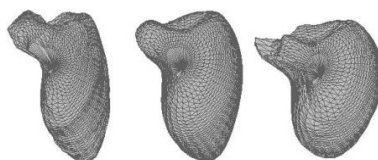
Model-based 3-D LV Shape Recovery in Biplane X-Ray Angiography: A-Priori Information Learned from CT

Roland Swoboda*, Josef Scharinger, Clemens Steinwender

University of Applied Sciences Upper Austria
Hagenberg, Austria

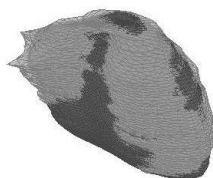
In coronary angiography, the gold standard for quantitative LV analysis is based on the evaluation of 2-D endocardial contours gathered from non-rotational 2-D x-ray image sequences. As 3-D information is lost due to projection, diagnostic parameters like EF are only approximated and wall motion is only assessable for surface areas whose boundary is visible in the projection images. This work presents a novel approach to recover the 3-D endocardial surface from two projections, so that LV function can be analyzed in 3-D.

The inherently sparse and noisy data available for reconstruction and the ill-posed nature of the inverse problem necessitates the incorporation of a-priori information. A statistical shape model (SSM) of the LV anatomy is therefore learned from 22 high-resolution datasets acquired with a 64-slice CT. Reconstruction is based on a non-rigid 2-D/3-D registration technique. To fit pose and shape of the model to the x-ray images of the patient, simulated projections of the model are calculated and the difference between real and simulated projections is minimized. Our cost function incorporates both contour and densitometric information derived from the projections. Different optimization strategies, like the Downhill Simplex and Particle Swarm algorithm, are applied and compared.



Deformable SSM of the LV anatomy
learned from CT

For patients where both CT and angiograms are available, the reconstructed LV shape is compared to the true shape known from CT. This allows an accurate evaluation of our approach. Simulated angiograms are derived from CT for further evaluation. Current results of volumetric similarity metrics like the difference-of-volumes and kappa statistics show a good correspondence between reconstructed and true shape: 91.00% and 85.88% for real angiograms, 94.56% and 87.12% for simulated angiograms, respectively. Using an approach based on SSM improves robustness and allows generating anatomically plausible and patient-specific shapes. A recovered shape is a potential base for further clinical evaluations.



Reconstructed vs. true
LV shape

Evaluation of Different Statistical Shape Models for Segmentation of the Left Ventricular Endocardium from Magnetic Resonance Images

Concetta Piazzese*, M Chiara Carminati, Andrea Colombo, Rolf Krause, Mark Potse, Lynn Weinert, Gloria Tamborini, Mauro Pepi, Roberto M Lang, Enrico G Caiani

Politecnico di Milano
Milan, Italy

S24

Introduction: Statistical shape models (SSMs) represent a powerful tool to segment medical images and to detect structures. SSMs incorporates a priori knowledge from training datasets that guide the model during deformation while it tries to match features of the analyzed image. The aim of this work is to evaluate segmentation accuracy of the left ventricle (LV) on magnetic resonance (MR) images using four different SSMs.

Methods: From a database of LV surfaces (Tomtec) segmented from transthoracic 3D echocardiographic (3DE) datasets obtained in 435 retrospective patients, four different SSMs containing respectively only end-diastolic frames (ED model), only end-systolic frames (ES model), both ED and ES frames (ED-ES model), and all frames (global model) were created. Each model was then roto-translated and scaled to fit the ED and ES frames in MR short-axis (SAX) image stacks of 15 patients with normal LV function, after manual initialization of 2 LV basal and one apical point on 2-chamber and 4-chamber long-axis images. The model was then deformed based on Principal Component Analysis to match the LV endocardial position simultaneously in the whole SAX stack. The LV volume resulting from each SSM was computed and compared to ED and ES volumes derived from the same SAX images analyzed by an experienced cardiologist (GS).

Results: Linear correlation and Bland–Altman analyses versus GS showed in all SSMs high correlation ($r^2 > 0.95$), non-significant biases, narrow limits of agreement, probably due to the large number of subjects included in the database, covering a large LV morphological variability.

Conclusions: We evaluated the accuracy of four different SSMs, based on LV endocardial surfaces extracted from 3DE images as training datasets, to segment the LV endocardium in MR SAX stack using a novel intermodality approach. All evaluated SSM strategies resulted in equivalent agreement when compared to LV volumes obtained by manual tracing.

A Nearly-Automated Approach for Left Ventricular Segmentation using Feature Asymmetry from Real-time 3D Echocardiography

Claudio Fabbri*, Simone Pertutti, Cristiana Corsi

Italy

Background: Quantification of left ventricular (LV) volumes is important for an accurate assessment of LV function for the diagnosis of cardiac diseases from 3D echocardiographic imaging. Tools available in clinical practice depend on cardiologist's experience in selecting the correct views for volume computation, tracing endocardial contours or selecting some feature points. Automated identification using image intensity is difficult in presence of speckle noise and low contrast in echocardiographic data. Therefore, the aim of this study was to develop a new LV segmentation algorithm driven by feature asymmetry (FA) information.

Methods: The proposed approach is based on a 3D modified Malladi-Sethian level-set algorithm, driven by FA as an edge indicator, followed by a curvature flow and isosurface extraction. The FA is obtained from the monogenic signal at different scales. The initialization procedure requires the selection of a point inside the LV and four points to allow the least square detection of the valvular plane. The algorithm was tested and validated on 3D echo data from CETUS 2014 challenge in 9 patients by correlation and Bland-Altman analysis for end-diastolic and end-systolic volume (EDV, ESV) and ejection fraction (EF). LV surfaces at ED and ES were compared by mean absolute distance (MAD), Hausdorff distance (HD) and Dice coefficient (D).

Results: Clinical indexes derived from the detected surfaces were in good agreement with the reference ones (EDV: $y=0.9x-13.2$, $r=0.98$, $\text{bias}=36.1\text{ml}$, $\text{SD}=20.9\text{ml}$; ESV: $y=0.9x-10.4$, $r=0.99$, $\text{bias}=25.3\text{ml}$, $\text{SD}=13.9\text{ml}$; EF: $y=0.8x+5.9$, $r=0.94$, $\text{bias}=-1.2\%$, $\text{SD}=5.2\%$). MAD, D and HD between surfaces were promising (MAD:2,58mm; D=0.88±0.028; HD=11.9±2.15mm).

Conclusions: The detection of LV surfaces using 3D level-set edge-based model driven by phase information is feasible. Derived LV function indexes are accurate compared to the ones derived by manual tracing of expert cardiologist. The proposed method allows accurate evaluation of chamber size and shape, even in case of irregular geometry.

BAN-Based Health Telemonitoring System for In-Home Care

Eliasz Kańtoch*

AGH University of Science and Technology
Kraków, Poland

S31

Introduction: Continuous monitoring of multiple health state parameters is crucial for early diagnosis of chronic diseases and its management. However, there are several challenges that needs to be faced to accelerate the development of patient telemonitoring at home. **Aims:** This study aimed to develop easy to implement and operate health monitoring system for in-home application for older people and patients suffering from chronic diseases.

Methods: The system consists of HCTU (home central transmission unit) and wireless battery operated sensors nodes: accelerometers, heart rate sensor, temperature sensor and body weight. The system analyzes incoming data and transmit it to the medical web server. Developed algorithms recognize unusual activity patterns and alert the user or doctors.

Results: The web-based graphical user interface enables to easily access patient data, supervise patient rehabilitation and variability of health parameters. Measurements of heart rate, body acceleration, body temperature and weight where collected from 12 patients (8 male, 4 female) during activities of daily living (ADL). Diagnosis can be supported or the effectiveness of ongoing treatment can be evaluated by acquired data.

Conclusions: Experimental results showed maximum 6% error compared to medical devices and proved that selected telemedical services involving analysis of the set of human health parameters can be successfully delivered remotely. Moreover, remote patient monitoring can reduce the number of clinic visits and improve the quality of the health care service.

A Multi-Channel Electrode-Tissue Impedance Detection Approach for Motion Artifact Suppression in Ambulatory ECG

Huanqian Zhang*, XiaoWei Du, Shulin Zhang, Qinghui Jin, Ruojie Tao, Qing Li, Jian Yang, Jianlong Zhao

China

S31

Aim: Due to the development of Internet of Things technology and telemedicine, increased attention has been paid to electrocardiogram (ECG) detection for individuals participating in outdoors activities, family activities, and exercise. During activities the interface between the electrode metal and the conductive adhesive as well as the stretch of the skin will introduce additional artifacts to the ECG signal. Processing these interference in ECG is highly difficult because motion artifacts (MAs) and ECG signals have similar frequency spectra. Adaptive filter can be used to remove MAs from ECG with a reference signal correlated with MAs. However, more sensors and leads should be employed to measure the reference signal, which will increase the complex and decrease the comfortability of the whole system.

Method: In this paper, we proposed a new multi-channel electrode-tissue impedance (MC-ETI) detection approach. It had one fewer electrode than the previously reported technologies, so that it was more suitable for long-term one-lead heart rate detection. An alternating current (AC) was injected into the human body through one electrode. Meanwhile, ECG and reference signals were detected by the other two electrodes independently.

Result: Three minutes measure data from each one of five healthy subjects, totaling in 547 heartbeats, were evaluated. Compared MC-ETI performance with conventional differential-channel electrode-tissue impedance (DC-ETI) detection, the experimental results shown that MC-ETI has significantly higher correlation with the motion artifacts in ECG signals than DC-ETI. The test data from the two approaches were applied to an adaptive filter. After filtering, the MC-ETI data were compared with the DC-ETI data, indicating that there were clear increases in the signal-to-noise ratio (3.5 dB), operational speed (7.4-fold), and convergence error accuracy (4.3%) for MC-ETI.

A Wearable Device for Physical and Emotional Health Monitoring

Srinivasan Murali*, Francisco Rincon, David Atienza

SmartCardia
Lausanne, Switzerland

S31

Personal health monitoring systems are emerging as promising solutions to tackle health-care costs and delivery. There is a growing interest within the medical community in developing ultra-small, portable devices that can continuously monitor and process several vital body parameters. In this work, we present a wearable device for physical and emotional health monitoring. The device obtains user's key physiological signals: ECG, respiration, Impedance Cardiogram (ICG), blood pressure and skin conductance and derives the user's emotion states as well. We have developed embedded algorithms that processes the bio-signals in real-time to detect any abnormalities (cardiac arrhythmia and morphology changes) in the ECG and to detect key parameters (such as the Pre-Ejection Period and fluid status level) from the ICG. We present a novel method to detect continuous beat-by-beat blood pressure from the ECG and ICG signals. We also present a real-time embedded emotion classifier operating under energy budget constraints that computes the emotion levels of the user based on the different physiological signals measured. Emotions are classified according to their attractiveness (positive valence) or their aversion (negative valence) in the horizontal valence dimension. The excitement level induced by the emotions is represented by high to low positions in the vertical arousal dimension of the valence-arousal space. The signals are measured either intermittently by touching the metal electrodes on the device (for point-of-care testing) or continuously, using a chest strap for long term monitoring. The processed data from device is sent from the device to a mobile phone by Bluetooth Low Energy protocol. The device can monitor the signals continuously for over 72 hours on a single battery charge. We will present case studies on how the technology can improve physical and emotional health of users and the key challenges encountered during the design process.

Wearable Monitoring: A Project for the Unobtrusive Investigation of Sleep Physiology Aboard the International Space Station

Marco Di Rienzo, Emanuele Vaini, Prospero Lombardi*

Fondazione Don Carlo Gnocchi ONLUS
Italy

S31

Objectives of the Wearable Monitoring project, part of the Futura Mission organized by the Italian Space Agency, are 1) to validate a new smart garment (MagIC-Space) for the comfortable assessment of vital signs during sleep in microgravity; and 2) to investigate sleep physiology aboard the International Space Station (ISS) by this device. MagIC-Space (the payload) is derived from a system previously developed in our lab. The original device was modified to meet the space qualification requirements. The final system is composed of a cotton vest including textile sensors for ECG and respiratory rate assessment; and a miniaturized electronic unit, containing a 3D accelerometer for the detection of the precordial vibrations caused by the heart contraction and blood ejection from the ventricles into the vascular tree (the seismocardiogram). Signals are locally stored on a memory card and then transferred to a laptop for the transmission to Earth. From the raw signals, indexes of heart contractility were estimated from the Q wave in the ECG and the instants of opening and closure of the aortic and mitral valves detected by the seismocardiogram. Information on the autonomic nervous control is obtained by the analysis of the heart rate variability. Six in-flight sleep recordings are planned from January till mid-May 2015 in one crewmember. The experiment is still in progress. After four in-flight recordings, the smart garment has been reported to be comfortable and easy to use because most of sensors and wirings are integrated into the garment. The quality of the recorded signals is good, with a very limited artifact rate ($< 2\%$). Further data will be available at the end of the experiments.

A Qualitative Dynamical Model for Cardiotocography Simulation

Alfredo Illanes, Michel Haritopoulos*, Felipe Robles, Francisco Guerra

Universidad Austral de Chile
Valdivia, Chile

S32

Introduction: In medicine, simulators can be used to assist clinical staff in the interpretation of the fetal cardiotocography (CTG), since they provide a risk free and controllable environment for training. However, currently available obstetric simulators and training programs provide limited realism and most of them simulate only static scenarios without the possibility of changing dynamics during the simulation. Moreover although several mathematical models has been proposed for CU and FHR signal generation separately, few of them put in relationship the dynamics of both signals. The aim of this work was to develop a qualitative dynamical model for simulation of normal and critical situations in labor and delivery as a training tool for educational purposes.

Materials and Methods: Based on the physiologic control of the fetal cardiovascular system, a dynamical model based simulator using matlab was developed on five interconnected blocks corresponding to: user's control panel (UCP), a fetal heart rate (FHR) generator, a uterine contraction (UC) generator, a random fetal movement (FM) generator, and a memory block, which allows to store dynamical information about the fetus state through a simple mathematical function. Results and

Discussion: The model provides the main dynamics of a CTG including baseline of the FHR, variability, accelerations and decelerations. The UCP allows the user to set different simulation parameters including the possibility of generate UC or FM online during the simulation. Simulated tracings were analyzed by two experts and evaluated in terms of signal realism and dynamics. Results show no significant differences between real and computer-generated CTG tracings.

Conclusions: This dynamical model of fetal cardiotocography fulfills the realism, adding the possibility of changes on line in any part of the tracing generation. The next step will be to integrate this model as a learning object on labor scenarios.

Fetal Heart Rate Complexity Measures to Detect Hypoxia

Óscar Barquero-Pérez*, Rebeca Goya-Esteban, Antonio Caamaño, Carlos Martín-Caballero, José Luis Rojo-Álvarez

Universidad Rey Juan Carlos
Fuenlabrada, Spain

S32

Background: Perinatal hypoxia is a severe condition that may harm fetus organs permanently or even cause death. When the fetus brain is partially deprived from oxygen, the control of the fetal heart rate (FHR) is affected. Objective. We hypothesize that the complex physiological mechanisms of the FHR are perturbed under perinatal hypoxia. We propose measure entropy and time irreversibility of the FHR to quantify the loss in the complexity.

Materials and methods: We estimated the complexity of the FHR signal using Sample Entropy (SampEn), Permutation Entropy (PE), and Time Irreversibility (TI). We compared the results with time (Short Time Variability, STV) and frequency domain (High Frequency Power, PHF) methods. We computed every one hour before delivery. FHR traces were preprocessed to remove artifacts. A database of 32 FHR recordings were acquired with cardiotocography, 15 controls and 16 cases. A case was declared whether: 1) the PH of the umbilical artery was ≤ 7.05 ; or 2) the APGAR score 5 minutes after delivery was ≤ 7 and a reanimation type III or greater was required. Resampling methods were used to establish the statistical differences.

Results: TI was significantly different for healthy and hypoxia fetuses (-0.38 ± 0.19 vs. -0.21 ± 0.37 , p -value=0.063). Entropy indices were higher for healthy fetuses (SampEn: 0.33 ± 0.12 vs 0.28 ± 0.09 , p -value=0.11; PE: 0.72 ± 0.04 vs 0.69 ± 0.07 , p -value= 0.12). STV (3.23 ± 1.15 vs 3.45 ± 1.35 , p -value=0.30) and PHF (0.40 ± 0.18 vs 0.43 ± 0.25 , p -value=0.31) indices showed no differences.

Conclusions: Complexity measures of the FHR were different for healthy and hypoxia fetuses. These indices may help to early detect hypoxia with less invasive methods.

Mutual Information Estimates of CTG Synchronization

Philip A Warrick, Emily F Hamilton

PeriGen Inc.
Montreal, Canada

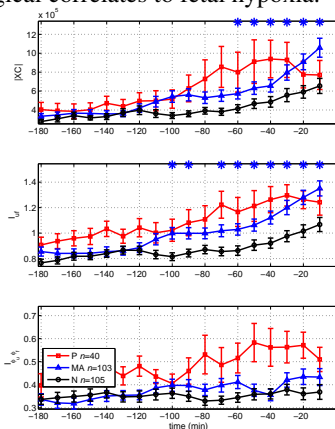
S32

Objectives: Assessing synchronization of the cardioctophography (CTG) signals uterine pressure (UP) and fetal heart rate (FHR) is a challenge because of noise and non-stationarity. We examined the use of mutual information (MI) and the instantaneous phase of the analytic signal to address this. MI was used to assess the UP-FHR coupling because it is suitable for non-linear systems with non-Gaussian noise. Estimating degree of synchronicity and UP-FHR delay length is useful since they are physiological correlates to fetal hypoxia.

Methods: The CTG records for this study consisted of 40 pathological (P), 103 metabolic acidotic (MA) and 105 normal (N) fetuses having >3 hours of labour. We calculated MI for both the raw UP and FHR signal pair $u(t)$ and $f(t)$ as well as their instantaneous phases $\phi_u(t)$ and $\phi_f(t)$ (calculated from the Hilbert transform). Binning was used for the probability densities $p(u)$, $p(f)$ and $p(u, f)$ required for MI calculation. We observed the time lag and value of the maximum MI over a range of possible UP-FHR lags using 20 min epochs with 50% overlap and compared these with cross-correlation (XC) estimates. Surrogate UP-FHR pairs generated by the amplitude-adjusted Fourier Transform technique were used to test MI significance.

Results: MI $I_{u,f}$ for the raw UP/FHR values discriminated N and MA fetuses more often (9 of 18 epochs) and earlier (100 min) than XC or phase MI $I_{\phi_u\phi_f}$ (see figure: statistically significant differences are indicated by *). Phase MI delay estimates (not shown) had much less variance than either of the other techniques, although it did not discriminate N and MA.

Conclusions: MI provides more discriminative estimates of UP-FHR synchrony earlier in labour compared to conventional linear cross-correlation.



Group mean \pm standard error of UP-FHR synchronization in the last 3 hours of labour and delivery using cross-correlation (top), mutual information (middle) and phase mutual information (bottom).

Fetal ECG Extraction Using Hybrid BSS Techniques

Luis Sarmiento, Alberto González, José Millet*

Unidades Tecnológicas de Santander, Colombia

S32

In the task of extracting the fetal ECG from abdominal ECG, often blind source separation is used as an intermediate step. To solve this problem is generally employed PCA and ICA. PCA takes advantage of time-structure of the sources, whereas ICA takes advantage of non-Gaussianity of the sources. However, realistic mixtures are many times compound of sources which present both diverse time-structure and non-Gaussianity. The COMBI and MULTI-COMBI algorithms offer novel schemes for combining PCA and ICA, enabling exploit the strengths of both techniques. In this work, the performance of the algorithms COMBI, MULTICOMBI, EFICA and traditional JADE algorithm are compared.

We used two database, the Noninvasive Fetal ECG Challenge 2013, as performance parameter we used the fetal RR interval measurement; and a semi-synthetic database compound of 26 abdominal ECG records, where real 3-D ECG signals representing maternal and fetal cardiac components are mixed by volume conduction transfer matrices, in which, the fetal to mother ratio SIR and fetal to noise ratio SNR are controlled. As performance parameter, we used the signal to error relation SER, varying SIR between -5dB to -30dB, and SNR between 0dB to 30dB in all possible combinations. In all case, it is found that the COMBI and MULTICOMBI algorithms show better performance than the JADE, and EFICA algorithms. For example, for SIR values between -5dB to -30dB whit SNR=10dB white noise, the mean SER is 8.42 ± 0.23 , 8.26 ± 0.15 , 8.02 ± 0.08 and 7.83 ± 0.05 dB; and 8.44 ± 0.52 , 8.9 ± 0.2 8.73 ± 0.07 and 8.52 ± 0.1 dB for pink noise, MULTICOMBI, COMBI, EFICA and JADE algorithms respectively.

While the COMBI and MULTICOMBI results are better, it is also true that they are the most dispersed. This is because are ad hoc algorithms, therefore in future works, must be optimized for the task of separating the sources in the abdominal ECG.

Quantification of the Ionic Current Contributions to Alterations in the Action Potential Repolarization by means of Piecewise-Linear Approximation

Michelangelo Paci*, Jari Hyttinen, Stefano Severi

Finland

S33

Prolongation and shortening of the action potential (AP) are important proarrhythmic markers at the cardiac cellular level. To investigate the ionic mechanisms underlying such phenomena it would be useful to quantify the contribution of each membrane current to the changes in AP duration (APD). We propose a novel method to quantify the contribution of each current to the repolarization of *in silico* APs by splitting among the currents the APD prolongation/shortening (ΔAPD_{90}) due to a perturbation from a basal to another condition. The method is based on a piecewise-linear approximation of the AP. (i) From the AP peaks, both the basal and the perturbed APs are dissected into uniform “discrete decreases” ΔV (e.g. -1 mV), splitting the repolarization timecourses into unevenly long time intervals. (ii) For each ΔV , APs are approximated by a linear decreasing trend and each current by its mean value; under this assumption the local contributions of each current to the prolongation/shortening are computed based on the variation of its mean value caused by the perturbation. (iii) The global contribution of each current to ΔAPD_{90} is the sum of all its local contributions. We tested our method on diverse perturbations, APD rate adaptation and current blocks, in the O’Hara-Rudy model. For example, in case of increased pacing rate from 60 to 120bpm, immediately after perturbation ΔAPD_{90} is -27ms, as the net result of the shortening contributions of I_{NaCa} , I_{NaL} , I_{Kr} , I_{Ks} and I_{CaL} (-20, -19, -15, -6 and -6ms, respectively) and some counteracting prolongation, e.g. I_{to} (+45ms). At steady state ΔAPD_{90} is -37ms and current contributions significantly change, e.g. I_{NaK} contribution becomes the greatest, changing from -1 to -73ms. Our method computes the current contributions to AP repolarization changes in response to perturbations, allowing a quantitative characterization of the direct and compensatory mechanisms implemented by the cell.

Drug Toxicity on Cardiac Pacemaking: A Multiscale Modelling Study

Xiangyun Bai, Henggui Zhang, Kuanquan Wang, Yongfeng Yuan, Qince Li, Na Zhao

School of Computer Science and Technology, Harbin Institute of Technology, Harbin, Heilongjiang 150001, China

S33

Introduction: Drugs, such as cisapride, have to be withdrawn from clinical uses due to their severe side effects, i.e., cardiotoxicity. As an agonist, cisapride can activate 5-Hydroxytryptamine 4 (5-HT₄) receptors which are localized in sinoatrial node (SAN) and atrium. It is unclear how the actions of cisapride alone and its combined effects with 5-HT₄ receptors impair cardiac pacemaking. The aim of this study was to investigate the functional impacts of cisapride on impairing cardiac pacemaker.

Method: The Zhang *et al.* model of action potentials of rabbit central and peripheral sinoatrial node (SAN) cells were modified to incorporate the actions of cisapride. Its action on the rapid rectifier potassium channel current (I_{Kr}) was simulated by simple pore blocking of I_{Kr} based on experimental data. Its action on the activation of 5-HT₄ receptors were modelled by increasing the L-type Ca²⁺ current (I_{CaL}) and shifting the activation curve of the funny current (I_f) toward more positive potentials. Single cell models were then incorporated into an anatomically detailed 2-D model of the intact SAN-atrium, in which effects of cisapride and 5HT₄ receptors activation on atrial cellular electrophysiology were also simulated. Using the multi-scale models, we quantified the effects of cisapride and its activation of 5-HT₄ receptors on cardiac pacemaking action potentials and their conduction.

Results: At single cell level, the action of cisapride on I_{Kr} alone had positive chronotropic effect in the central SAN cell (increasing the pacemaking rate by 11.4%), but had virtually no effect on the peripheral cell. When its activation to 5-HT₄ receptors was considered together with I_{Kr} blocking, cisapride increased the pacing rate (PR) (by 67%) in centre SAN cell, which dominates the heart rhythm; but decreased the PR substantially in the periphery SAN cell (by 21.4%). At the tissue level, cisapride increased the PR in the intact SAN-atrium, and amplified the tachycardia effect of 5-HT₄ receptor activation, leading to pacemaking site shift. It altered the activation sequence of cardiac excitation waves and reduced the maximum up-stroke velocity (dv/dt_{max}) of the atrium. In addition, early afterdepolarization was observed in the atrium.

Conclusion: Our simulation study substantiates the causative link between cisapride and cardiac pacemaking dysfunctions. It also suggests that activation of 5-HT₄ receptors by cisapride may account for atrial arrhythmogenesis, which should be taken into consideration for screening new drugs that activate SAN and atrium 5-HT₄ receptors.

Diabetes Affects the Temporal Dynamics of the Repolarization Properties of Cardiomyocytes

Olivier Meste*, Marianna Meo, Sergio Signore, Marcello Rota

University of Nice-Sophia Antipolis
France

S33

The duration of the action potential (AP) in cardiomyocytes is an important variable controlling the electrical properties of the normal and pathological myocardium. Prolongation of the AP in myocyte of the diabetic heart is coupled with increased risk of arrhythmia, but the determinants of these abnormalities remain to be elucidated. We raised the possibility that the diabetic condition is associated with alterations in the temporal dynamics of the AP profile in myocytes, a factor that may originate electrical instability. Thus, APs in isolated left ventricular myocytes obtained from control and streptozotocin-induced diabetic mice were measured by patch-clamp. The progressive changes in the repolarization phase of the AP for individual cells were tested on a set of 100 consecutive excitations at 2 Hz pacing rate. Each repolarization was normalized and fitted with a strictly decreasing function by using an original approach. The temporal properties of the repolarization function were automatically evaluated for the set of consecutive APs and the obtained indices were tested with linear regressions to define the dynamic characteristics of the repolarization over time. Specifically, whether the train of stimulations resulted in a stable pattern of APs or led to prolongation/shortening of the early and late repolarization phases was tested. In both control and diabetic groups prolongation and shortening of the AP were observed. Importantly, the progressive stimulation led to a faster late repolarization phase of the AP in the diabetic cells, as documented by a Wilcoxon signed rank test ($p < 0.001$). In contrast, AP indices for control myocytes were overall preserved over time. The dynamic changes of the AP profile in the diabetic group were restricted to the late repolarization phase, whereas the early phase behaved similarly for the two groups of cells. Thus, temporal dynamics of repolarization properties of cardiomyocytes are altered with diabetes.

Real-Time Simulation of I_{K1} in Cardiomyocytes Derived from Human Induced Pluripotent Stem Cells

Rosalie ME Meijer van Putten, Isabella Mengarelli, Kaomei Guan, Jan G Zegers, Antoni CG van Ginneken, Arie O Verkerk, Ronald Wilders*

Academic Medical Center, University of Amsterdam
Amsterdam, The Netherlands

S33

Background: Cardiomyocytes derived from human induced pluripotent stem cells (hiPSC-CMs) are widely used in studying basic mechanisms of ventricular arrhythmias. However, their action potential profile—and consequently the profile of individual ionic currents active during that action potential—differs substantially from that of native human cardiomyocytes, which is largely due to an almost negligible expression of the inward rectifier potassium current (I_{K1}). The Kir2.1 protein, encoded by the *KCNJ2* gene, is the main constituent of the I_{K1} channel in human ventricle.

Aim: We attempted to ‘normalize’ the action potential profile of our hiPSC-CMs through real-time simulation of the lacking I_{K1} .

Methods: Recordings were made from single isolated hiPSC-CMs in the dynamic clamp configuration of the perforated patch clamp technique, which allows the injection of a voltage-dependent *in silico* I_{K1} . The current-voltage characteristics of the simulated I_{K1} were based on data from voltage-clamp experiments on HEK-293 cells expressing Kir2.1 channels. The injected I_{K1} was modified to simulate the effects of loss-of-function and gain-of-function mutations in the *KCNJ2* gene.

Results: Without injection of I_{K1} , our hiPSC-CMs showed nodal-like spontaneous beating with a maximum diastolic potential of -56 ± 4 mV (mean \pm SEM, $n=9$), a maximum upstroke velocity of 10 ± 7 V/s, an action potential amplitude of 73 ± 9 mV, and an action potential duration at 90% repolarization of 162 ± 27 ms. Upon injection of an *in silico* I_{K1} with a peak outward density of 6 pA/pF, these values became -81 ± 1 mV, 178 ± 33 V/s, 123 ± 5 mV, and 171 ± 25 ms, respectively, unmasking the ventricular-like nature of our hiPSC-CMs. Proarrhythmic action potential changes were observed upon real-time simulation of both loss-of-function and gain-of-function mutations in I_{K1} , as associated with Andersen-Tawil syndrome type 1 and short QT syndrome type 3, respectively ($n=6$).

Conclusion: We conclude that injection of *in silico* I_{K1} makes the hiPSC-CM a more reliable model for investigating mechanisms underlying ventricular arrhythmias.

Real-Time Probabilistic Heart-Beat Classification and Correction for Embedded Systems

Grégoire Surrel*, Francisco Rincón, Srinivasan Murali, David Atienza

École Polytechnique Fédérale de Lausanne
Lausanne, Switzerland

S34

With the emergence of wearable and non-intrusive medical devices, one major challenge is the real-time analysis of the acquired signals in real-life and ambulatory conditions, as the accuracy of the recorded signals is not always optimal, which makes this new generation of devices more prone to misclassifications due to artifacts, such as, muscular noise. This paper tackles this situation by presenting a new algorithm for on-line heart-beat classification and correction that relies on a probabilistic model to determine whether a heart-beat is likely to happen under certain timing conditions or not. More specifically, it can quickly decide if a beat is occurring at an expected time or if there is a problem in the series (e.g., a skipped, an extra or a misplaced beat). Then, if an error is detected, the series is repaired accordingly. The proposed algorithm is crucial for this new generation of wearable devices as they run classification algorithms that rely on an accurate detection of the beats, like heart-rate variability, and the quality of such analyses can be easily compromised by the occurrence of erroneous beats. The algorithm has been carefully optimized to minimize the required processing power and memory usage, in order to enable its real-time embedded implementation on a wearable sensing device. Our experimental results, based on the PhysioNet Fantasia database, show that the proposed algorithm achieves 99.5% sensitivity in the detection and correction of erroneous beats. In addition, it features a fast response time when the activity level of the user changes, thus enabling its use in situations where the heart-rate might quickly change. Finally, we present how different time-domain (RMSSD, SDNN) and frequency-domain (LF/HF) analysis are affected by artificially corrupted heart-beat series, in order to illustrate how this algorithm allows significant improvement of these calculations after the correction of the beat series.

Evaluation of Short-term Individual Variability on the Contribution of Spectral-based Predictors to Cardiac Arrest Neurological Performance and Survival Outcomes

Conrado J Calvo*, David Filgueiras-Rama, Santiago Jimenez-Serrano, Francisco Castells, Francisco J Chorro, José Millet

Spain

Introduction: Early neurological prognosis in patients suffering from cardiac arrest and comatose status due to ventricular fibrillation (VF) is limited. VF waveform properties may provide a reliable estimation of VF duration after the initial onset helping to early assess cerebral performance (FNP) and survival outcomes (S). Here we analyze the relative contribution of VF spectral predictors to the development of a reproducible stratification risk score (RS).

Methods: VF prior to the first documented DC-shock was extracted from LII standard ECG from cardioverter defibrillators (n=70). Up to 5s artifact free segments were considered (1KHz sample rate). Non-parametric Welch method was used to extract fundamental spectral variables and derive high-to-low frequency ratios and non-linear high-order moments. Predictive models were obtained by stepwise multiple regressions using a backward elimination approach in the retrospective cohort (n=31). A fixed temporal sliding window of 3-5s was defined to assess the implications of spectral predictors variability from short segments prior DC-shocks to the outcome stratification in the prospective cohort (n=29). Ten controls without comatose status and known FNP were used for reference.

Results: A RS of three spectral predictors and the number of shocks delivered prior return to spontaneous circulation had the greatest performance prediction accuracy for FNP, where spectral predictors held most of the predictive power (Se=88%, Sp=91% and Acc=90%). In turn, the best clinical model had significantly lower predictive power (Se=50%, Sp=71% and Acc=69%). Low and Very Low risk patients had the greatest RS variability yet confidence intervals felt down within expected FNP or non-FNP accurately (98%). The model showed a correct and reproducible classification in 93% of patients.

Conclusions: Intrinsic VF spectral variations prior DC-shock do not alter the reproducibility of a new developed spectral-based risk score highly associated with FNP and S at hospital discharge.

On the Derivation of the Spatial QRS-T Angle from Mason–Likar Leads I, II, V2 and V5

Daniel Guldenring*, Dewar Finlay, Raymond Bond, Alan Kennedy, James McLaughlin

Ulster University
United Kingdom

S34

The spatial QRS-T angle (SA) has been identified as a marker for changes in the ventricular depolarization and repolarization sequence. The determination of the SA requires vectorcardiographic (VCG) data. However, VCG data is seldom recorded in monitoring applications. This is mainly due to the fact that the number and location of the electrodes required for recording the Frank VCG complicate the recording of VCG data in monitoring applications. Alternatively, reduced lead systems (RLS) allow for the derivation of the Frank VCG from a reduced number of electrocardiographic (ECG) leads. Derived Frank VCGs provide a practical means for the determination of the SA in monitoring applications. One widely studied RLS that is used in clinical practice is based upon Mason-Likar leads I, II, V2 and V5 (MLRL). The aim of this research was two-fold. First, to develop a linear ECG lead transformation matrix that allows for the estimation of the Frank VCG from the MLRL system. Second, to assess the accuracy of the MLRL derived SA (MSA). We used ECG data recorded from 545 subjects for the development of the linear ECG lead transformation matrix. The accuracy of the MSA was assessed by analyzing the differences between the MSA and the SA using the ECG data of 181 subjects. The differences between the MSA and the SA were quantified as systematic error (mean difference) and random error (span of Bland-Altman 95% limits of agreement). The systematic error between the MSA and the SA was found to be 7.69° [95% confidence interval: 5.31° to 10.08°]. The random error was quantified as 63.80° [95% confidence interval: 56.51° to 73.66°]. The findings of this research suggest that the random error can not be overlooked when using the MSA as a substitute for the SA.

ECG-derived respiration for ambulatory monitoring

Carolina Varon, Sabine Van Huffel

KU Leuven, Leuven, Belgium

S34

Aims: Respiration plays an essential role in the diagnosis and monitoring of different conditions. However, its recording is often associated with invasive and intrusive sensors such as respiratory belts and thermistors. These sensors are regularly used in a hospital setting and it is very rare to find them in ambulatory systems. Hence, several studies have focused on the computation of the so-called ECG-derived respiration (EDR). In this context, this research aims to evaluate different EDR algorithms on ECG signals that contain non-stationarities and noise.

Methods: Algorithms like the one based on the R-peak amplitude, principal component analysis (PCA), and kernel PCA, were evaluated. These were implemented on single-lead ECG signals extracted from the Physionet Fantasia and apnea-ECG datasets. First, all ECG and respiratory signals were segmented into epochs of one minute. Next, the EDR signals were computed for each ECG segment, and then compared against the real respiration using correlation, and coherence. Furthermore, different features were derived from the EDR signals, and differences between respiratory events in the apnea dataset were evaluated for each EDR algorithm.

Results: When non-stationary segments are taken into account, big differences are observed in the correlation and coherence between the EDR signals obtained with PCA and kPCA, and the real respiration. Moreover, it is clear that the R-peak amplitude method appears to be less sensitive to noise. Concerning apnea events, no significant differences were found between the different EDR signals.

Conclusions: These findings can be considered in real life applications, where transients, artifacts, changes in baseline, and noise contaminate the ECG. In addition, the simplest method to extract respiratory information from the ECG offers reliable and robust performance, when compared to methods based on PCA. However, some complex interactions between respiratory movements and the morphology of the ECG might be missing with this simple algorithm.

Inter-study Repeatability of Left Ventricular Strain Measurement using Feature Tracking on MRI Cine Images

Jérôme Lamy*, Gilles Soulat, Alban Redheuil, Morgane Evin, Elie Mousseaux, Nadjia Kachenoura

France

S35

Background: Feature tracking (FT) is an emerging approach for the evaluation of myocardial strain from standard cine magnetic resonance images (MRI). Contrary to MRI tagging techniques, an advantage of FT is its ability to analyze all cardiac chambers, regardless of their wall thickness. However, several technical challenges, including interstudy repeatability of FT techniques need to be investigated and this is the aim of our study.

Methods: We studied 10 healthy individuals (59 ± 9 years, 4 females), who underwent 2 MRI exams, within two weeks. For each exam, cine short-axis slices in left ventricular (LV) basal, mid- and apical locations were analyzed, by the same operator, using a custom FT software to extract: 1) radial thickening (Err), 2) circumferential strain (Ecc), and 3) endocardial radial motion (Erm) global peaks. Briefly, the FT, based on spatial correlation, was applied to the endocardial and epicardial contours initially drawn on a single phase of the cardiac cycle. Reproducibility between the 2 MRI exams was studied using Bland-Altman analysis, and consistency of our strain values was studied in terms of associations with age.

Results: Bland-Altman analysis revealed low bias for comparison between the 2 exams, especially for Ecc and Erm (mean bias [$\pm 1.96 \times$ standard deviation] were: 0.02 [-0.11,0.14]% for Err, 0.00 [-0.04,0.05]% for Ecc, 0.00 [-0.05,0.06]% for Erm). As expected, strain magnitudes, averaged over the 2 MRI exams decreased with age, resulting in the following correlation coefficients: $r = -0.59$ for Err, $r = -0.51$ for Ecc, $r = -0.53$ for Erm.

Conclusions: The application of an automated FT on cine data commonly acquired during standard MRI exams provided consistent and reproducible LV myocardial strain measurements. Extending such study to left atrium and right ventricle might be of major clinical usefulness, since regional function of such chambers remains poorly explored because of the lack of robust tools.

Speckle Tracking Analysis for Early Detection of Cardiotoxicity in Breast Cancer Patients

Cinzia Lorenzini, Claudio Lamberti, Michele Aquilina

DEI, University of Bologna, Bologna, Italy
IRST, Meldola, Italy

S35

Breast cancer and cardiovascular diseases are serious concerns for public health worldwide. The efficacy of anthracycline agents is, in patients with breast cancer, limited by serious side effects including cardiotoxicity. Echocardiography is the method of choice for the evaluation of patients before, during, and after cancer therapy. The use of 3D echocardiography has been shown to improve the accuracy and reproducibility of the left ventricular ejection fraction (LVEF) and may be preferable to 2D techniques. Although in clinical practice LVEF is considered the main parameter to evaluate cardiac function, it is not sufficiently sensitive to detect subclinical or regional myocardial dysfunction. The aim of this retrospective study was to detect early cardiotoxicity by speckle tracking analysis. We analyzed 2D and 3D echocardiographic datasets (2DE and 3DE) in 65 patients treated for breast cancer with anthracycline and trastuzumab. We compared the temporal variations of LVEF obtained analyzing 2D and 3D datasets and of the strain values computed before, during and after chemotherapy administration. In addition, in a subgroup of 45 patients a complete echocardiographic examination was performed 6 months after completion of therapy. Following clinical definition of cardio-toxicity onset (reduction of the LVEF, major than 10 percentage points, or to an absolute value $< 53\%$) the definition varies depending on the method used to compute LVEF (16.9% by 2DE and 50.8% by 3DE). Thirty-three patients developed cardiotoxicity. Nine of them showed a reduction of longitudinal and radial strain values before LVEF reduction at the 16th week. Through 3D speckle tracking analysis early diagnosis of the cardio-toxicity onset seems achievable allowing the planning of cardio protective therapy without interrupting chemotherapy administration.

Comparison of Novel Image Fusion Algorithms for Echocardiography and Cardiac Computed Tomography

Tim Nordenfur, Aleksandar Babic, Ivana Bulatovic, Anders Giesecke, Jonaz Ripsweden, Eigil Samset, Reidar Winter, Matilda Larsson

Medical Engineering, KTH Royal Institute of Technology
Stockholm, Sweden

S35

Aims: Treatment decision in patients with coronary artery disease can be based on stenosis morphology from coronary computed tomography angiography (CCTA) and hemodynamic effect from 3-dimensional echocardiography (3DE). Visualization of 3DE and CCTA in a single fused image might provide incremental diagnostic value. The aim of this study was to develop and compare novel 3DE/CCTA image fusion algorithms.

Methods: 13 patients with coronary artery disease underwent CCTA (Light Speed VCT XT, GE Healthcare) and 3DE (Vivid E9, GE Healthcare). The left-ventricular (LV) endocardium was segmented in 3DE using EchoPac 4D Auto-LVQ and in CCTA using a model-based edge-detection algorithm. The CCTA and 3DE images of matching cardiac phase were rigidly fused in three different ways: *ICP*: Iterative Closest Point alignment of the LV meshes. *3ch+base*: alignment of the three-chamber planes, mitral-apex lines and mitral centers. *3ch+apex*: alignment of the three-chamber planes, mitral-apex lines and apices. Fusion quality was quantified by the distances between corresponding CCTA and 3DE features, as identified by a cardiologist before fusion.

Results and conclusions: Each of the three developed algorithms performed fusion within an error margin of 1-2 cm for any landmark, as shown in the table. The results indicate that CCTA/3DE image fusion is feasible and provides anatomically correct results. The two three-chamber-based algorithms performed better than the ICP-based, possibly due to the large differences in LV shape between CCTA and 3DE images, suggesting that a landmark-based approach is to be preferred. The figure shows a fused image of one patient's coronary artery tree from CCTA and LV endocardium from 3DE.

Landmark error for each proposed image fusion algorithm			
Feature	Distance (mean \pm SD, $n = 13$)		
	ICP	3ch+base	3ch+apex
apex (cm)	1.4 \pm 0.6	1.6 \pm 0.6	0.9 \pm 0.4
mitral center (cm)	1.2 \pm 0.6	0.9 \pm 0.4	1.2 \pm 0.3
aortic center (cm)	2.5 \pm 1.0	1.6 \pm 0.9	2.0 \pm 0.6
mitral-apex line (deg)	10.2 \pm 6.8	6.8 \pm 3.8	6.8 \pm 3.8



Spectral Analysis of Electroanatomical Maps for Spatial Bandwidth Estimation as Support to Ablation

Margarita Sanromán-Junquera, Inmaculada Mora-Jiménez, Arcadio García-Alberola, José Luis Rojo-Álvarez

Universidad Rey Juan Carlos
Fuenlabrada (Madrid), Spain

S35

Introduction and Aim. Spatial and temporal processing of intracardiac electrograms (EGM), both in Cardiac Navigation Systems (CNS) or Electrocardiographic Imaging, provide with relevant information on the arrhythmia mechanism for supporting ablation. In our previous work, we first proposed Manifold Harmonics Analysis (MHA) for establishing the spatial sampling rate in ElectroAnatomical Maps (EAM) accounting for anatomical and bioelectrical features (e.g., voltage or activation time). Although a quantitative framework was provided, the sampling rate was computed by comparing the number of relevant coefficients in MHA with a simplified version of the EAM in terms of the EAM reconstruction error. Here, we propose a theoretically founded method for spectrum representation in terms of spatial frequencies from MHA. This new approach can determine the minimum number of EGM registered at different spatial positions for accurate EAM with a cut-off spatial bandwidth.

Methods. The EAM spectrum magnitude is obtained by cross-correlation between the original spatial anatomical and bioelectrical features, and the corresponding spectral coefficients projected onto the manifold harmonic basis (MHB). The reconstructed EAM is obtained by incrementally considering the spectral coefficients projected onto the MHB. The cut-off spatial frequency is computed according to a threshold value ($TH \in [0, 1]$), accounting for the EAM reconstruction quality.

Results. TH was scrutinized in high quality anatomical meshes from tomography images, and in simulated and real EAM from CNS. Experiments showed $TH > 0.95$ required to obtain accurate both anatomical meshes and EAM. Both simulated and real EAM showed strong dependence of the cut-off spatial frequency on the arrhythmia mechanism. Figure 1 shows an example of unipolar voltage EAM reconstruction for a $TH=0.95$ and $TH=0.99$.

Conclusions. The new proposed MHA methodology opens the field towards a new set of fundamental tools for principled spatio-feature analysis of EAM and improved knowledge on arrhythmia mechanisms.

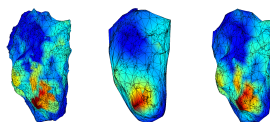


Figure 1: Unipolar voltage EAM (left), and reconstructed ones with a $TH=0.95$ (middle) and $TH=0.99$ (right).

Cardiology eHealth Messages Routing Policies Management Driven by Dynamic Bayesian Networks

Nachoua Guizani*, Jocelyne Fayn

University of Lyon
Lyon cedex 08, France

The emergence of eHealth, ubiquitous computing and the proliferation of mobile healthcare computing devices has led to a large increase in message transfers among remote healthcare providers and patients. Different scenarios in cardiology, such as the follow up of chronic heart diseases at home, monitoring and post-surgery rehabilitation of cardiovascular patients, etc., obviously require intelligent and reliable eHealth messages communication policies that should proactively react in case of unexpected events (exceeded deadlines for reply) or context changes (cardiologist unavailability, chest pain aggravation). Hence, such routing policies should contribute to reduce the overall cardiac mortality and morbidity, especially in emergency situations. In this context, we propose a model-driven system providing an orchestration of information systems and services for the support of context-aware, personalized, intelligent and adaptive eHealth message routing policies. Several contextual data from the source (patient clinical signs/social environment), the target (healthcare professional localization/trust level), and the message content itself (priority, type) are taken into account for processing the message transfers. The message content is compliant with the HL7 Reference Information Model specifications. Based on artificial intelligence methods, the system reasons about contextual data to determine the routing parameters requirements (healthcare professional profile type, routing means (SMS, mail, etc.)), and searches for the most relevant destinations that are closest to the inferred profile type. It also supervises unexpected events and dynamic context changes (localization) and adapts its routing decisions and behaviors accordingly. As a consequence, and because of the dynamicity that characterizes some contextual data and message statuses of the healthcare workflow chain, the messages may follow several routing policies over time. We finally demonstrate the process of inferring routing parameters in function of different context values by means of Dynamic Bayesian Networks and we also highlight the routing policy adaptation process.

S41

Designing Reliable Cohorts of Cardiac Patients Across MIMIC II and eICU

Catherine* Chronaki, Abdullah Chalin, Roger Mark

HL7 Foundation
Brussels, Belgium

S41

Background/Objective: i2B2/SHRINE proposed the notion of patient cohorts as first class objects that can be shared, grouped, and recruited for research purposes. Since 2003, MIMIC-II serves as a valuable resource to researchers worldwide offering detailed anonymized patient data from Intensive Care Units (ICU). The eICU data warehouse developed to evaluate the Philips eICU program in 30+ states/150+ ICUs supports research initiatives on patient outcomes, trends, and best practice protocols. The aim of this work is evaluate use of standard terminologies and nomenclature such as LOINC for lab observations and ICD9-CM/SNOMED-CT for diagnosis in designing reliable cohorts for cardiac patients across MIMIC-II and eICU.

Methods: Patients in MIMIC-II and eICU with a primary diagnosis of the circulatory system (ICD9CM 390–459) were selected. A correspondence of lab observations in MIMIC-II (75% with LOINC) and eICU was created and quality assured. Based on the ICD9-CM to SNOMED-CT map of the National Library of Medicine, correspondence of ICD9-CM codes to SNOMEDCT terms was sought. For ICD9 codes with multiple maps or is not specified elsewhere, the diagnostic strings in eICU and the ICD9 codes of highest frequency were employed to identify the appropriate SNOMED-CT code.

Results: MIMIC II v3.0 and eICU share a common set of 122 laboratory observation types and 714 diagnostic codes in ICD9CM (82 for primary cardiac discharge diagnosis). A unique SNOMED-CT code can be found in 36% of the ICD9 cardiac codes (71% of those in common). For the rest, rules from medical guidelines can be helpful. **Conclusions and Next Steps:** Structured data on Diagnoses (ICD9-CM) and Labs (LOINC) along with demographics can define complex cohorts of cardiac patients. Combining these in selecting SNOMED-CT terms, can select cohorts of higher quality and reliability and provide insights on MIMIC III, a public, multi-center, international data archive for critical care research.

Web Application for Data Exchange and Follow-up in Heart Rate Turbulence

Cristina Soguero-Ruiz, Alfonso Sánchez-Caro, Inmaculada Mora-Jiménez, Luis Lechuga-Suárez, Arcadi García-Alberola, José Luis Rojo-Álvarez*

Spain

Background: The technical differences when working with several Hospital Information Systems (HIS) exhibit some interoperability limitations. To overcome this drawback, it is necessary to develop web technologies based on clinical knowledge models (archetypes). On the other hand, cardiovascular risk stratification is widely used in clinical practice. However, many predictors of cardiac risk indices, proposed in the literature, are rarely used in clinical practice due to the lack of scientific evidence and data support. Heart Rate Turbulence (HRT) is an example of a sudden cardiac death prediction index with clear and concise guidelines. Objective. We developed a web application based on a built HRT archetype for data exchange and follow-up for HRT domain. The goal was to build a web tool to collect HRT related data from different HIS to clinical decision support.

Materials and Methods: CEN/ISO EN13606 standard aims to define an information architecture for communicating EHR between heterogeneous systems. It is based on a dual model that defines separation between information and knowledge. The information is supported by a Reference Model containing the basic entities for representing any information of a specific domain. The knowledge is supported by an Archetype Model (archetype), a structured and constrained combination of entities of a Reference Model that represents a particular clinical concept. The nodes (clinical terms) and constraints (such as ranges of allowed values) of the built archetype are used to define the HRT domain in the web application. This web application not only allows to collect and manage HRT data, but also it provides functionalities like editing or viewing the information related to a patient.

Conclusions: HRT follow-up to be used by the clinical community independently of technical limitations is obtained by combining web technologies and archetypes. Archetypes achieve semantic interoperability when exchanging data from different HIS.

S41

A Context-Aware Approach for Wellness Monitoring of Cardiac Patient using Social Network Service Expansion

Abdur Rahim Mohammad Forkan*, Ibrahim Khalil

RMIT University and NICTA
Australia

S41

Cardiac disease is very common in older adult around the world. We propose a framework for wellness monitoring of an elderly patient who leave alone in home and suffers from cardiac disease. The focus here is the integration of context-aware social networking services with conventional remote monitoring services by utilizing a common scalable platform. Using social networking services the goal is to expand patient's social linkage using similarity in cardiac conditions. Here we propose a cloud-based context-aware framework that captures heart rate, ECG, activity, calories burned using fitbit device and ECG sensors. The raw data are sent the Amazon cloud where data is converted to high level context. Using social networks this high level context information is send to patient's friends, family and doctors who are interested to know about his/her health condition. The interested parties get notified by Facebook when the context-aware system detects any changes. That is, using this platform a cardiac patient who live alone and need continuous monitoring, not only always get connected with virtual community by means of personal information but also using his health information. To retain the privacy context data is only sent to the people of known virtual community. This is a new architectural framework that utilizes the context data generated by wearable sensors to create interesting social networking services. The system is also designed to promote cardiac patients to interact with their community of interest using various context-aware social services.

Interactive Progressive-based Approach to Aid the Human Interpretation of the 12-lead Electrocardiogram

Andrew Cairns, Raymond Bond*, Dewar Finlay, Cathal Breen, Daniel Guldenring, Robert Gaffney, Patrick Henn, Aaron Peace

Ulster University
Newtownabbey, Co. Antrim., United Kingdom

Background: Cardiovascular disease (CVD) kills 17 million people per year. The 12-lead Electrocardiogram (ECG) is an important diagnostic support tool. 33% of ECGs are incorrectly interpreted and clinicians often impulsively provide a diagnosis based on their first impression/intuition. It is therefore imperative to optimise how physicians interpret the 12-lead ECG. An ECG currently presents the reader with the 12 lead signals on paper, each lead having a 2.4 second duration and a rhythm strip with 9.6 second duration. This presentation format delivers a significant cognitive load. We argue that the potential to reduce ECG interpretation errors will be advanced by using interactive touch screen devices, which would facilitate a sequential and systematic approach to aid ECG interpretation.

Methods: Following a literature review and interviews with expert clinicians and teaching professionals, we developed a set of interactive questions and prompts to guide a reader through a series of tasks when interpreting an ECG. This has been named 'Interactive Progressive based Interpretation' (IPI) and abstracted in the PDF supplement. The IPI system was implemented using emerging web technologies, i.e. HyperText Markup Language (HTML5), JavaScript and Cascading Style Sheets (CSS3). Using this model, the 12-lead ECG is segmented into five parts and presented over five web pages. Page one presents the rhythm strip, page two presents lead II, page three presents the limb leads, page four presents the precordial leads and the last page presents the full 12-lead ECG. Each displays a prompt and a series of interactive questions that require input before the reader can 'progress' to the next page. Refer to <http://tinyurl.com/IPI-system-demo>.

Conclusions: A new model has been proposed to aid ECG interpretation where interpreters systematically and sequentially interpret the 12-lead ECG as a series of sub-tasks. We hypothesise that this will reduce the number of errors and increase diagnostic accuracy.

S41

Dynamic Coupling Between Ventricular Repolarization Duration and RR-Interval Phase-Rectification Analysis in Chagas Disease

Olivassé Nasario-Junior, Paulo R Benchimol-Barbosa, Roberto Coury Pedrosa, Jurandir Nadal

Universidade Federal do Rio de Janeiro, Rio de Janeiro, Brazil

Dynamic ventricular repolarization duration (VRD) vs. RR-interval coupling relates to tachyarrhythmia vulnerability, particularly in chronic Chagas disease (ChD). Phase-rectification of RR-interval series separates acceleration (AC) and deceleration (DC) phases (Figure 1), reflecting sympathetic and parasympathetic influences on heart rate, respectively. This study investigated VRD and phase-rectification-driven RR-interval coupling to assess dynamic

repolarization adaptation in healthy and chronic ChD subjects. Healthy sedentary (Control, $n = 11$) and ChD ($n = 11$) groups were studied. All were in sinus rhythm and underwent 60 min head-up tilt table test. ChD group were submitted to MIBG scintigraphy to assess cardiac sympathetic innervation. Histogram of RR-interval series was calculated, with 100 ms class, ranging

from 600 ms to 1200 ms. For each class, mean of normal RR-intervals (MRR) and mean of the peak-to-peak R-to-T wave interval (MRT), representing VRD, were calculated and analyzed in the whole series (T), and in DC and AC phases. Linear regression model of MRT vs. MRR were computed for each group, and respective slopes calculated ($sMRT_T$, $sMRT_{DC}$ and $sMRT_{AC}$). Correlation coefficients were tested before analysis, and Student t-test compared groups ($\alpha < 0.05$). MRT_T , MRT_{AC} and MRT_{DC} significantly increased as a function of MRR in all groups, and slopes were significantly different between groups in phase-matched comparisons (Table 1). All ChD subjects presented reduced cardiac MIBG uptake. In a linear model of VRD RR-interval coupling, average RT-interval increases as a function of RR-interval, in both ChD and healthy subjects during tilt-table test. However, in ChD subjects showing sympathetic denervation, average RT-interval is longer and exhibited a flatter slope in a linear RR-interval coupling model.

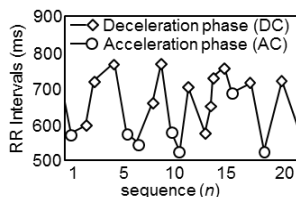


Fig 1. DC and AC phases represented in respective RR-intervals.

Table 1 – Slopes of MRT vs. MRR regression lines and intervals duration per group:

Group	$sMRT_T$	$sMRT_{DC}$	$sMRT_{AC}$	MRR(ms)	MRT(ms)
Control	$0.156 \pm 0.005^{\ddagger}$	$0.161 \pm 0.007^{\ddagger}$	$0.158 \pm 0.005^{\ddagger}$	$806 \pm 72.4^{\ddagger}$	$265 \pm 11.6^{\ddagger}$
ChD	$0.115 \pm 0.009^{\ddagger}$	$0.110 \pm 0.010^{\ddagger}$	$0.132 \pm 0.002^{\ddagger}$	$906 \pm 51.6^{\ddagger}$	$273 \pm 10.6^{\ddagger}$

Values are mean \pm SD; ‡ p < 0.05 intergroup comparison

Optimizing the Short- and Long Term Regression for QRS Detection in Presence of Missing Data

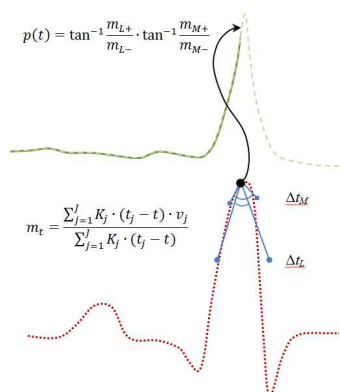
Piotr Augustyniak

AGH-University of Science and Technology
Krakow, Poland

S42

Although automatic detection of the heart beats has been investigated since the beginning of digital electrocardiography, current applications require robust algorithms performing well independently on missing data, local distortions or uneven lead connection. Our new algorithm uses a detection function based on the value of angle between two regression segments adjacent in a given point. The optimization of these segments, representing long-term and short-term acceleration of heart activity, is presented in this paper.

The algorithm is based on four simple steps: (a) iterative linear regression based on samples selected in two windows of different length Δt_L and Δt_M (b) calculation of series of angle values between regression segments adjacent to each point, (3) expressing the synchronicity in both series as a detection function and (4) adaptive thresholding of the detection function.



Regression-based QRS detector

The method was tested with original records from MITDB and their variants calculated by (a) resampling to 200-500 Hz, (b) inserting randomly distributed isolated outliers and (c) deleting groups of 1 to 4 adjacent samples. The problem addressed in this paper was proper definition of length for long- and short-term activity yielding best performance of the detection expressed by sensitivity and specificity. The performance was tested for different combinations of length values and measured by the area under the ROC curve.

QRS detection accuracy

signal source	Se %	Sp %
orig. MITDB	99.91	99.87
MITDB @ 200Hz	99.88	99.86
outliers 100ms	99.71	99.80

For the normal ECG, the values yielding the highest area of ROC for sensitivity and specificity of QRS detection are respectively: $\Delta t_L = 61$ ms and $\Delta t_M = 20$ ms. Thanks to sampling-independent internal data representation, the detection supports ECG records of wide range of sampling frequency and shows consistently high performance in presence of outliers or missing data in the signal.

supports ECG records of wide range of sampling frequency and shows consistently high performance in presence of outliers or missing data in the signal.

Robustness of the Segmented-beat Modulation Method to Noise

Angela Agostinelli, Corrado Giuliani, Sandro Fioretti, Francesco Di Nardo, Laura Burattini*

Università Politecnica delle Marche
Ancona, Italy

S42

Typically, an electrocardiographic (ECG) signal is corrupted by noise of different nature, mainly baseline wander (BW), electrode motion artefact (EM) and muscular artefact (MA). To get rid of it, the ECG is usually pre-filtered by application of linear techniques. However, the noise frequency-components that fall within the ECG frequency band survive pre-filtering and may change its morphological characteristics, limiting the ECG clinical usefulness. In these cases further signal processing is required. Template-based techniques may help, but most of them have the major limit of not being usually able to reproduce physiological heart-rate variability and morphological variability. Recently, a new template-based filtering procedure, the segmented-beat modulation method (SBMM), has been presented by ourselves to overcome such limit by adaptively adjusting each reconstructed beat to the original beat-length. More specifically, the SBMM first segments each cardiac beat into QRS and TUP segments, respectively independent and proportional to preceding RR interval, and then performs a modulation/demodulation procedure on the TUP segments. The SBMM has not being tested yet in noisy conditions. Thus, the aim of the present study was to evaluate the SBMM robustness to noise. The SBMM was applied to one synthetic and 18 clinical ECG tracings before and after corruption with BW, EM and MA. Results indicate that, in all cases, clean ECGs are estimated with errors <0.15 mV, typically greater in the QRS than in the TUP segments ($0-123 \mu\text{V}$ vs. $0-25 \mu\text{V}$, $p<10^{-5}$). Moreover, MA little affected ECG estimation ($5-46 \mu\text{V}$), while BW and EM caused higher errors ($4-101 \mu\text{V}$ and $10-123 \mu\text{V}$, respectively) especially in the QRS segment which however remained quite small. In conclusion, the SBMM proved to be a useful tool for providing clean ECG estimations of tracings affected by the most common kinds of noise, which are BW, EM and MA.

Spectral Analysis of QT Interval Variability and Muscle Sympathetic Nerve Activity in Normal Subjects During Head-Up Tilt

Fatima El-Hamad, Elisabeth Lambert, Mathias Baumert*

Australia

Beat-to-beat variability of the QT interval (QTV) is sought to provide an indirect non-invasive measure of sympathetic nerve activity, but a formal quantification of this relationship has not been provided. In this study we used power contribution analysis to study the relationship between QTV and muscle sympathetic nerve activity (MSNA). Here, ECG and MSNA were recorded in 10 healthy subjects in the supine position, followed by a 40° degree head-up tilt. Power spectrum analysis was performed using a linear autoregressive model with two external inputs (RR and MSNA). Total and low frequency power of QTV was decomposed into contributions by RR, MSNA, and sources independent of RR and MSNA. Results show that the percentage of MSNA power contribution to QT is very small, and does not change with tilt. The RR power contribution to QT power is notable and decreases with tilt, while the greatest percentage of QTV is independent of RR and MSNA in both, the supine position and after head-up tilt. In conclusion, beat-to-beat QTV in normal subjects does not appear to be significantly affected by the rhythmic modulations observed in MSNA. Therefore MSNA oscillations may not represent a useful surrogate for cardiac sympathetic nerve activity or, alternatively, sympathetic influences on QTV are complex and not quantifiable with linear shift-invariant autoregressive models.

S42

A Noise Robust QRS Delineation Method Based on Path Simplification

Tomás Teijeiro*, Paulo Félix, Jesús Presedo

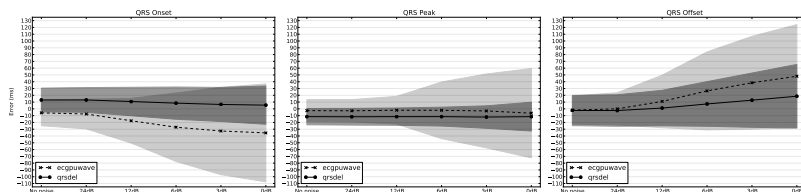
Centro Singular de Investigación en Tecnoloxías da Información (CITIUS), University of Santiago de Compostela, Spain

Aims: In this work we present *qrsdel*, a new multi-lead algorithm for the delineation of QRS complexes in ECG signals. The main objective is to provide a robust method that gives acceptable results even under severe noise conditions in the input signal, as often happens in continuous bedside or home monitoring, trying to overcome the difficulties found by classical algorithms when applied in scenarios presenting a low signal quality compared with the training databases.

Methods: Our method is based on relevant point selection using a path simplification algorithm, assuming a waveform representation as the sequence of linear segments between every pair of relevant points. Then, a clustering strategy is applied, using as features the slope of each segment and its distance to an estimation of the QRS peak. This result is combined with a qualitative description of the waveform in order to select the most promising segments to include inside the QRS limits. Finally, multi-lead aggregation is obtained by combining the single-lead limits ordered by a signal quality estimator.

Results: The validation was performed by adding electrode motion noise to the records of the QT database at different Signal-to-Noise ratios, and then comparing our proposal with the *ecgpuwave* approach. While *ecgpuwave* experiences a sensitivity degradation up to the 15% and an increase in the standard deviation of the errors in a factor of 4, *qrsdel* only reduces the sensitivity in a 1%, and the standard deviation increases up to a factor of 2 at the highest noise levels.

Conclusions: A noise robust QRS delineation method can be very valuable in poorly controlled monitoring environments, and therefore we have released our algorithm as free software. We also published the source code needed to generate the test database and replicate the experiments performed in this work.



Delineation error and standard deviation comparison between *qrsdel* and the reference *ecgpuwave* algorithm.

T-P Interval Estimation in Case of Overlapping Waves

Hervé Rix*, Aline Cabasson, Michal Kania, Olivier Meste

Univ. Nice-Sophia Antipolis
Sophia Antipolis, France

Assuming two positive overlapping signals, with known shapes, the proposed method estimates the distances between mean positions, and width and area ratios. The data are two profiles representing the component shapes: no parametric model is assumed. The algorithm seeks shape equality (using the Distribution Function Method) between a linear combination of observation and first component, and the second component, in function of the area ratio. At the minimum shape difference the three parameters (distance between components, scaling factor and area ratio) are estimated. After theory, simulations are presented on Gaussian signals. As examples of the robustness, for SNR=10 dB, the CV on distance estimation is 2% when the distance (expressed in standard deviation of the first component), scaling factor and area ratio are respectively fixed to 2, 1 and 1; CV=3.3 % when these values are fixed to 1.5, 0.3 and 0.6. Then, the method was applied on ECG signals from BSPM device during exercise on healthy people. The aim is to get time distance between each T-wave and the P-wave of the following beat, on a given lead, even in case of overlapping. Shape and width of the T-wave were shown to be constant before P-wave interference. So such a real T-wave was taken as first component model. Due to high noise level, the shape of the P-wave model is not crucial: assuming the same shape for the second component gave good results. Finally, all the T-P intervals between the mean positions of the waves were estimated. In case of overlapping, knowing P-wave position will improve (in a further work) PR estimation.

S42

Quantitative Comparison of Two Cardiac Electrical Imaging Methods to Localize Pacing Sites

Jaume Coll-Font*, Petr Stovicek, Dana H Brooks, Peter M van Dam

Northeastern University
Boston, United States

S43

Cardiac electrical imaging (CEI, AKA Electrocardiographic Imaging (ECGI)) has great potential in for pre-procedure planning for ventricular ablation. However it is an ill-posed problem and thus highly sensitive to noise. On the other hand, the depolarization sequence has a strong structure which can be used to characterize temporal dynamics to improve inverse solutions. Our groups (Radboud University Medical Center, RUMC, and Northeastern University, NU) have worked separately on this problem, each one taking a distinct approach. RUMC used a restrictive temporal model that imposes a known step function waveform on the transmembrane potentials. This reduces the unknowns to the time shift of these step functions at each position on the heart. The inverse problem is then non-linear, requiring initialization, done via the fastest route algorithm. The NU approach is more data-driven, fitting a high-dimensional spline with a small number of knot-point parameters to the body surface potentials, imposing smoothness in time, and using that temporal structure in the reconstruction. The result is a potential-based inverse at few reference times which characterizes the complete sequence. We present a comparison of both approaches using data from ventricular pacing of 3 subjects. We used 120 body surface ECG measurements, and a partially accurate geometry of the torso and heart derived from CT of the heart region only. Pacing locations came from the CARTO system. We report the results in terms of pacing site localization accuracy. RUMC method generally located initial activation more accurately and stably than NU (mean 31.58 and 36.79 mm respectively). However, the initialization step of RUMC was the most accurate (mean 30.25mm), suggesting that use of an inaccurate volume conductor model may limit inverse accuracy, and that further efforts are needed to develop hybrid methods to cope with this realistic level of geometric uncertainty.

In-vivo Evaluation of Reduced-Lead-Systems in Noninvasive Reconstruction and Localization of Cardiac Electrical Activity

Matthijs JM Cluitmans, Joël MH Karel, Pietro Bonizzi, Monique MJ de Jong, Paul GA Volders, Ralf LM Peeters, Ronald L Westra

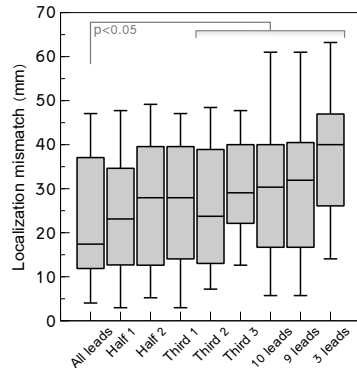
Maastricht University, Maastricht, the Netherlands

Noninvasive imaging of electrical activity of the heart has increasingly gained attention over the last decades. Epicardial potentials can be reconstructed from a torso-heart geometry and body-surface potentials recorded from tens to hundreds of body-surface electrodes. However, it remains an open question how many body-surface electrodes are needed to accurately reconstruct epicardial potentials.

In a canine model, we reconstructed epicardial electrograms from 39 beats, investigating the use of a full-lead system, consisting of 169 well connected body-surface electrodes, and reduced-lead systems: using half or a third of the electrodes, or a minimalistic set of the default 12-lead ECG (10 or 9 electrodes). Invasively recorded epicardial electrograms were used to evaluate the quality of the reconstructed electrograms. In 27 paced beats, also the mismatch between the known pacing location and reconstructed location of earliest activation was compared.

Correlation coefficients indicate that the quality of the reconstructed electrograms remains stable from 169 (full set) to 59 (a third) electrodes, and decreases with fewer electrodes. The mismatch between the detected origin of a beat and known pacing location increases with fewer electrodes, see Figure. However, it is remarkable that with only 9 or 10 electrodes, the median mismatch between detected and known pacing location is 30mm, only marginally higher than when half of the electrodes is used.

This study indicates that for specific goal such as detecting the origin of an extrasystolic beat, a lower number of body-surface electrodes can provide non-invasive reconstructions that can be still useful in clinical practice. However, especially when using only a 12-lead setup as suggested by others, it is important to realize that although the median results are reasonable, there is a large spread of the error, up to a 65mm mismatch.



Local Conduction Velocity Mapping for Electrocardiographic Imaging

Corentin Dallet*, Mark Potse, Laura Bear, Josselin Duchateau, Nejib Zemzemi, Valentin Meillet, Yves Coudière, Rémi Dubois

Electrophysiology and Heart Modeling Institute (IHU LIRYC), Bordeaux, France
Pessac, France

S43

Introduction: Slow conduction is a well-known pro-arrhythmic feature for tachycardia and fibrillation. Cardiac conduction velocity (CCv) mapping can be extremely helpful for investigating unusual activation patterns. Although methods have been developed to estimate velocity from ex-vivo preparations (e.g. from optical mapping recordings), the estimation of velocity from in-vivo electrograms (EGMs) remains challenging.

Aim: This paper presents a new method specifically designed for EGMs reconstructed non-invasively from body surface potentials using electrocardiographic imaging (ECGI). The algorithm comes in two versions: a computationally efficient version which assumes a locally linear activation wavefront (CCv1), and the second assuming a local quadratic wavefront (CCv2).

Methods: Two datasets were used: 1) from a realistic heart model providing i) the action potentials (APs) at epicardial points ($n=1629$), ii) reconstructed EGMs using ECGI on body surface electrodes ($n=252$), and iii) the local velocity (reference) for 3 patterns of paced activation; and 2) from an anesthetized pig where high-density potential maps were recorded simultaneously on the torso ($n=170$) and on the epicardium of the ventricles ($n=239$) during 10 different epicardial pacing protocols. Wavefront velocities were computed and compared to the reference for the local angular (θ_{error}) and velocity (v_{error}) errors.

Results: On the simulated data, CCv1 and CCv2 gave comparable results when applied directly to both the APs ($\theta_{\text{error}} = 10.62^\circ$ vs 10.52° , $v_{\text{error}} = 0.36$ m/s vs 0.35 m/s) and the reconstructed EGMs ($\theta_{\text{error}} = 38.67^\circ$ vs 38.94° , $v_{\text{error}} = 2.80$ m/s vs 2.78 m/s). For reconstructed EGMs in pig, CCv1 performed better than CCv2 ($\theta_{\text{error}} = 37.44^\circ$ vs 41.65° , $v_{\text{error}} = 1.85$ m/s vs 2.01 m/s) when compared to directly recorded epicardial data.

Conclusions: The proposed method allows the assessment of wavefront velocities from ECGI data. On the experimental data, CCv1 gave better results and is more computationally efficient.

Inverse Localization of Ischemia in a 3D Realistic Geometry: A Level Set Approach

Carlos E Chávez, Felipe Alonso-Atienza, Nejib Zemzemi, Yves Coudière, Diego Álvarez

Carlos III University of Madrid
Leganés, Madrid, Spain

S43

Background. The reconstruction of cardiac ischemic regions from body surface potential measurements (BSPMs) is usually performed at a single time instant which corresponds to the plateau or resting phase of the cardiac action potential. Using a different approach, we previously proposed a level set formulation that incorporates the knowledge of the cardiac excitation process in the inverse procedure, thus exploiting the spatio-temporal correlations contained in the BSPMs.

Aim. In this study, we extend our inverse level-set formulation for the reconstruction of ischemic regions to 3D realistic geometries, and analyze its performance in different noisy scenarios.

Methods. We use a 3D mesh of torso and heart surfaces obtained from a CT-scan of a 43 years old woman. The heart and torso domains are discretized using finite element triangular meshes of 5842 and 719 nodes, respectively. BSPMs are corrupted by AWGN with different signal-to-noise ratios (SNRs).

Results. Our method is benchmarked against zero-order Tikhonov regularization (see comparative Table). The inverse reconstruction of the ischemic region is evaluated using the correlation coefficient (CC), the sensitive error ratio (SN), and the specificity error ratio (SP).

Conclusions. Our algorithm outperforms zero-order Tikhonov regularization, specially in highly noisy scenarios (low SNRs).

Comparative quality metrics

	Tikhonov			Level Set		
SNR	CC	SP	SN	CC	SP	SN
5	0.59	0.43	0.34	0.77	0.22	0.21
10	0.64	0.37	0.30	0.80	0.19	0.19
15	0.68	0.29	0.33	0.79	0.20	0.19
20	0.74	0.22	0.27	0.76	0.28	0.17

Effect of the Torso Conductivity Heterogeneities on the ECGI Inverse Problem Solution

Najib Zemzemi*, Laura Bear, Mark Potse, Corentin Dallet, Yves Coudière, Remi Dubois, Josselin Duchateau

NRIA Bordeaux Sud-Ouest
Talence, France

S43

Aims: The effect of torso conductivity heterogeneities on the ECGI inverse problem solution is still subject of debate. In this study we present a method to assess the effect of these heterogeneities.

Methods: We used numerical simulations to construct reference data. The torso geometry was constructed from a CT scan of a 43-years-old woman. The geometry contained the body surface, the lungs, the bones, and the heart surface. We distinguished three different conductivity values: lungs, bones, and the rest of the tissue. In order to construct the body surface potentials, we used the bidomain model in the heart and the Laplace equation with heterogeneous conductivities in the torso. After adding different levels of noise on the body surface potentials (BSP), and without filtering, we solved the inverse problem based on an optimal control approach using a first order Tikhonov regularisation for both homogenous and heterogeneous torso conductivities.

Results: For zero value of noise, the mean values of the correlation coefficient (CC) and relative error (RE) were 0.95 and 0.26, respectively, for the heterogeneous inverse, whereas for the homogenous inverse CC was 0.88 and the RE was 0.48. Adding 0.5mV (respectively 1mV, 2mV) error on the BSPs comes with CC= 0.76 (respectively CC=0.59, 0.38) and RE=0.78 (respectively RE= 1.4, 2.7), whereas in the heterogeneous case, CC=0.71 (respectively CC=0.54, 0.35) and RE=0.70 (respectively RE= 1.5, 2.7).

Conclusions: For low values of error in the BSP measurements, the effect of torso heterogeneities is clear: there is a gain between 5 to 10% of accuracy in terms of CC and 10 to 20% in terms of RE if these heterogeneities are accounted for in the inverse model. This gain decreases when the noise in the BSP measurement increases.

Comparison of Temporal Dimensionality Reduction Methods for Constrained Inverse in Cardiac Electrical Imaging

Jaume Coll-Font*, Danila Potyagaylo, Walther Schulze, Olaf Doessel, Dana H Brooks

Northeastern University
Boston, United States

Cardiac electrical imaging, that is, reconstructing cardiac electrical activity from body surface measurements, is a technology with great potential. However, the ill-posedness of this problem continues to motivate the search for improvements on current methods to enhance attractiveness for clinical adoption. One direction for improvement is to better use the strong temporal structure of the cardiac electrical activation in the imaging model. Along those lines, Messnarz et al. introduced an algorithm that constrains the reconstructed transmembrane potential to be non-decreasing over time during QRS. This physiologically meaningful constraint reduces the solution space of the problem and regularizes the solution. However, this approach is computationally intensive and can become prohibitive as spatial and temporal resolution on the heart increase. Here we compare three distinct options to reducing the computational load: downsampling the measurements in time (M), linearly interpolating the potentials in time using the method of Huiskamp and Greensite (HG) and non-linearly interpolating the potentials with a spline-based method (SP). The data used were simulated transmembrane heart potentials that were forward propagated to the body surface in a densely sampled geometry. The resulting body surface potential simulations were corrupted with noise and the inverse computed using a much coarser mesh to take geometry errors into account. The results indicate that the downsampled version of the Messnarz algorithm generally performed better than the interpolation approaches. Within the interpolation methods, the non-linear approach had similar results to the downsampled case while the linear interpolation performed worse. For example, correlation coefficients between reconstructed activation maps and ground truth ranged from M: (0.62 - 0.84), HG: (0.49 - 0.87), SP: (0.37 - 0.76) On the other hand, the computational requirements of the spline interpolation method was much lower than the other two approaches, suggesting room for improving accuracy while maintaining the computational advantage.

S43

Synchronization of Respiratory, Heartbeat and Blood Pressure Signals: 3D Plots and Indices

E. Gatsori, G. Manis

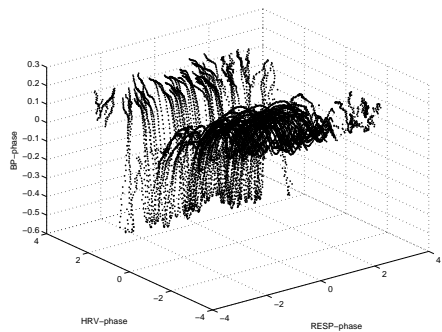
University of Ioannina, Dept. of Computer Science & Engineering
Ioannina, Greece

In coupled oscillating systems, “synchronization” means presence of certain relations between their phases and frequencies. Synchronization, also referred as “phase locking” or “coupling”, is widely used in experimental studies and the modeling of interaction between different physiological systems showing oscillating behavior.

In this paper we study the correlation of respiration, heartbeat and blood pressure signals in 3D space using phase coupling. To the best of our knowledge, it is the first time that the correlation of these signals is investigated in 3D space. We produce 2D and 3D phase plots and examine phase coupling in all cases. We calculate the mutual information which is a widely used metric for estimating such correlations between two signals. For examining signals in 3D space we compute the multivariate mutual information.

The multivariate mutual information is not a simple generalization of mutual information and reveals different information detecting the correlation among all three examined signals. Additionally to the common metrics for signal synchronization, we examined the use of the gradient, in order to extract and quantify the relations as depicted in the 3D plots.

Results showed us a stronger correlation between blood pressure and heartbeat signals and a relatively small correlation between respiratory and heartbeat signals, as well as between respiratory and blood pressure signals. Also, a very interesting observation is the strong correlation among all three signals which is very clear from the 3D phase plots and is also verified from both multivariate mutual information and the gradient.



3D Plot depicting the correlation of respiratory, heartbeat and blood pressure signals of a subject.

Comparison of Methods to Measure Baroreflex Sensitivity in Brugada Syndrome

Mireia Calvo*, Virginie Le Rolle, Daniel Romero, Nathalie Béhar, Pedro Gomis, Philippe Mabo, Alfredo Hernández

Université de Rennes 1
Rennes, France

Aim: Baroreflex sensitivity (BRS) is a valuable index to assess cardiovascular autonomic control and therefore to provide prognostic evaluation in many cardiac diseases. Although several methods have been developed to noninvasively capture spontaneous BRS, they are difficult to compare and often provide conflicting results. This study analyzed eight different BRS estimates obtained from a clinical series of patients suffering from Brugada syndrome, in order to quantify the agreement between measures.

Methods: Thirty-seven patients diagnosed with Brugada syndrome took part in a head-up tilt test while noninvasive blood pressure recordings were collected. The test was divided into three phases, leading to 111 BRS results for each method: i) supine rest for 10 minutes, ii) tilting with an inclination of 60° for 45 minutes or until the test was positive and iii) rest in supine position for 10 minutes. Eight BRS estimates were compared in all phases: (1) BRS+/- and (2) BRS-/- from sequence analysis, (3) BRS-LF, (4) BRS-HF, (5) BRS-LHF, (6) BRS-TF1 and (7) BRS-TF2 from cross-spectral analysis and (8) BRS-SD.

Results: Measures resulting from the sequence method failed to provide results in over 30 recordings, whereas BRS-SD and BRS-TF2 gave results in all cases. All methods captured a decrease in response to tilting, but BRS+/- and BRS-/- obtained higher BRS after the test with respect to baseline. Moreover, these estimates showed low agreement with the remaining methods based on intra-class correlation coefficient results (BRS+/-: $r = 0.21 \pm 0.12$, BRS-/-: $r = 0.27 \pm 0.15$). Assuming an age-associated reduction in BRS, which has been previously reported, the lowest Pearson's correlation coefficients came from sequence analysis results ($r = -0.28 \pm 0.03$).

Conclusions: Among the analyzed BRS estimates, those derived from sequence analysis showed a lower reliability when capturing baroreflex function in a clinical series of Brugada syndrome patients.

S44

Heart Failure, End-Systolic Pressure-Volume Relation

Rachad M Shoucri

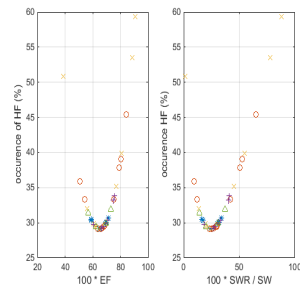
Royal Military College of Canada
Kingston, Ontario

The problem of heart failure with normal or preserved ejection fraction (HFpEF) has been the subject of numerous studies. Mathematical relations between ejection fraction (EF) and the parameters describing linear or non-linear end-systolic pressure-volume relation (ESPVR) have been derived that point to the possibility of relations between observed percentage of heart failure (HF) and EF on the one hand, and indexes derived from the ESPVR on the other hand. This study shows that important information can be derived from the ESPVR that can give better insight into the mechanics of ventricular contraction. Applications to clinical data published in the literature show the consistency of the mathematical formalism used to calculate the non-linear ESPVR, which is based on the theory of large elastic deformation of the myocardium.

The figure shows two relations between percentage of occurrences of HF with EF (left side), and with SWR/SW (right side) (SW = stroke work, SWR = stroke work reserve = SWx - SW, SWx = maximum possible stroke work calculated from the area under the ESPVR). The results shown in the figure are presented for five clinical groups: normal *, aortic stenosis o, aortic valvular regurgitation +, mitral regurgitation ^, miscellaneous cardiomyopathies x. Note that the normal group (*) appears around the minimum of both curves. For the left side curve the minimum of occurrences of HF appears around $EF \approx 0.67$ or about 2/3. For the right side curve the minimum of occurrences of HF appears around $SWR/SW \approx 0.34$ or about 1/3.

The results presented in the figure are one example of several interesting indexes that can be derived from the ESPVR in order to assess the mechanics of ventricular contraction. When ratios of pressures are used, those indexes can be calculated in a non-invasive way and they can be used to classify the state of the left ventricle in three categories, normal state of the heart, mildly depressed state of the heart corresponding to $SWR \approx 0$, or severely depressed state of the heart in which an increase in afterload results in a severe decrease of stroke work SW causing cardiac insufficiency.

Results also show that bivariate (or multivariate) analysis of data is superior to univariate analysis of data (like by using only EF) for segregation and classification of different clinical groups.



Aortic-finger Pulse Transit Time vs R-derived Pulse Arrival Time: a Beat-to-Beat Assessment

Emanuele Vaini*, Prospero Lombardi, Marco Di Rienzo

Italy

Pulse Transit Time (PTT), is commonly defined as the time it takes the blood pressure (BP) wave to travel from the aortic valve to a distal artery (usually the fingertip). Given the difficulty in the time localization of the Aortic valve Opening (AO), PTT is usually surrogated by the Pulse Arrival Time (PAT), in which AO is approximated by the R peak in the ECG signal. Thus PAT provide a distorted estimation of PTT because it includes the electromechanical time, i.e. the extra time from the electrical stimulation of the ventricles till AO. While the difference between the PTT and PAT mean values is known, little knowledge exists on the difference in their beat-to-beat dynamics. Aim of this pilot study was to get a first insight into such an unexplored issue. In a sitting healthy subject we simultaneously recorded ECG, continuous finger BP and the chest micro accelerations produced by the heart contraction (the seismocardiogram, SCG) for 5 minutes. A specific algorithm was developed to automatically detect in each SCG waveform the time position of the fiducial point associated to the AO (this association has been previously verified by ultrasound measures). PAT, PTT and the Pre Ejection Period (PEP) were estimated for each heart beat from the timing between AO and the Q and R peaks in the ECG. Data analysis indicates that, when compared to PTT, PAT is characterized not only by the expected greater mean value (223ms vs. 134,4ms) but also by a larger variability (sd=7,02ms vs. 4,63ms). Additionally, while the PTT power spectrum was almost flat, PAT power displays a marked peak at the respiratory frequency. From the analysis of PEP, it appears that PAT beat-to-beat variability is much more similar to PEP than to PTT dynamics. Investigations are in progress to validate these preliminary findings.

S44

Changes of Pulse Wave Velocity in Lower Limbs in Hypertensive Patients

Magdalena Matejkova*, Vlastimil Vondra, Ladislav Soukup, Filip Plesinger, Ivo Viscor, Josef Halamek, Pavel Jurak

International Clinical Research Center, St. Anne's University Hospital, Brno
Brno, Czech Republic

S44

Increased arterial stiffness is connected with vascular aging and cardiovascular diseases. Arterial stiffness correlates with Pulse wave velocity (PWV) which can be measured by bioimpedance method. Plethysmography signal was measured by non-invasive Multichannel Bioimpedance Monitor and PWV was calculated by PulseWave software in thigh and calf on both legs beat-to-beat. Protocol: 2-minute supine position (horizontal position), 5-minute head-up tilt test 70° (vertical position). Subjects: 25 healthy (14 women and 11 men) non-smoking volunteers (normal) and 24 patients treated for hypertension (12 women and 12 men). PWV values of last 60 seconds during different positions of subject was evaluated for right and left leg separately and averaged. The relative $PWV_r = PWV_{vertical}/PWV_{horizontal}$ was calculated. Unpaired t-test was used to test differences between groups. There were no significant differences ($p=NS$) in basic parameters normal/patients: age $58.0\pm 9.8 / 63.0\pm 13.8$, weight $75.5\pm 13.8 / 81.8\pm 19.0$ kg, height $1.71\pm 0.10 / 1.69\pm 0.11$ m, systolic blood pressure $125.2\pm 14.4 / 126.3\pm 16.8$ mmHg, diastolic blood pressure $74.3\pm 8.6 / 70.6\pm 8.8$ mmHg. The only significant difference were in the PWV_r parameter ($p<0.05$): 1.27 ± 0.17 for normal group and 1.17 ± 0.15 for patients. Decrease PWV_r in patients treated for hypertension was statistically significant in comparison with the healthy group with the same blood pressure, weight and height. This result reflects increased arterial stiffness in the treated hypertensive group and demonstrates that a simple test could provide an early diagnosis of loss of vessel compliance.

Computational Study of Altered Pressure induced Arterial Remodeling

Linxia Gu*, Shijia Zhao, Abdullah Ibrahim

University of Nebraska-Lincoln
United States

The goal of this work is to develop a predict model for better capturing the altered pressure induced artery remodeling, including the histories of both geometrical and material adaptations. The calculated local mechanical parameters in terms of wall stress and shear stress were used to form the governing law of the remodeling process. An adaptive material remodeling strategy combined with the element birth and death techniques for the geometrical growth were implemented in the commercial finite element codes. The numerically predicted remodeling results in terms of the wall thickness, inner diameter and the ratio of elastin to collagen content of the artery were compared with and fine-tuned by the experimental data in a rat model from the literature. Results demonstrated the good predictability of our computational model, which could capture and illustrate the higher pressure induced arterial thickening and stiffening. In addition, the roles of geometrical growth and material remodeling were isolated to better understand the contributions of each element to the arterial remodeling and their coupling effect. Finally, this framework was applied to a patient-specific artery generated from computer tomography to demonstrate its heterogeneous remodeling process. Results suggest that altered pressure induced arterial remodeling are quite heterogeneous due to both nonlinear geometry and material adaptation process. The developed computational model directly predicted and interpreted time-varying three-dimensional snapshots of intermediate morphologies during arterial remodeling, which could complement the discrete experimental data for improving the clinical management. The proposed computational framework could also be extended to simulate other types of the mechanics-related tissue remodeling including in-stent restenosis and grafting.

S44

Automated Home Monitoring of Atrial Fibrillation in Heart Failure Patients

Silviu Dovancescu¹, Saeed Babaeizadeh²

¹Philips Research, Eindhoven, The Netherlands

²Philips Healthcare, Andover, MA, USA

Background: A wearable monitor (fluid accumulation vest, FAV) was de-signed to aid disease management of chronic heart failure (HF) patients. The FAV allows patients to perform and transmit self-assessments of transthoracic bioimpedance. The data is primarily analyzed for indications of intra-thoracic fluid accumulation associated with worsening HF. Each measurement also in-cludes a non-conventional ECG signal which might enable an automated mon-itoring of cardiac arrhythmias. The most common arrhythmia amongst HF pa-tients is atrial fibrillation (AF) known as a harbinger of HF worsening.

Aim: This study aims to investigate the feasibility of using FAV self-assessments for monitoring AF in HF patients.

Methods: Eleven HF patients with persistent AF were followed with the FAV for up to one year as part of an observational home monitoring study. Patients used the FAV to perform daily measurements with a duration of 5 minutes. The ECG signals were analyzed by an AF detection algorithm based on Markov modelling of inter-beat-intervals (IBI). After identifying normal QRS complexes, the model calculates a dynamic score for the irregularity of the IBIs which reflects the relative likelihood of observing such intervals in AF versus outside of AF. The algorithm was trained on a database of ambulatory holter recordings.

Results: During the study period, sinus rhythm was restored in one patient by means of electrical cardioversion, and two other patients were implanted with cardiac pacemakers (pacing >99%). All patients resumed FAV self-assessments after the procedures. Analyzing 2183 true AF and 425 non-AF measurements the algorithm achieved a sensitivity of 98% and a specificity of 94%.

Conclusions: Using the FAV non-conventional ECG, our AF algorithm de-tected the presence and termination of persistent AF in HF patients. Detecting AF in patients monitored with the FAV is feasible and may be valuable for those at risk of incident and recurrent AF.

A Novel Model of Atrial Fibrillation: Episode Recurrence and Disease Progression in a Virtual Patient Population

Eugene TY Chang*, Yen Ting Lin, Julie Eatock, Kanwal K Bhatia, Tobias Galla, Richard H Clayton

University of Sheffield
Sheffield, United Kingdom

Motivation Atrial fibrillation (AF) is a leading cause of morbidity and mortality. AF prevalence increases with age, which is attributed to pathophysiological changes that aid AF initiation and perpetuation. Recording and modelling atrial electrical activity can identify and inform hypotheses surrounding AF mechanisms. Current state-of-the-art biophysical models are only capable of simulating short periods of atrial activity at high spatial resolution, whilst clinical recordings generate infrequent temporal datasets of limited spatial resolution, on which multi-year epidemiological studies are based. A model that combines biophysical knowledge, clinical data and epidemiological studies, to predict the increased susceptibility of a patient to future AF episodes and estimate disease progression would be of significant interest. Method We propose a proof-of-concept mathematical model to simulate AF recurrence and disease progression within a virtual patient population based on non-Markovian continuous-time stochastic processes. AF is modelled as a binary state time series, considering the contribution of known determinants – predisposition to AF, effects of ageing and other risk factors, and episode-related remodelling – to alter transition probabilities between AF and no-AF. The model contains 13 parameters affecting the vulnerability of the atrium and episode-related remodelling; parameters are estimated from literature where possible. Following analytic derivation of the survival functions for each event, exact sample paths were simulated numerically and continuous-time Monte Carlo simulations were used to measure the statistical properties of the AF process. Results and Conclusions In an initial exemplar study, we evaluated a virtual patient population with first AF episode at age 55 over several decades, to simulate progression from paroxysmal to persistent AF. Monte Carlo simulation of the model (n=100,000) revealed a bifurcation in AF episode duration at ~85 years, indicating progression to persistent AF. We conclude that the model may be useful for informing and generating hypotheses of AF initiation and maintenance.

S51

Drifting Rotors Prevalence Is Associated with Dominant Frequency Reduction after Persistent Atrial Fibrillation ablation

JL Salinet, MS Guillem, TP Almeida, X Li, G Goroso, GS Chu, G André Ng, FS Schindwein

Mogi das Cruzes University, Brazil; Heart Institute, Brazil; Universitat Politècnica de València, Spain; University of Leicester, UK.

S51 Introduction: Identification and target of arrhythmogenic atrial regions remains an evident challenge during persistent fibrillatory mechanisms in atrial fibrillation (AF) patients. This study aimed at investigating the spatio-temporal behavior of atrial regions hosting dominant frequency (DF) and phased rotors to better understanding this arrhythmia.

Method: 8 persistent AF patients undergoing first catheter ablation procedure (pulmonary vein isolation) were included in the study. Non-contact AF electrograms (2048 EGMs; up to 1 minute) were recorded around the entire left atrial chamber for off-line analysis. Ventricular far-field influence was removed prior to the analysis. DF areas within 4 to 12 Hz and phase singularity (PS) points located where there is $[-\pi + \pi]$ phase progress were automatically identified and tracked over consecutive high density maps. Rotors were defined as PS trajectories lasting for at least 100 ms. The spatio-temporal correlation on the LA areas hosting high DF peaks areas and PS rotors propagation was also investigated.

Results: Persistent AF patients presented multiple PS points. They are not spatio-temporally anchored at specific regions and drift over different areas of the LA with preferential locations (Figure 1). After ablation, the number of rotors across the LA was reduced from 11.8 ± 3.9 to 8.0 ± 4.3 ($-34.7 \pm 27\%$, $p=0.05$), especially in the pulmonary vein areas (4.8 ± 2.6 vs. 1.2 ± 1.3 , $-79.8 \pm 19.5\%$, $p<0.05$). DF analysis presented a similar trend with the highest DFs (DF_{max}) decreasing from 7.3 ± 0.4 Hz to 7.1 ± 0.8 Hz. Although the reduction prevalence has been seen on both metrics, DF_{max} areas did not match with higher PS incidences.

Conclusion: Both frequency and phase analyses seem to have a role at identifying areas that might be perpetuating persistent AF. Concatenated real-time phase and frequency mapping may contribute as an auxiliary tool for AF ablation.

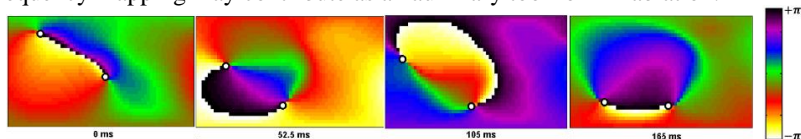


Figure 1 - Consecutive 2D phase mapping with PS drifting point moving across the LA.

Spectral Variation in Intracardiac Impedance as a Predictive Marker During Internal Cardioversion of Atrial Fibrillation

Philip Walsh*, Omar Escalona, Vivek Kodoth, David McEneaney, Ganesh Manoharan

Centre for Advanced Cardiovascular Research (CARC), University of Ulster, Newtownabbey, UK.

Background: Intracardiac impedance (ICI) influences the success of internal cardioversion as it inversely relates to the electrical current density delivered during defibrillation. However, few studies have examined spectral variation across frequency of ICI during internal cardioversion of atrial fibrillation (AF).

Methods: In this study, thirty patients (age 58.13 ± 12.29 years; male/female: 9:1; average BMI 32.75) with persistent AF (30.93 ± 31.13 months) were randomised to a biphasic very-low-tilt-rectilinear (B-VLTR) or monophasic very-low-tilt-rectilinear (M-VLTR) shock waveform using a step-up protocol (50-300V; 50V steps). The primary end-points were cardioversion outcome with respect to waveform type and energy delivered. Data was subsequently grouped into four categories; successful cardioversion with B-VLTR and M-VLTR (Group-I and Group-III, respectively) and failed cardioversion with B-VLTR and M-VLTR (Group-II and Group-IV, respectively). Variation of ICI within the time domain (ΔZT ; change in ICI between shocks) and frequency domain ($\Delta IAMSA$; change in impedance amplitude spectrum area) was calculated across each group and the statistical significance of changes between shocks evaluated.

Results: Sinus rhythm was restored in 14 patients (46%). The mean voltage, current, energy and ICI measured across all groups was $270.53 \pm 35.96V$, $3.68 \pm 0.80A$, $9.12 \pm 3.73J$ and $70.82 \pm 13.46\Omega$, respectively. In the time-domain, all patients who cardioverted exhibited a significant reduction in ICI between the first and third shock (Group-I,III: $\Delta ZT(S1-S3) = 4.95\Omega (SD=2.71)$, $p < 0.009$ and $\Delta ZT(S1-S3) = 5.00\Omega (SD=1.62)$, $p < 0.003$, respectively) while no significant reduction was measured in patients who failed to cardiovert (Groups-II,IV: $\Delta ZT(S1-S3) = 3.30\Omega (SD=5.63\Omega)$, $p > 0.154$ and $\Delta ZT(S1-S3) = 8.12\Omega (SD=6.61\Omega)$, $p > 0.051$, respectively). In the frequency domain, a meaningful variation in the impedance amplitude spectrum area (IAMSA) between first and third shock in patients that were successfully treated versus those that failed to cardiovert was also observed.

Conclusions: A significant decrease in ICI within the time domain and a relative reduction of the IAMSA value within the frequency domain were identified as positive markers for success of internal cardioversion.

Technological Challenges of Computing in Cardiology in AF Management

Nadir Saoudi*

This session will be completed with an open discussion led by N Saoudi and accompanied by a direct live feed of an RF ablation procedure. Please plan to stay after the oral presentations to participate in the discussion.

S51

The PhysioNet/Computing in Cardiology Challenge 2015: Reducing False Arrhythmia Alarms in the ICU

Gari Clifford*, Ikaro Silva, Benjamin Moody, Qiao Li, Danesh Kella, Abdullah Shahin, Tristan Kooistra, Diane Perry, Roger Mark

Emory University and Georgia Institute of Technology
United States

False alarms rates in the ICU are as high as 90%, decreasing quality of care by slowing staff response times while increasing patient delirium through noise pollution. This year's Challenge provides a set of multiparameter ICU data segments with 2,500 associated life-threatening arrhythmia ICU alarms, and challenges the general research community to address the issue of false alarm suppression using all ICU signals. Each data segment was 5 minutes long (for real time analysis), ending at the time of the alarm. For retrospective analysis we provided a further 30 seconds of data after the alarm was triggered. A total of 750 data segments were made available for training and 500 were held back for testing in each arm of the competition. Each alarm was reviewed by expert annotators, at least two of whom agreed that the alarm was either true or false. The scoring algorithm assesses the percentage of alarms correct, but with a penalty that weights the suppression of true alarms five times more heavily than acceptance of false alarms. We created four baseline algorithms: The first accepted all alarms as true and scored 30.14. The second used the prior probability of the alarm being true (33% Asystole, 27% Extreme Bradycardia, 82% Extreme Tachycardia, 33% Ventricular Tachycardia, 24% Ventricular Flutter/Fibrillation) and scored 43.19. The third used open source algorithms for signal quality checks on the blood pressure or the photoplethysmogram to decide which signal to use to estimate heart rate and scored 45.24. The fourth used the match between an open source QRS detector and pulse onset detector to decide if the signals were measuring the same activity, and scored 50.14. A total of 43 teams made a total of 230 competition entries. The min/median/max score in the first phase was 31.40 / 50.14 / 76.62.

S52

A multimodal approach to reduce false arrhythmia alarms in the intensive care unit

Sibylle Fallet, Sasan Yazdani, Jean-Marc Vesin

Swiss Federal Institute of Technology
Lausanne, Switzerland

Purpose: High false alarm (FA) rates are a persistent concern in the Intensive Care Unit (ICU). Limited performance of ICU monitoring devices results in the desensitization of the medical staff and longer response times. This work aims at lowering FA rates, while not suppressing the true alarms.

Method: The database consists of 1250 life-threatening alarm recordings, each categorized as a bradycardia, tachycardia, asystole, ventricular tachycardia or ventricular flutter/fibrillation arrhythmia. Each record contains two ECG leads and at least one pulsatile waveform (photoplethysmogram and/or arterial blood pressure). The nature of each alarm was manually labeled by a team of expert. Based on the quality of available signals, heart rate was either estimated from pulsatile waveforms using an adaptive frequency tracking algorithm or computed from ECGs using an adaptive mathematical morphology approach. Furthermore, we developed a supplementary measure based on the spectral purity of the ECGs to determine if a ventricular tachycardia or flutter/fibrillation arrhythmia has taken place. Finally, alarm veracity was determined based on a set decision rules on HR and spectral purity values.

Results: Our method achieved an overall score of 72.95 for the first phase of the challenge, with a TPR of 94% and a TNR of 71%. The following results were obtained for each arrhythmia: asystole (score = 76.42, TPR = 92%, TNR = 78%), bradycardia (score = 73.53, TPR = 96%, TNR = 66%), tachycardia (score = 80.0, TPR = 96%, TNR = 60%), ventricular flutter/fibrillation (score = 79.55 TPR = 83%, TNR = 88%) and ventricular tachycardia (score = 67.38, TPR = 93%, TNR = 65%).

Conclusion: With an overall FA suppression rate of 71%, our method could contribute in suppressing FA rate in the ICU. The method is still being improved and will be further tested during the next stage of this challenge.

Results (phase 1):

Arrhythmia	TPR	TNR	Score
Asystole	92%	78%	76.42
Bradycardia	96%	66%	73.53
Tachycardia	96%	60%	80.00
Ventricular Flutter/Fibrillation	83%	88%	79.55
Ventricular Tachycardia	93%	65%	67.38
Real-time	93%	65%	68.15
Retrospective	95%	77%	77.82
Overall	94%	71%	72.95

S52

False Alarms in Intensive Care Unit Monitors: Detection of Life-threatening Arrhythmias using Elementary Algebra, Descriptive Statistics and Fuzzy Logic

Filip Plesinger*, Petr Klimes, Josef Halamek, Pavel Jurak

Institute of Scientific Instruments of the ASCR
Brno, Czech Republic

Aims: A false alarm ratio of up to 86 % has been reported in Intensive Care Unit (ICU) monitors. Such a high value can lead to reduced staff attention and patient deprivation. This paper presents a method for detection of specific arrhythmias – asystole, extreme bradycardia, extreme tachycardia, ventricular tachycardia and ventricular flutter/ fibrillation – in accordance with the “2015 Physionet/CinC Challenge”. **Data:** The method was trained with the use of 750 records and tested on 500 records from ICUs provided by Physionet and scored by specialists for the presence of specific arrhythmia and alarm validity. The records (300 or 330 seconds long) were sampled at 250 Hz and consisted of two ECG leads and one or two blood pressure signals.

Methods: First, invalid data areas are detected in each of the channels. Next, QRS complexes and RR intervals are found in all signals using a different QRS detection approach according to the specific signal type. Information regarding low-frequency (2–9 Hz) activity is acquired in the case of ECG signals. The RR series obtained are tested for regular heart activity (based on standard deviation, heart rate and QRS temporal distribution). An arrhythmia-specific test is processed if none of examined RR series is regular activity. Tests for individual arrhythmias are based on examination of QRS temporal distribution, comparison of heart rate with known limits, observation of low-frequency ECG activities (in the case of ventricular tachycardia and ventricular fibrillation) and fuzzy logic in indeterminate cases.

Results: Training-set sensitivity and specificity of 92.09 % and 86.18 % were achieved. A hidden test set resulted in an overall score of 76.62 points (CinC Challenge Phase I).

S52

Reducing False Arrhythmia Alarms Using Robust Interval Estimation and Machine Learning

Christoph Hoog Antink, Steffen Leonhardt

Philips Chair for Medical Information Technology,
RWTH Aachen University, Aachen, Germany

False alarms in the intensive care unit (ICU) lead to a decreased quality of care. In today's clinical practice, arrhythmia alarms are usually generated using the electrocardiogram (ECG) only. This approach can fail if the ECG is disconnected or contaminated with artifacts while other modalities like the photoplethysmogram (PPG) or the arterial blood pressure (ABP) might still contain usable information.

Our approach is based on the assumption that most false arrhythmia alarms can be suppressed if accurate beat-to-beat interval information is available. Thus, a robust interval estimator, based on the similarity in morphology of consecutive heart beats, is implemented. The signal 16 seconds prior to the alarm is analyzed in terms of self-similarity using autocorrelation, absolute magnitude difference, and maximum amplitude pairs functions. An adaptive moving window ensures that no averaging across multiple intervals is performed. Moreover, the three self-similarity measurements are applied individually to all available channels containing a cardiac signal. The results are fused using a Bayesian approach and used to determine the interval I_n as well as the quality of estimation Q_n for all $n \in N$ analysis windows. Several features are derived from the interval estimation ($\min(I)$, $\max(I)$, $\text{std}(I)$, etc.) and the quality metric ($\text{mean}(Q)$, $\text{median}(Q)$) using ECG only, ABP / PPG only, and all channels simultaneously. Those features are used to train a classification tree and a regularized linear discriminant analysis classifier; the table lists the results for a combination of both.

While false alarms for tachycardia can be suppressed perfectly, the performance for ventricular flutter / fibrillation and ventricular tachycardia is suboptimal. Here, the assumptions that the interval information suffices and that the beat morphology does not change can be violated. To improve performance, waveform-describing features should be added.

	TPR	TNR	Score
Asystole	58%	91%	72.95
Bradycardia	92%	71%	70.83
Tachycardia	100%	100%	100.00
Ventricular Flut./Fib.	33%	91%	58.93
Ventricular Tach.	84%	69%	64.26
Real-time	86%	74%	66.90
Retrospective	90%	82%	75.18
Overall	89%	78%	70.98

Reduction of False Critical ECG Alarms using Waveform Features of Arterial Blood Pressure and/or Photoplethysmogram Signals

Wei Zong*

Philips Healthcare
Andover, United States

Introduction: This article presents a practical algorithm to reduce false positive critical ECG alarms, using waveform features of arterial blood pressure (ABP) and/or photoplethysmogram (PPG).

Methods: Waveform features of ABP and/or PPG, such as pulse-to-pulse intervals, pulse amplitudes, and pulse signal quality, were extracted on a beat-by-beat basis in real-time. A pulse detector similar to PhysioNet wabp (an open-source ABP pulse detector) was employed. For each detected pulse (or a forced detection, if there is no pulse detected for 2s), five event-feature indicators (EFIs), which indicate the likelihood of event-presence to the corresponding five critical ECG alarms, were calculated from the waveform features of a group of pulses prior to the current pulse (or forced detection). To validate a critical ECG alarm, in the real-time mode, values of the corresponding EFI for those pulses in a prior window (4s) to the alarm time were checked; and in the retrospective mode, the EFI values for those pulses in the prior window and an after window (3s) to the alarm time were used. Physiological reasoning-based decision rules were used in the algorithm for validating each type of the critical ECG alarms.

Results: An entry was made to the PhysioNet/Computing in Cardiology 2015 challenge in Phase I. On the test set, the algorithm's TPR, TNR, and Score, for the real-time mode, were 99%, 44%, and 59.45; for the retrospective mode, were 95%, 51%, and 61.65; and for the overall, were 97%, 48%, 60.58; respectively. The average and maximum running times were 0.105% and 0.193% of quota, respectively.

Discussion: Using waveform features of ABP and/or PPG is a reasonable and effective way to reducing false critical ECG alarms. For maximum results, further options such as sophisticated ECG signal processing on all available leads and respiration signal processing would need to be considered.

S52

Decreasing the False Alarm Rate of Arrhythmias in Intensive Care using a Machine Learning Approach

Linda M Eerikäinen*, Joaquin Vanschoren, Michael J Rooijackers, Rik Vullings, Ronald M Aarts

Eindhoven University of Technology
Eindhoven, Netherlands

We present a novel algorithm for classifying true and false alarms of life-threatening arrhythmias in intensive care. This algorithm was entered in the PhysioNet/Computing in Cardiology Challenge 2015 “Reducing False Arrhythmia Alarms in the ICU”. Arrhythmias triggering the alarms are divided into five classes: asystole, extreme bradycardia, extreme tachycardia, ventricular flutter or fibrillation, and ventricular tachycardia. The algorithm performs a binary classification of the alarms for a specified arrhythmia type by combining signal quality information and heart rate features from multiple sources, such as electrocardiogram (ECG), photoplethysmogram (PPG), and arterial blood pressure (ABP), depending on availability. A modified low-complexity R-peak detector was applied to the ECG. Beats from PPG and ABP were detected with an open-source algorithm that employs a sum slope function and adaptive thresholding. Beat matching between multiple signals was applied to extract heart rate even when the quality of signals from all sources was poor. Classifiers were trained separately for every type of arrhythmia. Hence, the complete algorithm leverages five different predictive models. Features were selected separately for each type of arrhythmia, e.g., for ventricular tachycardia information about the presence of ventricular beats was included. Various machine learning techniques, such as classification trees and Random Forests, were compared in the selection process of classifiers. K-fold cross-validation was applied during training. Classification sensitivities of true alarms 67–99% (mean 83%) on the training set and 17–97% (mean 87%) on the unrevealed test set. Classification specificities on the training and test set were 63–93% (mean 79%) and 69–100% (mean 80%), respectively. The best performance was for tachycardia, whereas the poorest results were for ventricular arrhythmias. The overall challenge score was 70.03. The performance of the algorithm is expected to improve by further refining the features, especially for ventricular arrhythmias, and by applying more complex classification models.

S52

A Robust Detection Algorithm to Identify Breathing Peaks in Respiration Signals from Spontaneously Breathing Subjects

Chathuri Daluwatte*, Christopher G Scully, George C Kramer, David G Strauss

US FDA
Silver Spring, United States

Introduction: Assessing respiratory and cardiovascular system coupling can provide new insights into disease progression, but requires accurate analysis of each signal. Respiratory waveform data collected during spontaneous breathing are noisy and respiration rates from long term physiological experiments can vary over a wide range across time. There is a need for automatic and robust algorithms to detect breathing peaks in respiration signals for assessment of the coupling between the respiratory and cardiovascular systems. We developed an automatic algorithm to detect breathing peaks from a respiration signal.

Methods: The breathing peak detection algorithm consists of several parts. The preprocessing consists of a band pass antialiasing filter, power line noise filtering, baseline wander correction, and down sampling. Signal slope characteristics were used to detect candidates for breathing peaks and an adaptive thresholding criterion was used to discriminate breathing peaks from noise artifacts. A dynamic signal quality index was developed using Fourier transform to quantify the quality of the respiration signal as it varies over time, and this was used to remove peaks appearing due to noise. A peak quality index was developed using the signal quality around each peak to characterize the reliability of each detected peak. Comparison of the detected peaks against human annotations was performed to assess the algorithm.

Results: The algorithm was tested on respiration signals from conscious ovine hemorrhage models (N=5, total length = 6.1h) with breathing rate varying from 20 to 100 breaths/min. The sensitivity of the algorithm was 97.7% with a positive predictive value (PPV) of 96.3%.

Conclusions: The developed algorithm presents a promising approach to detect breathing peaks in respiration signals from spontaneously breathing subjects. The algorithm was able to identify breathing peaks consistently while the breathing rate varied from 20 to 100 breaths/min.

A Comparison of Obstructive Sleep Apnoea Detection using Three Different ECG Derived Respiration Algorithms

Nadi Sadr, Philip de Chazal

School of Elect. and Inf. Engineering, University of Sydney, Australia

Aims: An ongoing research goal is to reduce the number of diagnostic signals for sleep apnoea detection. In this paper, the ECG signal was used to detect sleep apnoea episodes.

Methods: Three different algorithms (QRS amplitude, PCA and kernel PCA) were applied to the ECG signal to extract information of the respiratory activity. Features were then extracted from the respiratory activity and used to classify sleep apnoea episodes using an Extreme Learning Machine classifier. Data from the first 60 minutes of the 35 ECG signal recordings from the MIT PhysioNet Apnea-ECG database was used throughout the study. Performance was measured with leave-one-record-out cross validation. The fan-out number for the ELM classifier was varied between one and ten.

Results: The results showed that the performance of the PCA algorithm was equal to or outscored the other two algorithms at all fan-out numbers we explored. Its highest test-set performance was an accuracy of 79.4%, a sensitivity of 48.8%, and a specificity of 87.7% at a fan-out of ten.

Conclusion: The results showed that linear PCA algorithm improved OSA detection by EDR features compared to the other two algorithms.

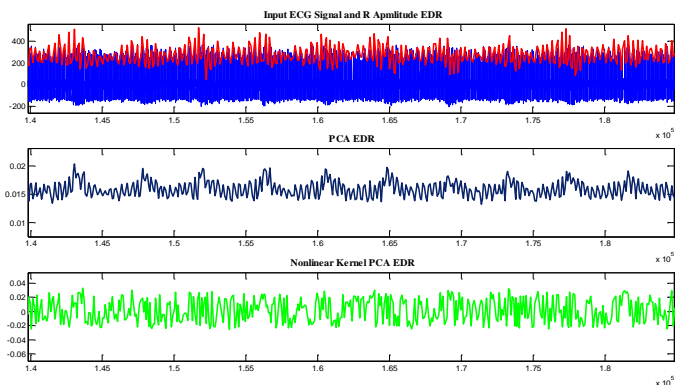


Figure 1. Example outputs from the three different methods for estimating the ECG derived respiration signal. Input ECG signal (blue), the QRS amplitude EDR (red), PCA EDR (dark blue), and kernel PCA EDR (green) signals.

Identification of Respiratory Phases using Seismocardiogram: A Machine Learning Approach

Vahid Zakeri, Kouhyar Tavakolian*

University of North Dakota
Grand Forks, United States

Aim: This study was aimed at developing an algorithm that could identify the respiratory phases, i.e. inspiration (I) or expiration (E), by analysing seismocardiogram (SCG) cycles.

Methods: In order to better assess SCG cycles, it is needed to discriminate the cycles based on their position in the respiratory phases. The electrocardiogram (ECG), respiration, and SCG signals of 45 subjects were recorded. The SCG cycles were obtained using the ECG's R-peaks, and for each cycle the corresponding respiratory phase was found according to the respiration signal. The total 2146 SCG cycles were studied, in which 1109 cycles were in phase I, and the rest in phase E. The support vector machine (SVM), a powerful machine learning algorithm, was employed to classify the SCG cycles into I or E. Each SCG cycle in the time-domain was divided to 32 equal bins, and the average of each bin was computed. An augmentation of all these averages formed the feature vector for each cycle. The SVM algorithm was trained using 51% of data (567 cycles in phase I, and 530 in phase E), and then was tested on the rest of data. There was no overlap between testing and training data.

Results: The developed SVM algorithm could correctly classify 88% of the testing data (1049 cycles). The testing data included 542 cycles in phase I and 507 in phase E, and their classification accuracies were 92% and 85% respectively.

Conclusions: The machine learning algorithms, in particular support vector machines, seems a promising approach for identifying the respiratory phases of SCG cycles. The results of this study establish a solid ground for further analysis in order to increase the identification accuracies in future works.

Sleep Apnea Detection Directly from Unprocessed ECG through Singular Spectrum Decomposition

Pietro Bonizzi*, Joel Karel, Stef Zeemering, Ralf Peeters

Maastricht University
Maastricht,, Netherlands

Aims: ECG-based detection of obstructive sleep apnea (OSA) is generally based on heart rate related indices. Computation of these indices require an ECG record to be pre-processed and the R-peak locations to be estimated. This study proposes a novel method to detect OSA events directly from an unprocessed ECG through singular spectrum decomposition (SSD).

Methods: SSD is a recently proposed technique for decomposition of nonlinear and nonstationary time series in narrow-banded components. Given an ECG record, SSD was applied to non-overlapping 10 seconds segments and the dominant frequency (DF) of the main component in the frequency band [0.02-0.5]Hz was estimated. Each segment was binary classified based on the corresponding DF (1, if DF larger than a defined threshold (TH), 0 otherwise). For every minute, the SUM of the six corresponding binary values was then used to classify that minute as normal or apnea (with higher SUM meaning possible apnea). Validation was based on the Apnea-ECG Database, including 20 apnea (A) recordings, 5 borderline (B), and 10 control (C) (sampling rate 100Hz). Group A was randomly split into 14 training and 6 test records. Multiple round cross-validation was used to determine the optimal values for TH (in the range [0.02-0.5]Hz) and SUM (in the range 0 to 6) and performance analysis. The optimal model was then used to classify B and C.

Results: The optimal values for TH and SUM given by cross-validation were 0.25Hz and 3, respectively. The average sensitivity and specificity were 0.65 and 0.28. When applied to groups B and C, the optimal model showed a sensitivity of 0.70, and a specificity of 0.25.

Conclusions: Although performance of the proposed model is still poor in avoiding false positive, the preliminary results reported in this study suggest that detection of OSA directly from unprocessed ECG is possible.

S53

Ballistocardiogram Amplitude Modulation Induced by Respiration: a Wavelet Approach

Quentin Delière*, Jens Tank, Irina Funtova, Elena Luchitskaya, David Gall, Philippe van de Borne, Pierre-François Migeotte

Cardiology Dept., Erasmus Hospital, Université libre de Bruxelles, Belgium

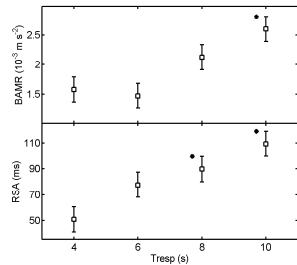
Aims: Ballistocardiography (BCG) records the accelerations of the human body consecutives to the heart beating activity. In the past, BCG was mainly used for cardiac contractility and stroke volume (SV) assessment and the influence of respiratory phase has been demonstrated. Here we present a method for the estimation of Ballistocardiogram Amplitude Modulation induced by Respiration (BAMR). It is based on wavelet analysis and is comparable to the analysis of respiratory sinus arrhythmia (RSA).

Methods: BCG, ECG and respiration were simultaneously recorded on four subjects during a stepwise imposed controlled breathing protocol with four increasing breathing periods: $T_{resp}=[4,6,8,10]$ s. For each step the following methods were applied: (1) a continuous wavelet transform (CWT) analysis of the BCG signal to compute its energy and Ea_{max} , the maximum energy of BCG acceleration during the systolic phase of the cardiac cycle. Time series of Ea_{max} were then constructed and analyzed using a second CWT analysis where the total energy in the breathing frequency band is our BAMR estimate. (2) RSA amplitude was similarly estimated using CWT on RR-Intervals (RRI) time series. (3) Average amplitude of maximum systolic BCG acceleration (a_{max}) and RRI were computed.

Results: As expected, the traditional RSA analysis shows a linear dependence: RSA amplitude increases with T_{resp} ($p < 0.05$). BAMR presents a similar and significant ($p < 0.05$) dependence. By contrast, a_{max} decreases with T_{resp} ($p < 0.05$) while RRI remains constant.

Conclusion: In this study, we developed a wavelet based method to estimate the respiratory modulation of ballistocardiogram (BAMR) which demonstrates, for the first time, a significant increase with the breathing period similar to RSA dependence. As Ea_{max} is supposed to be related to SV, these results have important implications on physiological interpretation of RSA.

S53



BAMR and RSA vs T_{resp}

Real-Time Detection of Sleep Respiratory Disorders

Delphine Feuerstein*, Laurence Graindorge, Amel Amblard, Aziz Tatar, Gustavo Guerrero, Sylvain Christofle-Boulard, Corinne Liodice, Alfredo Hernandez, Jean-Louis Pepin

Sorin CRM SAS, Clamart, France
Clamart, France

Background: Sleep apnea syndrome (SAS) is an under-diagnosed disease with high prevalence in patients suffering from cardiovascular diseases. Usual diagnosis tools detect breathing disorders by retrospective analysis of the recorded signals. We evaluated a real-time detection algorithm using a novel cardio-respiratory Holter (SpiderSAS, Sorin CRM). Here, abnormal respiratory events are detected as soon as they occur, before normal respiration has resumed. This real-time detection will enable triggering and/or adjusting an event-based SAS treatment.

Methods: The proposed breathing disorder detector is solely based on nasal airflow. Respiratory cycles are identified by the crossing of two independent thresholds that are adaptively updated, according to features from the patient's breathing pattern. Respiratory cycles with periods exceeding 8 seconds are identified as apneas. Successive respiratory cycles of low amplitude ($\leq 50\%$ of baseline) lasting more than 10 seconds are classified as hypopneas. The detection algorithm was assessed on 27 severe SAS patients, who underwent a full polysomnography (PSG). Simultaneously, the Holter measured nasal pressure. Apneas and hypopneas were detected on-line. Central reading of PSG was done by an expert, blinded core-lab. Events found were matched with those recorded by the Holter and the performance (sensitivity (SE) and positive predictive value (PPV)) of the real-time detector was assessed.

Results: A total of 3365 events were scored on the PSG. The real-time detector SE was 86% (90% for apneas, 81% for hypopneas) and the PPV was 63% (67% for apneas, 56% for hypopneas). The low PPV was mostly due to false detections while patients were awake.

Conclusions: The real-time detector showed a good sensitivity. The PPV would be sufficient for triggering treatment on-line during the apnea or hypopnea. This double-threshold algorithm could also set the basis of an off-line detector for SAS screening, whereby resumption of normal breathing would confirm the detection and improve the PPV.

Mathematical Modeling of the Role of Cooperativity Between Contractile and Regulatory Proteins in the Mechano-Calcium Feedbacks in Myocardium

Elena Shikhaleva, Tatiana Sulman, Arseniy Dokuchaev, Larisa Nikitina, Leonid B Katsnelson*

Institute of Immunology and Physiology of the Ural Branch of Russian Academy of Sciences
Ekaterinburg, Russian Federation

Mechano-Calcium Feedbacks (MCFs) provide a fine tuning of Excitation-Contraction Coupling (ECC) in cardiomyocytes with mechanical conditions of myocardium contractions. The feedbacks reveal themselves e.g. in load-dependent relaxation in isotonic twitches, in inactivating effects of quick deformations during isometric twitches, and in the specific responses of calcium transients and action potentials on the mechanical conditions of these twitches. A lot of experimental data supported by theoretical research shows that cooperative dependence of CaTnC kinetics on the cross-bridge concentration ($[Xb]$) is a key mechanism underlying MCFs in the intact cardiomyocytes in normal and pathological states. Nevertheless, a seeming discrepancy has arisen between this contribution of the cooperativity to the performance of the intact myocardium on the one hand, and experimental data obtained on skinned heart muscles, on the other hand. The latter data showed that mechanical conditions significantly affect only calcium sensitivity of the 'pCa-force' relationship rather than its Hill coefficient of cooperativity (see e.g. Konhilas et al; J Physiol, 2002). These findings have convinced many physiologists that cooperativity does not really contribute to the MCFs. We overcame this discrepancy in the framework of mathematical model where we suggested and tested a refined concept of Xb-CaTnC cooperativity that allows the cooperativity to reveal itself differently in steady-state and transitional processes. We incorporated equations formalizing the refined concept in our mathematical model used many times before to analyze electrical and mechanical activity of the heart muscle (see e.g. Katsnelson et al; PBMB, 2011). It turns out that the refined cooperativity underlies both mechano-dependence of calcium activation in the modeled intact myocardium and correct simulation of the above mentioned data obtained on the skinned muscles. These results overcome the described above seeming discrepancy at least within the model. Supported by RSF Grant 14-35-00005.

S54

From Microscopic Calcium Sparks to the ECG: Model Reduction Approaches for Multi-scale Cardiac Simulation

Michael Alan Colman*, César Parra-Rojas, Erick Andres Perez Alday

University of Manchester
United Kingdom

Introduction: Malfunction of the intracellular calcium handling system in cardiomyocytes is being increasingly linked to arrhythmogenesis. Feedback mechanisms in spatio-temporal calcium dynamics are critical for the development of spontaneous calcium waves, which may underlie the rapid focal activity associated with conditions such as atrial fibrillation and heart failure. Thus, microscopic fluctuations can manifest in whole-cell and even whole-organ dynamics. Computational modeling provides a powerful tool to explain and dissect the multi-scale mechanisms underlying cardiac function. However, single-cell models which account for spatio-temporal calcium dynamics are unsuitable for incorporation into organ-scale simulations due to their computational load, thus limiting the ability of multi-scale modeling approaches to describe tissue level arrhythmogenesis dependent on calcium handling malfunction. In this study we develop two methods to overcome this limitation.

Methods: The Gaur-Rudy ventricular cell model is selected for demonstration of the model-reduction approaches. From this 1D model is derived a 3D cell model as well as a non-spatial, deterministic version which will form the basis for integration into tissue models. The first reduction method is guided by empirical analysis of the 1D model and involves inducing transitions of the deterministic ryanodine receptor model to match the behavior of the microscopic model. The second method is based on mathematical analysis of the system, applying the large-N approximation to naturally capture stochastic feedback mechanisms in the non-spatial cell model. Results and

Conclusions: Both methods successfully reproduced the macroscopic consequences of microscopic fluctuations (i.e. spontaneous calcium sparks and waves) at only a hundredth of the computational cost. This allowed integration into large-scale tissue models and simulation of the electrocardiogram, used in the present study to demonstrate natural focal activity resulting from alterations to sub-cellular dynamics. Application of the large-N approximation provided a more powerful method which naturally accounts for alterations to sub-cellular dynamics than the empirically-guided approach.

S54

Calcium Alternans is a Global Order-Disorder Phase Transition: Robustness on RyR2 Release Dynamics

Enrique Alvarez-Lacalle*, Angelina Peñaranda, Inmaculada R Cantalapiedra, Blas Echebarria, Yohannes Shiferaw

Universitat Politècnica de Catalunya- BarcelonaTech
CASTELLDEFELS, Spain

Electromechanical alternans is a beat-to-beat alternation in the strength of contraction of a cardiac cell, which can be caused by an instability of calcium cycling. Using a distributed model of subcellular calcium units we showed recently that alternans occurs via an order-disorder phase transition which exhibits critical slowing down and a diverging correlation length. By introducing the different regulations of the RyR2 with dyadic and luminal calcium, which lead to different stereotypical sparks and inactivation mechanisms, we show here that the presence of the order-disorder transition is robust. As long as the local probability of release is a steep function of some local variable (local luminal or dyadic calcium, or number of locally recovered receptors), the ordering phase appears independently of the particulars of the RyR2 regulation. Different regulations lead to different local causes of the steep probability, and this is the key ingredient, together with diffusion, to produce the transition to alternans. This suggests that to be able to distinguish between different mechanisms, both in-silico and in-vivo experiments should analyze how global averages related to homeostasis, as for instance the global pre-systolic SR load, are affected by the different local RyR2 regulations.

S54

Papillary Muscles Contraction Does Not Change Ventricular Wall Mechanics

Jeremy Rice*, Slava Gurev

IBM Research
Yorktown Heights, United States

Papillary muscles play a crucial role to support valves in the ventricles. However, much less is known about the role in ventricular wall mechanics. The literature is inconclusive, showing both changes in wall strain and indications of no changes in strain after detachment of papillary muscles. We designed a high-resolution 3D model of canine ventricles to investigate the effects of papillary muscles on strain in the regions overlying papillary muscles. The finite element ventricular model employed P2/P1 tetrahedral elements with 800,000 displacement degrees of freedom to simulate a nearly-incompressible hyper-elastic orthotropic material of cardiac tissue with laminar sheet organization. The model anatomy was obtained from in-vitro MRI, and a realistic fiber geometry assumed transmural rotation in the ventricular wall. In papillary muscles, the fibers were aligned with the long axis and smoothly transitioned at the interface of the ventricular wall. Electrical activation was simulated using a monodomain model, and stimuli were applied at several locations on the endocardium including papillary muscles to reproduce a realistic activation of the canine ventricles during normal rhythm. The model was coupled to the CircAdapt lumped circulatory model. Boundary conditions were either: 1) the attached state in which movements of the papillary muscle tips are restricted to a plane parallel to the base of the ventricles; or 2) the detached state with no constraints placed on the muscle tips. All components of strain in the fiber coordinate system were measured at locations overlying anterior and posterior papillary muscles and then compared between attached and detached states. In simulations of typical physiological contractions, we found virtually identical patterns in all strain components in the two cases. This result is consistent with most but not all experimental findings. Further studies will be required to generalize the results to more anatomical reconstructions and a wider range of conditions.

S54

Customizing the Bull's-Eye to Improve the Clinician's Diagnostic Intuition

Ezio-Maria Ferdeghini*, Vincenzo Positano, Gianluca Di Bella, Alessandro Pingitore, Daniele Rovai

CNR
Pisa, Italy

In 2002 the Cardiac Imaging Committee of the Council on Clinical Cardiology of the American Heart Association defined a standard for segmentation, nomenclature and display of the tomographic images of the heart. The "bull's-eye" plot defines how to divide the left ventricular (LV) myocardium in 17 segments, giving a name to each segment and assigning individual segments to the main coronary perfusion territories. Such display has been widely accepted by all imaging modalities, as evidenced by the huge number of scientific quotations. However, the graphical display of a three-dimensional solid on a two-dimensional plane necessarily implies a distortion or a partial representation of the object. In the case of cardiac imaging such a distortion could affect the representation of the extent of a variety of pathological processes, such as myocardial perfusion deficits, wall motion abnormalities, left ventricular hypertrophy, or scars. With this in mind, we aimed to evaluate how the classical display in polar coordinates affects the visual assessment of myocardial infarct extension, and if this graphic display might be modified to provide a more likely information. Cardiac magnetic resonance was performed on 38 patients with myocardial infarction. The global and regional LV volumes, as well as the myocardial infarctum (MI) size, were measured using a validated semiautomatic method: boundaries were automatically traced and manually corrected when needed. All sizes were expressed as percent of LV mass, to be linked to the areas of the bull's-eye regions. The infarct size was assessed by the scores. To improve the clinician's perception of the heart, we propose some alternatives which take into account a more likely view of the percent distribution of the LV volumes on a two-dimensional representation, while keeping the conventional 17 segments organization, although providing a customized bull's eye closer to the real LV of each patient.

P61

Fetal Magnetic Resonance Image Denoising Based on Homogeneity Testing and Non Local Means

Kostas Haris, George Kantasis, Nicos Maglaveras, Anthony Aletras*

Aristotle University
Greece

Introduction A new edge-preserving denoising method for MR images is proposed. Local statistical homogeneity testing is combined with the Non Local Means denoising method. Preliminary qualitative results on real MR images are shown.

Materials and Methods: Non Local Means (NLM) is a relatively recent image denoising method that achieves excellent noise reduction while, at the same time, preserves image information encoded in intensity changes (edges). This is accomplished by exploiting the intrinsic pattern redundancy of the images. However, the required computational effort is enormous compared to other competitive denoising techniques such as anisotropic diffusion and wavelet-based denoising. In the proposed method, statistical homogeneity testing is used to decide if the neighborhood of the current pixel is homogeneous and, therefore, simple averaging is appropriate. In case of heterogeneity, the NLM algorithm is applied for the estimation of the central pixel value. The main idea behind the proposed method is that a large portion of pixel neighborhood (or patches) are homogeneous and therefore, their true central pixel intensity can be estimated optimally by the sample mean. On the other hand, in case of heterogeneity, the local neighborhood structure may be rich and complex. Therefore, it is reasonable to look for other patches with similar structure which is the idea behind the NLM method. The central pixels of the similar patches will contribute with the appropriate weight to the estimation of the current pixel value. This results in effective noise reduction while the image information is preserved. **Results** The proposed algorithm was applied to synthetic and acquired MR images. A qualitative indicator of the denoising performance is the method noise images. The method noise images should ideally contain only pure noise without any structural information. Our results show effective noise reduction with edge preservation at lower computational demands

P61

MRI Simulation-based Evaluation of ECV Calculation using MOLLI T1 Maps

Christos Xanthis, Anthony Aletras*

School of Medicine, Aristotle University of Thessaloniki, Greece
Thessaloniki, Greece

Introduction Quantification of myocardial extracellular volume (ECV) fraction has been recognized as an important biomarker for assessing specific cardiomyopathies. ECV maps are derived from pre- and post-contrast T1 maps of myocardium and blood, calibrated by the blood hematocrit value. Modified Look-Locker Inversion-recovery (MOLLI) method is the most widely used pulse sequence for T1-mapping. Previous study has shown a T2-dependent error in the MOLLI estimate of T1, but the dependency of MOLLI-based ECV measurement on T2 has not been explored yet. In this study, we investigate that T2-dependency with MR simulations of the MOLLI for a wide range of physiological T2 values for pre-contrast blood and myocardium. Methods A recently developed GPU-based (Graphics Processing Units) MR physics simulator was utilized. A clinical MOLLI (scheme 5-3s-3) was simulated for all physiological combinations of T1 and T2, resulting in a database of all possible physiological signal intensities. The MOLLI T1 estimates were then calculated for every database signal based on a 3-parameter fit. For the ECV calculation, the following “true” values were selected based on the literature: pre-contrast-T1myocardium=1045msec, pre-contrast-T1blood=1669msec, post-contrast-T1myocardium=407msec, post-contrast-T1blood=252msec and blood-hematocrit=0.4, resulting in a “true” ECV value of 26.7%. For the investigation of ECV’s T2-dependency, the ECV was calculated based on the MOLLI T1 estimates from the database for a wide range of physiological T2 values for pre-contrast blood (200- 300msec) and myocardium (20-100msec). Results MOLLI-based ECV calculation always demonstrates underestimation that becomes greater for low T2 values of pre-contrast myocardium and high T2 values of pre-contrast blood. Moreover, ECV calculation presents higher dependency on pre-contrast myocardial T2 values compared to the T2 values of pre-contrast blood. For pre-contrast myocardial T2 values of 45, 65, and 85msec (corresponding to normal, edematous and infarcted myocardium respectively) and pre-contrast blood T2 value of 250msec, the measured underestimation was 3.6%, 2.5% and 1.8% respectively.

P61

Framework to quantify the metabolic rate in the heart using Monte Carlo simulation and Compartmental Modeling

FLOREZ PACHECO Edward^{1,2}, FONSECA Henrique da¹, VIJAYAKUMAR Vani², FURUIE S Sergio¹.

¹School of Engineering, University of Sao Paulo, Brazil

²Department of Radiology, University of Mississippi Medical Center, USA

The Nuclear Medicine imaging using PET modality allows to evaluate the physiological condition of the heart (i.e. heart disease, perfusion, cardiac stress, physics disorders, etc.), by the use of small amounts of radioactive material. While the visual information provided by PET image is quite important and today is heavily used by the specialists, it is clear that having quantitative values of the metabolism would help to determine the real condition of the myocardium, to get a more accurate diagnosis and to apply a better treatment. Thus, we developed a framework using different tools to simulate a real PET exam focused in the heart in order to analyze the metabolic exchange in this organ. This research produced realistic PET exams by using GATE platform that perform Monte Carlo simulations, together with an anthropomorphic phantom of the whole body called MASH. This study contemplated the modeling of a commercial PET scanner with BGO detectors, where the MASH's thorax was imaged by the scanner. In order to enhance the realism of the simulation, clinical data was considered, like the quantity of radiotracer (FDG) injected, time of acquisition, number of frames along the time, among others. Next, the projections were reconstructed using STIR's algorithms. With the aim of obtaining a better quality of the volumes and to select the specific ROI, filters and segmentation algorithms were applied, respectively. Finally, the heart metabolic analysis was performed using a mathematical model that seeks to describe and to quantify the level of consumption and exchange of glucose in the heart through a model with three compartments. The metabolic parameters obtained were: $K_1=0.5690$, $k_2=0.2266$, $k_3=0.0718$, $k_4=0.0243$. It was evidenced that the process of metabolic quantification using compartmental modeling is significantly relevant because of its flexibility, noninvasively and reliability. Hereafter, we will apply this framework under real PET images.

P61

Left Ventricle Functional Geometry in Different Cardiac Pathology

Tatiana Chumarnaya*, Olga Solovyova, Yulia Alueva, Sergey P Mikhailov, Valentina V Kochmasheva, Vladimir S Markhasin

Institute of Immunology and Physiology of Russian Academy of Sciences; Ural Federal University
Yekaterinburg, Russian Federation

Functional geometry of left ventricle (FGLV) refers to the dynamical change in the ventricular shape during contraction and relaxation. It has been shown that FGLV significantly contributes to the regulation of contractility and cardiac pump function in health and disease. The aim of our work is to evaluate the FGLV in patients with various myocardial diseases. A control group of healthy people (n=24) was compared to the study groups of patients with ischemic heart disease (IHD, n=52) with preserved ejection fraction (EF); patients with dilated cardiomyopathy (DCM, n=25) before and after cardiac resynchronization therapy (CRT) and patients after heart transplantation (HT, n=9, 15 days after operation). Based on 2D-echocardiography the following FGLV parameters were evaluated: a regional heterogeneity index (RHI); a systolic asynchrony index (SAI); a Gibson sphericity index; an apical conicity index; a Fourier shape-power index (FSPI). Patterns of the spatial and temporal heterogeneity of LV regional systolic function and FGLV indexes were characterized in control group and in patients. Both RHI and SAI in IHD patients increased significantly (RHI: $26\pm 2\%$ vs $15\pm 2\%$; SAI: $18\pm 2\%$ vs $13\pm 2\%$, sensitivity of 34%; specificity of 99%), and a strong negative correlation between RHI and EF was shown. FSPI in IHD patients was statistically higher throughout the contractile cycle. In DCM patients before operation, FGLV characteristics dramatically differed from the control. In most patients responded to CRT by increased EF, normal FGLV characteristics restored in 5 days after operation. HT patients with no rejection had normal FGLV characteristics, but HT patients with acute rejection had deterioration of FGLV. The spatio-temporal heterogeneity of LV regional wall motion is one of the characteristic features of normal cardiac pump function. FGLV changes in pathology. FGLV abnormalities are early predictors of LV pump function disturbances. FGLV recovery is accompanied with an increase in LV pump function.

P61

Detection of fibrosis in LGE-cardiac MRI using Kernel DL-based clustering

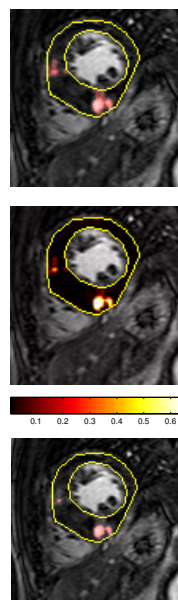
Juan Mantilla*, José Luis Paredes, Jean-Jacques Bellanger, Julian Betancur, Frédéric Schnell, Christophe Leclercq and Mireille Garreau

Université de Rennes 1, France

Aims & Background: Hypertrophic cardiomyopathy (HCM), as a common genetic cardiovascular disease, is characterized by the abnormal thickening of left ventricular myocardium. Myocardial fibrosis commonly presented in HCM can be detected in Late Gadolinium Enhanced (LGE) cardiac magnetic resonance imaging. Here, we propose the use of a Dictionary Learning (DL)-based clustering technique for the detection of fibrosis in LGE-Short axis (SAX) images.

Methods: For this study, the inner and outer contours were manually delineated by a cardiologist on LGE-SAX inversion recovery (IR) sequences at mid-diastole. Random image patches of size $[3 \times 3]$ are taken as input atoms to train a classifier based on the sparse codes obtained with a DL approach: 1) in an unsupervised step, two clusters are obtained from the similarity matrix among the training patches after performing a multisignal 1-D clustering based on wavelets, 2) a dictionary is constructed with the patches clustered in two classes: enhanced and non enhanced pixels, 3) a classifier (K -Nearest Neighbor) is trained with the sparse codes coefficients of the training patches obtained from a DL algorithm based on kernel 4) Finally, for a new LG-SAX image, the label of each pixel is predicted by using the trained classifier.

Results: Acquisitions obtained with a cardiac MRI Philips Achieva 3T were collected from 10 patients. Figure-top, shows a LGE-SAX image example with the automated detection of fibrosis using the proposed approach. Results can be compared with the results obtained using a method validated in the literature (fuzzy-c means approach) that provides the fibrosis detection (Figure-bottom), after thresholding a membership map of the enhanced pixels (Figure-middle). Our results, visually evaluated by an expert, show the capacity of detection of fibrosis without the needs of tuning threshold parameters.



P61

Effect of Interpolation on Electroanatomical Mapping

Margarita Sanromán-Junquera, Raquel Díaz-Valencia, Arcadio García-Alberola, José Luis Rojo-Álvarez, Inmaculada Mora-Jiménez

Universidad Rey Juan Carlos
Fuenlabrada (Madrid), Spain

Background and Aim. Cardiac navigation systems (CNS) are often used in electrophysiological studies to create spatial-electrical maps supporting the arrhythmia mechanism identification. Sequentially recorded electrograms yield the bioelectrical information from features such as voltage and activation times in terms of their spatial location, which are subsequently interpolated for building the electroanatomical map (EAM) of the cardiac chamber. Our goal was to evaluate quantitatively the effect of interpolation in the EAM accuracy.

Methods. Triangulated irregular networks (TIN), thin plate spline (TPS), and support vector machines (SVM) were assessed by using: (a) two detailed simulated time activation maps during flutter and sinus rhythm in both atria; (b) a set of real CNS maps, given by 13 activation time and 17 voltage maps, with 6 right atria (RA), 6 left atria (LA), 4 right ventricles (RV), and 14 left ventricles (LV). Interpolation methods were benchmarked using root mean squared error (RMSE), efficiency (EF), and Willmott distance (WD).

Results. (a) EF and WD were similar for yielding a clearer cut-off point than RMSE for the number of required samples, which was around 150 atrial locations. Better EAM accuracy was obtained using TPS, followed by SVM and TIN, except for flutter in the RA, where early-meets-late was smoothed by SVM. (b) EAM accuracy in RA (measured with WD) slightly outperformed LA (0.67 vs 0.61), whereas RV and LV were similar (0.74 vs 0.74); similar EAM accuracy was given by the interpolation methods (TIN 0.73 ± 0.12 ; TPS 0.75 ± 0.13 ; SVM 0.69 ± 0.20); higher accuracy was obtained for EAM in unipolar voltage (0.91 ± 0.02), in bipolar voltage (0.74 ± 0.07) and in activation time (0.61 ± 0.14).

Conclusions. The EAM accuracy is dependent on the map type and on the cardiac chamber.

P61

Classification of Doppler Ultrasound Signal Quality for the Application of Fetal Valve Motion Identification

Faezeh Marzbanrad*, Yoshitaka Kimura, Miyuki Endo, Marimuthu Palaniswami, Ahsan H Khandoker

The University of Melbourne
Parkville, Australia

One-dimensional Doppler Ultrasound (DUS) is a commonly applied technique for fetal heart rate monitoring in medical practice, but it can also be used to identify the timings of fetal cardiac valve motion. These timings are required to estimate the fetal cardiac intervals, which are fundamental and clinically significant markers of fetal development and well-being. Several methods have been proposed in previous studies to automatically identify the timings using 1-D DUS and fetal Electrocardiography (fECG) as a reference. However DUS is highly susceptible to noise and variable on a beat-to-beat basis. Therefore it is crucial to assess the DUS quality to ensure its validity for a reliable estimation of the valve movement timings. An automated quality assessment can provide the operator with an online feedback on the quality of DUS during data collection. This paper investigates automated classification of the DUS quality using Naive Bayes (NB) classifier. The quality of 345 beats of DUS signals collected from 57 fetuses was assessed by four independent annotators and used for training and validation of the classifier. Five quality levels were assumed for rating: very bad(1), bad(2), borderline(3), good(4) and very good(5). Inter-rater agreement results of Fleiss kappa test showed a fair agreement with overall kappa=0.300, and $p < 0.0001$ confirming that the observed agreement was not accidental. The signals with the average score of below 2.5 and above 3.5 were labeled as unacceptable and acceptable, while others were labeled as ambiguous. The classification was then performed on 121 and 120 DUS segments, rated as acceptable and unacceptable, respectively. Results of 10-fold cross validation showed an average classification accuracy of 86% on training and 84% on test data, sensitivity of 83% on training and 80% on test set; and specificity of 89% on training and 88% on test data.

P61

Classifying Lung Congestion in Congestive Heart Failure using Electrical Impedance - A 3D Model

Noam Omer*, Shimon Abboud, Marina Arad

Israel

Introduction: In congestive heart failure (CHF) patients an increased interstitial fluid, secondary to increased peripheral and pulmonary capillary pressure, leads to collection of fluids in the lungs which are major causes of mortality in CHF patients. Classifying and monitoring pulmonary congestions is a significant clinical challenge, due to lack of direct access to the pleural cavity. In this study, we investigate the feasibility of the parametric electrical impedance tomography (pEIT) technique in classifying and monitoring pulmonary congestions, such as pleural effusion and pulmonary edema and supplying essential findings regarding the congestion type, localization and bilaterally, using a computerized 3D model.

Methods: The investigation is based on pEIT with a reduced number of 5 electrodes applied in a computerized 3D model of the thorax segmented into tissue types, each assigned with appropriate electrical conductivity value. The Forward Problem for Poisson's equation in the human thorax is implemented using Finite Volume Method (FVM) to estimate the potentials developed on the body surface. These potential measurements are used to reconstruct information of the spatial conductivity distribution within the body (the Inverse Problem). We have modeled local and global congestions types resembling the pathologies and used the model results in order to develop a decision algorithm for identifying the congestion type, localization and bilaterally.

Results: Significant difference ($p < 0.02$) was found in 5 out of 8 independent projections between the results obtained in a model with edema and a model with unilateral (left/right) pleural effusion. Significant differences ($p < 0.02$) were found only in 2 out of 8 projections when comparing between left and right pleural effusion.

Conclusions: The results indicate that classifying between the two types of pulmonary congestions, pleural effusion and pulmonary edema is feasible. Localization and bilaterally of pleural effusion needs further investigation. It can be concluded that pEIT technique with only 5 electrodes might be useful in clinical practice.

P62

Causality in the Cardio-Postural Interactions During Quiet Stance

Ajay Verma, Amanmeet Garg, Andrew Blaber*, Reza Fazel-Rezai, Kouhyar Tavakolian

Grand Forks, United States

Physiological systems are understood to interact with each other to maintain equilibrium. Prolonged standing is known to induce postural sway, pre-syncope symptoms and muscle fatigue. Prior work has shown the presence of interactions between the cardiovascular and postural systems during quiet stance. The cause-and-effect relation between the representative signals of the two systems remains to be established. This preliminary work presents a study to identify the causal relationship between the blood pressure (BP) and center of pressure (COP), medio-lateral COP (COPx), and antero-posterior COP (COPy) during quiet stance. A 5-minute sit-to-stand experiment was conducted for 2 healthy young participants to acquire data for the BP and COP signals. The signals were band pass filtered between 0.001 Hz and 20 Hz frequencies. The statistical framework of Granger causality was applied to test for the bidirectional causal relation between the BP-COPx, BP-COPy signal pairs. The algorithm computed the F-statistic and critical value for null hypothesis of no causality between the signals. Data were extracted for a window of 15 seconds length, translated with an overlap of 5 seconds over the last 4 minutes of the quiet stance phase to obtain 23 time windows. Data for both subjects rejected the null hypothesis for both BP-COPx and BP-COPy signal pairs. Subject 1 showed bidirectional causal relation between BP and COPy, whereas, subject 2 showed bidirectional causality between BP-COPx and BP-COPy signal pairs. The results from this study suggest that during quiet stance both the antero-posterior and medio-lateral postural sway cause the blood pressure signal and vice-versa. Additionally, two characteristic behaviors were observed in the causal interaction where 1) both signals simultaneously cause each other and 2) the two signals alternate to cause the other in sequential time windows.

P62

Influence of Psychological Stress on Systolic-Diastolic Interval (SDI) Interaction Measured from Surface Electrocardiogram (ECG)

Chandan Karmakar*, Mohammad Hasan Imam, Peng Li, Marimuthu Palaniswami

Deakin University
Australia

Stress affects the ventricular repolarization by increasing the QT interval variability. QT and TQ intervals are considered as a surrogate of systole and diastole durations. The ratio of QT to TQ interval within a cardiac cycle (i.e. QTTQ ratio) represents the synchronized contraction and relaxation operation of the heart. It has been reported that increase of QTTQ ratio can be arrhythmogenic. Besides QTTQ, the ratio of TQ to RR interval (i.e. TQRR ratio) can also be used as a non-invasive measure of the diastolic function to analyse ventricular dysfunction. In this study, the effect of stress on systolic-diastolic interval (SDI) ratios is analysed to investigate stress related alteration in ventricular repolarization in healthy subjects. We analysed the subjects of drivedb database available in Physionet to investigate the stress related changes in these parameters. 15 Healthy individuals' ECG were analysed, where stress was induced through car driving in busy traffic condition. QT, TQ and RR interval time series derived from surface ECG were used to measure the beat-to-beat QTTQ and TQRR ratio. The mean and variance of QTTQ and TQRR time series were used to compare the SDI variability in unstressed condition from stressed condition of the subjects. The study results indicate that stress induction increases the mean QTTQ ratio and decreases the TQRR ratio indicating the effect of stress on systolic and diastolic functions. However, the difference between stressed and unstressed conditions was not significant ($p > 0.05$). The variability of SDI parameters (i.e. variance of QTTQ and TQRR ratios) can detect the induced stress in healthy individual and significantly ($p < 0.05$) differentiated the stressed condition from natural steady state relaxed condition of the same individual. The significant increase in variability in QTTQ and TQRR ratio indicate the increased probability of arrhythmogenesis due to sympathetic activation during stressed condition.

P62

Radial Artery Pressure Wave-Derived Systolic and Diastolic Duration in Healthy Adults: Relation to Heart Rate and Age

Peng Li¹, Chandan Karmakar^{2,3}, Chengyu Liu¹, Changchun Liu¹

¹School of Control Science and Engineering, Shandong University, Jinan, China

²Electrical & Electronic Engineering Department, University of Melbourne, Melbourne, Australia

³Centre of Pattern Recognition and Data Analytics (PRaDA), Deakin University, Geelong, Australia

The measurements of cardiac systolic duration (SD) and diastolic duration (DD) have been well accepted as helpful tools for evaluating the cardiac functionality. In clinical practice, SD and DD are generally measured using echocardiography or heart sound signals. Recent studies have seen the attempts of approximating SD and DD by electrocardiogram (ECG)-derived QT and TQ intervals, as well as radial artery pressure (RAP)-derived foot-to-notch and notch-to-foot intervals. The simplicity in measuring ECG and RAP signals allows the SD and DD measurements implemented in novel household intelligent medical devices. However, to the best of knowledge, currently there lacks deep elucidations on their performance when used as surrogate SD and DD data.

In the present study, we defined SD and DD from RAP signal and investigated the relation of SD, DD, and ratio of SD to DD (S/D) to heart rate (HR) and age in healthy adults. Sixty healthy subjects were enrolled in this study, and we recorded their ECG and RAP signals simultaneously in well-defined clinical protocol. SD was determined as the interval from the systolic foot to the diastolic notch of the same cardiac cycle, and DD was defined as the interval from the diastolic notch to the systolic foot of the next cardiac cycle. HR was calculated using the RR interval in ECG. Their mean values among 10 cardiac cycles were used in the analysis.

Results demonstrated a negative linear relationship between SD and HR, a negative nonlinear relationship between DD and HR, and a positive linear relationship between S/D and HR (all $p < 0.001$). In addition, age did not suggest statistically significant relationships with all three RAP-derived parameters. Our results were in common with previous publications, confirming that the RAP-derived foot-to-notch and notch-to-foot intervals are good surrogates for the cardiac systolic and diastolic duration.

Calculation of the pulse wave velocity from waveform of the central aortic pressure pulse in young adults

Jana Hruskova*, Eva Zavodna, Jiri Moudr

St. Anne University Hospital Brno
Brno, Czech Republic

Introduction: Cardiovascular diseases are the most common causes of morbidity and mortality in developed countries. Therefore, the correct determination of the parameters indicating the disease condition is critical in effective treatment of patients. One of the parameters evaluating arterial stiffness is determining the pulse wave velocity (PWV), but the method of determining faces a number of problems.

Methods: In the study was measured 20 healthy patients in age 15-23. Using applanation tonometry by SphymoCor was measured pulse wave from a. radialis and a. carotis. PWV was measured by standardized device SphygmoCor and calculated by our method of flow triangle using central aortic pressure pulse for determination PWV.

Results: Average value of PWV calculated by method of flow triangle was 8.35 ± 0.86 m/s and average value measured by SphygmoCor 7.2 ± 0.8 m/s. The variance differences of measured and calculated values PWV was 0.785 ± 0.575 m/s. The average value of the a.radialis- a.carotis distance was 485 ± 43.4 mm.

Conclusions: According to the results it can be assumed that the new method of analysis the forward and backward waves is relatively accurate, but it is very sensitive to standardize measurement. The results are affected by several factors, is necessary to propose further steps to accurate protocol for the more precise results.

Acknowledgement: This publication was written at Masaryk university as part of the project „Kardiovaskulární systém od buňky k lůžku pacienta”, MUNI/A/1326/2014. with the support of the Specific University Research Grant, as provided by the Ministry of Education, Youth and Sports of the Czech Republic in the year 2015. “Supported by European Regional Development Fund – Project FNUSA-ICRC (No.CZ.1.05/1.1.00/02.1023)”

P62

A Low-Cost Solution to follow the Evolution of Arrhythmic Patients

R Gonzalez-Fernandez, M Mulet-Cartaya, JD Lopez-Cardona, A Lopez-Reyes, R Lopez-Rodriguez, R Lopez-Creag

Central Institute for Digital Research
Havana, Cuba

The aim of this paper is to discuss the features of a system designed to study the evolution of arrhythmic patients doing their daily activities.

The system is composed by: a small battery-powered device to acquire and transmit, via Bluetooth, an ECG channel; an Android mobile application to process the ECG and a web application. The ECG device was designed to acquire and transmit the ECG continuously since it is turn on; information about pacemaker spikes presence and electrode status are transmitted too. The Android application receives the ECG data; QRS complexes are detected and classified and heart rate is computed. A GSM/GPRS network and HTTP protocol are used to upload the information to a web application. It stores each ECG file in a MySQL database; cardiologists can check ECG strips and analyze trend charts associated to each patient. Also, cardiologist can call any patient to adjust drug treatment. The ECG device is simple, patient only have to attach three electrodes to his skin and press the ON/OFF button.

Three ECG device's prototypes were tested according to the IEC 60601-2-47 standard successfully. Two hundred three-minute ECG strips were processed; Bluetooth communication was without errors. QRS complex detection algorithm was evaluated with MIT-BIH database; sensitivity was 99,02%. Web application provides graphical tools to analyze the trend of RR intervals, heart rate and ectopic beats. The MySQL database had not report any problem in data storing or recovering processes. A medical telephone terminal, based on the MSP430F5529 microcontroller, is being developed by the authors. This terminal will perform the same functions as the Android application, but at a lower cost.

The proposed system seems easy to use by arrhythmic patients and cardiologists; it could be an important tool to follow the cardiac arrhythmias evolution with limited resources and minimal discomfort for patients.

A Mobile Application for Cardiac Rhythm Study

R Gonzalez-Fernandez, M Mulet-Cartaya, JD Lopez-Cardona, R Lopez-Rodriguez

Central Institute for Digital Research
Havana, Cuba

The aim of this paper is the discussion of the main features implemented in an Android application for ECG processing.

The software was designed to use a mobile phone, connected to a battery-powered ECG device, as a signal acquisition layer in a Telemedicine platform oriented to implement several health services. The ECG device is able to acquire and transmit, via Bluetooth, the ECG continuously. The Android application receives the ECG data according to a simple protocol. The Bluetooth pairing process is made by the proposed software following the traditional procedure. ECG data is filtered using a FIR moving average filter. QRS complexes are detected and classified, as premature or not, RR intervals are measured and heart rate is computed. An energy collector, combined with heuristic rules, was implemented to detect QRS complexes. The classification process is made taking in count RR interval duration and QRS complex width. All these information is uploading to a web site using GSM/GPRS network and HTTP protocol. Also, all the data is store in a database implemented in the phone; this feature allows downloading that information into a personal computer to make other studies. The software was programming in Java language using Eclipse SDK and SQLite database engine.

The proposed software has been tested with five models of Android mobile phones, working without problems. Errors have not been reported in communications when the distance between the ECG device and the phone is less than ten meters. QRS complex detection algorithm was tested with MIT-BIH database and the QRS detection sensitivity was 99,02%.

The developed software seems a powerful tool to convert a mobile phone, combined with the appropriated ECG device, in a medical device for several Telecardiology services. Also, an event recorder or a medium-term Holter can be implemented.

P63

Continuous vital monitoring and automated alert message generation for motorbike riders

B. Schmitz¹, C. Hofmann¹, R. Maestre², A. L. Bleda², V. Melcher³, J. van Gent⁴

¹Fraunhofer Institute for Integrated Circuits IIS, Erlangen, Germany

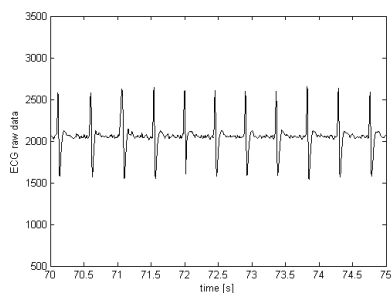
²CETEM Technologic Center, Yecla, Spain

³Fraunhofer Institute for Industrial Engineering IAO, Stuttgart, Germany

⁴Lookwell International BV, Eindhoven, Netherlands

Aims: The focus of the presented project is on a technical assistance system that avoids critical situations in traffic as well as the threat of an accident and sends an automated alert message in case of an actual accident. In addition to warnings of stress, inattentiveness or fatigue, the performed physiological monitoring is also used for driver motivation by indicating the “joy of riding” during a tour. To give first responders a basic impression on the possible severity, measurements of vital parameters from the accident site shall be provided.

Methods: The technical assistance system is based on two independently working sensor kits integrated into a driver’s equipment. The first kit puts together electrodes for ECG and EEG as well as sensors for ambient data (body temperature and humidity) and movement information based on inertial sensors into a helmet. The second kit features physiological monitoring



ECG data acquired during a motorbike ride

with primary sensors (ECG electrodes and respiration band) integrated into a garment, completed by ambient and inertial sensors inside an attachable electronics box. Both kits perform onboard biosignal processing in real-time and derive secondary parameters. The ECG is also processed for HRV specific parameters to derive the level of stress and relaxation. A Smartphone receives the data via BLE (Bluetooth Low Energy) and performs data fusion and context evaluation. In case of an accident or critical situation an alert message complying with EN 15722:2011 (eCall) is generated and sent out. Also a link to a data server is provided, giving first responders or physicians latest physiological states and trends from accident site.

Results: The sensor systems have been adapted for integration into rider equipment and work reliably during a ride. The acquired physiological signals have been compared with signal quality from wearables in other application scenarios (e.g. sports) and with signals gathered using medical adhesive electrodes.

Training-Induced Gene Expression Plasticity in Cardiac Function and Neural Regulation for Ultra-Trail Runners

María Maqueda*, Emma Roca, Daniel Brotons, J Manuel Soria, Alexandre Perera

Technical University of Catalonia (UPC)
Barcelona, Spain

Aims: This study aimed to assess the gene regulatory response from a group of 16 athletes and to observe the plasticity induced by their training on the gene expression (GE) response after their participation in an ultra-trail competition. Analyses only focused on genes annotated as belonging to circulatory system (CS) and neural regulation of cardiac function (CF) from the KEGG Pathways database.

Methods: We used microarray technology (HuGene2.0ST from Affymetrix, Inc., California) to analyse the GE profile of runners' blood samples that were collected before and after the race. Two subgroups were considered: Active and Elite based on their training hours per week (10 hours cutoff of aerobic training). A linear regression model was fit for each biomarker as a function of gender, training level, pre-post race and an interaction factor between the two last variables. In order to obtain a list of ranked genes with significant differential expression, a moderated t-test was performed for each regressor in the model (FDR adjusted p-value<0.05). Genes annotated in the selected pathways were matched to the former lists of prioritized genes.

Results: 1447 ranked genes were obtained when GE levels were evaluated before and after the race. Training regime modulated the response to exercise based on a list of 259 prioritized genes arisen from their interaction factor; where ALOX5, SORT1 and ARHGEF11 genes were identified as part of CS and neural regulation of CF pathways. Similarly, a total of 31 genes were matched to the pre-post ranking.

Conclusions: Runner training regime affects the GE levels of specific genes annotated as belonging to vascular smooth muscle contraction, neurotrophin signaling and serotonergic synapse pathways in the gene regulatory response to an acute exercise.

P63

Future Directions of Power Sources for Ambulatory ECG Monitors

Philip A. Catherwood¹, David Branagh², Dewar D. Finlay¹, James A. D. McLaughlin¹

¹Ulster University, Jordanstown, N. Ireland

²Intelesens Ltd, Belfast, N. Ireland

Introduction: There exists a technology gap between portable diagnostic healthcare devices and the energy sources that power them. Battery technology has been developing more slowly than microprocessor, wireless, and data storage technologies, yet is fundamental to every nomadic healthcare device.

Aims: This paper presents empirical results from a measurement campaign designed to quantify the power requirements for modern ambulatory ECG monitors which utilize various power-saving schemes. From this vantage point it is thus possible to critique existing battery technology and consider alternative power paradigms for future devices.

Methods: A number of commercially available ambulatory ECG monitoring devices were selected and power consumption rates observed for their assorted modes of operation. The devices utilize various battery technologies, the most popular being rechargeable lithium-polymer packs. Operation modes include –recording specific cardiac event data to an SD card or via a wireless link; sending data periodically (pre-scheduled) via an RF connection; and streaming live data continuously. Measurements were conducted for a number of devices and maximum run time (battery life) observed.

Results and Conclusions: The measurement campaign highlighted the power consumption requirements for the various ambulatory ECG monitors; from the results to be presented a subset is illustrated here. Pre-scheduled reporting using various fixed reporting frequencies yielded the following results for 1000mAh cells using Wi-Fi wireless links.

Reporting Frequency	Total Time (hours) ± std. dev.
60 min	33.80 ± 0.90
30 min	34.35 ± 2.29
15 min	34.50 ± 2.70
5 min	36.00 ± 1.88
1 min	29.73 ± 1.51

Results from across the datasets highlight the power consumption requirements by such ECG monitors and demonstrate a distinct deficit in modern battery capability (average run time being 33.68 hours (33 hours 41 minutes)) despite designers employing contemporary power supply technologies and novel power-frugal algorithms. A number of alternative power strategies are discussed and their suitability for ambulatory ECG monitors critiqued.

P63

A Usability Evaluation of ECGSim: A Simulation Tool to Aid Learning in Electrocardiology

Raymond Bond*, Eelco van Dam, Peter van Dam, Dewar Finlay, Daniel Guldenring

University of Ulster
Newtownabbey, United Kingdom

Understanding the Electrocardiogram (ECG) is a difficult challenge. The ECGSim software (www.ecgsim.org) was developed over the past two decades to reduce the burden of understanding difficult ECG concepts. ECGSim allows the user to modify action potentials and view how these changes affect the ECG. Nevertheless, the success of such tools is correlated to their 'usability'. Thus, this study quantified the usability of ECGSim during the 2014 Computing and Cardiology Conference. 14 subjects were recruited (10 males, 4 females, mean age=35, SD=10). Each subject session involved, (1) a pre-test survey, (2) eight tasks to be attempted by each subject using ECGSim (refer to PDF supplement) and (3) a post-test survey. Subjects were asked to think-aloud when attempting each task to elicit cognitive insights. Before attempting each task the subjects were asked to rate the perceived difficulty of the task. And after each task they were then asked to rate the task difficulty based on hindsight. Screen-recording software and a microphone was used record all user interactions. The experiment collated these ratings as well as the frequency of user errors and task completion times. Using statistical testing, only tasks 1 ($p = 0.05$), 6 ($p = 0.02$) and 7 ($p = 0.01$) were more difficult in comparison to what the user expected. The study also adopted the Systematic Usability Scale (SUS), which is an objective quantitative measure of usability. The mean and median SUS score was 72 (SD=17) and 78 respectively. A SUS score of 78 achieved a percentile rank of 82/100, indicating that ECGSim is quantifiably more useable than 82% of other software interfaces that were previously evaluated using the SUS mechanism (as the accepted baseline median SUS score is 68). When grading on the SUS curve, ECGSim achieved a score of B+ (out of a possible score from A-F).

P63

Cardiac Monitoring in Head Area for Motorcycle Applications

Andres L Bleda*, Rafael Maestre, Björn Schmitz, Christian Hofmann, Jose M Nacenta, Guadalupe Santa, Soledad Pellicer, Vivien Melcher

CETEM Technologic Center, Yecla, Spain
Yecla, Spain

In the case of an accident, motorcycles are a much riskier mode of transport than others. For example, the risk of death for motorcyclists is 20 times that of car occupants, and the number of deaths within the EU remains elevated. The i-VITAL project has been promoted with the goal of improving the emergency response of medical services for motorcycle accidents. The i-VITAL integrated system is capable of monitoring real-time vital sign readings so that the emergency team can prepare an adequate emergency response in advance, as well as selecting the most appropriate hospital for adequate assistance. The use of helmets is compulsory and they already include other enhanced functionalities (such as Bluetooth speakerphone, or even GPS support). However, ECG has been performed almost solely through skin contact to both sides of the body, whereas direct electrical heart signal monitoring in helmets remains an unsolved problem. Actually, to the best of our knowledge, there is no helmet capable of performing this function in a reliable manner. This paper presents a novel vital sign monitoring system for seamlessly integration into helmets, which is being developed under the i-Vital European project. An exhaustive study of signal quality of the measured ECG during bike rides in helmets has been carried out. This paper includes a brief description of the i-Vital project (vital sign monitoring in helmets and garments, accident detection system, enhanced eCall with vital signs information, and other related info is mentioned) containing real research tests to identify head zones where ECG can be measured with lower noise level and higher quality while using helmets as the integrator element. An exhaustive set of valuable real ECG tests in helmets have been performed during bike rides in order to achieve a reliable system. The final results are presented and discussed in this paper.

P63

Human Authentication Implemented for Mobile Applications Based on ECG-Data Acquired from Sensorized Garments

Daniel Tantinger*, Markus Zrenner, Nadine Lang, Heike Leutheuser, Bjoern Eskofier, Christian Weigand, Matthias Struck

Fraunhofer Institute for Integrated Circuits IIS Erlangen
Erlangen, Germany

Biometric procedures, like iris or finger print scans, are nowadays widespread methods for human authentication. Recent studies suggest that also the human electrocardiogram (ECG) is unique for each person and is therefore difficult to falsify. This fosters the use of ECG-signals as a promising method for biometric authentication. State-of-the-art solutions for biometric authentication using the ECG-signal rely on data recorded with multi-channel medical devices. However, on mobile applications the obtained signals are more difficult to handle due to motion artefacts and a lower signal-to-noise ratio. In this study a sensorized garment was used to derive a single-channel-ECG. The proposed method performs authentication based on ECG-data recorded by this mobile application. Several methods proposed in the literature were implemented - using fiducial points (Singh et. al, 2011), wavelets (Belgacem et. al, 2012), short-time Fourier transform (Odinaka et. al, 2010), autocorrelation (AC) and discrete cosine transform (DCT) (Wang et. al, 2007). Data recorded with the garment and from the PhysioNet database were evaluated and compared. Results showed that the proposed methods are not adequate to recognize a subject based on mobile recorded ECG-data. Therefore, a novel authentication technique was introduced that can cope with mobile ECG data. Based on R-peak detection, a combination of autocorrelation, DCT, and temporal and amplitude distances between detected fiducial points was applied on averaged ECG-segments to perform a one-class classification (identify a specific human amongst all others). For classification of the normalized features, a k-Nearest Neighbors classifier was used, whereby several settings of parameters were tested. Preliminary results showed that the classification rate with mobile recorded data is similar to the rate with PhysioNet data. As a consequence the introduced method can cope with noisier ECG-signals providing very few geometric features by maintaining the high classification rate of state-of-the-art methods for medical ECG-data.

P63

VitalSimML: A Well-Formed Data Structure to Capture Patient Monitoring Scenarios to Facilitate the Training of Nurses via Computer-Based Simulation

Jonathan Currie*, Raymond Bond, Paul McCullagh, Pauline Black, Dewar Finlay

Ulster University
Newtownabbey, United Kingdom

Research shows that the deterioration of a monitored patient is not always identified on time and this can ultimately lead to a poorer outcome for the patient. Those who supervise monitored patients may lack ‘accessible’ and ‘repeatable’ simulation based training. And such training could be provided using intelligent software/multimedia solutions. There is currently a lack of an open standard for capturing patient monitoring scenarios that could be freely exchanged between institutions. Such a standard would allow instructors to create bespoke scenarios that could then be parsed and visualised using a software simulator. This could be used to provide training to clinical staff and for assessing their proficiency. This study involved a review of the literature on patient monitoring. Search keywords included: patient monitoring, healthcare simulation, e-simulation, web-simulation and virtual patient. From this review, 10 patient monitoring cases were analysed for the required elements in terms of their structure and content. As a result, we designed a well-formed data structure called VitalSimML using the eXtensible Mark-up Language. VitalSimML can be parsed by software to simulate interactive healthcare scenarios, which can then be used for training nurses. VitalSimML will capture patient demographics (e.g. sex, race), the vignette (e.g. scenario description, patient history, media resources, correct diagnosis and treatment), vital signs (e.g. ECG, blood pressure, respiratory rate), an interaction model (e.g. decision logic) and the physical characteristics of the patient (e.g. height, weight, complexion). Refer to PDF supplement for an overview. In conclusion, we developed the first digital format for capturing patient monitoring scenarios. If this is adopted then trainees could ‘repeatedly’ rehearse a broader range of scenarios and practice their decision-making skills using a software simulator. This is an alternative to relying on a small number of traditional laboratory based sessions that are scheduled at a set time and involve expensive equipment.

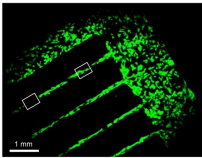
P63

Microscopic Modelling of Non-Linear Gap Junction Channels

Yves Coudière, Andjela Davidović*, Thomas Desplantez, Clair Poignard

Université de Bordeaux, Inria, IHU-LIRYC
Bordeaux, France

The usual way to model the propagation of the action potential through the cardiac tissue is to assume passive diffusive intracellular and extracellular domains, and ion channel dynamics on the cells' membrane. Gap junctions (GJ) are localised clusters of gap junction channels (GJCs) that connects electrically adjacent cells.



A patterned cell culture, Beauchamp et al (2012).

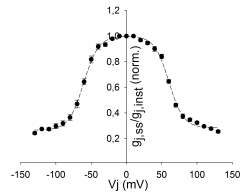
The importance of GJCs and their modifications in the signal propagation has been demonstrated in the experimental study of Beauchamp et al (2012). But, in the current mathematical models the behaviour of the GJCs is either neglected or assumed to be passive, i.e the conductance of GJCs is taken as a steady constant. On the other hand, the experimental results, obtained by the dual-voltage clamp technique, show that GJCs' conductances are time and voltage dependent.

Here we focus on describing one type of GJCs which are dominant in ventricular cells (Cx43). We use the Hodgkin-Huxley formalism to describe GJC conductance via one gating variable $g_j = g_j(t, V_j)$

$$\frac{dg_j}{dt} = \frac{g_{j,ss}(V_j) - g_j}{\tau(V_j)},$$

where the subscript *ss* stands for the steady state, and τ for the time to reach it. We incorporate the non-linear GJC current into the microscopic model of the tissue as a new boundary condition on specific parts of the cells' membranes.

Some 3D numerical experiments are currently being performed on a thin strip of cells, in order to compare the model's results with the experimental ones of Beauchamp et al (2012). We use a monolayer of 50×3 cells, represented by cylinders of $100\mu m$ length and $10\mu m$ radius, with $2\mu m$ inter-cellular distance. We model GJCs on the cross sections of the cylinders. Finally, we apply an external stimulus on the border of the domain, and observe the propagation of the AP.



Normalised $g_{j,ss}$, fitting the experimental results.

P64

Adaptation of Rabbit Ventricular Cell Model to Reproduce Action Potentials in Isolated Papillary Muscles.

Ask S Jensen, Cristian P Pennisi, Cristian Sevcencu, Jørn B Christensen, Jette E Kristiansen, Johannes J Struijk

Aalborg University
Aalborg, Denmark

Aims: The aim of this study was to establish a computational model of the rabbit ventricular action potential (AP), which would be suitable for investigation of drug effects on the AP of the isolated rabbit papillary muscle.

Methods: The data used in this study consisted of transmembrane AP recordings from isolated right ventricular papillary muscles from 21 rabbits. An existing detailed computational model of the rabbit ventricular AP was adapted to reproduce parameters of the experimental AP recordings. This adaptation was carried out by a reduction of the maximum conductivity of both the fast sodium current (I_{Na}) and the overall depolarizing current (I_{CaL} , I_{NaCa} , I_{NaK}) in order to optimally reproduce both the AP amplitude and the AP duration (APD, the 30%, 60%, and 90% repolarization durations) at multiple pacing rates. The resulting model was validated by comparison to data from the literature and the original model.

Results: At 2 and 0.5Hz pacing respectively, the experimentally recorded steady state 90% APD (APD_{90}) was 114 ± 11 ms and 150 ± 13 ms. After adaptation to experimental data, the model produced a steady state APD_{90} of 131ms at 2Hz and 143ms at 0.5Hz. Validation showed that the adaptation maintained model stability and did not substantially affect internal Ca dynamics or responses to stimuli.

Conclusion: A model of the rabbit ventricular AP was adapted in order to reproduce parameters of experimental transmembrane AP recordings from the isolated right ventricular rabbit papillary muscle. This adapted model is useful for computational model based analysis of drug effects on the rabbit papillary AP.

T-wave Morphology Depends on Transmural Heterogeneity in a High-Resolution Human Left-Ventricular Wedge Model

Massimo W Rivolta*, Graham H Bevan, Viatcheslav Gurev, John J Rice, Coeli M Lopes, Jean-Philippe Couderc

Italy

Aims: The role of spatial heterogeneity on the T-wave is still controversial. Here, we use a high-resolution in-silico cardiac wedge model to evaluate the role of the transmural heterogeneity on T-wave morphology.

Methods: Computer simulations were performed in which the transmural electrograms were recorded at a heart rate of 60 BPM. The QT interval, TpTe interval and TpTe/QT ratio were extracted. We used: i) a high-resolution 3D cardiac wedge model (~4 millions cells, 0.2 mm spacing) excised from a left ventricle bi-ventricular human heart model (~30 million cells); and ii) a modified version of the Ten Tusscher 2006 cardiac cell model with late sodium current added. Heterogeneity was generated by changing the spatial distribution of cell types across the wedge. The region from endocardial surface to a defined depth (0 to 100%) was filled with M-cells with a long APD; the remainder was Epicardial cells with a short APD. Activation was in the direction of endocardium to epicardium.

Results: A negative T-wave was obtained when no heterogeneity was present because depolarization and repolarization were in the same direction. A positive T-wave requires the repolarization in the reverse direction by having longer APDs toward the endocardium. QT interval duration monotonically increased with the thickness of the M-cells layer. In contrast, TpTe and TpTe/QT were longest when the layer of M-cells was approximately 60% of the total wall thickness. Further, increasing M-cell layer to 100% reduced TpTe and TpTe/QT because of decreased heterogeneity. Similar results were obtained by spatially mixing cell types versus discrete separation into layers.

Conclusions: T-wave morphology depends on the distribution of cell types. In particular, we observed a high correlation between QT interval and the thickness of the M-cell layer, while TpTe and TpTe/QT were the longest when the cell distribution was more balanced between the different cell types.

P64

Influence of gap junction dynamics on the stability of reentrant waves in cardiac tissue

Claudia Hawks*, Jorge Elorza, Jean Bragard, Inma R. Cantalapiedra+, Angelina Peñaranda+, Blas Echebarria+

University of Navarra
Pamplona, Spain

+Polytechnic University of Catalonia
Barcelona, Spain

Aims: In the literature, simple models assuming constant conductivities often model the electrical connection between cardiac cells. However, experimental studies have shown that gap junctions (GJ) actually connect adjacent cardiac myocytes. These GJ are complex proteins of the connexin family (Cx40; Cx43; Cx45 being the most commonly found in human cardiac tissue). These GJ possess their own dynamics and this dynamics interacts with the propagating action potential (AP) by remodeling the conductivities of the cardiac tissue (in analogy to the plastic behavior of the brain cells). The aim of the present paper is to study the influence of the GJ dynamics on the stability of the AP.

Methods: The model that we have used is a one-dimensional ring of cardiac tissue of size L (size is varied between 6 to 10 cm) where the electrical activity is modeled by the bidomain formulation. In addition, the Beeler-Reuter model and the Peñaranda *et al.* model [1] for the active properties of the membrane have been used. The GJ dynamics is described following the works of Lin [2] and Desplantez [3]. The bidomain model has been reformulated in terms of the intra- and extra-cellular electrical potential in order to model more accurately the GJ dynamics.

Conclusions: The addition of the GJ dynamics in the model of cardiac propagation has modified the stability producing alternans dynamics rather than regular dynamics observed in the case of constant conductivity. We have also observed the appearance of conduction block when the AP was stable in the constant conductivity case.

References:

[1] Peñaranda A, Cantalapiedra IR, Bragard J, Echebarria B., Cardiac dynamics: a simplified model for action potential propagation. *Theoretical, Biology and Medical Modelling*, 2012; **9**: 50 doi:10.1186/1742-4682-9-50.

[2] Lin X, Crye M, Veenstra RD. Regulation of Connexin43 Gap Junctional Conductance by Ventricular Action Potentials. *Circ Res*. 2003; **93**:e63-e73.

[3] Desplantez T, Halliday D, Dupont E, Weingart R. Cardiac connexins Cx43 and Cx45: formation of diverse gap junction channels with diverse electrical properties. *Eur J Physiol* 2004; **448** :363375.

Parameter Sensitivity from Single Atrial Cell to Tissue: How Much does it Matter? A Simulation and Multivariate Regression Study

Eugene TY Chang*, Richard H Clayton

University of Sheffield
Sheffield, United Kingdom

Motivation: Initiation and maintenance of atrial arrhythmias are poorly understood and computational models are used to understand cellular and multicellular electrical activity. We previously performed parameter sensitivity analysis in the Courtemanche-Ramirez-Nattel (CRN) human atrial cell model, and sought to extend this to address sensitivities across spatial scales. Thus, in this study we investigated how input variability and uncertainty at cellular level propagates through to affect tissue level dynamics.

Methods: We simulated action potential (AP) propagation in a strip of cardiac tissue, using the monodomain and CRN tissue/cell models. Input maximal conductances ($p=12$) within the CRN model were varied within $\pm 1/3$ of baseline, and points in parameter space selected by Latin hypercube sampling. The tissue was paced for twenty beats at 1Hz (S1), and 6 metrics of AP shape were derived for the final beat (max dV/dt , max voltage, resting voltage, action potential duration to 90% repolarization (APD90), resting voltage and APD to 50% repolarization (APD50)). S1 pacing was followed by a single ectopic beat (S2) at different intervals, at one end and the midpoint of the tissue. Additional tissue metrics were calculated, including conduction velocity (CV), CV and APD restitution and the size of the tissue vulnerable window. Subsequently, parameter sensitivity on both tissue and cell level outputs was performed using partial least squares regression following Sobie (2009). Simulations and postprocessing were performed in Nektar++ and Matlab (Mathworks). Results/Conclusions Regression values were smaller in tissue compared to cell (APD90/max dV/dt $R^2=0.30/0.35$ in tissue vs $R^2=0.92/0.93$ in cells). AP metrics exhibited stronger sensitivities to maximal ionic conductances in single cell compared to tissue simulations (sensitivity indices 0.93/0.98 for max dV/dt /max voltage to G_{Na} in cell vs 0.50/0.58 in tissue) while CV was sensitive to G_{Na} (0.61). Further analysis of functional metrics in tissue will determine sensitivity of tissue to cellular changes.

P64

Effects of Enhanced Sodium Currents in Mathematical Model of Heterogeneous Myocardium

Nathalie Vikulova^{1,2,*}, Anastasia Khokhlova^{1,2}, Olga Solovyova^{1,2}, Leonid B. Katsnelson¹

¹Institute of Immunology and Physiology, Ural Branch of the Russian Academy of Sciences

²Ural Federal University, Yekaterinburg, Russia

Aims: Some mutations in the SCN5A gene encoding cardiac sodium channels cause the long QT interval syndrome. However, possible effects of enhanced function of sodium channels on transmural gradient in electrical and mechanical properties of myocardium has not been sufficiently studied. We used our mathematical models to investigate effects of enhanced sodium current on both electrophysiological and mechanical activity of heterogeneous myocardium.

Methods: We utilized our sub-epicardial (EPI) and sub-endocardial (ENDO) guinea pig cell models, which take account for transmural differences in several ionic currents and myofilament contractile mechanisms between the cells, and our 1D continuous model of heterogeneous myocardial tissue comprising mechanically and electrically coupled EPI and ENDO cardiomyocytes. Rhythm disturbances in the models were induced by increasing the density of intermediate (I_{NaIm}) and late (I_{NaL}) components of sodium currents during isometric contraction at 1 Hz.

Results: An increase in I_{NaIm} led to delayed afterdepolarizations and extra action potentials (APs) prior to regular stimuli, which almost stopped contractions in EPI, but not in ENDO cell. However, the 1D tissue strand demonstrated more stable behavior than isolated cells, beat-to-beat increase in APs duration due to intercellular coupling resulted in an increase in the dispersion of repolarization.

An increase in I_{NaL} led to early afterdepolarizations (EADs) in ENDO, but not in EPI cell. The 1D tissue strand demonstrated EADs propagation from ENDO to EPI cells via electrical coupling resulting in extra APs in EPI cells. The strand generated isometric force with unstable amplitudes alternating around the control force.

Conclusions: Enhanced I_{NaIm} and I_{NaL} induced abnormalities in activity of both cell types, but scenario of rhythm disturbances was different. The 1D heterogeneous myocardial tissue demonstrated more regular behavior under increased I_{NaIm} , while enhanced I_{NaL} produced alterations in electrical and mechanical activity of the strand.

Supported by the Russian Science Foundation (#14-35-00005).

Influence of Right and Left Atrial Tissue Heterogeneity on Atrial Fibrillation Perpetuation

Adrian Luca*, Vincent Jacquemet, Nathalie Virag, Jean-Marc Vesin

Swiss Federal Institute of Technology, Lausanne, Switzerland
Lausanne, Switzerland

Purpose. Atrial electrical and structural remodelling has been consistently linked with AF initiation and maintenance. We propose a biophysical modelling approach to separately investigate the impact of right and left atrial (RA/LA) electrical heterogeneity on AF perpetuation.

Methods: A Courtemanche atrial cellular model with modified channel conductance was used to simulate self-terminated AF episodes. The baseline AF substrate was based on 4:1 anisotropy ratio and uniform membrane properties. AF was initiated by a ramp pacing protocol applied in the pulmonary veins region. Once AF was observed, random patchy heterogeneities in action potential duration (shorter action potential duration inside the patches) were further introduced in the cellular model for the subsequent simulation of AF. The simulations were performed separately for the RA/LA heterogeneities in the range 20-80% of the size of each atrium (the characteristic length scale of patches was 7.5mm). The effect of tissue heterogeneity on AF perpetuation was quantified by the duration of AF episodes (an AF episode lasting more than 50s was considered as non-terminated).

Results: The mean AF episode duration was 21.6 ± 13 seconds for homogeneous tissue and increased to 40.4 ± 18 sec ($p < 0.05$; 52 simulations) in the presence of heterogeneities. For high percentages of heterogeneities, the mean AF episode duration and the number of non-terminated AF episodes were significantly higher for RA heterogeneity compared to the LA heterogeneity (48 ± 9 sec vs. 32.8 ± 21 sec, $p < 0.05$; 25 vs. 15 non-terminated AF episodes in 26 simulations). No significant differences were found for low percentages of heterogeneities. However, in the latter case, a large variability of AF duration with respect to the spatial localization of tissue heterogeneities was observed.

Conclusions: The results are evidence of a direct link between the mechanism underlying AF and the spatial extent/localization of tissue heterogeneities, with the right atrial substrate more likely to be involved in persistent AF.

P64

Computer Analysis of Isolated Cardiomyocyte Contraction Process via Advanced Image Processing Techniques

Jan Odstrcilik*, Vratislav Cmiel, Radim Kolar, Marina Ronzhina, Larisa Baiazitova, Martin Pesl, Jan Pribyl, Ivo Provaznik

St. Anne's University Hospital – International Clinical Research Center (ICRC)
Brno, Czech Republic

Introduction: Isolated cardiomyocytes have been used as valid and useful model in experimental cardiology research for decades. A single cardiomyocyte is considered as a functional unit with electrical, signaling, and mechanical functions of cell excitation-contraction process. The contraction function is usually measured via expensive and complex instruments which can either damage the cell or take much time for setting up (AFM – Atomic Force Microscopy). In contrary, recent development of optical microscopy and digital cameras suggests utilization of touch-less cardiomyocyte video acquisition in connection with advanced image processing techniques for automatic and precise evaluation of cardiomyocyte contraction process.

Methods: A typical adult cardiomyocyte is a cylindrically-shaped cell (approx. with length $100\mu\text{m}$ and diameter $25\mu\text{m}$) that can be observed as a bright structure surrounded by dark curve in bright-field optical microscopy. The dark curve surrounding the cardiomyocyte is formed by cell membrane that blocks and scatters visible light. The proposed paper presents an automatic membrane detection method via computer processing of acquired video-sequences by utilization of dynamic active contour model. Evaluation of detected cell area is consequently used for estimation of cardiomyocyte contraction function and its beating parameters.

Results: A set of eight isolated cardiomyocyte video-sequences was acquired using bright-field optical microscopy equipped with high-speed scientific camera with framerate 50-100 fps and 512×512 pixel resolution. A contraction function was extracted from video-sequences and compared with synchronized contraction measurement by AFM. The results show high correlation ($R>0.9$) between the cardiomyocyte beating parameters derived from estimated contraction function and standard AFM measurement. The results signalize the proposed methodology can be used for evaluation of cardiomyocytes contraction processes, which can be useful in drug screening. The method is also robust against the cell rotation and translation during contraction as well as in case of low-intensity imaging, which allows its utilization for fluorescence applications.

Voltage Sensitive Dye di-4-ANEPPS Prolongs Impulse Conduction Through Ventricles, but not Through AV Node in Isolated Rabbit Heart

Veronika Olejnickova*, Marina Ronzhina, Oto Janousek, Jana Kolarova, Katerina Fialova, Ivo Provaznik, Marie Novakova

Masaryk University
Brno, Czech Republic

Aim: Voltage sensitive dye di-4-ANEPPS is widely used in studies of cardiac electrophysiology. Although reduction of cardiac impulse propagation and prolongation of RR interval in the presence of di-4-ANEPPS is known, the effect on impulse conduction through AV node has not been studied yet. The aim of this study was therefore quantification of di-4-ANEPPS impact on duration of impulse conduction through AV node and ventricles in isolated rabbit hearts.

Methods: Isolated hearts from 12 New Zealand adult rabbits were included in this study. Study was performed at Langendorff model perfused with Krebs-Henseleit solution (1.25 mM Ca²⁺, 37°C, 70 mmHg). After 20 minutes of stabilization, 6 hearts were stained with 2 µM di-4-ANEPPS for 25 minutes followed by 25 minutes of wash out of redundant dye. Another 6 hearts were subjected to 50 minutes of perfusion without di-4-ANEPPS immediately after stabilization. Three orthogonal touch-less electrograms were recorded during the whole experiment. The changes in PQ interval, QRS duration, and incidence of AV block of the second and third degree were subsequently analysed.

Results: Voltage sensitive dye di-4-ANEPPS statistically significantly ($\alpha = 0.05$) prolongs PQ duration between 13-16 minutes of staining period and QRS duration after 14 minutes of staining period as compared with non-stained hearts. During wash out period changes in QRS duration persist, while changes in PQ period reverted. AV blocks of the second and third degree were detected only in sporadically.

Conclusions: It can be concluded that voltage sensitive dye di-4-ANEPPS leads to prolongation of cardiac impulse conduction through the ventricles. Conduction through AV node is impaired only slightly.

P64

Quantification of the Effects of Electrical Remodelling due to Hypertrophic Cardiomyopathy on Human Ventricular Electromechanical Activity and Energetics

Gareth M Jones*, Michael A Colman, Ismail Adeniran, Henggui Zhang

University of Manchester
Manchester, United Kingdom

Introduction: Hypertrophic cardiomyopathy (HCM) is an inherited disease that affects approximately 1 in 500 people worldwide. It is associated with mutations in sarcomeric proteins and leads to asymmetrical left ventricular hypertrophy, interstitial fibrosis and ventricular arrhythmias. Inefficient utilization of energy by mutant proteins may be the cause of energetic compromise seen with the disease. Despite experimental evidence detailing electrical remodelling, the mechanisms and contributions to cardiac malfunction in HCM are unclear.

Methods: The O'Hara-Rudy model of human ventricular single cell electrophysiology is updated to incorporate descriptions of (i) reactive oxygen species (ROS) production, (ii) mitochondrial energetics and (iii) force-generation, based on recent models for each component. HCM is included by adjusting cell model parameters to reproduce electrical remodeling based on recent experimental data. Currents modified include I_{CaL} , I_{NaL} , I_{NCX} and I_{K1} . A leftward shift of the force- Ca^{2+} relationship was included, reproducing the increased myofilament sensitivity to Ca^{2+} associated with the disease.

Results: Electrical remodelling due to HCM prolonged the action potential duration (APD) by 57% and enhanced the intracellular Ca^{2+} transient, leading to a 46% increase in contractile force. Greater developed force is accompanied by a higher tension cost, resulting in energetic compromise shown by a reduced phosphocreatine to ATP ratio. An increase in mitochondrial ROS production of 18% resulted in higher levels of active CaMKII with resultant increases in the population of phosphorylated target channels, including L-type Ca^{2+} and late Na^{+} . Levels of CaMKII were in agreement with those seen experimentally.

Conclusions: In this study we have developed an integrated single cell model of the human ventricle which simultaneously accounts for electrophysiology, energetics and force generation. The model demonstrates the coupled nature of these systems; ROS production enhanced the effect of HCM remodelling on inward currents through CaMKII activation; both electrical and myofilament remodelling contributed to increased contractile force.

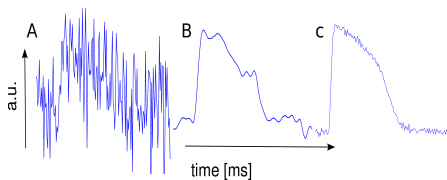
P64

Robust Framework for Quantitative Analysis of Optical Mapping Signal without Averaging

Ilija Uzelac, Flavio . H. Fenton

School of Physics, Georgia Institute of Technology, Atlanta, USA

Aims: Trans-membrane voltage V_m , and intracellular free calcium concentration $[Ca_i]^{+2}$ signals obtained from optical mapping experiments are often corrupted with noise, with S/N ratio sometimes close to one (fig1a). This is due to the low light



Zebra fish Action Potential Duration. a) Raw b) Spatio-temporal filtering c) Stacked signal.

intensities and very short exposure times when recorded with cameras at frames rates of 500-1000 fps. General approach is to apply strong spatial and temporal filtering at the expense of signal degradation and loss of critical information (fig1b). In this paper we present and analyze an oversampling signal/image processing technique where due to the cycling processes in cardiac activity can be performed repetitive and deterministic measurements.

Methods/Results: By pacing the heart at a specific cycle length it is possible to record multiple repetitions of voltage and calcium propagating waves. The timing of the pacing stimuli is precisely controlled with a microcontroller to know the exact times for stacking of the images/signals. The stacking reduces noise effectively as the square root of the number of stacked images. Signals obtained by our stacking method have significantly reduced noise levels (fig1c) allowing precise quantification of the wavefront, wave-back and action potential duration. This technique is of great use when requiring the computing and analyzing of electrophysiological tissue characteristics with great precision.

Conclusion: This method is easy to implement in optical mapping recordings of cardiac dynamics where repetitive and deterministic measurements can be performed. We show examples of accurately obtained conduction velocities, APD restitution and alternans (spatial patterns), and bifurcations on several animal hearts (fish, rabbit, cat and pig).

P64

3-D Modeling of the Thorax for Seismocardiography

Alexandre Laurin*, Kouhyar Tavakolian, Andrew Blaber, Sébastien Imperial, Philippe Moireau, Dominique Chapelle

Vancouver, Canada

Seismocardiography (SCG) is measurement of sternal acceleration caused by heart beats. With the proliferation of inexpensive and ultra-sensitive accelerometers in smart phones, SCG is becoming a cost-effective and easy-to-use alternative to traditional cardiac monitoring, with built-in telemedicine capabilities. In order to interpret and analyze SCG, we must have a representation of the system capable of modeling it. No physiological 3-D model of the thorax and its interactions with the beating heart exists to interpret seismocardiograms. We identified the mechanical properties of the relevant tissues in the thorax in terms of shear and Young's moduli. We thus defined material properties for sternal and costal bone, as well as for costal cartilage. We developed a 3-D mesh of the heart and thorax, obtained by adapting an existing life-like 3-D mesh of an entire male body. We identified the regions of the thorax that come in contact with the heart and input physiologically reasonable forces there. The system reacted in a way consistent with SCG observations. In a final step, we will couple the thoracic deformation model to a 3D beating heart model previously developed by our M3DISIM collaborators. This coupling will incorporate contact boundary conditions that take into account the pericardium. Ultimately, we will create a thoracic model capable of returning seismocardiogram signals. This model will open the door to further work in solutions to inverse problems, and patient-specific modeling.

P64

Massively Parallel CUDA Simulations of Cardiac and Embryonic MRI on a Cloud-based Cluster

George Kantasis, Christos Xanthis, Anthony Aletras*

Thessaloniki, Greece

Introduction Magnetic Resonance Imaging (MRI) simulations have been used for pulse sequence optimization and training purposes. Recently, advanced experiment setups became feasible using CUDA-technology which resulted in faster cardiac and embryonic MRI simulations. However, in cases of more complex experiments (cardiac motion, blood flow) more advanced hardware configurations are needed. In this study we hypothesized that a cloud-based application of advanced MR simulations could address that concern. The aim was to distribute a previously developed MR simulator on a scalable cloud-based infrastructure. **Methods** The MapReduce algorithm was used for the distribution of the recently developed MR simulation platform MRISIMUL on the cloud. In this study, a Gradient-Echo pulse sequence (241601 timesteps) was simulated on a 3D anatomical model of a human embryo (1101824 isochromats). The model was evenly shared among the nodes of the cluster. The Mapper step was implemented on each node by executing the simulation on the corresponding part of the model. The Reducer step was implemented by gathering the resulting k-space matrices on a central node, summing them up and performing the Fourier-transform. Amazon Web Services (AWS) was selected as the cloud service provider for hosting the cluster infrastructure. The cloud-based experiments were performed on g2.2xlarge instances equipped with one NVIDIA GRID K520 GPU of 4GB global memory. To evaluate scalability, the execution times of the simulations were recorded for an increasing number of available nodes in the cloud (1-16 nodes). **Results** For the current experiment configuration, the total simulation time was described by the following formula: $\text{Total Time(sec)} = 1232\text{sec}/(\text{Nodes}) + 92\text{sec}$, resulting in a speedup of about 8 times on a sixteen-node cluster compared to the single-node setup. The GPU execution time showed an almost linear speedup with a slope close to 1 whereas a roughly constant overhead (92sec), associated with processing and gathering the data, was always present.

P64

Robust Statistical Modeling of the Atrioventricular Node during Atrial Fibrillation

Mikael Henriksson*, Valentina DA Corino, Leif Sörnmo, Frida Sandberg

Lund University
Lund, Sweden

Introduction: The atrioventricular (AV) node plays a central role during atrial fibrillation, influencing the conduction of atrial impulses and, therefore, heart rate. Statistical modeling represents a non-invasive approach to characterizing certain AV nodal properties. Such modeling may be useful, for example, when evaluating the efficacy of antiarrhythmic drugs. A statistical dual pathway AV node model has previously been proposed by our group. Since the number of parameters defining that model sometimes implies estimates with larger variance, a new model is considered with a reduced number of model parameters.

Method: In the new model, it is assumed that every atrial impulse attempts to pass through each pathway with equal probability, irrespective of the pathway taken by the previous impulse. This approach eliminates the need for a model parameter which accounts for the ratio between ventricular activations caused by pulses conducted in either pathway. The present model is defined by the following five parameters: one parameter describing the mean arrival rate of atrial impulses to the AV node and four parameters describing functional refractory periods and prolonged refractoriness due to concealed conduction/relative refractoriness. A maximum likelihood approach is employed for estimating the four AV node parameters.

Results: 292 24-h Holter recordings from the RATAF (RATe control in Atrial Fibrillation) database were analyzed (recorded during administration of beta blockers and calcium channel blockers). Using a wavelet-based performance measure related to the RR interval histogram, the new model accounted for 89% of the analyzed segments, while the previous model accounted for 90%. On the other hand, the standard deviations of the parameter trends were considerably lower than those of the previous model, suggesting that more robust estimates are produced.

Conclusions: The results suggest that the new model offers information similar to the previous model, but with more reliable parameter estimates.

P65

Characterization of AV-nodal Properties during Atrial Fibrillation using a Multilevel Modelling Approach

Mikael Wallman*, Frida Sandberg

Fraunhofer-Chalmers Centre
Sweden

Background: The atrioventricular node (AVN) plays an important role during atrial fibrillation (AF) since it prevents the heart from racing by blocking atrial impulses. Rate-control of AF is a commonly used treatment and several randomized clinical trials have shown that it may be as effective as rhythm-control medication. In order to optimize rate control and improve clinical decisions there is therefore a need for quick and reliable characterization of the individual AVN.

Methods: We employ a multi-level modelling approach, combining a previously presented functional model (M1, allowing rapid estimation of 6 statistical parameters), with a novel, more detailed network model (M2, allowing detailed description of impulse propagation through the AVN using 18 parameters). Using a genetic algorithm, we estimate >200 sets of M2 parameters from ventricular activation sequences (RR-series) derived from clinical ECGs from two distinct AF-patients (P1, unimodal RR-series, and P2, bimodal RR-series) and compare these to the corresponding M1 parameters.

Results: For P1, the estimated M1 parameters indicated that the functional refractory periods were 390ms and 590ms for the slow (SP) and the fast pathways (FP), respectively. Corresponding values for P2 were 320ms and 340ms. In the M2 parameters, the conduction delays for P1 and P2 were virtually identical (FP: 1-56 ms, SP: 23-80 ms). Conversely, the effective refractory periods differed, with ranges for SP estimated to 250-450ms (P1), 120-270ms (P2), and ranges for FP estimated to 300-750ms (P1), 210-480ms (P2).

Conclusions: We have demonstrated that a fixed set of statistical properties for the RR-series correspond to limited ranges of electrophysiological properties of the AVN, and that these can be estimated from ECG. Estimated parameters suggest that the refractory properties of FP and SP play a larger role than the conduction delay in the emergence of bimodal RR-series under AF.

P65

Influence of Left Atrial Geometry on Rotor Core trajectories in a Model of Atrial Fibrillation

Konstantinos N Tzortzis*, Caroline H Roney, Norman A Qureshi, Fu Siong Ng, Phang Boon Lim, Spencer J Sherwin, Nicholas S Peters, Chris D Cantwell

Imperial College London, London, UK

Background and Aim: Rotors, which are the organizing sources of atrial fibrillation (AF), have been known to exist in various animal models and there is increasing evidence about their existence in human AF patients. Rotor generation and maintenance is affected by myocardial architecture and geometry and ectopic discharges in the pulmonary veins (PV) of the left atrium (LA). The present study is an *in silico* investigation into the influence of the LA geometry, in isolation, on the spatiotemporal dynamics of rotors.

Methods: The computational methodology involved the reconstruction of an anatomically accurate LA geometry using MRI data from a patient with persistent AF. Changes representing electrical remodeling in AF were also incorporated into the computational model, and spiral wave simulations were performed using the Nektar++ spectral/*hp* element framework. To aid analysis, the three-dimensional mesh was mapped to a two-dimensional distance-preserving surface representation and the spatiotemporal organization of rotors was investigated by tracking over time singularities in the phase of the action potential.

Results: In contrast to other studies, the homogeneous isotropic substrate used in this study was found not to inhibit rotor drifting and rotor attraction by PVs. Furthermore, after meandering for a short period of time, rotors become spatially stable over time in various LA regions. Moreover, PVs, and especially the right superior and left inferior PVs can function as rotor attractors, responsible for the initiation of PV re-entrant waves which continue for extended durations. The overall trajectory and fixed points of attraction of rotors are highly sensitive to the location where sustained rotors and spiral waves were generated.

Conclusion: Our *in silico* results show that the LA geometry itself plays an important role in the perpetuation of fibrillatory activity as other relevant clinical studies have suggested.

P65

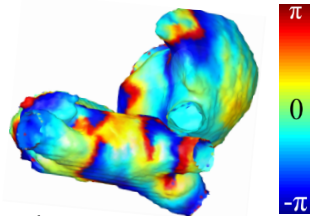
Methods for analyzing signal characteristics of stable and unstable rotors in a realistic heart model

Markus Rottmann¹, Laura Anna Unger¹, Gunnar Seemann¹, Amir S. Jadidi², Thomas Arentz², Olaf Dössel¹

¹ Institute of Biomedical Engineering, Karlsruhe Institute of Technology Karlsruhe, Germany

² Arrhythmia Division, University Heartcenter Freiburg-Bad Krozingen, Germany

Atrial fibrillation is the most common cardiac arrhythmia. Until today many mechanisms are not well understood and the typical signal characteristics near rotor tips need to be quantified. In this work, signal characteristics of a stable and a more unstable rotor in a realistic heart model including fiber orientation were analyzed with the following methods: peak to peak amplitude, Hilbert phase, approximate entropy and RS-difference. In this simulation model the stable rotor rotated within a cycle length of 145 ms and stayed in an area of 1.5 mm x 3 mm and another more unstable rotor with a cycle length of 190 ms wandered in an area of 10 mm x 4 mm. In a distance of 2 mm to the rotor tip, the peak to peak amplitude decreased significantly by a maximum factor of 4 whereas the RS-difference and the approximate entropy were maximal. The rotor center trajectories were automatically located by phase singularities determined by the Hilbert transform. We show that more unstable rotors result in more amplitude changes over time and also the cycle length differs more. Furthermore, we present typical activation patterns of the circular Lasso catheter centered at the rotor tip with a coverage of about 85 percent of the cycle length and in a distance of 5 mm to the rotor tip. We suggest that cardiologists use a combination of the described methods to determine a rotor tip position in a more robust manner.



Phase map

P65

Surface ECG Spectral Analysis to Predict Atrial Fibrillation Catheter Ablation Long-term Outcome

R Alcaraz¹, F Hornero², L Fácila³, JJ Rieta⁴

¹ Research Group in Electronic, Biomedical and Telecommunication Engineering, University of Castilla-La Mancha, Cuenca, Spain

² Cardiac Surgery Department, General University Hospital Consortium of Valencia, Spain

³ Cardiology Department, General University Hospital Consortium of Valencia, Spain

⁴ Biomedical Synergy, Universidad Politécnica de Valencia, Spain

Nowadays, catheter ablation (CA) is widely recommended to deal with persistent atrial fibrillation (AF). However, optimal patients selection for this procedure remains a challenge, because no reliable predictors of its long-term outcome have been found yet. Indeed, typical clinical markers, such as AF duration or left atrial size, have provided conflicting results. As an alternative, the dominant atrial frequency (DAF) analysis from the surface ECG has been widely studied in recent years, showing promising results for some CA strategies. However, no much attention has been paid to other non-invasive spectral metrics.

This work focuses on analyzing for the first time three spectral indices to predict non-invasively CA outcome based on analyzing the atrial activity spectral characteristics. Precisely, the dominant atrial frequency (DAF) as well as its 3 dB bandwidth (BW) and the median frequency (MF) were computed for the atrial activity signal extracted from lead V1 of 12 persistent AF patients undergoing a CA procedure based on ablating atrial sites with maximal DAF. Ten second-length ECG intervals just before the CA procedure were considered for the study. After an average of 12 ± 7 months of follow-up, 6 (50%) out of the 12 patients were free from AF.

Results showed higher DAF and lower BW for patients in SR at the end of follow-up (6.60 ± 0.46 Hz; 0.47 ± 0.15 Hz) than for those who relapsed to AF (6.20 ± 0.96 Hz; 0.42 ± 0.12 Hz), respectively. However, statistical significance was no relevant in any case. In contrast, the MF revealed statistically significant differences between both groups, being 6.42 ± 0.17 Hz and 6.03 ± 0.30 Hz for patients in SR and AF, respectively. Moreover, this marker provided sensitivity, specificity and accuracy values of 100%, 83.33% and 91.67%, respectively. In view of these preliminary results, the MF could be considered as a more promising harbinger of long-term CA outcome than the DAF. Nonetheless, further studies with wider databases will be developed in the next future.

The Lagged Central Tendency Measure Applied to Assess P-wave Duration Variability Improves Paroxysmal Atrial Fibrillation Onset Prediction

R Alcaraz¹, A Martínez¹, JJ Rieta²

¹ Research Group in Electronic, Biomedical and Telecommunication Engineering, University of Castilla-La Mancha, Cuenca, Spain

² Biomedical Synergy, Universidad Politécnica de Valencia, Gandia, Spain

Despite of its high prevalence, the mechanisms leading to the onset of paroxysmal atrial fibrillation (PAF) are still not entirely understood. Intensive efforts have been carried out in the last decade to find out markers able to predict PAF onset from the surface electrocardiogram (ECG). To this respect, linear and non-linear estimations of the P-wave duration variability just before the onset of PAF have provided very promising results. However, these analyses have not paid attention to the possible scale-dependent variations in the P-wave duration variability over time. Therefore, the main goal of this work was to assess whether the P-wave duration variability computed from different scales could reveal useful information to improve the prediction of PAF onset.

For that purpose, the two hours preceding a PAF episode from lead V1 of 46 patients were extracted from Holter recordings. This interval was divided into two 1 hour-length segments. After delineating all the P-waves with a previously published algorithm and computing their duration, the central tendency measure (CTM) with lags between 1 and 10 was computed from the obtained time series. Statistically significant differences between both groups were obtained for every lag. Moreover, CTM values were always higher for ECG segments far from PAF (e.g. 0.991 ± 0.014 for lag 2) than for those close to PAF (e.g. 0.935 ± 0.105 for lag 2), thus indicating a higher P-wave duration variability when the onset of PAF approximated. CTM values obtained with lags 2, 3 and 4 also improved classification with regard to the first lag. Precisely, diagnostic accuracy for lags 1, 2, 3 and 4 was 0.804, 0.837, 0.814 and 0.804, respectively. These results suggest that the transition from sinus rhythm to PAF may be a process with a scale variant structure, which seems to be coherent with the highly inhomogeneous and fragmented atrial conduction preceding the onset of PAF. Nonetheless, further studies are required to validate this finding.

P65

Far-Field Effect in Unipolar Electrograms Recorded from Epicardial and Endocardial Surface: Quantification of Epi-Endo Dissociation During Atrial Fibrillation in Humans

Piotr Podziemski, Stef Zeemering*, Elham Bidar, Pawel Kuklik, Arne van Hunnik, Ulrich Schotten

Warsaw University of Technology
Warsaw, Poland

Background: High-density unipolar contact mapping is used to characterize wave conduction patterns during cardiac arrhythmias such as atrial fibrillation (AF). However, due to nature of the unipolar electrogram it reflects local as well as remote electrical activity and great care should be taken in accurate identification of local activity. Here, we explore whether endo-epicardial dissociation during AF can explain origin of far-field components in unipolar electrograms.

Methods: To assess the number of far-field deflections in unipolar electrograms that have a source on the other side of the atrial wall, we used simultaneous endo-epicardial high-resolution contact mapping. 30s endo-epicardial electrograms were recorded using two 64 electrode arrays directly opposing each other, placed on the right atrial wall in 5 patients with persistent AF. Conduction along the lines of conduction block was detected in recorded activation patterns. Changes of the amplitude of the electrogram with increasing distance from the conduction block were assessed to predict the amplitude of far-fields as a function of the distance from wavefront. For all far-field deflections, which could not be explained by local activation within the same plane, we searched for a source of activity on the other side of the atrial wall.

Results: $74\pm 3\%$ of detected far-field deflections could be explained by activation on the same side of the atrial wall. Within the remaining deflections, $42\pm 5\%$ had a source in the activity happening directly on the other side of the atrial wall and $15\pm 3\%$ of detected far-fields were of unknown origin.

Conclusions: Significant proportion of the far-field deflections detected using contact mapping during AF results from endo-epicardial dissociation. This may have an impact on proper annotation of local activity and therefore on accurate identification of conduction patterns. The number of far-field deflections in unipolar electrograms due to endo-epi dissociation may help to quantitatively describe transmural dissociation.

P65

Towards Application of Complexity Measures of Atrial Electrograms to Predict Outcome of the Ablation Procedure

Katarzyna Kořna*, Piotr Podziemski, Paweł Kuklik, Daniel Steven, Jan J Źebrowski, Stephan Willems

Poland

Background: Atrial fibrillation (AF) is the most common and the most complex sustained arrhythmia. Up to date, complexity assessment of AF electrograms has been mostly used to target areas for ablation. The aim of this study was to assess the reliability of the complexity analysis of a single electrogram as a predictor of spontaneous cardioversion.

Methods: Left and right atrial endocardial bipolar electrograms from two locations (High Right Atrium - HRA and Coronary Sinus - CS) were recorded before ablation treatment of AF (at baseline) in 36 patients. Information about the ablation outcome (CV-cardioversion or TERM-spontaneous termination) was collected. For all electrograms, algorithmic complexity was calculated and compared with other parameters used in electrogram complexity assessment: Complex Fractionated Electrogram Indices (mean CFE, ICL, SCI) and Shannon Entropy. To check significance of the results, ANOVA variance analysis and ROC analysis were performed.

Results: Baseline electrograms from electrodes located in HRA had significantly lower algorithmic complexity than from electrodes located in CS. Only the Shannon Entropy of electrogram measured at CS showed significant difference between CV and TERM ($p=0.03$), while in case of algorithmic complexity only a trend towards significance was found ($p=0.08$). Area under ROC curve for algorithmic complexity was no lower than 0,63 and for Shannon Entropy no lower than 0,66.

Conclusions: Complexity methods may be useful in the assessment of the ablation immediate outcome, however the choice of the complexity measure is an important and open question. Electrogram complexity parameters used in clinical practice did not distinguish the ablation outcome groups with Shannon entropy showing the most significant difference.

P65

F-wave Amplitude Stability on Multiple Electrocardiogram Leads in Atrial Fibrillation

Marianna Meo, Antonio R. Hidalgo-Muñoz, Vicente Zarzoso, Olivier Meste, Decebal G. Latcu, Nadir Saoudi

Brigham and Women's Hospital, Harvard Medical School
Boston, MA, USA

Fibrillatory wave (f-wave) amplitude correlates with left atrium (LA) size in certain electrocardiogram (ECG) leads and other clinical markers of atrial fibrillation (AF). Hence, it is regarded as a predictor of ablation therapy outcome. This study aims at assessing the temporal stability of f-wave amplitude measures throughout the recording and determining the minimum signal length necessary to characterize them accurately in standard ECG leads.

We examined a set of 12-lead ECGs acquired in 34 persistent AF patients. Duration of the atrial activity signal (AA) resulting from TQ interval concatenation ranged between 30 and 60 seconds. We first determined the minimum temporal window length W needed for assuring an accurate correlation of the related amplitude value with that obtained on the full signal in leads I, II, V_1 - V_6 (threshold Pearson's coefficient $R = 0.9$). A further intrarecording correlation was tested by comparing amplitude values computed in two distinct W -second AA signal excerpts, at the beginning and the end of the signal, to avoid overlap influence. This step was performed both on the W -second raw signal and on the principal component analysis (PCA) rank-1 approximation with same duration.

The first experimental step yielded $W = 5$ seconds. Amplitude correlation between the beginning and the end of the recording was generally accurate in all leads of the raw signal for $W = 5$ s ($R_{min} = 0.799$, V_1 ; $R_{max} = 0.999$, V_3). Interestingly, PCA revealed that more stable amplitude measures are determined in proximity to LA ($R(V_1) = 0.975$; $R(V_2) = 0.993$; $R(V_3) = 0.989$; $R(II) = 0.841$).

Our findings confirm the temporal stability of f-wave amplitude measures and the robustness to the duration of the signal examined. Moreover, a preprocessing stage based on PCA improves the stability of this parameter in leads closer to LA.

Teager Energy Based Approach to Detect Atrial Peaks to Predict Atrial Fibrillation Recurrence

Raquel Cervigón*, Javier Moreno, José Millet, Francisco Castells

Spain

Atrial fibrillation (AF) is the most common cardiac arrhythmia encountered in clinical practice with significant morbidity and mortality. Radiofrequency catheter ablation is currently used widely and successfully to treat AF, whose success is limited in part by uncertainty in the mechanisms that sustain AF. AF intracardiac recordings were registered in 41 patients immediately before AF ablation procedure. They were divided in 2 groups according to AF recurrence outcome: 26 of them remained in sinus rhythm, where 50% were in persistent AF (n=13) and the other 15 turned back to AF, where 10 patients were in paroxysmal AF. There was no statistically significant difference between clinical parameters from recurrent and non-recurrent AF patients in both groups. A 24-pole catheter (Orbiter, Bard Electrophysiology, 2-9-2 mm electrode spacing) was positioned to record right atrium (RA) and left atrial (LA) electrical activity as well. All patients were monitored after ablation, and were divided in 2 groups according to AF recurrence outcome 3 months after ablation procedure. Atrial peaks are extracted from the envelope obtained by teager energy operator. Teager energy reflects the changes occurring in the envelope of the atrial electrical signal. Subsequently, statistical parameters were calculated from atrial rate signal. Results showed differences between RA in both groups, maximum of the histogram showed a value of 176.51 ± 38.90 ms in the group without recurrences vs. 152.27 ± 23.85 ms in the recurrent AF group ($p=0,03$). Moreover, differences between both atria were found in AF non-recurrent patients, with 168.28 ± 39.37 ms in the RA vs. 183.76 ± 28.63 ms in the LA ($p=0.04$), nevertheless only small differences along atria were found in the recurrent AF group. High frequency values, especially without a gradient between both atria, predict AF recurrence. This suggests that when the atrial electrical activity is more irregular and similar in both atria, the reversion to sinus rhythm is more difficult.

P65

Dynamic Coupling Between Atrio-Ventricular Duration and RR-Interval Histogram Phase-Rectification Analysis in Chronic Chagas Disease

Paulo R Benchimol-Barbosa, Olivassé Nasario-Junior, Roberto Coury Pedrosa, Jurandir Nadal

Universidade Federal do Rio de Janeiro, Rio de Janeiro, Brazil.

Dynamic atrio-ventricular duration (AVD) vs. *RR*-interval coupling assess AV conduction facilitation and susceptibility to arrhythmia. Phase-rectification of *RR*-interval series allows separation of deceleration (DC) and acceleration (AC) phases (Figure 1), reflecting sympathetic and parasympathetic influence on heart rate, respectively. This study assessed chronic Chagas disease (*ChD*) status on dynamic AVD and phase-rectification-driven *RR*-interval coupling. Healthy sedentary (Control, $n = 11$) and *ChD* ($n = 11$) groups were studied. All had 1:1 AV conduction in sinus rhythm, and underwent 60 min head-up tilt table test. *ChD* group was submitted to MIBG scintigraphy to assess cardiac sympathetic innervation. Histogram of *RR*-interval series was calculated, with 100 ms class, ranging from 600 ms to 1200 ms. For each class, mean normal *RR*-intervals (MRR) and mean peak-to-peak *P*-to-*R* wave interval (MPR), representing AVD, were calculated and analyzed in the whole series (T), and in DC and AC phases. Linear regression model of MPR vs. MRR were computed and respective slopes calculated ($sMPR_T$, $sMPR_{DC}$ and $sMPR_{AC}$). Correlation coefficients were tested before analysis, and Student t-test compared groups ($\alpha < 0.05$). MPR_T , MPR_{AC} and MPR_{DC} significantly increased as a function of MRR in Control (Table 1). In *ChD*, increase was significant only in MPR_{DC} . All *ChD* subjects showed reduced cardiac MIBG uptake. In healthy subjects, *PR*-interval increases as a linear function of *RR*-interval, in a wide physiological range of *RR*-interval variation during tilt-table test. In *ChD* subjects showing sympathetic denervation, however, *PR*-interval increases only in DC phase, confirming loss of sympathetic driven (AC phase) *RR*-interval variation.

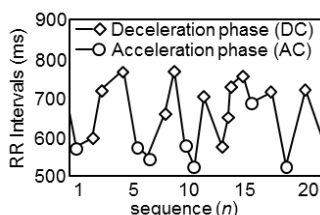


Fig 1. DC and AC phases represented in respective *RR*-intervals.

Table 1 – Slopes of MPR vs. MRR regression lines and intervals duration per group:

Group	$sMPR_T$	$sMPR_{DC}$	$sMPR_{AC}$	MRR(ms)	MPR(ms)
Control	$0.100 \pm 0.006^*$	$0.134 \pm 0.003^*$	$0.102 \pm 0.007^*$	$806 \pm 72.4^\ddagger$	$131 \pm 8.5^\ddagger$
<i>ChD</i>	0.002 ± 0.004	$0.031 \pm 0.002^*$	0.006 ± 0.005	$906 \pm 51.6^\ddagger$	$140 \pm 7.8^\ddagger$

Values are mean \pm SD; * $p < 0.05$; $^\ddagger p < 0.05$ intergroup comparison

Comparison of Electric and Magnetic Cardiograms Produced by Myocardial Ischemia in Models of the Human Ventricle and Torso

Erick Andres Perez Alday*, Chen Zhang, Michael Alan Colman, Haibo Ni, Zizhao Gan, Henggui Zhang

University of Manchester
Manchester, United Kingdom

Introduction: Myocardial ventricular ischemia results from a lack of blood flow to the heart. This decreases partially or completely the oxygen supply to the cell, which can damage the muscle. Significant ischemic regions within the heart can promote abnormal conduction and repolarisation patterns and ventricular arrhythmias which can lead to sudden cardiac death. Thus, identification of acute transient ischemia through non-invasive techniques may prove vital in early diagnosis and treatment. Unfortunately, the standard 12-lead electrocardiogram (ECG) may not provide sufficient information for satisfactory diagnosis; the 12-lead ECG of patients with ischemia may only differ by 70-85% compared to normal patients. The magnetic field, however, may provide a greater level of detail because it is more sensitive to currents tangential to the surface of the chest than the electric field. In this study we compare and quantify the effect of the presence of ventricular ischemia on the ECG and magnetocardiogram (MCG) Methods Biophysically detailed computational models of the human ventricles in 1D, 2D and 3D are incorporated into a heart-torso model. A boundary element method is used to compute the electric and magnetic potentials on the surface of the body, from which cardiograms are derived. We consider the 12- and 36-lead ECG and the 36-lead MCG. Multiple electrophysiological and structural types of ischemia are included. Results During normal conditions, the simulated QRS complex and T-waves of the cardiograms show strong agreement with experimental data. The 12-lead ECG showed very few differences between the control and ischemia conditions; more information is provided by both the ECG and MCG with 36 leads, wherein the ST-segment and T-wave are affected by the presence of ischemia. Conclusion Our results confirm that the 12-lead ECG is insufficient to provide effective diagnosis of ischemia, whereas the 36 lead ECG and in particular MCG offer advantages in identification.

P66

The Effect of Voltage Sensitive Dye di-4-ANEPPS on the RT/RR Coupling in Rabbit Isolated Heart

Petr Veselý*, Marina Ronzhina, Kateřina Fialová, Jana Kolářová,
Josef Halánek, Marie Nováková

Czech Republic

Aims: Voltage sensitive dye di-4-ANEPPS is ordinary used for optical measurement of action potential in experimental cardiology. In this work, the effect of the dye on the RT/RR coupling measured in electrograms (EGs) recorded on rabbit isolated hearts during experiments with di-4-ANEPPS application was studied.

Methods: The experiments were performed on 16 male rabbits: di-4-ANEPPS-treated (n=10) and control (n=6) groups. In the first group, the experimental protocol consisted of stabilization (S), di-4-ANEPPS loading (L), and wash-out (W) (each of 20 min duration). Voltage-sensitive dye di-4-ANEPPS was added to the perfusate in concentration of 2 $\mu\text{mol/l}$ during the phase of di-4-ANEPPS loading. The second protocol included only 60 min stabilization without any pharmacological interventions. EGs from three orthogonal leads were continually recorded (fs=2 kHz, 16 bits). The R waves and the end of T waves were automatically detected. The differences of RR, RT and RT/RR between the last and second minute in each experimental phase were computed in the first group. In the second group, these measures were calculated at corresponding time moments for comparison.

Results: The results were expressed as a median and interquartile range (Q0.75-Q0.25) and the significance between the groups was determined with Kruskal-Wallis test. $\Delta(\text{RT/RR})$, in S, L and W, was -0.095, 0.061; -0.093, 0.043; -0.027, 0.039 in di-4-ANEPPS-treated group and -0.127, 0.071; 0.006, 0.016; -0.001, 0.025 in control group. The significant difference ($P<0.01$) was found between two groups in L phase. Additionally, there was the significant difference in ΔRR [ms] which was 120.9, 74.8 in di-4-ANEPPS-treated group and 6.94, 19.28 in control group in the same phase.

Conclusions: The significant difference in $\Delta(\text{RT/RR})$ between both groups shows a possible effect of di-4-ANEPPS on the RT/RR coupling which is mainly caused by the prolongation of RR interval during loading with the dye.

A Novel Method for Automatic Standardization of Digital Electrocardiographs

Eduardo Freitas*, João Salinet, Tiago Almeida, Henrique Oliveira

Mogi das Cruzes University, Brazil

Mogi das Cruzes, Brazil

Introduction: It is crucial to assure the recording's quality for correct ECG interpretation. This research aimed at developing an automated standardization method to gauge digital electrocardiography (EC) devices.

Method: The developed microprocessed gauge equipment (MGE) is divided into digital and analog circuits and an embedded software to control them. One circuits group contains conditioned reference signals (CRS) from Physionet Bank to simulate cardiac activity. Another circuits group analyses the outputs from MGE (or EC) comparing them with CRS. The self-check mode runs all circuits MEG to gauge it. At the EC check mode, CRS are sent to EC. The commercial EC equipment (Contec, model ECG80A) was used to MGE validation following the IEC60601-2-51:2005 (amplitude variation <5%; timing accuracy <5ms; signal stability against noise influence <5%). The assessment is performed by statistical correlation analysis R2 for the self-check (1% tolerance) and Kolmogorov-Smirnov (KS) for EC check.

Results: At the EAM self-test, temperature and humidity were changed (17 to 35°C and 30 to 85%) and R2 correlation value maintained ≥ 0.99 as designed. The KS test established with 1% of significance level for EC assessment resulted in KS=0.012 for amplitude accuracy, 0.0028 for timing accuracy and 0.021 for signal stability against noise influence. All KS values were lower than their respective critical values (0.073, 0.097 and 0.072) and are presented at the customer report indicating a tolerance of 1% that is more rigorous than that recommended by the standard (5%). Finally, visual inspection between EC signals and CRS on printed graph paper at a standard scale certifies the EC reliability.

Conclusions: The proposed method shows evident advantages when compared with the traditional approaches of ECs standardization increasing productivity and eliminating subjectivity at the gauge protocols.

P66

Comparison of Intensity-based B-splines and Point-to-Pixel Tracking Techniques for Motion Reduction in Optical Mapping

Jaime Yagüe-Mayans, Conrado J Calvo*, Antonio Cebrián, Francisco J Chorro, José Millet

Universidad Politécnica de Valencia
Spain

Introduction: Suppression of motion artifacts (MA) in OM requires uncoupling of cardiac contraction by restriction techniques, which have important effects on cardiac physiology and deteriorates the quality of acquisitions and their interpretation. In this study, we propose to assess the performance of two independent intensity-based methods for efficient registration to minimize MA.

Methods: A method based on based point-to-pixel block matching similarity with tracking with displacement interpolation approach (PPBMA) was compared to a classical non-rigid registration algorithm where the deformation field is obtained using cubic splines (DFCS). Both alternatives were tested under controlled conditions using phantoms and real image sequences (n=5). Spatiotemporal trajectory loops and total directional displacement were compared before/after registration. Computation of action potential duration (APD) and activation properties were obtained to evaluate the accuracy of reconstructed AP and its reliable interpretation.

Results: Our results showed that motion was greatly suppressed at automatically preselected key-points and extended to broader percentage areas using DFCS method. Maximum displacement after registration was in the sub-pixel to pixel range (0.92 ± 0.15 vs 0.89 ± 0.21). DFCS showed better performance by reducing MA in larger areas by an average of 13.13% greater extension (63.36% vs 76.49%). The latter allowed for more accurate estimation of APD across the epicardium (APD80 (ms): 101.2 ± 38.1 vs 86.5 ± 9.4 ms) reducing the coefficient of variance to that observed in presence of the uncoupler blebbistatine (CoV: Uncorrected: 19.10%, PPBMA: 2.94%, DFCS: 1.84%, Blebb: 1.58%). Even though both methods show minimization of MA, DFCS had a negative effect on upstroke velocities and spatial smoothing on the activation isochronal maps greatly affecting its interpretation depending upon spatiotemporal resolution of acquired sequences.

Conclusions: Intensity based methods are useful for MA correction via registration due to its accuracy tracking frame-to-frame geometrical displacements in large areas of the heart. Yet, special care must be taken to preserve upstroke information intact.

P66

Cardiac Resynchronization Efficiency Estimation by New Ultra-High-Frequency ECG Dyssynchrony Descriptor

Tereza Reichlova*, Pavel Jurak, Josef Halamek, Filip Plesinger, Jolana Lipoldova, Miroslav Novak and Pavel Leinveber

International Clinical Research Center, Brno, Czech Republic

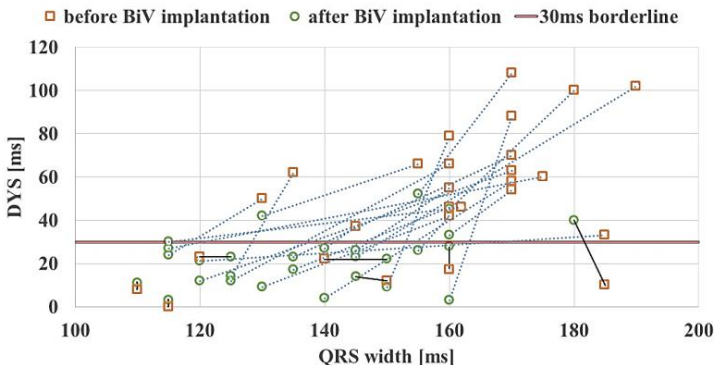
Biventricular implantable pacemaker (BiV) is usually recommended for heart failure patients with LVEF $\leq 35\%$ and QRS duration $> 120\text{ms}$. We introduce promising marker evaluating appropriateness and efficiency of Cardiac Resynchronization Therapy (CRT) recipients.

Data: 12-lead UHF-ECG, 25 kHz sampling, 10 minute resting measurement, 28 CRT subjects, each before BiV and with BiV on, VV delay 0. Methods: A new parameter DYS was computed as time difference between two maxima of UHF envelopes computed from V1 and V6 leads in QRS complex in 500-1000Hz frequency band. DYS was calculated before and after implantation of BiV pacemaker. The two values of DYS were compared with standard QRS width.

P66

The assumption for being responder for BiV is high value of DYS before CRT and significant DYS decrease during biventricular pacing. Subjects with no synchrony improvement of electrical activation between V1 and V6 are under the borderline of $\text{DYS} = 30\text{ms}$ in the lower part of the Figure. There is DYS increase in these patients. They have simultaneously DYS before stimulation $\leq 30\text{ms}$.

Thus the DYS parameter can serve as a new marker for prediction of BiV pacemaker efficiency. This information cannot be derived from standard QRS width values prior BiV implantation.



DYS and QRS width parameters before and after BiV implantation

Feasibility of Compression Depth Estimation from the Acceleration Signal during Cardiopulmonary Resuscitation in Long-Distance Trains

Digna M González-Otero, Sofía Ruiz de Gauna, Jesús Ruiz, Beatriz Chicote, Sandra Plaza

University of the Basque Country (UPV/EHU)
Bilbao, Spain

Introduction: Early cardiopulmonary resuscitation (CPR) and early defibrillation are key for survival during out-of-hospital cardiac arrest. Long-distance trains are increasingly being equipped with defibrillators to ensure a quick response to the emergency. CPR feedback devices help rescuers to deliver chest compressions with an adequate depth. Most of them are based on accelerometers placed beneath the rescuer's hands to estimate the chest displacement. However, in a moving train the measured acceleration is a combination of the acceleration of the chest and that of the train. We wanted to evaluate the accuracy of accelerometer-based systems in the estimation of chest compression depth in this scenario.

Materials: Four volunteers delivered chest compressions on a resuscitation manikin equipped with a distance sensor for depth reference during the Zaragoza-Bilbao train route. CPR was performed with a triaxial accelerometer placed between the manikin's chest and the rescuer's hands. We acquired 3-min records between consecutive stations, delivering compressions with target depths of 35 mm and 50 mm. Six records corresponding to intervals with different average velocities were selected.

Methods: We applied a time-domain (td) method that approximated the double integration combining a linear filter and the trapezoidal rule, and a frequency-domain (fd) method based on the analysis of the harmonic content of the acceleration in 2-s intervals. We evaluated the accuracy of both methods when using a single axis of the accelerometer (a_1) and when composing the three axis (a_3).

Results: The median (IQR) unsigned error in mm was 6.44 (3.66-10.10), 5.88 (2.92-10.06), 1.78 (0.78-3.08) and 1.95 (0.96-3.55), for tda_1 , tda_3 , fda_1 and fda_3 , respectively.

Conclusions: Chest compression depth could be accurately estimated from the spectral analysis of the acceleration in a moving train. However, the accuracy of the time-domain method was severely compromised, with median errors above 10% of the target depth.

In Silico Investigation of the Pro-arrhythmogenic Effect of KCNQ1-G269S Mutation in Human Ventricles

Haibo Ni, Wei Wang, Erick A Perez Alday, Henggui Zhang

Biological Physics Group, University of Manchester
Manchester, UK

Introduction: A recent study identified a modest loss-in-function mutation KCNQ1-G269S in long-QT patients who remain asymptomatic during rest but exhibit prolonged QT intervals during exercise, suggesting a possible impaired response of cardiac I_{Ks} current to adrenergic stimulations. The aim of this study was to investigate the pro-arrhythmogenic effect of such genetic variant using biologically detailed computational models.

Methods: O'Hara-Rudy model of human ventricular cells was modified to incorporate the effects of beta-adrenergic stimulation on ion channels and intracellular Ca^{2+} handling system. The I_{Ks} formulation was updated based on the experimental data in the wild type (WT) and variant mutations (WT-G269S and G269S). Beta-adrenergic stimulation was considered only for a saturating concentration of isoprenaline. Tissue vulnerability was quantified using a one-dimensional model representing transmural ventricular strands. The pro-arrhythmogenic effects were investigated using a 3D ventricular model with realistic structure and myofibre orientation. QT intervals were quantified in a torso-heart model.

Results: The KCNQ1-G269S mutation showed moderate change to electrical activities in the absence of adrenergic stimulation. It produced insignificant (14 ms) but marked (48 ms) action potential duration (APD) prolongation in the absence and presence of isoprenaline, respectively. It also induced early after-depolarisations in the mid-myocardial cells with application of isoprenaline. The APD heterogeneity among regional cells was enhanced by the mutation, which was further increased by adrenergic stimulation, leading to increased vulnerability of the tissue to genesis of unidirectional conduction block. Results from the 3D model suggested that the mutation augmented activation-repolarisation interval in the ventricles, resulting in prolongation in QT intervals, which was further augmented in the presence of isoprenaline.

Conclusions: The blunted activation of I_{Ks} to beta-adrenergic stimulation by KCNQ1-G269S mutation is the primary contributor to the significant increase in cardiac APD and QT intervals under adrenergic stress, leading to increased vulnerability to arrhythmogenesis in human ventricles.

P66

Electrocardiographic Detection And Monitoring of Pulmonary Hypertension

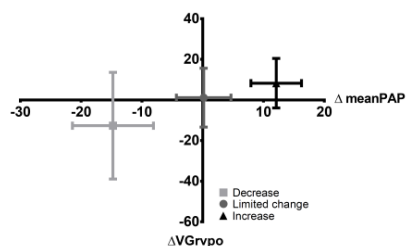
Marjolein C. de Jongh, Vivian P. Kamphuis, Sumche Man, Arie C. Maan, Hubert W. Vliegen, Cees A. Swenne
Cardiology Department, Leiden University Medical Center
Leiden, The Netherlands

Background. Early detection of pulmonary hypertension (PH) and monitoring its course is of vital clinical importance. A change in RV afterload alters the action potential morphology of the involved myocardium, thus instantaneously affecting the ECG. We previously demonstrated in a transversal study that a projection of the electrocardiographic ventricular gradient optimized for right ventricular overload (VG_{rvpo}) correlates well with the invasively measured mean pulmonary arterial pressure (PAP) [1]. Here we attempt to detect changes in mean PAP within patients by serial ECG analysis.

Methods. We retrospectively selected patients from the previous study group who underwent a right heart catheterization (RHC) because of suspected PH [1], who had 2 ECGs made within 3 months from the right heart catheterization (RHC), and within 3 months from an echocardiogram made 6-24 months either before or after the RHC, respectively. We computed VG_{rvpo} , and changes within patients were related to changes in mean PAP as measured during RHC or assessed by the echocardiogram. Mean PAP changes were divided in three groups: decrease >7.5 mmHg, increase >7.5 mmHg, or limited change (within the $-7.5 \dots +7.5$ mmHg range).

Results. A total of 39 patients (15/24 male/female, age 60 ± 12 years) were evaluated. The VG_{rvpo} change in the PAP-increase group was significantly larger than the VG_{rvpo} change in the PAP-decrease group (unpaired t-test, $P < 0.05$).

Discussion. Our first results indicate that ECG-based trend detection in patients with PH or at risk of developing PH is feasible. Further validation should preferably be done in a prospective study with ECGs made immediately preceding (preferable invasively measured) PAP assessment.



Mean \pm SD changes in mean PAP and VG_{rvpo} in the study group.

[1] Kamphuis et al. J Electrocardiol 2014;47:175-182

Reliability of APD-Restitution Slope Measurement: Quantification and Methodological Comparison

Michele Orini*, Neil Srinivasan, Peter Taggart, Pier Lambiase

London, United Kingdom

Introduction: The restitution of the action potential duration (APDR) is a mechanism whereby cardiac excitation and relaxation adapt to heart rate changes. The APDR curve is drawn by plotting the function $APD = f(DI)$, being DI the diastolic interval. A steep APDR curve is associated with increased vulnerability to fatal arrhythmias. Accurate estimates of the APDR slope (α -APDR) are required in order to assess cardiac risk and to elucidate the mechanisms underlying arrhythmogenesis. This is challenging because of noise and small number of (DI,APD) points that can be collected during experimental studies. The aims of this study are: (1) Derive a decomposition of α -APDR into its main determinants and show how they affect α -APDR estimates. (2) Compare the most commonly used methodology to estimate α -APDR in real-like scenarios.

Methods: We derive an analytical expression for α -APDR, as a function of its main determinants. We use 43 restitution curves recorded from the endo- and -epicardium in 3 patients with structural normal hearts. We generated reference APDR curves by fitting real data and we altered them by: (1) Adding Laplacian noise with different amplitudes (Anoise) to the main determinants of α -APDR (selectively or in combination); (2) Under-sampling APDR curves. Linear-piecewise and exponential interpolation were used to estimate α -APDR.

Results: Even small changes in the APD of the basic cycle length, repolarization and activation time of the premature beat induces significant changes in α -APDR, with mean absolute error $> 20\%$ for Anoise > 3 ms. Piecewise linear outperformed exponential fitting for Anoise < 3 ms (in terms of correlation and mean absolute error). However, it was more sensitive to downsampling.

Conclusion: α -APDR is sensitive to noise. The linear method provides estimates that correlate better with reference α -APDR than the exponential method. APDR curves can be compared only when constructed over the same number of (DI,APD) points.

P66

Role of Mechanics in Rhythm Disturbances in 1D Mathematical Model of Myocardial Tissue with Local Ca^{2+} -Overload

Alexander Kursanov^{1,2}, Olga Solovyova^{1,2}, Leonid Katsnelson¹, Vladimir S. Markhasin^{1,2}

¹Institute of Immunology and Physiology UB of RAS

²Ural Federal University, Yekaterinburg, Russia

Possible contribution of the mechanical factors to the arrhythmogenesis in Ca^{2+} overloaded cardiomyocytes has been under appreciated. Earlier developed mathematical model of cardiomyocyte electromechanical function predicted a significant role of the intra- and extracellular mechanical factors in arrhythmogenesis.

We utilized a cellular model to study effects of the electromechanical coupling between cardiomyocytes in a 1D heterogeneous muscle strand formed of 90% of normal (N) cardiomyocytes and 10% of sub-critical (SC) cardiomyocytes with moderately decreased Na^+ - K^+ pump activity.

Single SC cardiomyocytes did not demonstrate spontaneous activity during isometric contractions at a reference length. Regular fiber twitches at the reference initial cell length were induced by 1 bps electrical stimulation applied at an edge of the strand. Excitation spread along the tissue via electrodiffusional cell coupling followed by cell contractions and force development in the fiber. Mechanical interactions between N- and SC-cells in the tissue resulted in the spontaneous activity emerged in the SC zone between the regular stimuli. If the excitation wave spreads from SC- to N-region, the SC-cells developed delayed after-depolarizations (DAD) that caused a slowly developing beat-to-beat decrease in the force of fiber contraction. If the excitation spreads in the opposite direction, DAD in the SC-cells induces reflected downward excitation waves capturing the normal region and followed by extrasystoles in the whole fiber.

The results suggest that ectopic activity may emerge in a sub-critical myocardial region and expand by capturing normal regions in myocardium due to the electromechanical coupling between cardiomyocytes.

P66

Pulse Annotation of Automatic External Defibrillators Recordings during Out of Hospital Cardiac Arrest

Clément Neyton*, Sarah Ménétré, Daniel Jost, Fabielle Angel, Bernard Gény, Vincent Lanoë, Jean-Philippe Didon

Schiller Médical
Wissembourg, France

BACKGROUND: Obtaining information about the circulatory status of a patient during resuscitation is crucial. However, current guidelines advise that lay persons should not check for a palpable pulse as it has proven to be time consuming and unreliable. The lack of information about the hemodynamic status during out of hospital cardiac arrest (OHCA) has made the validation of pulse detection algorithms integrated into automated external defibrillators (AED) a challenging task. This study aims at proposing an annotation scheme for the assessment of pulse in OHCA. **METHOD:** For a patient undergoing an OHCA, impedance cardiogram (ICG) and ECG records are extracted from the analysis period of the AED. The pulse presence is checked clinically by educated first responders after each analysis leading to a non-shockable rhythm and upon arrival of the physician. Given the unreliability of pulse check, additional annotations were necessary. Expert reviewers annotated the rhythm types on the ECG and they used the ICG to correctly identify pulseless electrical activity (PEA) -organized rhythm without a pulse- from pulse-generating rhythms (PR). PEA episodes were restrictively selected when no pulse was clinically detected and when thoracic impedance variations weren't synchronous with cardiac contraction. PR episodes were annotated when both responders detected a pulse in presence of an organized rhythm.

Results: Between November 2010 and September 2011, the BSPP (Fire Brigade of Paris) recorded 965 interventions from which 6,497 analysis were extracted. After removing episodes unsuitable for the classification, the database contains 2,852 segments of which 2,798 were annotated as no pulse (2,025 asystoles, 318 ventricular fibrillations, 455 PEA) and 54 as PR.

Conclusion: This annotation scheme is a mandatory step toward validating a pulse detection algorithm into AEDs. Being independent from the recording device, several databases could be annotated using the same protocol.

P66

Sample Entropy as a Shock Outcome Predictor during Basic Life Support

Beatriz Chicote*, Unai Irusta, Elisabete Aramendi, Daniel Alonso, Carlos Jover, Carlos Corcuera

University of the Basque Country (UPV/EHU)
Bilbao, Spain

Aim: To improve accuracy and minimize the analysis time to predict defibrillation success based on the pre-shock Ventricular Fibrillation (VF) waveform analysis for patients treated by Basic Life Support (BLS) services. Futile defibrillation attempts imply unnecessary chest compression interruptions and potentially worsen outcome. A shock outcome predictor would contribute to optimal defibrillation timing during BLS in a resuscitation scenario. **Materials:** Data collected by the Basque BLS ambulances in the years 2013-2014 was reviewed. Only cases containing defibrillation shocks during VF and continuous ECG tracings pre-shock (analysis) and post-shock (annotation) were included. Defibrillation was annotated as successful if it restored a rhythm with QRS complexes and rate above 30 bpm within 60 seconds. The final dataset had 255 shocks from 92 patients, 65 were successful and 190 unsuccessful.

Methods: Using a 5-s pre-shock ECG segment, 13 classical VF waveform features were computed measuring amplitude, slope, spectral characteristics and complexity. In addition, Sample Entropy (SmpEnt) was introduced as shock outcome predictor. An optimal detector of successful shocks was designed for each feature minimizing the Balanced Error Rate (BER), thus balancing Sensitivity (SE) and Specificity (SP). Repeated shocks within a patient were weighted, and performance was evaluated using a leave one patient out cross-validation. Finally, the minimum pre-shock segment duration assuring an accurate shock outcome prediction was determined.

Results: For 5-s segments SmpEnt was the best predictor with BER 0.18, SE 84% and SP 80%. The best slope and spectral features had a BER of 0.21 (SE 81%, SP 77%) and 0.24 (SE 74%, SP 78%), respectively. Furthermore, BER for SmpEnt was under 0.22 for pre-shock segments as short as 1.5-s.

Conclusions: SmpEnt is an improved shock outcome predictor, even for VF-segments as short as 1.5-s. During BLS, SmpEnt could be used as a decision support tool to guide optimal timing for defibrillation.

P66

Alternatives to Estimate the Compression Depth from the Acceleration Signal during Cardiopulmonary Resuscitation

Sofía Ruiz de Gauna, Digna M González-Otero, Jesús Ruiz, Beatriz Chicote, Noelia Vidales

University of the Basque Country (UPV/EHU)
Bilbao, Spain

Introduction: Feedback devices improve the quality of chest compressions provided during cardiopulmonary resuscitation (CPR). These devices are usually based on accelerometers and estimate the chest displacement by double integration. This procedure is inherently unstable and requires additional reference signals to ensure a good performance. We described and evaluated the accuracy of three alternatives for the estimation of the chest compression depth using exclusively the acceleration signal.

Materials: A resuscitation manikin was equipped with a displacement sensor for depth reference. Chest compressions were provided in sternal position by six volunteers (two per record), with a tri-axial accelerometer placed beneath the rescuer's hands. We compiled twelve 10-min records, with a target depth of 50 mm and four target frequencies (80, 100, 120, and 140 cpm). For each record, volunteers alternatively provided 2-min series of 30 compressions.

Methods: The first method estimates the compression depth by approximating the double integration using a two-step combination of a linear filter and the trapezoidal rule. The second method estimates the velocity signal (one-step integration) and computes its area between the zero-crossing instants detected for each compression cycle. The third method computes the average compression depth from the spectral analysis of the harmonic components of the acceleration signal, using non-overlapping 2-s windows. For each method, the unsigned error between the detected compression depth and the reference was computed.

Results: The median (IQR) unsigned error (in mm) for each method was, respectively: 4.01 (2.05-6.15), 3.93 (2.03-6.18), 1.25 (0.58-2.08).

Conclusions: Globally, the method based on the spectral analysis of the acceleration provided the best performance. The method relies on the idea that the acceleration signal is quasi-periodic during short chest compression intervals, and the average compression depth in that interval can be estimated from the magnitudes and phases of the first harmonics of the acceleration.

P66

A Wavelet-Based High-Frequency Analysis of Fragmented QRS Complexes in Patients with Myocardial Infarction

Chun-Cheng Lin*, Weichih Hu, Yu-Wei Lin

National Chin-Yi University of Technology
Taichung, Taiwan

Fragmented QRS (fQRS) is an important and noninvasive marker for evaluating myocardial scar in patients with coronary artery disease, which is defined as additional spikes within the QRS wave. It is not easy to detect the fQRS accurately because of a variety of fQRS morphology. This study is to analyze the high-frequency (HF) potentials of fragmented QRS complexes using a continuous wavelet transform-based method in patients with myocardial infarction (MI). A HF parameter was defined as the root-mean-square (RMS) value of wavelet coefficients at central frequencies of 100Hz, 150Hz, 200Hz, or 250Hz, and was further normalized by the RMS value of entire QRS complex, which is defined as the HF ratio. There were 76 MI patients and 43 Normal subjects recruited in this study. All of the ECG recordings are obtained from the PTB Diagnostic ECG Database including the conventional 12-lead and Frank XYZ lead ECGs. A signal averaging technology was adopted to reduce the background noise. The fragmented QRS complexes were defined by the presence of an additional R wave, or notching in nadir of the S wave, notching of R wave, or the presence of more than one R prime. The study results demonstrate that although of the mean HF ratios of MI patients are significantly larger than those of normal subjects in Frank lead ECGs, if the fragmented QRS complexes were excluded, there were no significant differences of mean HF ratios between MI patients and normal subjects. All of the mean HF ratios of fragmented QRS complexes are significantly larger than those of non-fragmented QRS complexes ($p < 0.001$). The total accuracy of the HF ratio for detecting the fragmented QRS complex is about 80% (specificity 84% and sensitivity 60%) in 12-lead ECGs, and is about 84% (specificity 88% and sensitivity 65%) in Frank lead ECGs.

P67

Robust detection of ECG waves

Anna Wojdel*, Vicent J Ribas Ripoll, Miguel Teixidó-Roman, Pablo Ramos, Josep Brugada

Custom Software and Electronics
Barcelona, Spain

Objectives: This study aims at developing an ECG wave detector that can support doctors in assessing heart functionality. It separates cardiac cycles and delineates specific waves (P, QRS, T) in for each cycle of the incoming ECG signal, in an automated and robust manner.

Methods: Our ECG wave detector is designed for a standard 12 lead ECG sampled with sampling rate of 500~Hz and 10~second segments. The system developed is robust against changes in sampling rate, recording noise and missing leads. We work in the wavelet domain by applying dyadic discrete wavelet transforms to each lead separately. The representation obtained is merged into a single signal, which is processed uniformly and independently of the initial number of leads. Wave is done in two steps: (i) QRS complex localization and removal, and (ii) P- and T-wave localization.

Results: The performance of our ECG wave detector was assessed on 182 pathological ECGs diagnosed (only abnormal durations) by a cardiology service. Absolute performance of our approach is summarized by the following average errors: QRS duration $E_{qrs}=12.9\text{ms}$ (131), P duration $E_p=28.8\text{ms}$ (38), PR interval $E_{pr}=18.8\text{ms}$ (71), QTc interval $E_{qtc}=29.8\text{ms}$ (11). Numbers in brackets refer to number of manual measurements available in our dataset for a given type of duration. These results compare well with the commercially available HES (Corscience, Germany) software not only on the accuracy ($E_{qrs}=12.8\text{ms}$, $E_p=21.2\text{ms}$, $E_{pr}=42.1\text{ms}$, $E_{qtc}=16.4\text{ms}$), but most notably, on the robustness against bad or difficult data acquisition.

Conclusions: Our method for ECG measurement extraction proves to be very robust against problematic input data, with no accuracy loss. It exhibits only few systematic errors (especially in QTc), which can be addressed in further development, the system is promising for deployment in an ER environment.

P67

Detection of Irregular Heartbeats Using Tensors

Griet Goovaerts^{1,2}, Ofelie De Wel¹, Bert Vandenberg³, Rik Willems³, Sabine Van Huffel^{1,2}

¹ KU Leuven, Department of Electrical Engineering-ESAT, STADIUS Centre for Dynamical Systems, Signal Processing and Data Analytics, Belgium.

² iMinds, Medical Information Technologies, Belgium.

³ Department of Cardiovascular Sciences, KU Leuven, Leuven, Belgium

Introduction Automatic classification of heartbeats in different categories such as atrial premature beats or premature ventricular contractions is important for ECG analysis. The number of irregular heartbeats in a signal can for example be used as a risk stratifier for sudden cardiac death. Current heartbeat classification methods typically use time or frequency domain features to characterize heartbeats. We propose the use of tensors to incorporate the structural information that is present in multilead ECG channels. Since different ECG leads provide information on a particular orientation in space, more robust detection can be done if all leads are considered.

Methods We present a novel tensor-based method for irregular heartbeat detection in multilead ECG signals. After preprocessing and heartbeat detection using wavelet-based methods, the ECG signal is segmented beat-by-beat. The different heartbeats are then placed in a three-dimensional tensor with dimensions time, space and heartbeats. Canonical Polyadic Decomposition is used to decompose the tensor. The results are three loading vectors, corresponding to the dimensions of the original tensor. Through analysis of these loading vectors, irregular heartbeats can be detected using a simple thresholding procedure.

Results and conclusion The method has been applied to a subset of the St.-Petersburg Institute of Cardiological Technics 12-lead Arrhythmia Database available on Physionet. The dataset consists of recordings of 30 minutes and contains 12 standard leads. When applying the method to the first 10 signals, we obtain a mean sensitivity and specificity of more than 90%. These results indicate that the presented method is a new and reliable way of performing irregular heartbeat detection.

P67

ECG Baseline Wander Removal with Recovery of the Isoelectric Level

Antonio Fasano, Valeria Villani*

Università Campus Bio-Medico di Roma
Roma, Italy

Aims: In this paper we propose a novel approach to ECG baseline wander (BW) removal that is able to recover the isoelectric level in the detrended signal. Since BW affects all ECGs, its removal is an unavoidable preliminary step in ECG processing. The cubic spline interpolation (CSI) is the only method for BW removal that does not alter the isoelectric level. However, it exhibits poor detrending performance in comparison with more recent techniques.

Methods: We have recently proposed an approach to BW removal that is based on quadratic variation reduction (QVR). It estimates BW by solving a constrained convex optimization problem where quadratic variation enters as a constraint. This approach has been shown to outperform state-of-the-art algorithms. However, it does not restore the isoelectric level in the detrended signal. To overcome this limitation, we introduce additional constraints in the optimization problem and constrain the amplitude of few fiducial points to be close to isoelectric segments. Conversely to CSI, which requires a fiducial point for each beat, the proposed algorithm requires in total very few points: in the limit one fiducial point is sufficient.

Results: ECG records from the MIT-BIH Arrhythmia Database (PhysioNet) exhibiting frequent premature ventricular complexes were considered. Portions mostly free from BW were isolated and corrupted by different realizations of BW extracted from the record nstdb/bw from the MIT-BIH Noise Stress Test Database. Performance was assessed through a statistical analysis of the error in estimating baseline and recovering the isoelectric level. For all realizations of BW, both quantities were lower for the proposed approach than CSI.

Conclusions: The proposed approach, being an extension of the one based on QVR, inherits its properties and outperforms state-of-the-art algorithms in estimating BW. Additionally, it is able to recover the isoelectric level.

P67

Low-Delay Estimation of the Real-Time Respiratory Rate from the ECG using a Bank of Notch Filters

Leila Mirmohamadsadeghi*, Jean-Marc Vesin

Swiss Federal Institute of Technology
Lausanne, Switzerland

Purpose: The respiratory rate (RR) can be estimated from the ECG thanks to the modulation of the latter by respiration. However, current methods yield estimates with large delays. The purpose of this study was to use a bank of FIR notch filters to estimate the RR simultaneously from two ECG-derived respiratory waveforms, namely respiratory sinus arrhythmia (RSA) and R-peak amplitudes (RPA), in a real-time and computationally simple way.

Methods: The output power of a notch filter is small if the input frequency is close to the notch frequency. A bank of order-3 FIR notch filters, characterized by a pair of complex-conjugate zeros, are applied to the RSA and RPA. At every sample, the filtered RSA and RPA are multiplied together. The resulting product, after inversion and smoothing, is used in a weighted sum of the notch frequencies to compute the common frequency of the inputs, i.e., the RR. The accuracy and delay of this scheme were evaluated on the entire Physionet Fantasia dataset, which contains simultaneous recordings of the ECG and respiration from 20 young and 20 elderly subjects. The reference RR was computed from the respiration signal using a combination of classic frequency estimation methods.

Results: The proposed method resulted in a mean error of 2.60 ± 2.51 breaths-per-minute (bpm) over the young (compared to 2.65 bpm for the state-of-the-art, $p < 0.01$) and 3.05 ± 2.98 bpm over the elderly subjects (compared to 3.17 bpm for the state-of-the-art, $p < 0.01$). The delay of the estimates was 5.27 ± 4.22 seconds (compared to 10.12 seconds for the state-of-the-art, $p < 0.01$).

Conclusions: The proposed method provides low-delay RR estimates from the ECG that are better than the state-of-the-art in accuracy and estimate delay. This method is computationally simple and can be implemented on portable monitoring devices requiring a continuous and low-delay real-time RR estimate.

Table 1: Mean error (young and elderly) and delay of the proposed method compared to the state-of-the-art over the Fantasia dataset.

	error (bpm)	delay (seconds)
state-of-the-art (W-OSC)	2.91	10.12
proposed	2.82	5.27

Causality Analysis of Atrial Fibrillation Electrograms

David Luengo*, Gonzalo Rios-Muñoz, Víctor Elvira

Univ. Politecnica de Madrid
Madrid, Spain

Multi-channel intracardiac electrocardiograms (electrograms) are sequentially acquired during heart surgery performed on patients with sustained atrial fibrillation (AF), which is one of the most common heart disorders, to guide catheter ablation for patients not responding to drug therapies. These electrograms are used by cardiologists to determine candidate areas for ablation (e.g., areas corresponding to high dominant frequencies or fractionated electrograms). In this paper, we introduce a novel hierarchical causality analysis method for the multi-output sequentially acquired electrograms. The proposed approach allows us to discriminate among signals corresponding to normal propagation (sinus rhythm) or atrial fibrillation (e.g., the presence of a rotor or an ectopic focus). Furthermore, the causal model obtained will provide important information regarding delays among signals as well as the direction and strength of their causal connections. The tool developed will ultimately serve to guide cardiologists towards problematic areas that may require catheter ablation. Results on synthetic signals and several real data (both for sinus rhythm and atrial fibrillation) acquired during ablation therapy are used to validate the proposed approach.

P67

Neural network approach for T-wave end detection: a comparison of architectures

Alexander A. Suárez León¹, Danelia Matos Molina¹, Griet Goovaerts²
 Carlos R. Vázquez Seisdedos¹, Steven Vandepuut², Sabine Van Huffel²

¹ Universidad de Oriente, Cuba; ² KU Leuven, Belgium

Aim: This study aimed to propose and evaluate a new approach for T wave end location based on Multilayer Perceptron (MLP) architectures.

Methods: The approach consists on a neural network acting as a regression function that estimates the T wave end location using the samples contained in a window which includes Te point, see figure. QTDB database was used for training and validation. For each annotated beat, a 100 samples vector (400 ms) is extracted from a reference point at R + 200 ms (R is the R-peak location of the current ECG beat). The resultant vectors were reduced dimensionally using the following techniques: (1) Principal Components Analysis (PCA); (2) Discrete Cosine Transformation (DCT) and (3) down-sampling (RES) with a down-sampling factor equal to 6.

Up to 16 components were taken from the output of this stage to build the global dataset. The target output is calculated subtracting the annotated Te point from the current reference point and dividing this result by 100.

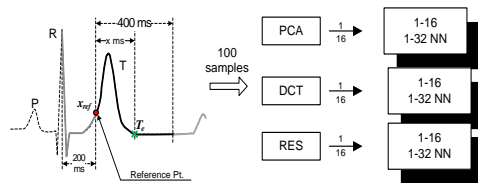


Diagram for MLP-based Te detector

For each technique, a set of three layer's MLP networks were trained varying the number of input neurons from 1 up to 16, and the number of hidden neurons from 1 up to 32 resulting in 512 architectures for each technique. The activation functions for the hidden and output layers were tanh and linear function, respectively. The training function was Backpropagation-Bayesian Regulation. The 30% of the global dataset was selected for training. The validation was performed over the global dataset. The training set is selected randomly from the global dataset every time the number of neurons in the input layer changes.

Results: The table shows the best detectors using the three above methods.

Best results for each dimensional reduction method.

Method	Neural Network	Error: $m \pm std$ (ms)
DCT	16-31-1	-0.06 \pm 15.45
PCA	16-29-1	-0.50 \pm 15.34
RES	16-19-1	-0.12 \pm 15.06

A Comparison of Three Methodologies for the Computation of V-index

Ebadollah Kheirati Roonizi*, Massimo W Rivolta, Luca T Mainardi, Roberto Sassi

Università degli Studi di Milano
Crema, Italy

Aims: Spatial dispersion of ventricular repolarization (SHVR) can be assessed from ECGs using the V-index. The metric is derived from a biophysical model, representing the ECG as a linear combination of scalars (“lead factors”) and a single waveform (DTW: “dominant T-wave”), with its derivatives. In this study, we tested three methodologies for V-index computation, by means of computer simulations and Holter recordings.

Methods: Two new methodologies (M1 & M2) were introduced and compared with the original algorithm (M0). M1 and M0 are both based on a numerical approximation of the DTW and its first derivative. However, in M1 all nearby beats share a common DTW. Imposing that the shape of transmembrane potentials during repolarization does not change increases noise resilience. M2 employs, instead, an analytical model based on sinusoidal waveforms. This functional set is closed under differentiation, which removes the necessity for a nonlinear iterative optimization procedure, while allowing higher-order terms in the DTW model. Analysis were performed using synthetic 8-lead ECGs generated with a forward electrophysiological model (SHVR in the range 10-70 ms). Then, the V-index was computed on Holter recordings collected before and after moxifloxacin administration (a drug known to slightly affect repolarization heterogeneity).

Results: On simulations, M2 generally displayed a lower mean square error between V-index estimates and SHVR. Only for low values of SHVR (10 ms), where higher-order terms were not necessary, M0 outperformed ($p < 0.05$). On real data, all methods were able to detect the effects of moxifloxacin. However, the linear correlation between the three V-index estimates was smaller than 0.7 ($p < 0.05$), suggesting inter-method variability.

Conclusions: All the three methods were able to estimate the V-index in both synthetic and real ECG. However, M2 seemed to provide more reliable estimates of SHVR, in particular for large SHVR.

P67

Fractal Pattern of Heart Rate Variability Revealing Unknown Very Low Frequency Properties

Dorota Kokosińska*, Jan Gierałowski, Jan Żebrowski

Poland

Our analysis of heart rate variability night-time recordings involves 8 groups of patients: 38 healthy, 103 - aortic valve stenosis, 36 - hypertrophic cardiomyopathy, 32 - atrial fibrillation, 82 - cardiac arrest, 17 - congestive heart failure and 700 patients from PhysioNet CAST database. We also used 13 matched case-control pairs.

We applied Multiscale Multifractal Analysis (MMA), which presents the scaling properties of fluctuations and allows us to analyze long-range correlations. Hurst surface $h(q,s)$ – the final results of MMA, describes dependence of local Hurst exponent, as a function of the multifractal parameter q – magnitude of fluctuation and the scale s – data window width.

Special 6 general diagnostic criteria let us assess characteristic shapes of Hurst surfaces for all subjects, giving result “ill” or “healthy”. Percentages of correct results (accuracy) for general 6 criteria were: 70% - patients with cardiac arrest, 61% - patients with hypertrophic cardiomyopathy, 86% - patients with atrial fibrillation, 79% - patients with aortic valve stenosis, 95% for patients with arrhythmia suppressed by encainide, flecainide and moricizine, 80% - patients with congestive heart failure and 85% for matched pairs case-control. In general for all of our groups (1034 patients), we obtained 91% of correct results. These results show us that MMA can be used as an effective screening examination method. We also prepared the additional conditions, detecting fibrillation atrial and subjects from CAST study, which both present clear and highly repetitive HRV multifractal patterns. The Hurst surface for fibrillation atrial, which is often considered to be white noise-like, has raised area for high values of s , so for very low frequencies (for white noise it should be flat) which we find to be very interesting and promising result, considering atrial fibrillation studies.

P67

Angular Velocity Transition Along the QRS Loop Aid in the Detection of the QRS Complex End and Detection of Acute Myocardial Infarction

Vito Starc*, Todd T Schlegel

University of Ljubljana Faculty of Medicine
Ljubljana, Slovenia

Automated ECG-based detection of acute myocardial infarction (AMI) is often challenging, especially in inferior wall AMI. In both healthy individuals and in patients with AMI, we developed a new method for determining QRS end and compared its performance to that of more established methods. Our method is based on angular velocity changes around the QRS loop formed by the projection of a derived vectorcardiogram on a unit sphere. Specifically, we determined the rate of change of angular velocity in the direction of change, $d(t)$, using Frank leads reconstructed from standard 12-lead ECG recordings from the Physionet PTB Database. Possibly due to its relatively sharp transition with high, narrow peak that disappeared at the end of the QRS complex, the $d(t)$ signal enabled more reliable and reproducible determination of the QRS end than the more established automatic methods. Whereas in patients with anterior AMI, $d(t)$ performed similarly to the established methods, in patients with inferior AMI, the $d(t)$ -determined angular velocity transition (AVTr) typically preceded that of QRS end determined by the established methods, and by more than 5 ms in 28% of cases. While AVTr precedence coincided with diagnostic ST elevation in only a minority of recordings with recent inferior AMI, the use of AVTr precedence as a complement to the more established methods increased the sensitivity for detecting inferior AMIs from 23% to 43% without notably compromising specificity in healthy individuals.

P67

A LightWAVE Plug-in for Semi-automatic Annotation of Heart Beats from ECG Time Series

Luca Citi*, Claudia Olariu, Riccardo Barbieri

University of Essex
Colchester, United Kingdom

LightWAVE (<http://physionet.org/lightwave/>) is an open-source web-based software for viewing ECGs and other physiologic waveforms and associated annotations (such as heart-beat markers). It also allows PhysioNet administrators and users to add and revise annotations in the course of creating new data collections and curating existing ones. At present, most users run the raw ECG through an automated QRS detector and later use LightWAVE to review and correct the detected heart beats. Although this 2-stage procedure may work well with clean signals, it is inefficient and time consuming when the recordings are contaminated by noise, artefacts or recurring ectopic events. To overcome this limitation, we developed a LightWAVE plug-in for semi-automatic annotation of heart beats from ECG time series. This plug-in is written in JavaScript using the JQuery library and integrates nicely within the LightWAVE client-side software. While the algorithm automatically identifies most QRS complexes, it stops - asking for manual intervention - whenever the confidence of a detection falls below a given threshold. The algorithm learns from the user input and improves over time by adapting to the specific characteristics of the time series, such as unusual QRS morphology or recurring artefacts (e.g. the gradient switching noise of a MRI scanner). We tested the software extensively on time series with a wide range of different characteristics, including records from the MIT-BIH arrhythmia database and signals recorded during MR imaging sessions. Especially on noisy data, its use dramatically reduced the time needed to produce annotation files for previously unannotated records. The plug-in is written in an extensible, modular fashion to allow the use of different detection algorithms within the same user interface. Our plug-in extends the functionality of LightWAVE and brings it closer to one of its design goals, i.e. to provide a comfortable and efficient method of annotating physiologic data.

P67

Novel Algorithm for Estimation ST-Segment Parameters

Vadim Konuhov, Sergey Akulov, Anna Akulova*

Samara State Aerospace University
Samara, Russian Federation

In modern cardiac practice estimation of ST-segment parameters is widely used for myocardial ischemia diagnosis. The conventional algorithm includes the following steps: low-pass filtering, QRS-complex detection, baseline drift correction, ST-segment averaging, determination of K and J points. However, it does not provide the ability for estimation of each ST-segment as well as stability to baseline wander correction. In this paper we propose the novel algorithm for ST-segment estimation based on “asymmetric” wavelet transform. The point is in the different mother wavelet functions for direct and inverse wavelet transforms. Application of proposed algorithm for ECG analysis results in baseline wander removal and amplification of ST-segment’s frequency components. Comparative analysis of standard and proposed algorithm was made. Ten records from MIT/BIH ECG database were tested. Random noise was added to the initial signals to obtain different value of signal-to-noise ratio. We used the value of variance estimate dependent on the value of signal-to-noise ratio as a criterion of efficiency. The results of the research show, that the mean variance estimate of ST-segment parameters for proposed algorithm was less than 70% compared with a standard in the wide range of signal-to-noise ratio values. Algorithm of “asymmetric” wavelet transform proposed in this paper might also be used for various purposes in automatic ECG analysis, e.g. QRS-complex shape determination, T-wave parameters estimation and signal denoising.

P67

A robust, simple and reliable measure of Heart Rate Variability using relative RR intervals

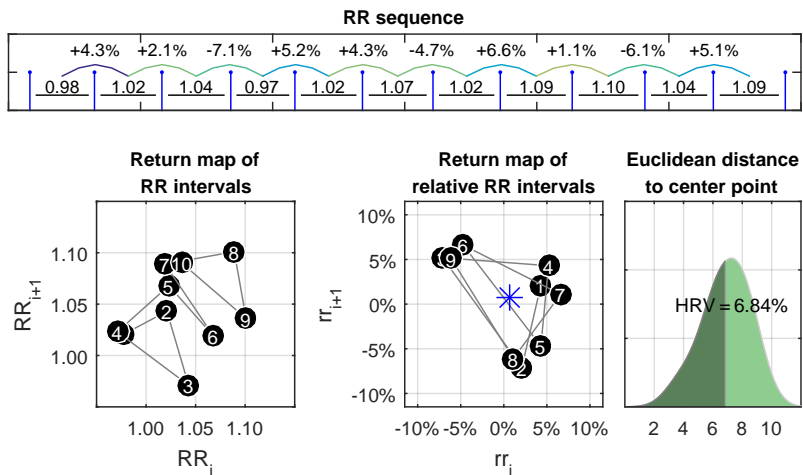
Marcus Vollmer

University of Greifswald
Greifswald, Germany

Background: Heart Rate Variability (HRV) is a physiological marker of the autonomic activity of the heart. For patients with cardiological diseases it has been used for risk stratification and health prediction. Other applications extend from psychology to sports science. However, in case of heart rate changes many standard measures are unreliable.

Methods: A new geometric measure for HRV is introduced. It is based on relative RR intervals, the difference of consecutive RR intervals weighted by their mean.

Results: The proposed measure is simple, robust and reasonable for computing HRV. It can be applied even to short RR sequences with artifacts and missing values.



Top: RR intervals in seconds and corresponding relative intervals rr in percent. Bottom: The return maps of absolute (left) and relative RR intervals (center) provide insights into heart beat dynamics (quasi periodic orbit). Relative RR intervals are adjusted for heart rate changes. The median distance to the center point can be used as HRV (right: kernel density function).

P67

Assessment of Autonomic Nerve Activity by Circadian Rhythm at Different Stages after Acute Myocardial Infarction Based on Holter Data

Hongduoer Liu*, Ping Zhan, Zhigang Wang, Yi Peng

Institute of Basic Medical Sciences, Chinese Academy of Medical Sciences & School of Basic Medicine, Peking Union Medical College, Beijing 100005, China
China

This project is aimed to perform study concerning the state of autonomic nerve system (ANS) at different stages after acute myocardial infarction (AMI), based on the assessment of circadian rhythm reflected by heart rate variability (HRV). The data were provided by the Telemetric and Holter ECG Warehouse (THEW), among which two databases were extracted. 61 Holter recordings were selected from database AMI (E-HOL-03-0160-001), containing the recordings of two stages for a patient after AMI, one between 24-48 h after AMI (AMI- I) and the other between 5th and 10th day after AMI (predischarge, AMI- II). And 189 Holter recordings were selected from database Normal (E-HOL-03-0202-003) as normal controls. Two episodes in resting state lasting 2 h were to be selected in each Holter record, one in the period of 7:00~20:00 (day), the other in 0:00~6:00 (night). Non-Gaussianity index (λ) with the scale at 25 s was calculated in each 2 h RR interval series. The λ of day (λ_{day}) and night (λ_{night}), as well as the ratio of them ($\lambda_{day}/\lambda_{night}$), were included. Results showed that there was significant difference between λ_{day} and λ_{night} (0.33 \square 0.07 v 0.46 \square 0.09) for

I (0.34(0.28-0.38) vs 0.38 \square 0.10), and significant difference between λ_{day} and λ_{night} for AMI- II (0.36(0.30-0.40) vs 0.40(0.35-0.46)). $\lambda_{day}/\lambda_{night}$ was significantly lower in Normal (0.75 \square 0.24) th AMI- I (0.89(0.75-1.2))and AMI- II (0.92(0.72-1.08)). Moreover, there existed no significant difference for $\lambda_{day}/\lambda_{night}$ between AMI- I and AMI- II. Though circadian rhythm regained to some extent for post-AMI patients predischarge, it might not mean that it reached to the normal level. Since the loss of circadian rhythm is revealed to be a typical symbol of autonomic dysfunction, it is suggested that further monitoring and assessment of circadian rhythm is necessary for post-AMI patients.

P67

Causal relationships in cardiovascular system revealed by transfer entropy

Dorota Wejer, Luca Faes, Danuta Makowiec, Beata Graff
 Institute of Theoretical Physics and Astrophysics, University of
 Gdańsk, Poland

Introduction: A switch in a body position from supine to upright results in liquids displacement in the body and may lead to postural-related syncope. The autonomic nervous system (ANS) controls the cardiovascular system to preserve homeostasis of the blood supply. Analysis of time intervals between subsequent heart beats (RR-intervals) and systolic blood pressure (SBP) provides a noninvasive way to get insights on couplings between cardiac (CS) and vascular (VS) systems driven by the ANS.

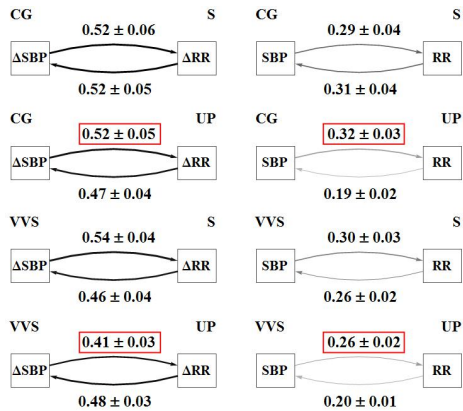
Aims: We ask how the alternation in the body position modifies the exchange of information between CS and VS in healthy people and how this alternation changes in patients suffering from vasovagal faints.

Methods: Series with RR-intervals and SBP signals were obtained during the head-up tilt test from 27 healthy people - CG group, and 54 patients who had a vasovagal syncope during the test - VVS group. The couplings between CS and VS in the supine (S) and in upright (UP) positions were assessed by transfer entropy between RR and SBP, and between beat-to-beat changes in RR, ΔRR and in SBP, ΔSBP , by using the so-called non-uniform embedding procedure. The statistically significant results were pooled in the subjects \times position groups.

Results:

Although there are differences in CS-VS couplings between CG and VVS group at supine and in upright position, the strong difference appears in response to upright position. In both groups we observe the domination of SBP but in case of VVS this domination is weaker. Moreover, considering increments of signals, we see the superiority of CS over VS.

S71



The mean values of the subjects \times position groups with standard error.

Parameter Estimation of a Mathematical Model Describing the Cardiovascular-Respiratory Interaction

Layli S Goldoozian, Antonio R Hidalgo-Muñoz, Vicente Zarzoso*, Edmond Zahedi

Iran (Islamic Republic of)

Aims: Short-term interaction between heart rate (HR) and physiological measures like blood pressure and respiration reveals relevant information about autonomic nervous system (ANS) function. Complex mathematical models for describing their couplings have been proposed in the literature. However, an accurate estimation of their parameters in an inverse modeling problem is crucial and remains a challenge. This study considers a physiologically-based model of the cardiovascular-respiratory system and ANS control that presents the neural and mechanical effects of respiration separately.

Methods: Model parameters are divided into high- and low-sensitivity groups according to the sensitivity analysis outcome. The estimation of the high-sensitivity parameters is carried out by the Nelder-Mead method in two steps: firstly the optimization of the parameters linked to the low frequency part of the outputs and secondly the parameters related to the high frequency (respiration rate range) while fixing those computed at the first level.

Results: The estimation method is applied on synthesized signals generated by random perturbation of the model parameters up to 30% from their nominal values. An accurate estimation of the highest-sensitivity model parameter (intrinsic HR) is achieved with an error of $4.9 \pm 3.8\%$ over the actual values. One of the parameters reflecting the amplitude of the respiratory-mediated variations presents an even better approximation with a mean relative error as low as $3.8 \pm 2\%$. Some other parameters presenting less sensitivity are roughly estimated, although a highly accurate global model fitting is always obtained.

Conclusions: Our results show that most of the high-sensitivity parameters can be well approximated regardless of their initial values, including the respiratory-related parameters specifically considered in our physiologically-based framework.

S71

Investigation of Causal Interactions Between Ventricular Action Potential Duration, Blood Pressure and Respiration

Stefan Van Duijvenboden*, Michele Orini, Nick Child, Jaswinder S Gill, Peter Taggart, Ben Hanson

University College London
United Kingdom

Recently, it has been shown that the ventricular action potential duration (APD) exhibits cyclical variation related to respiration in subjects with healthy ventricles. The exact mechanisms are at present incompletely understood, but mechanical electrical coupling and central gating of autonomic drive by central respiratory networks have been proposed as potential explanations. This study aims to improve our understanding of the underlying mechanisms of the APD oscillations by investigating the causal interactions between APD, blood pressure and respiration at the respiratory frequency. The study included 12 subjects with normal ventricles undergoing routine clinical electrophysiological procedures for supraventricular arrhythmias. Synchronized measurements were made from ventricular unipolar electrograms, femoral arterial systolic blood pressure (SBP) and respiratory activity (RESP). Breathing was regulated at a fixed frequency of 0.25Hz and heart rate was clamped by right ventricular pacing. The APD was estimated from the unipolar electrogram by measuring the activation recovery interval (ARI). A trivariate linear autoregressive model that accounts for lagged and instantaneous effects was then used to compute the directed coherence (DC) between RESP, ARI and SBP. The results show that the average DC between RESP and ARI, and RESP and SBP were higher compared to the average DC between ARI and SBP: 0.64 (RESP driving ARI) and 0.76 (RESP driving SBP) vs. 0.05 (SBP driving ARI) and 0.08 (ARI driving SBP). The first study on the origin of cyclical APD modulation by respiration suggests that it is not simply driven by a mechanical component performed by respiratory activity on the arterial pressure, but is the result of more complex interactions.

S71

Information-Theoretic Assessment of Cardiovascular-Brain Networks during Sleep

Luca Faes*, Daniele Marinazzo, Giandomenico Nollo

University of Trento
Trento, Italy

This study was aimed at detecting the structure of the physiological network reflecting the autonomic modulation of the cardiovascular and brain systems during normal sleep. To this end, time series of the overnight time course of cardiac parasympathetic activity and brain wave activities were measured as the normalized spectral power of heart rate variability in the high frequency band (HF) and of the EEG power in five different bands (delta, theta, alpha, sigma, beta), computed from the polysomnographic recordings of ten healthy subjects. Then, the causal statistical dependencies within and between these six time series were assessed in the information domain evaluating the internal information of the heart system and the brain subsystems and the information transfer between pairs of systems. The conditional self entropy (SE) and the transfer entropy (TE) were defined as measures of internal information and information transfer, and were then computed considering two estimation approaches: a linear method exploiting multiple regression models and a nonlinear method combining nearest neighbor entropy estimation with dimensionality reduction. The statistical significance of SE and TE was assessed using an F-test for the linear method, and an empirical randomization test for the nonlinear method. Both approaches consistently detected structured networks of physiological interactions, revealing strong internal information in all systems (SE was significant in all subjects) and information transfer directed predominantly from heart to brain (significant outgoing/incoming TE links at the HF node: 26/12 (linear), 24/16 (nonlinear)). Both methods detected bidirectional interactions between HF and beta, and the nonlinear method evidenced higher information flowing out of the delta node. These results highlight the potential of the information-theoretic framework to assess linear and nonlinear dynamics manifested in the functional network that underlies the autonomic regulation of cardiovascular and brain functions during sleep.

S71

Visualizing Evolving Clinical Sentiment using Vector Representations of Clinical Notes and Distributed Stochastic Neighbor Embedding

Mohammad Mahdi Ghassemi*, Roger Mark, Shamim Nemati

Massachusetts Institute of Technology
Cambridge, United States

Background: ‘Big Data’ has allowed researchers and clinicians alike to launch countless inquiries into critical care practice. Yet despite the use of sophisticated approaches with attractive p-values, much of the peer-reviewed literature is still seen as a poor substitute for actual clinical expertise. As researchers, we observe large variances in care practice for patients with seemingly similar conditions and backgrounds, presumably because clinicians are considering features that we may not be able to infer from the available structured data. With an ever-increasing volume of unstructured free text, which documents the observations of the clinical staff over the course of a patient’s stay, there is an unprecedented opportunity to understand what these experts may be seeing that the machine is blind to.

Methods: In this paper, we visualized how clinical language use and sentiment is associated with several commonly population level parameters including: age, marital status, mortality, gender and race. Our analysis utilizes 7 years of unstructured free text notes from the Multiparameter Intelligent Monitoring in Intensive Care (MIMIC) database. After removing stop words, text data was partitioned by our parameters, and transformed into numerical feature vectors using Google’s word2vec algorithm, a power natural language processing tool utilizing the Skip-gram approach. We compared visualizations of the first two principal components of our word vector features across each of the parameter categories (male/female, lived/died etc.). We also extracted representative words from clusters arising in the word feature space. Lastly, we inferred the general sentiment of the clinical notes towards each parameter by gauging the average distance between positive and negative keywords, and all other terms in the space.

Results: Our preliminary results are promising with statistically significant differences in word feature distribution observed across mortality and age according to a two sample non-parametric test ($p < 0.05$).

S72

Heart Rate Estimation in Photoplethysmogram Signals using Nonlinear Model-Based Signal Processing

Federico Wadehn, Yue Zhao

ETH Zurich
Zurich, Switzerland

Introduction: Unobtrusive monitoring of the heart rate with wrist-worn pulse oximeters during physical activity features the challenge of signals that are heavily contaminated by motion artifacts (MA). The photoplethysmogram signal (PPG) acquired by a pulse oximeter consists of quasi-periodic pulses, which correspond to the volumetric changes of blood in peripheral tissue. The pulses in the PPG signal are rather peaked as shown in Fig.1 and are thus only poorly modeled with a pure sinusoid, which is though the underlying assumption in spectral estimation based methods. Starting from the Beer-Lambert law, we model the MA-free PPG signal with an exponential of a sinusoid, whose frequency corresponds to the heart rate (cf. Fig.1). This model allows us further to treat the amplitude modulated PPG signal contaminated by MA as an additive mixture of sinusoids in the log-domain. Using spectral information of three-axis accelerometer recordings, MA are classified as either periodic or aperiodic, according to the number of significant peaks in their spectrum. For periodic MA the PPG spectrum is cleaned from these spurious peaks.

Algorithm: The heart rate estimation algorithm consist of: 1.) Sub-division of the PPG signal into 8s long segments; 2.) Impulsive MA (outlier) removal using a saturating function such as a sigmoid; 3.) Taking the logarithm of the nonnegative PPG signal; 4.) Spectral estimation (Goertzel algorithm) on both the PPG and the accelerometer signals with a resolution of 1 BPM; 5.) Weighting

spectral peaks of the PPG signal with the inverse of the normalized energy in the accelerometer signal in that specific frequency band to reduce the effect of periodic MA; 6.) Following a smoothness condition (HR changes < 20 BPM) the heart rate is either set to the spectral peak or the previous heart rate.

Results: A dataset of 10-min long PPG recordings of 12 healthy subjects during treadmill exercise was used to asses the algorithm. The average absolute heart rate estimation error was 1.3 BPM with a standard deviation of 2.4 BPM.

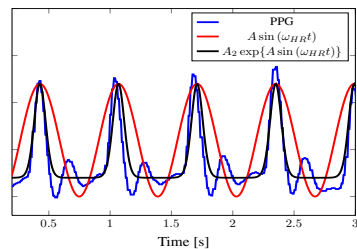


Fig.1 Sine and Exp. of Sine fitted to PPG

S72

Comparison of Four Smartphone Compatible Blood Pressure Monitors

Roderick Treskes*, Enno van der Velde, Daniëlle Eindhoven, Martin J Schalijs

Leiden University Medical Center
Leiden, Netherlands

Background: Over the past 4 years, several smartphone compatible blood pressure (BP) monitors, potentially to be used in home BP monitoring, received a CE mark. To our knowledge, no study comparing such smartphone compatible BP monitors has been performed yet. It is the purpose of this study to compare five automatic BP monitors with a handheld sphygmomanometer.

Methods: Individuals aged 18 to 30 years were selected for the study. Individuals with a history of congenital heart disease, vasculitis or irregular cardiac arrhythmias were excluded. In each individual, BP measurements were performed with six different systems (one measurement per monitor in each individual). Five automatic BP monitors were used (automatic monitors). Four monitors were smartphone compatible: Withings (Withings, Issy-les-Moulineaux, France) Wireless Blood Pressure Monitor, Qardioarm (Qardio Inc., San Francisco, CA), iHealth BP5 and iHealth BP7 (iHealth Lab, Inc. Mountain View, CA). One was a regular automatic monitor: Omron M7 (Omron, Kyoto, Japan). Furthermore, a handheld sphygmomanometer (Welch Allyn, Skaneateles Falls, NY) was used. In each individual, the order in which the monitors were tested was randomized. Measurements with Welch Allyn were done by a trained physician, blinded to BP measurements from automatic monitors. Finally, SPSS (IBM, Armonk, NY) was used to perform a linear mixed model. Bonferroni was used to adjust for multiple comparisons.

Results: So far, 13 individuals were included in the study. Mean age was 26.1 years, 46% was male and mean body mass index was 22.7 kg/m². Mean systolic and diastolic BP, measured by the handheld Welch Allyn, were 115±11 mmHg and 70±7 mmHg, respectively. Differences in systolic or diastolic BP between Welch Allyn and automatic monitors were not significant.

Conclusions: No systematic differences between a handheld sphygmomanometer and automatic monitors, of which four were smartphone compatible, were detected. Further research will be done to corroborate these findings.

A Novel Algorithm for Estimating Beat-to-Beat Systolic and Diastolic Blood Pressure using Chest Based ECG and Photoplethysmography

*Xinhui Yang, Kevin Xu, Gang Chen, Shiping Li, Jordan Davis (Xuelin Xu)

Bluer Technology
United States

Aims: Cuffless blood pressure measurement has been a hot research topic recently. This study aimed to propose a novel wearable system to estimate both systolic blood pressure (SBP) and diastolic blood pressure (DBP) on beat-to-beat basis with the same accuracy as existing ambulatory blood pressure monitoring system.

Methods: Bluer Technology has developed a novel wearable device to collect real time vital data from patients' chest. The device has differential ECG sensors and SpO2 sensors. ECG sensors enable accurate measurement of ECG signals, in this case Modified Lead II type signal, while SpO2 sensors collect blood oxygen saturation level(SpO2) and photoplethysmography signal(PPG). The blood pressure was estimated based on modified lead II ECG and PPG. Due to the short pulse transit time (PTT) of PPG signal on chest, an algorithm has been developed to compensate for PTT. Mean PTT over a period of multiple beats were used as compared to single beat in conventional algorithms.

Results: We have achieved a mean error of ± 5 mmHg and a standard deviation of 6mmHg in both SBP and DBP estimation. These numbers meets the standards of ANSI.AAMI SP10:2002 for noninvasive blood pressure accuracy(± 5 mmHg mean error and 8mmHg standard deviation).

Conclusions: A novel algorithm is developed to accurately estimate SBP and DBP blood pressure based on vital signals collected from patient chest. Results meet AAMI standard. An easy-to use wearable device to implement the algorithm has been designed.

S72

Self-Terminating Re-Entrant Cardiac Arrhythmias: Quantitative Characterization

Alan P Benson, Barrie Hayes-Gill, Arun V Holden*, Rosa Matthews, Aneela Naz, Stephen Page, Eleftheria Pervolaraki, Muzahir Tayebjee

University of Leeds
Leeds, United Kingdom

Introduction: Atrial and ventricular tachyarrhythmia are often sustained by re-entrant propagation. Episodes of paroxysmal atrial fibrillation are by definition self-terminating, and ~20% episodes of recorded endogenous or induced ventricular fibrillation self-terminate before they are defibrillated. A quantitative, stochastic description of self-termination provides an alternative to the current paradigm for re-entrant tachyarrhythmia - that of triggers and a substrate, modelled by parametrically heterogeneous deterministic partial differential equations.

Methods: We assume normal sinus rhythm and re-entrant tachycardia are clearly distinguishable, over time scales of seconds to tens of years, and in an individual can be modelled stochastically by the transition probabilities of initiation and termination of the tachyarrhythmia. Atrial and ventricular data was from recordings obtained during routine clinical monitoring and treatment, either noninvasively (ECGs- foetal from maternal abdomen, adult 12 lead, Holter recordings), or invasively (endocardial recordings during electro-anatomical mapping and ablation, from implanted pacemakers and ICDs). The transition probabilities can be estimated from longitudinal recordings in an individual, from the rate of episodes and their duration.

Results: The ventricular transition probabilities range from a notional 0.000000004 (one terminal re-entrant tachyarrhythmic event in a lifetime) to ~ 0.1 /s (a torsade storm in an LQT patient). Foetal arrhythmias occur in a few percent of recordings, but ventricular transition probabilities of initiation of ~0.001 and termination ~ 1 have been estimated. These wide ranges require logarithmic axes for an initiation/termination transition probability space, within which a patient's history is a line.

Conclusions: These transition probabilities can be related to probability estimates from population studies, and provide a measure of the effect of remodelling. They can be decomposed into probabilistic networks for excitable wave dynamics, and related, via birth and death models for rotor phase singularities, to pharmacologically addressable electro-physiological parameters.

Sustained re-entry in a 3D Regionally Ischemic Human Heart. A Simulation Study

A. Mena-Tobar¹, J.M Ferrero², J.F. Rodriguez-Matas^{1,3}

¹CIBER-BBN, Univeridad de Zaragoza, Zaragoza, Spain

²Universidad Politécnica de Valencia, Valencia, Spain

³Politecnico di Milano, Italy

Introduction: Ventricular tachycardia and fibrillation are known to be two types of cardiac arrhythmias that usually take place during acute ischemia and frequently lead to sudden death. In this work, we have studied the vulnerable window in a human heart during acute ischemia.

Method: A 3-D geometrically and anatomically accurate regionally ischemic human heart is considered, along with a modified version of the ten Tusscher 2006 action potential (AP) model. The ischemic region was composed of transitional border zones (BZ), a normal zone (NZ), and the central zone (CZ) of ischemia. In the CZ, $[K^+]_o$ was set to 9.9 mM, the inward Na⁺ and L-type currents were scaled by a factor of 0.85 to imitate acidosis, and the intracellular ATP and ADP concentration were set to 5 mM and 99 μ M respectively. A wash-out zone in the endocardium was simulated as affected by mild hyperkalemia. The model was stimulated at a frequency of 1.25Hz for 45 seconds, for preconditioning, followed by an extra-stimulus located in the subendocardial border zone with different coupling intervals (CI).

Results: Results indicate spatial heterogeneities in the propagated action potential, as reported experimentally, throughout the regional ischemic tissue, such as resting membrane potential (-86.1 mV in NZ, and -70.3 mV in the CZ, with potentials varying between these values in the BZ). For CIs in the range 265-295 ms, reentry occurred in the tissue. The reentry activity originated in the endocardium as a single rotor, that propagated transmurally toward the epicardium. Sustained re-entrant activity was found within the vulnerable window, being stable even under the presence of normal sinus rhythm stimulation.

Conclusion: The model predicts the generation of sustained re-entrant activity in the form of a rotor around the ischemic zone. The re-entrant activity originates in the endocardial surface and propagates transmurally towards the epicardium

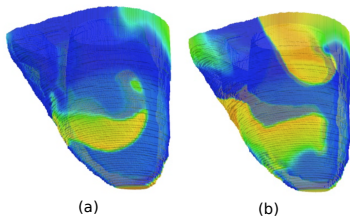


Figure 1. Snapshot of the reentrant pattern in the acute ischemic heart for two different CIs. A) CI = 270 ms, B) CI = 280 ms.

Multiple Virtual Electrodes Widen the Unpinning Interval

Sebastian Berg*, T K Shajahan, Tariq Baig, Valentin Krinsky, Stefan Luther

Max Plank Institute for Dynamics and Self-Organization
Germany

Cardiac cells, such as other excitable media, commonly show spiral waves. Once initiated, these spiral waves can continue rotating indefinitely in the medium and have to be driven out by external stimuli as they cause life threatening arrhythmias. One easy way to remove spiral waves is to deliver high frequency stimuli locally to the excitable medium. However, this method works only in a homogeneous excitable medium. Cardiac tissue contains heterogeneities in various sizes and properties, including scar tissues, muscles, and vasculature and a spiral wave in the vicinity of such a heterogeneity tends to rotate along its boundary. To eliminate these pinned spiral waves, they have to be unpinned first. An electrical stimulus given very close to the spiral core can unpin the wave if the stimulus is given within a small time window known as the unpinning window of the spiral. This stimulus can also be generated by an external field where the heterogeneity to which the spiral is pinned acts as a virtual electrode. Most studies have focused on the interaction of a single virtual electrode. In this study we use chicken cell monolayers with a hole drilled into the center which acts as the pinning center for an induced spiral wave. We then delivered electric field pulses in any chosen phase of a vortex rotation. These pulses cause waves to be emitted from the central heterogeneity as well as the boundary and smaller heterogeneities. We observed that multiple virtual electrodes can fall into the unpinning window and this happens at different phases of the spiral wave. Further, these results are supported using numerical simulations. Thus, we find that the time interval in which unpinning by an electric field stimulus is possible can be larger due to the presence of multiple virtual electrodes.

S73

A New Low-Energy, Far-Field Defibrillation Mechanism

Niels F Otani, Valentin Krinski, Stefan Luther

Rochester Institute of Technology
Rochester, New York, USA

Introduction. Experimental research activity has recently focused on a promising new method for low-energy defibrillation. Called far-field defibrillation, the method imposes electric field pulses that engage the bulk of the heart tissue, in contrast to other methods that deliver electrical energy locally through implanted electrodes. The effectiveness of this method can potentially depend on the timing of the delivery of the pulses. Here we describe a new mechanism by which these electric field pulses might terminate reentrant waves, which operates independently of shock timing. **Method.** A three-dimensional finite-difference monodomain computer simulation, which includes a full ion channel model and resistive gap junction coupling, is run in rectangular domains of different widths, designed to represent heart walls of varying thicknesses. Once a reentrant action potential scroll wave is established in the system, an electric field stimulus is delivered with varying field vector orientations through the imposition of its effect on the domain boundary conditions. **Results.** We find that, once the surface perpendicular to the scroll wave filament is depolarized by the electric field, termination of the scroll wave always results. Termination is nearly immediate in the case of thin walls (0.5 cm). In thicker walls (e.g., 2.0 cm), interaction of the induced wave with the scroll wave results in an L-shaped filament, which then shrinks and disappears by the same mechanism by which scroll wave rings terminate. Termination thus occurs independently of wall thickness, timing, and electric field orientation, as long as the latter has a normal component sufficient (about 1 V/cm) to elicit a wave. This new mechanism will likely operate alongside other mechanisms, and thus has the potential to lower the defibrillation threshold.

S73

Classification of Cardiac Arrhythmia in vitro based on Multivariate Complexity Analysis

B. Xu^{1,2}, S. Jacquir³, S. Binczak³, H. Yahia², R. Dubois¹

¹LIRYC, Bordeaux. ²Team GéoStat, INRIA Bordeaux Sud-Ouest.

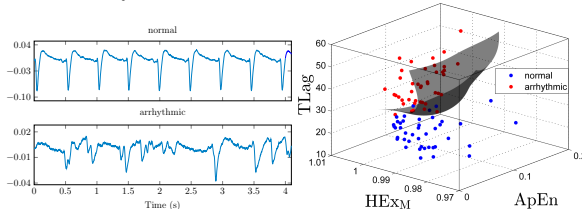
³CNRS UMR 6306, LE2I Université de Bourgogne, France.

Background: The animal models (in vitro or in vivo) provide an excellent tool to study heart diseases, among them the arrhythmia remains one of the most active research subjects. It can be induced or treated by drugs, electrical stimulation, hypothermia etc.

Problems: However, the inducing or treating effects in cardiac culture often happened long after the initial applications or in some relatively short time windows. So, it is necessary to capture and classify rapidly the signal change. Human-assisted monitoring is time-consuming and less efficient. An automatic classification method for real-time use would be useful and necessary.

Methods: Since electrocardiological signals are features by repetitive or similar patterns reflecting the intrinsic information about the patient (or culture), analyzing these patterns could help not only to monitor the status's change but also to evaluate/explore the physiologic control mechanisms. Methods based on complexity analysis are of considerable interest in this case.

Aims: Compare different complexity analysis methods in order to find the most appropriate ones to discriminate the normal cardiac signals from arrhythmic ones acquired from a cardiac cell culture in vitro. The selected features are then used by a SVM classifier.



Left: Electrical field potential (EFP) of in vitro cardiac culture on Multielectrodes Array.

Right: SVM classification of normal and arrhythmic EFP signals.

Results: Among the six complexity analysis methods, Time Lagging (TLaG) method allowed obtaining the best discrimination index (normal vs. arrhythmic, p -value, $9e-23$). The proposed Modified Hurst Exponent (HEX_M) showed better performance than original Hurst Exponent with well-improved p -value (from 0.019 to $2e-9$). The Approximate Entropy (ApEn), Sample Entropy (SampEn) and Detrended Fluctuation Analysis gave good discrimination ratio but with larger p -values (at order 10^{-3}). Combination of TLaG, HEX_M and ApEn can provide a more robust classifier and allow monitoring and classifying in an automatic way the electrical activities' changes in the cardiac cultures.

Logistic Regression to Enhance Risk Assessment by Left Ventricular Ejection Fraction and f99

Corrado Giuliani, Cees A Swenne, Sumche Man, Angela Agostinelli*, Sandro Fioretti, Francesco Di Nardo, Laura Burattini

Università Politecnica delle Marche
Ancona, Italy

Introduction: Despite recent advances in the treatment of life-threatening ventricular arrhythmias, sudden cardiac death remains one of the leading causes of death in developed countries. Left ventricular ejection fraction (LVEF) and f99 are two noninvasive indexes of cardiovascular risk (traditional the former and innovative the latter) which, taken singularly, have not shown sufficiently high predictive power for the occurrence of major cardiac events to justify preventive actions. Thus, the aim of the present study was investigate if their combination improves predictability of ventricular arrhythmias.

Methods: To this aim, ECG recordings from 266 patients with an implantable cardiac fibrillator (ICD) because of a depressed LVEF were used. All patients underwent a 4-year follow-up at the end of which they were classified as either ICD_Cases (76 patients) if they had developed ventricular tachycardia or ventricular fibrillation, or ICD_Controls (190 patients) otherwise. The ECG of each patient was used to compute the f99, a repolarization index defined as the frequency at which the cumulative power energy reaches 99%. Eventually, a logistic regression between LVEF and f99 was performed in order to derive a combined predictor (CP) of ventricular arrhythmia. Goodness of each index was evaluated by its ability to discriminate ICD_Cases from ICD_Controls in terms of the area under the receiver operator curve (AUC).

Results: When used singularly, LVEF and f99 were respectively significantly lower and significantly higher in the ICD_Cases than in the ICD_Controls (median LVEF: 32% vs. 36%, $P < 10^{-4}$; median f99: 37 Hz vs. 30 Hz, $P < 10^{-3}$) and respectively provided an AUC of 0.67 and 0.64. When combined to get $CP = -0.15 - 0.05 \cdot LVEF + 0.03 \cdot f99$, CP was significantly lower in the ICD_Controls than in the ICD_Cases (median CP: -1.1 vs. -0.7, $P < 10^{-6}$) and provided an AUC of 0.71.

Conclusions: Use of logistic regression improves LVEF and f99 predictability of ventricular arrhythmias.

S74

Big-Data Analytics for Arrhythmia Classification using Data Compression and Kernel Methods

José María Lillo-Castellano*, Inmaculada Mora-Jiménez,
Rafael Moreno-González, María Monserrat-García-de-Pablo,
Arcadi García-Alberola and José Luis Rojo-Álvarez

Rey Juan Carlos University
Fuenlabrada, Madrid, Spain

Background. Big-data analytics is broadly used today in multiple research fields to discover and analyze hidden patterns in large databases. Although Cardiac Arrhythmia Classification (CAC) has been studied in depth to date, new CAC methods need to be still designed.

Methods. Intracardiac Electrograms (EGMs) of arrhythmia episodes stored by Implantable Cardioverter Defibrillators (ICDs) in a national scientific big data service are used. A committee of six expert cardiologists ensured high quality of EGMs, evaluating and classifying each episode into eight arrhythmia classes (8-class): *sinus tachycardia*, *atrial fibrillation*, *flutter*, *uncertain supraventricular tachycardia*, *sustained monomorphic ventricular tachycardia*, *sustained polymorphic or ventricular fibrillation*, *T-wave oversensing*, and *noise*. A grouping of these classes according to the arrhythmia origin into three major sets was carried out (3-class): *atrial*, *ventricular* and *other*. A new big data analytics method for automatic CAC of EGM episodes is proposed. The method combines the effectiveness of a fast computational measure based on data compression concepts (Jaccard dictionary similarity) and the classification power of kernel methods, requiring minimal EGM preprocessing and allowing dealing with EGMs of different duration. We compare the performance of two classifiers, k -Nearest Neighbors (k -NN) and Support Vector Machines (SVM) when considering four different input spaces in 8-class and 3-class CAC scenarios.

Results. Experiments with 6848 EGMs from 629 patients showed that k -NN worked better than SVM when previous episodes from the same patient were available in the classifier design, and vice-versa. For the best cases, k -NN and SVM yielded accuracies near to 95% and 85%, respectively.

Conclusion. Big-data analytics combining data compression and kernel methods is a useful criterion to classify arrhythmia episodes EGMs stored by ICDs quickly and efficiently. The proposed method can be used as a high-quality big data service for CAC, providing a support to cardiologists for improving the knowledge on patient diagnosis.

Automatic Diagnosis of Complete Left Bundle Branch Block from Standard 12-lead Electrocardiogram

Xiaojuan Xia*, Anne-Christine Ruwald, Martin Ruwald, Nene Ugoeke, Barbara Szepietowska, Valentina Kutyifa, Mehmet Aktas, Poul Erik Bloch Thomsen, Wojciech Zareba, Arthur Moss, Jean-Philippe Couderc

University of Rochester
Rochester, United States

Automatic diagnosis of the Complete Left Bundle Branch Block from standard 12-lead Electrocardiogram. XJX, ACR, MHR, NU, BS, VK, MKA, PEBT, WZ, AJM, JPC.

Introduction: A strict Left Bundle Branch Block (LBBB) criteria was recently proposed to identify patients with complete LBBB who benefit the most of Cardiac Resynchronization Therapy. The aim of our study was to automate the strict LBBB criteria in order to facilitate broader application of the criteria which requires the measurements of subtle QRS patterns from standard 12-lead ECGs.

Methods and Results: We developed a series of algorithms to automatically detect and measure the QRS parameters required for strict LBBB criteria. The algorithms were developed using training (n=20) and validation (n=592) sets consisting of signal-averaged 12-lead ECGs(1000Hz SamplingRate) recorded from 612 LBBB patients from MADIT-CRT. In this study, 4 trained clinicians independently and blinded performed adjudication on 185 assigned ECGs which included 148 different ECGs for comparing automatic and manually adjudicated results, 13 ECGs for evaluation of intra-observer variability and 32 ECGs for inter-observer variability. We assessed the performance of automated algorithms, using manually adjudicated results as references. Overall sensitivity and specificity for detecting complete LBBB were 95% and 86%. The mean absolute deviation(MAD) of QRS duration and notch/slur locations for the automated method vs. the manual method was below 1ms, and MAD values were lower than 2ms for inter-observer and intra-observer variability. Sensitivity and specificity for detecting notch and slur locations were 87% and 78% for notches and 96% and 90% for slurs, respectively, using the automatic method. In addition 95% and 90% agreements for notches and 93% and 88% agreements for slurs were reached for inter-observer and intra-observer variability.

Conclusions: The proposed algorithms automatically measure QRS features required for the diagnosis of complete LBBB. Our study shows good performance in reference to manual results.

S74

Orthogonal Component Analysis to Remove Ventricular Far Field in Non Periodic Sustained Atrial Flutter

Gustavo Lenis, Tobias Oesterlein, Dan-Timon Rudolph, Olaf Dössel*

Karlsruhe Institute of Technology (KIT)
Karlsruhe, Germany

Automatic signal processing of intracardiac electrograms (EGM) plays a decisive role in the diagnosis and treatment of supraventricular arrhythmias. During sustained atrial flutter (AFlu) a repetitive signal is measured in the atrium. However, the ventricular far field (VFF) may overlap with the atrial activity (AA) and compromise the automatic signal processing tools during the intervention. Recently, an innovative method based on periodic component analysis (PiCA) was proposed as artifact removal technique. This method exploits the periodicity of sustained AFlu to reconstruct the corrupted AA. Even though PiCA proved to be a very successful method in many scenarios, it cannot be securely applied when the atrial activity is not highly periodic. Small deviations in the period of the signal or the morphology of each AA lead to wrong reconstructions. Therefore, we propose a new method based on orthogonal component analysis (OCA) that can be used to reconstruct the original AA in the case of non periodic sustained AFlu. The idea behind OCA is to learn how the clean, not corrupted AA are distributed in a low dimensional space spanned by a few principal components and to extrapolate that knowledge to reconstruct the original AA from the corrupted EGM. The same principal components obtained for the distribution of pure AA are used to represent and correct the corrupted AA. After the correction is carried out, the scores in the corrected distribution have the same mean and standard deviation as the scores of the original distribution of pure AA. Using the proposed method, we were able to show that it can be applied successfully for the reconstruction of corrupted AA in the case of periodic and non periodic sustained AFlu. Specially the latter was demonstrated to be an impossible task for known methods such as PCA or PiCA.

S81

Validation of the V-index as a Metric of Ventricular Heterogeneity in Endocavitary Recordings

Michele Orini, Claudio Blasi, Malcom Finlay, Ben Hanson, Pier Lambiase, Roberto Sassi, Luca Mainardi*

Politecnico di Milano
Italy

Aims: Spatial dispersion of ventricular repolarization (SHVR) is an important factor influencing the arrhythmogenic properties of the ventricles. We recently introduced the V-index, an estimator of SHVR obtained from the analysis of T-wave shapes on ECG leads in successive beats. A direct relation between V-index and SHVR has been demonstrated theoretically and using numerical simulations employing a mathematical model of the ECG. In this work, we validate the relation using concurrent endocavitary recordings and surface ECG. Additionally, we also tested the correlation between SHVR, V-index and Tpeak-to-Tend (Tpe), a common ECG marker of repolarization dispersion.

Methods: We analyzed data from 10 patients, which underwent simultaneous recording of endocavitary and surface 12-Leads ECG during two experimental phases: baseline and mental-stress. Endocavitary recordings were performed by 3 catheters (placed in the right and left ventricles and in the epicardial coronary vein) and 10 unipolar recordings were obtained from each catheter. For each beat, fiducial points of repolarization activity (T-onset, T-peak, T-end and local repolarization time obtained using Wyatt method) were first automatically detected on each recordings. Then, they were reviewed and manually corrected using dedicated semi-automatic software. SHVR was computed as the range of the temporal median of local repolarization times of each cardiac site (DRT). This value was compared with V-index and Tpe values, obtained from surface ECG.

Results: Linear correlation between the V-index and DRT was high during baseline ($\rho=0.83$, $p<0.01$), but lower during mental stress ($\rho=0.50$, $p<0.17$). However, when data were pooled together, a significant linear correlation was observed ($\rho=0.64$, $p<0.001$). Correlation between V-index and SHVR was always higher than correlation between Tpe and SHVR.

Conclusions: This work highlights the relationship between V-index and a direct measure of repolarization heterogeneity obtained from endocavitary recordings, and it demonstrates that the V-index is a better marker of repolarization dispersion than Tpe.

S81

Determining the Connection between Capacitively Coupled Electrocardiography Data and the Ground Truth

Anna Böhm*, Christoph Hoog Antink, Steffen Leonhardt, Daniel Teichmann

RWTH Aachen University
Germany

Capacitively coupled ECG (cECG) has been investigated by many groups in the past years. Its benefit is contactless measurement and therefore improved comfort for patients compared to the standard ECG. However, due to its capacitive coupling, the cECG signal differs from the conductive ECG in terms of morphology. Additionally, the cECG's amplitude is attenuated and it is more artifact-prone. Hence, one difficulty of cECG, if no ground truth is available, is to deduce what the actual ECG would look like. The possibility to determine transfer functions based on mathematical modeling of the electrode-skin contact has been shown in the past. However, given such a model, it is difficult to correctly estimate its parameters. In this paper, a different approach based on a multiple-input-single-output (MISO) blind deconvolution technique is taken. The aim was to reconstruct a single-lead reference ECG from multiple cECG channels. To that end, the deconvolution process was performed in the frequency domain, where convolution becomes a simple multiplication. The time-domain estimation can then be obtained via inverse transformation. In order to test this approach, data from previous studies were selected. These recordings consisted of three cECG and one reference ECG channels from several test subjects. Data with acceptable quality were chosen automatically by an algorithm, discarding sections that contained artifacts in all channels. Subsequently, blind deconvolution was performed. Finally, cross-validation was used to assess the results. According to our findings, the estimation of the reference ECG from three cECG channels with deconvolution is feasible. The root-mean-square error (RMSE) of the reference ECG signal to its estimation obtained via deconvolution was lower than to each of the unprocessed cECG channels (estimation=0.6217; cECG1=1.2211; cECG2=1.0162; cECG3=0.8143). While this is a promising result, its applicability to other cECG setups has to be shown in future studies.

S81

A Principal Component Analysis Approach for Heart Rate Turbulence Assessment in Chagas Disease

Alex C Alberto*, Gabriel A Limeira, Jurandir Nadal

Universidade Federal do Rio de Janeiro
Rio de Janeiro, Brazil

The analysis of heart rate turbulence (HRT) is a powerful method to estimate the baroreflex from the 24 h Holter ECG signals, by considering that an isolated premature ventricular contraction (PVC) causes an immediate cardiac acceleration followed by a deceleration in subjects with low risk of sudden death. This study aims at developing a method for risk stratification of sudden death in chronic Chagas cardiopathy, by applying Principal Component Analysis (PCA) to the tachogram segments extracted for HRT analysis. HRT analysis was applied to a database of high resolution ECG from Chagas disease patients, with 10 min signals in XYZ leads, sampled with 16-bit resolution at 1000 Hz. From a set of 115 records that presented PVC, it was possible to extract at least one valid tachogram segment of 19 RR intervals with an isolated PVC in the third position in just 51 signals. The valid segments from each ECG record were taken to compute a coherent mean, used them for measuring the well-known parameters turbulence onset (TO) and turbulence slope (TS). From this dataset, two groups of eight signals were extract, according to the estimated risk of sudden death: high risk ($TO \geq 0$ and $TS \leq 2,5$ ms/RR interval) and low risk ($TO < 0$ and $TS > 2,5$ ms/RR interval). PCA was thus applied to this set of 16 coherent means with 19 samples to reduce data representation to three principal components (PC), which represented 98.2% of the original variance. Applied to the respective PC scores, a logistic regression allowed the separation of groups with 94% accuracy – 88% sensibility and 100% specificity. As a conclusion, PCA has a potential for baroreflex assessment throughout HRT in Chagas disease, but this method should be validated with a larger sample with long duration ECG records.

S81

Algorithm for Real-time Prediction of Neurally Mediated Syncope Integrating Indexes of Autonomic Modulation

R. Couceiro, P. Carvalho, R. P. Paiva, J. Muehlsteff, J. Henriques, C. Eickholt, C. Brinkmeyer, M. Kelm, C. Meyer

University of Coimbra
Coimbra, Portugal

Background. Neurally mediated syncope (NMS) is a transient and self-limited loss of consciousness that affects all ages and is associated with high rates of falls and hospitalizations. One of the most common triggers of NMS is orthostatic stress. This causes an initial rise in sympathetic tone, which is followed by “paradoxical” sympathetic withdrawal and an overshoot parasympathetic activation. This results in bradycardia, hypotension, and syncope.

Objective. In this study we propose a new algorithm for real-time prediction of NMS that integrates indexes of autonomic modulation (among other parameters), which is based on the analysis of the electrocardiogram (ECG) and photoplethysmogram (PPG) alone.

Protocol. ECG and PPG signals were acquired from 43 patients with suspected NMS, during scheduled diagnostic head-up tilt table (HUTT) tests. 21 patients experienced syncope during the test and 22 patients did not.

Methods. Heart rate variability (HRV) indexes were integrated in an algorithm comprising surrogates of chronotropic, inotropic, blood pressure and vascular tone changes. From the ten selected features, one index from the time-domain (SDNN) and two indexes from the frequency-domain (normalized low- and high-frequency areas) were found to be the most relevant. NMS was predicted based on the distance of the selected features to the stable orthostatic state using a threshold-based approach.

Results. The proposed algorithm was validated in 43 subjects using a three-way data split approach and the results are presented in Table 1.

Conclusion. HRV indexes improved the algorithm specificity (SP), positive predictive value (PPV) and false positive rate per hour (FPRh) in the train/validation phase and the prediction time (PreTime) in the test phase, showing the importance of autonomic modulation indexes in real-time prediction of NMS.

Table 1 – Results achieved by the proposed algorithm with and without HRV indexes

Algorithm	Phase	SE (%)	SP (%)	PPV(%)	FPRh (h ⁻¹)	PreTime (s)
W/ HRV indexes	Train/Validation	93.3	100	100	0	56.1±36.8
	Test	100	92.3	85.7	0.15	256.7±239.4
W/o HRV indexes	Train/Validation	93.3	96.7	94.8	0.15	61.0±38.6
	Test	100	92.3	85.7	0.15	243.3±242.5

SE: Sensitivity; SP: Specificity; PPV: Positive Predictive Value; FPRh: False positive rate; PreTime: Prediction time

Reliability Loss with Sampling Rate Reduction

Paulo Sousa, Rute Almeida, Marta João Silva, Ana Paula Rocha

Faculdade de Ciências, Universidade do Porto
Porto, Portugal

High sampling frequency is not usually considered in hospital monitoring systems, what can limit the usefulness of the data, namely for repolarization measures. In this work the reliability of beat-to-beat measures using low sampling frequency is quantified with respect to the original rate.

PTB Diagnostic ECG Database (PTB: 289 patients/files) and Holter from intensive care patients (ICU: 21 patients, 45 files) recordings originally at 1000Hz were downsampled to 500, in PTB, and 250Hz, in both databases, and delineated producing marks for each lead (SL) and a combined annotation (SLR). RR and QT intervals were extracted from a normal beat per recording at PTB and 20 random beats of each ICU recording. The reliability (R) was measured considering Lin's concordance correlation coefficient (CCC), intraclass correlation coefficient (ICC), and Information-based measure of disagreement (IBMD: 1-R). Reliability was evaluated in PTB for each of the 15 SL, SLR and mean interval (M), and in ICU for each file, considering all 20*45 beats (G1) and one arbitrary beat per file (G2). The conventional interpretation was considered: excellent ($R > 0.9$) and good ($R > 0.7$).

Regarding CCC and ICC, for RR at 500Hz, $R > 0.7$ always, with $R > 0.9$ for SLR, M and 10 SL; at 250Hz $R > 0.7$ for SLR, M and all but 1 SL, with $R > 0.9$ for 4 SL, G1-2 and 30 ICU files. For QT at 500Hz, $R > 0.9$ for all cases while at 250Hz $R > 0.7$ for all but 17 ICU files, with $R > 0.9$ for SLR, M, 11 SL, G1 and 16 ICU files. IBMD < 0.1 (excellent) was found in all cases except at 2 ICU cases for QT.

Results indicate that at 250Hz RR and QT measures are still reliable compared with the values at 1000Hz: measurement errors are small in comparison to the true differences between subjects.

S81

The Origin of Diastolic Micro-Signals Observed in Defibrillator Recipients Might Be Qualitatively Explained by a Simple Computational Model

Aldo Casaleggio*, Paolo Rossi, Michele Migliore

Italy

Background: In previous studies, investigating intracardiac electrograms (Egm) obtained from implantable cardioverter defibrillators (ICD), the presence of Diastolic Micro-Signals (DMS) preceding the initiation of ventricular tachyarrhythmias (VT) has been observed [1] both in coronary artery disease (CAD) and in dilated cardiomyopathy (DCM).

Purpose: to propose an explanation of DMS for the case of ischemic cardiomyopathy, using a recently published computational model.

Methods: a computational model of the electrical cardiac activity able to reproduce erratic arrhythmias in a bi-dimensional network of Beeler-Reuter cardiac cells has been recently published [2]. The model has been validated in the presence of scar-ischemia related, and it assumes that gap-junction conductance can be fluctuating and rectifying.

Results: the computational model assumes that the scar causes an inner loop in which the electrical activity may propagate without generating cardiac beats. However, the inner activity may occasionally propagate outside the scar through an exit door, initiating premature cardiac beats. Movies showing this effect and the connection with DMS will be presented and discussed.

Conclusions: this study is at its initial stage and it only considers a bi-dimensional network of cardiac cells. However it supports the hypothesis that, in patients with ischemic cardiomyopathy, DMS reveal the presence of an electrical activity embedded within the scar, that can be monitored by an intracardiac electrocatheter placed in the proximity of the scar lesion. References 1. Casaleggio A, Guidotto T, Malavasi V, Rossi P. *Comput in Cardiol* 2010;37:737-740. 2. Casaleggio A, Hines ML, Migliore M. *PLoS ONE* 9(6): e100288 (2014).

S82

Investigation of the Functional Effects of KCNJ2-linked Short QT Syndrome on Electrical Conduction at Purkinje-Ventricle Junction at Low- and High-Frequency

Cunjin Luo*, Kuanquan Wang, Qingjie Wang, Yongfeng Yuan, Zhili Li, Ming Yuan, Henggui Zhang

China

Introduction: Genetic KCNJ2-linked short QT Syndrome (SQT3) arises due to Ik1 ion channel mutations leading to accelerated ventricular repolarization and arrhythmias. However, ionic mechanisms of the SQT3 are incompletely understood. The aim of this study was to utilize the heterogeneous Purkinje-ventricular models to investigate the functional impacts of the SQT3 on the electrical wave conduction at the Purkinje-ventricle junction. Methods and

Results: Detailed Stewart et al. model of human Purkinje fibre cells and ten Tusscher et al. models of human ventricular cells were coupled together to construct a heterogeneous 2-D model of Purkinje-ventricular tissue. Previously validated Ik1 channel formulations for SQT3 (including WT, WT-D172N and D172N mutations) were incorporated in each cell. Rate-dependent effects of the mutations were considered by the implementation of low (0.5 Hz), normal (1.25 Hz) and high (2.66 Hz, 3.33 Hz) stimulation frequencies. In simulations, APD90 and APD90 dispersion across the strand in the middle of the 2-D sheet tissue for the WT, WT-D172N and D172N mutation conditions were measured; the conduction velocity at different areas of the tissue model were calculated; and pseudo-ECGs were simulated. Compared with the WT condition, although the APD across the strand was reduced by the WT-D172N and D172N conditions, the APD gradient was markedly increased at some local regions across the Purkinje fibre and ventricular strand. Compared with 1.25 Hz frequency of electrical stimulation, the measured APD90 across the strand did not change noticeably at 0.5 Hz, but was reduced at 2.66 Hz. Simulated ECG showed similar characteristics at 0.5 Hz, 1.25 Hz and 2.66 Hz. At 3.33 Hz of electrical stimulation, 1:1 response of electrical excitation wave to stimuli failed in WT condition, but sustained in the mutant conditions.

Conclusions: Increased Ik1 due to the D172N mutation accelerates ventricular repolarization, and reduces APD spatial dispersion along the Purkinje-ventricle tissue, which facilitates the conduction of rapid electrical excitation waves, which otherwise fails to conduct in WT condition. Such a loss of protective effect of cardiac tissue to high frequency of electrical stimulation, together with abbreviated APD and ERP, may account for the initiation of ventricular tachycardia and fibrillation.

Epicardial-Limited Electrophysiological Heterogeneities do not Facilitate Ventricular Arrhythmia Induction: An Experimental Study

Antonio Guill, Alvaro Tormos, Conrado J Calvo, Eduardo J Roses, Antonio Cebrian, Luis Such-Miquel, Luis Such, Manuel Zarzoso, Francisco J Chorro, Jose Millet*

Universitat Politecnica de Valencia
Valencia, Spain

Introduction: The electrophysiological heterogeneities of the myocardium are associated with vulnerability to arrhythmias. Temperature variations can give rise to changes in cell refractoriness and electric propagation. The present study describes a heterogeneity model induced by epicardial cooling / warming. The ventricular activation-recovery interval (ARI) and conduction velocity (CV) are determined, and an analysis is made to determine whether the induced dispersion is accompanied by an arrhythmogenic effect.

Methods: An experimental study was carried out in isolated rabbit hearts (n=8), using a specific electrode device including a thermoelectric element for controlled cooling and warming of a limited epicardial zone of the left ventricle, with simultaneous recording of the electrograms in the zone. Recordings were likewise made in another zone of the same ventricle. The recordings obtained were used to calculate ARI under sinus rhythm, and programmed pacing was used to assess CV and the induction of ventricular arrhythmias.

Results: With respect to baseline, ARI in the modified zone was prolonged (137 ± 22 ms vs 111 ± 13 ms, $p < 0.05$) under maximum hypothermia ($22.3 \pm 0.6^\circ\text{C}$ vs $36.7 \pm 0.8^\circ\text{C}$) and was shortened (98 ± 13 ms vs 107 ± 16 ms, $p < 0.05$) under conditions of hyperthermia ($41.8 \pm 0.3^\circ\text{C}$ vs $37.3 \pm 0.4^\circ\text{C}$). The CV decreased (70 ± 17 cm/s vs 76 ± 17 cm/s, $p < 0.05$) under hypothermia and increased (79 ± 20 cm/s vs 75 ± 21 cm/s, $p < 0.05$) under hyperthermia. There were no changes in the unmodified zone. Repetitive responses were observed in four experiments, with no dependency between the appearance of responses and the induced modifications.

Conclusions: Thermally induced dispersion of ARI and VC did not favor the induction of ventricular arrhythmias, probably because only a limited zone of the ventricular epicardium was affected.

Control of Ventricular Tachycardia under Myocardial Ischemic Conditions and Infarction

Edda Boccia*, Stefan Luther

Max Planck Institute for Dynamics and Self-Organization
Goettingen, Germany

Myocardial ischemia arises when blood supply of substrates doesn't meet tissue's metabolic demands. It can degenerate to acute ischemia and infarction. Ischemia is followed by profound metabolic changes: hyperkalemia (increment of extracellular potassium), hypoxia (deprivation of oxygen supply) and acidosis (increment of acidity in the blood). We present a modified version of the Luo-Rudy I model, adopted to investigate action potential propagation under ischemia and infarction. The domain is represented by a 2D virtual sheet of myocardial tissue, where heterogeneity is introduced by subdividing it in three distinct zones: a central circular ischemic area (CZ), a ring-shaped border zone (BZ, linear transition between physiological and ischemic values) and normal tissue. As a first approximation, hyperkalemia and acidosis were simulated and parameters were changed in the CZ and in the BZ at each time after the onset of ischemia. We study the interaction of propagating waves with ischemic regions and the onset of cardiac arrhythmias, including ventricular tachycardia (VT) and fibrillation (VF). We investigate pinning and unpinning of rotating waves to and from infarction zones using pulsed electric fields. We will discuss the implications of our findings for the development and optimization of low energy control of cardiac arrhythmias including Low-Energy Anti-Fibrillation Pacing (LEAP, Luther & Fenton et al., Nature 2011).

S82

Effects of Early Afterdepolarizations on Ventricular Tachycardia in Human Heart

Jieyun Bai, Kuanquan Wang*, Yinghui Li, Henggui Zhang

Harbin, China

Aim: Early afterdepolarizations (EADs) are classically generated at slow heart rates and suppressed by fast intrinsic heart rates. However, experimental studies suggest EADs may also occur at rapid heart rates as a consequence of tachyarrhythmias. The aim of this study was to investigate the interaction between EAD and rapid reentrant excitation waves and assess its effects with electrocardiogram (ECG).

Methods: A 3D human ventricular conduction model was developed by integrating Purkinje fiber network system and anatomically detailed ventricular geometry of the human heart with detailed electrophysiology in the format of mono-domain model. For simulating EADs, both ICaL and IKr equations of the ten Tusscher and Panfilov (TP06) model were modified based on experimental conditions. The standard S1-S2 stimulation protocol was implemented to induce reentrant excitation waves. ECGs were computed from a site 2cm distance from the epi-cardiac surface of the heart.

Results: At the cellular level, reduced repolarization reserve by IKr contributed to action potential duration (APD) prolongation (ENDO: 302ms vs. 402ms, MIDDLE: 414ms vs. >1000ms, EPI: 298ms vs. 397ms) and genesis of EADs only in MIDDLE cells. In the 3D model, EADs caused drift of rapid rotors. Multiple focal excitations arising from EADs kept regeneration of reentrant excitation waves by breaking excitation wave fronts. ECGs presented periodic features with stable reentry in control condition, but degenerated into irregular and complex features in EADs condition. These observations were characteristic of the differences between ventricular tachycardia and ventricular fibrillation, which are in good agreement with clinical reports.

Conclusions: The MIDDLE cells are prone to genesis of EADs at rapid heart rates, which play an important role in degenerating ventricular tachycardia into ventricular fibrillation.

S82

Left Ventricular–Aortic Coupling in Sickle Cell Disease Underlies Diastolic Dysfunction

Emilie Bollache*, Nadjia Kachenoura, Roberto Lang, Victor Mor-Avi, Amit Patel

U1146 INSERM-UPMC UM CR 2-CNRS 7371
Paris cedex 13, France

Left ventricular (LV) diastolic dysfunction (DD) is associated with increased mortality in sickle cell disease (SCD) but its mechanisms are not well known, preventing the development of effective therapies. Our hypothesis was that DD in SCD may be due to changes in aortic properties. We studied 31 SCD patients (32 ± 7 yrs) and 12 normal controls (29 ± 10 yrs) who underwent echocardiography and MRI on the same day. LV diastolic function was assessed from echocardiography. MRI included velocity-encoded images of the aorta to measure ascending aortic cross-sectional area, stroke volume, distensibility, as well as volumes of the forward (FFV) and backward (BFV) blood flow. Compared to controls, SCD patients had increased aortic area, stroke volume, and both FFV and BFV, while distensibility was similar. DD was found in 5/31 patients (16%), in whom the increase in BFV and BFV/FFV ratio was even more pronounced, when compared to the remaining patients. Our findings suggest a potential mechanism of DD in SCD patients. Increased cardiac output induced by chronic anemia might be associated with aortic dilation, which may increase LV afterload (BFV), ultimately leading to LV DD. If confirmed in larger studies, these aortic changes could be targets for specific therapies as a way to prevent the development of DD in SCD.

P83

Phase Contrast MRI: Development of a User-Friendly Platform for Fast-Automated Segmentation and Fluid-Dynamic Post-Processing

Selene Pirola, Filippo Piatti*, Francesco Sturla, Emiliano Votta, Igor Nesteruk, Massimo Lombardi, Alessandro Della Corte, Malenka Bissell, Alberto Redaelli, Enrico Caiani

Politecnico di Milano
Milano, Italy

Aims: 3D Phase Contrast MRI (4D-flow) provides in vivo quantitative blood flow assessment. However, its usability in clinical practice is challenging due to laborious post-processing. To overcome this limitation, we aimed at: 1) developing a dedicated user-friendly platform for fast and semi-automated aortic lumen segmentation and 4D-flow analysis; 2) validating segmentation results with manual tracing; 3) testing its clinical applicability on patients with bicuspid aortic valve (BAV).

Methods: 4D-flow images (3T, Siemens) of 5 BAV patients were used to extract the cartesian velocity components and velocity magnitude. A dedicated semi-automated Region Growing and Thresholding (Rg-Th) algorithm, exploiting texture properties in different image regions, was applied to segment the lumen, thus providing the 3D region in which computing the fluid-dynamic parameters from velocity images. After automated definition of the vessel centerline, manual interaction was required only to place a seed in the slice of interest, from which fluid-dynamic and morphological variables are computed: blood velocity contours and vectors, lumen area, blood flow rate, flow displacement, flow jet angle, local normalized flow helicity, and wall shear stress.

Results: Validation of Rg-Th with manually traced aortic contours by two blinded observers in 52 sagittal slices resulted in high correlation ($r^2=0.98$), small bias (-4% of area lumen) and narrow limits of agreement ($\pm 15\%$), with DICE similarity >0.9 and comparable to that obtained between the two observers. Fluid-dynamic and morphological analysis pointed out the significant impact of BAV alterations on the ascending aorta.

Conclusions: We developed a comprehensive analysis platform potentially able to increase usability of 4D-flow MRI to investigate aortic fluid dynamics. Validation with manual tracings showed the good performance of the applied lumen segmentation method, at the basis of fluid-dynamic parameters computation. This analysis may help in providing multiple parameters that could be used for effective stratification of BAV severity.

Design of Anthropomorphic Atherosclerotic Carotid Artery Flow Phantoms for Ultrasound Images

Francesca Galluzzo, Filippo Leonardo, Alessandro Ceruti, Luca De Marchi, Cristiana Corsi

DEI-DIN, University of Bologna, Bologna, Italy

Beside classical applications, flow phantoms can be used as test objects to explore novel ways of enhancing the US-based carotid atherosclerosis diagnosis. To achieve this goal carotid phantoms (CaPs) should be anatomically realistic both in terms of geometry, acoustic and physical properties.

We propose a framework for designing CaPs of healthy and atherosclerotic arteries. It consists in the following steps: (i) by using CAD software and 3D printing, an anthropomorphic negative outer vessel mold and several inner cores modeled for mimicking different pathological conditions were produced; (ii) the cavity between inner and outer molds was filled with a polyvinyl alcohol solution, which undergoes several freeze/thaw cycles to change cryogel stiffness and mimic several atherosclerotic conditions affecting the whole vessel wall or some portions and eventually embedding additional materials to mimic composite vessel occlusions; (iii) the resulting phantom was embedded in agar-based tissue-mimicking material, and (iv) a blood-mimicking fluid based on nylon-scatterer solution, was pumped through it with pulsatile flow.

To verify the framework effectiveness we constructed three CaPs: healthy, with a hard/soft plaque causing a 30%/65% vessel narrowing. Then, we acquired B-mode images of the CaPs, and performed their geometric characterization. The CaPs wall thickness, measured from B-mode images, ranged between 1.2÷2.12mm for the normal wall and between 2÷4.63mm in presence of stenosis, which are in good agreement with real wall thickness values (~1mm, >1÷4mm). Lumen diameter ranged between 7.21÷7.63mm for CCA, 6.88÷7.57mm for ICA and 6.38÷6.75mm for ECA. These measurement, verified by means of a caliper, are in good agreement with value of in-vivo measurement. The proposed framework allows to easily realize anthropomorphic CaPs at low cost, reproducing different atherosclerotic conditions.

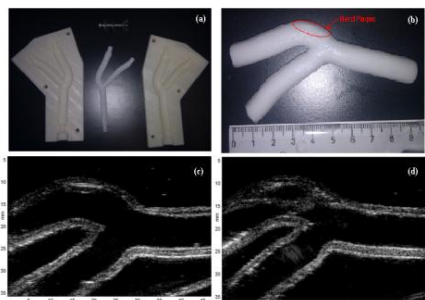


Figure: 3D Printing negative outer mold and inner cores (a); CaP with hard plaque (b); B-mode images obtained from hard (c) and soft (d) plaque CaPs.

Aortic Pulse Wave Velocity using Wavelet Analysis in Magnetic Resonance Imaging

Ioannis Bargiotas*, Elie Mousseaux, Wen-Chung Yu, Bharath Ambale Venkatesh, Emilie Bollache, Alain De Cesare, Joao A C Lima, Alban Redheuil, Nadjia Kachenoura

France

Background: Pulse wave velocity (PWV) is a major predictor of cardiovascular mortality. It can be measured from MRI (aoPWV) as the ratio between aortic length and transit time (TT) necessary for the flow wave to travel between two aortic locations. Although MRI has an excellent anatomical coverage enabling reliable measurement of arterial length, accurate TT determination remains challenging, and is the purpose of this work.

Methods: We studied 71 healthy individuals (45 ± 15 years, 29 females) with aortic MRI velocity acquisitions and gold-standard tonometry carotid-femoral PWV (cfPWV). We developed a multiresolution method, based on wavelet cross-spectrum, to estimate TT from ascending and descending aortic MRI flow curves. This method (aoPWVwu) combines the robustness of Fourier-based methods (aoPWVf) to temporal resolution with the possibility to restrict the analysis to reflectionless systolic upslope of the flow curves, as performed in the time domain (aoPWVtu). The three aoPWV were compared according to their linear correlations with age, cfPWV and the effects of decreased temporal resolution.

Results: Correlation with age was highest for wavelet-based method (aoPWVwu: $r=0.84, p<0.001$; aoPWVtu: $r=0.74, p<0.001$; aoPWVf: $r=0.63, p<0.001$). Associations with cfPWV were highest when using techniques restricted to the flow curve upslopes (aoPWVwu: $r=0.58, p<0.001$, aoPWVtu: $r=0.58, p<0.001$, aoPWVf: $r=0.40, p<0.001$). Furthermore, while a 4-fold decrease in temporal resolution had only minor effect on correlation with age for aoPWVwu (r decreased from 0.84 to 0.80) and aoPWVf (r decreased from 0.63 to 0.51), we found major alteration of this relationship for aoPWVtu (r decreased from 0.74 to 0.38).

Conclusions: MRI measurement of TT using systolic upslopes resulted in a better correlation of aoPWV with age and cfPWV, as compared to a Fourier-based approach applied on the entire cardiac cycle. Furthermore, methods based on harmonic decomposition were less affected by low temporal resolution. Since the wavelet-based approach combines these two advantages, it might help to overcome current technical limitations related to low MRI temporal resolution.

A Fully Automated Approach to Aortic Distensibility Quantification from Fetal Ultrasound Images

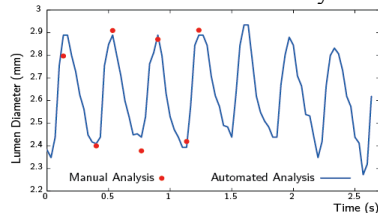
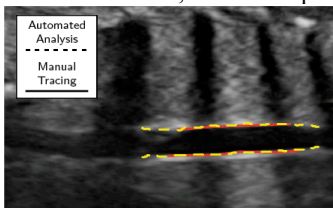
G Tarroni¹, S Visentin², E Cosmi², and E Grisan¹
¹ University of Padova, Italy; ² University Hospital of Padova, Italy

Background. Several conditions (e.g. intrauterine growth restriction, IUGR) that might occur during fetal development have been associated with increased cardiovascular mortality during adulthood. IUGR induces cardiovascular remodeling, including a decrease in aortic distensibility (AD). AD can be evaluated from fetal ultrasound (US) image sequences, potentially improving IUGR assessment. AD quantification requires the estimation of the maximum change in aortic lumen diameter (ΔD), which relies on tedious and operator-dependent manual tracing performed over a series of visually identified end-diastolic (ED) and end-systolic (ES) frames. The aims of this study were to develop and test a fully automated technique for ΔD quantification from US image sequences.

Methods. The aortic lumen is automatically identified through convolution with a set of discriminative kernels learned from a training dataset using an AdaBoost classifier. Then, segmentation is performed using anisotropic filtering and level-set methods. Lumen diameter is computed for at least 3 cardiac cycles. The obtained time curve is fitted with a sinusoidal function, whose amplitude represents the estimated ΔD . Image sequences were acquired from 20 subjects. An experienced interpreter traced lumen contours on ED and ES frames, allowing ΔD extraction: 10 sequences were used to train the discriminative kernels, while the other 10 were used for testing. Frame-by-frame lumen diameter values as well as subject-by-subject ΔD values were compared between automated and manual analyses by means of Bland-Altman, linear regression and correlation analyses.

Results. Automatically estimated lumen diameter values were highly correlated to manually extracted ones ($R=0.94$, $y=0.90x+0.2$). Bland-Altman analysis showed small bias (bias=-0.21mm) and narrow limits of agreement (std=0.38mm) compared to the mean value (4.54mm). Automatically estimated ΔD values were in good agreement with manually obtained ones ($R=0.74$, $y=1.04x+0.08$, bias=0.11 mm, std=1.13mm, mean value=0.78mm).

Conclusion. Fully automated ΔD quantification from fetal US image sequences is feasible, and thus a potential alternative to manual analysis.



Measurement of IMT with Fuzzy Segmentation in Carotid Ultrasound Images

Nader Jafarnia Dabanloo*, Faezeh Foolad, Gholamreza Attarodi, Emad Fatemizadeh

School of Electronic and Electrical Engineering, University of Leeds, Leeds, UK
Leeds, United Kingdom

The most public indicator in cardiac-vessel is the IMT(intima- media thickness) in carotid artery. Given that the existing methods are manually , that are costly and time consuming or fully automatic with low accuracy , So we're looking for a way to use the user's knowledge while automatic, To increase accuracy and reduce computational time and cost calculation. the proposal algorithm have four step, first pree-processing ,second feature extraction, Spatial, wavelets and gray level co-occurrence matrix (GLCM) features are extracted from carotid artery ultrasound images. Redundant and less important features are removed from the features set using genetic search process. Finally, segmentation process is performed on optimal or reduced features. Intima-media thickness (IMT) is measured from the images segmented by the proposed approach .Then put a point on the wall and move it in the desired class to obtain maximum IMT of image . finally classify the images into normal or abnormal. Using this method reduces the error by using the knowledge of users and reduce computational time. The new objective functions of proposed algorithms are realized by incorporating the noise clustering concept into the entropy based fuzzy C-means algorithm with suitable noise distance which is employed to take the information about noisy data in the clustering process. We use a class of robust non-Euclidean distance measures for the original data space to derive new objective function. The efficiency of clustering methods using DBI and Silhouette indexes and number of iterations have shown. The superiority of the proposed methods has been examined through the experimental study on medical images. The results indicated that the proposed algorithm work more accuracy than standard algorithms. Finally we achieve 95% classification accuracy. segmentation and classification of carotid artery ultrasound images have less computational cost and more accuracy rather than other techniques.

P83

The PhysioNet/Computing in Cardiology Challenge 2015: Reducing False Arrhythmia Alarms in the ICU

Gari Clifford*, Ikaro Silva, Benjamin Moody, Qiao Li, Danesh Kella, Abdullah Shahin, Tristan Kooistra, Diane Perry, Roger Mark

Emory University
Atlanta, United States

False alarms rates in the ICU are as high as 90%, decreasing quality of care by slowing staff response times while increasing patient delirium through noise pollution. This year's Challenge provides a set of multiparameter ICU data segments with 2,500 associated life-threatening arrhythmia ICU alarms, and challenges the general research community to address the issue of false alarm suppression using all ICU signals. Each data segment was 5 minutes long (for real time analysis), ending at the time of the alarm. For retrospective analysis we provided a further 30 seconds of data after the alarm was triggered. A total of 750 data segments were made available for training and 500 were held back for testing in each arm of the competition. Each alarm was reviewed by expert annotators, at least two of whom agreed that the alarm was either true or false. The scoring algorithm assesses the percentage of alarms correct, but with a penalty that weights the suppression of true alarms five times more heavily than acceptance of false alarms. We created four baseline algorithms: The first accepted all alarms as true and scored 30.14. The second used the prior probability of the alarm being true (33% Asystole, 27% Extreme Bradycardia, 82% Extreme Tachycardia, 33% Ventricular Tachycardia, 24% Ventricular Flutter/Fibrillation) and scored 43.19. The third used open source algorithms for signal quality checks on the blood pressure or the photoplethysmogram to decide which signal to use to estimate heart rate and scored 45.24. The fourth used the match between an open source QRS detector and pulse onset detector to decide if the signals were measuring the same activity, and scored 50.14. A total of 43 teams made a total of 230 competition entries. The min/median/max score in the first phase was 31.40 / 50.14 / 76.62.

S84

Enhancing Accuracy of Arrhythmia Classification by Combining Logical and Machine Learning Techniques

Vignesh Kalidas*, Lakshman S Tamil

The University of Texas at Dallas, Richardson, TX, USA

Introduction: This paper aims to develop an algorithm to reduce occurrence of false arrhythmia alarms in ICUs. The algorithm was trained using alarm-annotated Physionet dataset comprising ECG, photoplethysmogram (PPG) and/or arterial blood pressure (ABP) signals. Augmenting ECG features with PPG/ABP features minimizes false classifications, thereby increasing prediction accuracy

Method: Peak-to-peak interval (PPI) thresholds and ECG frequency-spectrum statistics were used to classify different arrhythmias. A pre-processing stage that included assessment of signal-quality for detecting flat/zigzag lines and spikes, followed by basic baseline wander removal increased the accuracy in identifying signal peaks. Pan-Tompkins algorithm was used to determine R, S-peaks and QRS-complex durations for the ECG. PPG/ABP peaks, corresponding to heart rate, were derived from zero-crossing points of first-order derivative of the PPG/ABP signal. Different PPI thresholds were used in classifying bradycardia, tachycardia and asystole. ECG in conjunction with PPG/ABP determined the alarm status. Identification of dominant frequency component followed by verification of the presence/absence of ECG fiducial points, both inferred from frequency analysis of ECG, were used in classifying ventricular flutter/fibrillation. Thresholds for S-peak to R-peak ratio and QRS-complex widths, together with ECG frequency analysis were used in classifying ventricular tachycardia.

Results: Our algorithm, based on constraint logic, achieved 93% sensitivity and 81% specificity for 750 training records and 86% sensitivity and 71% specificity for 500 test records in Phase I. In Phase II, methods such as moving-window analysis, secondary thresholds, wavelet analysis for efficient R-peak classification along with support vector machines technique for machine learning are incorporated to increase the accuracy.

Table 1. Results for Phase 1

Arrhythmia	Training Phase		Test Phase	
	Sensitivity	Specificity	Sensitivity	Specificity
Asystole	95.03%	90.00%	75.00%	89.00%
Bradycardia	95.74%	86.13%	85.00%	82.00%
Tachycardia	97.75%	76.93%	97.00%	60.00%
Ventricular Flutter/Fibrillation	83.50%	94.31%	33.00%	100.00%
Ventricular Tachycardia	90.04%	59.13%	80.00%	55.00%
Real Time Dataset	96.73%	82.92%	89.00%	67.00%
Retrospective Dataset	89.32%	78.35%	83.00%	76.00%
Overall	93.05%	80.64%	86.00%	71.00%

Validation of Arrhythmia Detection Library on Bedside Monitor Data for Triggering Alarms in Intensive Care

V Krasteva^{1*}, I Jekova¹, R Leber², R Schmid², R Abächerli^{2,3}

¹Institute of Biophysics and Biomedical Engineering, Sofia, Bulgaria

²Schiller AG, Baar, Switzerland

³CRIB, University Hospital Basel, Switzerland

There are studies reporting that only 2 to 9% of alarms in Intensive Care Unit (ICU) are important for patient management, 6 to 40% are true but clinically insignificant, while ICU false alarms are prevalent with rates as high as 86%. False alarms mainly induce stress in patients and clinical staff, and decrease the quality of care that is reported to significantly increase the hospital recovery time and re-hospitalization rates. Aiming to reduce the incidence of ICU false alarms, the 2015 PhysioNet/CinC Challenge encourages the development of algorithms for analysis of bedside monitor data for robust detection of life-threatening arrhythmias (asystole, bradycardia, tachycardia, ventricular tachycardia, ventricular flutter/fibrillation (VF)) in “real-time”, using 10s of data before the alarm (Event 1) and “retrospectively”, using up to 30s of data after the alarm (Event 2). Two Challenge datasets are announced: training set (750 recordings), blinded test set (500 recordings, publicly unavailable for purpose of scoring), including 2 ECG leads and up to 2 pulsatile waveforms (photoplethysmogram, arterial blood pressure), sampled at 12-bit, 250Hz, passed through FIR band pass filter [0.05-40Hz] and mains notch filter.

We participate in the Challenge Events 1 and 2 with a closed source entry, aiming at training and test-validation of the Arrhythmia Detection Library (ADLib, Schiller AG) for detection of ICU alarms. The main ADLib module analyses the ECG leads, providing QRS detection, VF detection and heart-beat classification. Additional modules might be included for analysis of the ECG quality and the pulsatile signal. The alarm decision module scans the ADLib output over 10s prior to the alarm to take a decision for true or false alarm. The overall performance is evaluated as: running time (8.5% (average), 8.8% (maximum) of quota), true positive rate (TPR), true negative rate (TNR) and blinded score given in the Challenge Phase I (see Table1).

Table 1. Score received in Phase I entry of the Challenge.

	Training set		Blinded test set		Score
	TPR	TNR	TPR	TNR	
Asystole	86%	77%	75%	89%	78.07
Bradycardia	91%	68%	81%	66%	54.76
Tachycardia	96%	55%	96%	60%	80.00
Ventricular Flutter/Fibrillation	84%	89%	33%	88%	57.14
Ventricular Tachycardia	73%	68%	80%	68%	60.31
Real-time	-	-	88%	75%	68.88
Retrospective	-	-	82%	75%	62.26
Overall	88%	72%	85%	75%	65.44

Reduction of False Alarms in Intensive Care Unit using Multi-feature Fusion Method

Chengyu Liu*, Lina Zhao

School of Control Science and Engineering, Shandong University, Jinan, China

* Corresponding author: bestlcy@sdu.edu.cn

False alarms in the intensive care unit can cause the ceaseless and boring noises, thus leading to decreased quality of care. So the intelligent identifying method for false alarms, especially for the life-threatening arrhythmia alarms, plays an important role for clinical application. However, accurately classifying the alarms into true and false ones is still full of challenges.

In the present study, we aimed to propose a multi-feature fusion method for accurately classifying the true or false alarms for five life-threatening arrhythmias. Firstly, we used the sample entropy method to assess the signal quality for each 10 s segment from the two ECG channels. Then we detected the R-wave peaks for the ECG segments with good signal quality and thus determined one segment with the minimum standard deviation of RR intervals for each ECG channel respectively. The selected segment was used to obtain the heart rate, ECG amplitude and ECG template. For each of the five life-threatening arrhythmias, we also calculated the heart rate and waveform matching features for the ECG signals at the alarm moment using different time windows. Meanwhile, we used the algorithms provided by the Challenge to calculate the signal quality and different heart rate features for the arterial blood pressure (ABP) and/or photoplethysmogram (PPG) signals. Finally, we fused all the features from ECG, ABP and PPG signals to classify all alarms into true or false ones. The obtained results are: asystole with true positive ratio (TPR) 58% and true negative ratio (TNR) 88%; extreme bradycardia with TPR 92% and TNR 89%, extreme tachycardia with TPR 91% and TNR 60%, ventricular tachycardia with TPR 58% and TNR 53%, and ventricular flutter/fibrillation with TPR 83% and TNR 68%. The final scores are 59.60 for Event 1, 53.64 for Event 2 and 56.49 for overall.

S84

Heart Beat Fusion Algorithm to Reduce False Alarms for Arrhythmias

Chathuri Daluwatte*, Lars Johannesen, Jose Vicente, Christopher G Scully, Lorian Galeotti, David G Strauss

1Division of Biomedical Physics, Office of Science and Engineering Laboratories, CDRH, US FDA, Silver Spring, MD, USA
Silver Spring, United States

Introduction: There is a need for patient monitoring algorithms to reduce alarm fatigue by rejecting clinically irrelevant alarms. We developed an algorithm using multimodal physiological waveforms (electrocardiogram (ECG), blood pressure (BP), photoplethysmogram (PPG)) to improve arrhythmia detection by reducing the incidence of false alarms while maintaining a high true alarm rate as part of the Physionet Challenge 2015 (2015-Challenge). **Algorithm Description:** Individual beat detectors are applied to ECG, BP, and PPG signals. Global annotations are generated by fusing individual beat location estimates. Arrhythmia alarm criteria specified in the 2015-Challenge are applied to the global annotations to declare the alarm as either true or false. **Validation**

Method: The 2015-Challenge provided a 750 record training set and 500 record test set including ECG, BP and/or PPG signals. In each record, the physiological monitor detected an arrhythmia alarm in the last 10 seconds of the record. Expert human annotators reviewed and labeled each alarm as true or false; 456/750 of alarms in the training set were considered false. Algorithm performance was scored as true positive rate (TPR: True Positives/All Positives) and true negative rate (TNR: True Negatives/All Negatives).

Results: Human annotators considered 456 of the 750 (61%) monitor generated alarms false. Our algorithm was able to discard 429 of these false alarms (TNR of 94%), while correctly classifying 238 of the 294 true alarms (TPR of 81%). When applied to the test set, we achieved a TPR of 78% and TNR of 93%.

Conclusions: We developed an algorithm to classify arrhythmia alarms as true or false. Our results support that false alarms can be reduced in the clinic by combining information from multiple physiological signals. Ongoing work will attempt to increase the true positive rate by improving signal quality indices.

Suppression of False Arrhythmia Alarms using ECG and Pulsatile Waveforms

Paula Couto, Ruben Ramalho, Rui Rodrigues*

Faculdade de Ciencias e Tecnologia da Universidade Nova de Lisboa,
Portugal
Portugal

False alarms in the Intensive Care Unit(ICU) are disturbing for patients and staff, leading to decreased quality of care. The 2015 PhysioNet/CinC Challenge promotes the development of algorithms to detect false arrhythmia alarms in the ICU. The alarms present in the challenge are Asystole, extreme bradycardia, extreme tachycardia, ventricular tachycardia and ventricular fibrillation or flutter. Our method uses simultaneous ECG and pulsatile waveforms, photoplethysmogram or arterial blood pressure to suppress false arrhythmia alarms. There are a good number of published QRS detection methods, and also open source software, for ECG and for pulsatile waveforms. Therefore, it is possible to obtain, for each waveform, a set of QRS detections that can be used to decide if an arrhythmia alarm is a false alarm or not. Often the results of the different waveforms are contradictory because some of those waveforms may be contaminated by noise or the signal simply gets lost for a while. Evaluating the signal quality of each waveform is necessary to check if an alarm is true or not. But the signal quality evaluation is a very difficult task, and it must be done in relation to the results one wants to reach: in this case it is a correct detection of the heart beats. For each type of waveform, ECG, arterial blood pressure (ABP) or photoplethysmogram (PLETH) we use a different method to evaluate the signal quality. There are two other key steps in our method: detection of ventricular beats to can verify Ventricular tachycardia alarms and detection of ventricular fibrillation. The overall score of our method in the unofficial phase is 60.40, corresponding to true positive rate of 77% and a true negative rate of 78%.

S84

Automatic Generation of Surface Meshes for Right Ventricle with 1-to-1 Vertex Correspondence from Cine-MR Images

Y. Su¹, M.L. Tan¹, S.K. Teo¹, L. Zhong^{2,3}, R.S.Tan^{2,3}

¹Institute of High Performance of Computing, A*STAR, Singapore

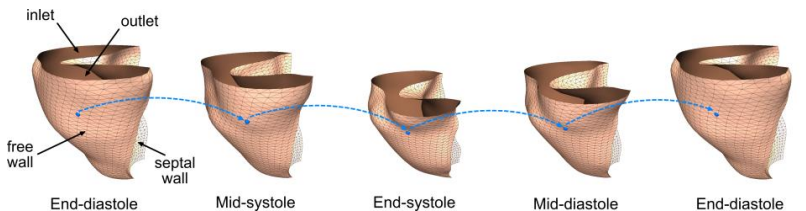
²National Heart Centre, Singapore

³Duke-NUS Graduate Medical School, Singapore

An automatic method is developed to generate 1-to-1 corresponding surface meshes of the right ventricle (RV) over the whole cardiac cycle. The inputs are a set of 3D RV surface meshes independently reconstructed from border-delineated magnetic resonance imaging (MRI) data at each frame/phase of the cardiac cycle. These meshes do not have correspondence relationship in terms of the number of vertices and mesh topology.

To generate point correspondence, a template model of the free wall and septal wall of the RV (represented by cylindrical mesh-pair) is modified to fit the actual shape of the RV at each time frame. In the initial rough matching stage, mesh matching between the template and the target is achieved using a radial basis function morphing process. The feature points on the template and target meshes are automatically identified using a parameterization method. In the second fine matching stage, a progressive mesh projection process is used to conform the rough estimate to fit the exact shape of the target. This process incorporates an optimization process based on non-linear elastic energy minimization to achieve superior mesh quality and smooth point motion.

Eight healthy volunteers were recruited for MRI scanning and the algorithm was tested on the acquired data. It was observed that the algorithm took an average of approximately 70 seconds to complete. The maximum absolute deviation between the matched model and actual ground truth was 0.187 mm on average.



Selected instances of 1-to-1 corresponding RV meshes in the cardiac sequence. The blue dot shows the position of a tracked point in time.

Automatic Detection of Microvascular Obstruction in Patients with Myocardial Infarction

Trygve Eftestøl, Erlend Singsaas, Kjersti Engan, Leik Woie, Stein Ørn

University of Stavanger
Stavanger, Norway

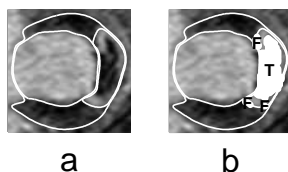
Aims: The presence and extent of microvascular obstruction (MO) in patients with myocardial infarction (MI) is an important prognostic indicator. In late Gadolinium (Gd) enhanced cardiac magnetic resonance images (LGE-CMRI), pixels within the MI will appear with very high signal intensity (SI) due to the effect of the Gd contrast agent. Gd does not enter areas of MO which will therefore appear as areas with low SI within the infarction. In image applications of LGE-CMRI where properties of the infarction are analysed, it is important to identify MO-regions. Therefore we have designed an automatic method to detect MO-regions.

Methods: The scar, epicardial and endocardial boundaries in LGE-CMRI from 22 patients were manually traced. Candidate MO-regions within the scar were determined by areas of pixels with SI values below a threshold adaptively determined from discriminative information in scar, normal appearing tissue and natural clusters within the scar. Each MO-region was labelled as true (T) or false (F) MO.

Each region was characterised by features like area, centroid and orientation. As small false regions will typically be at the scar boundary, the dilated area around each region was determined. Proportions of this area positioned inside scar and outside myocardium were added as features. Different feature combinations were used to design a classifier for discriminating true from false MO-regions. In the classifier design both parametric and non-parametric classifiers were tested in a cross validation strategy.

Results: In the selection of features and training of the candidate classifiers, the best performing classifier (mean(std.dev.)) used all features except the centroid with a total accuracy, true positive and negative rates of of 0.85(0.03), 0.70(0.11), and 0.97(0.03) respectively.

Conclusion: The results of these preliminary experiments indicate that automatic detection of MO areas is feasible.



Original infarcted MRI (a), with candidate MO-regions (white) detected as true (T) or false (F) (b).

Feasibility of Variable Step Size Least Mean Squares for intra-MRI ECG Artefact Reduction

André Guillou*, Sarah Ménétré, Grégory Petitmangin, Jacques Felblinger, Laurent Bonnemains

Schiller Médical
Nancy, France

In order to achieve high spatial and temporal resolution during cardiac magnetic resonance imaging (MRI), acquisitions need to be spanned over multiple heart beats. Therefore, the detection of cardiac cycles on ECG is of paramount importance. However, during cardiac MRI, fast switching gradients cause artifacts on the electrocardiogram (ECG), disturbing both triggering and monitoring. To cancel this noise, the Least Mean Squares (LMS) algorithm is a simple and efficient method. LMS uses one main parameter, its step size, which influences the quality of artifact reduction. While the step size is usually chosen arbitrarily, we propose a method to choose this parameter accurately using information about the sequence played by the MR imager. The proposed method consists of calculating the optimal step size using the MR gradient variance during the sequence. An intra-MRI ECG database previously acquired with various MR sequences (i.e. FIESTA, Diffusion, EPI, SSFSE...) was used to generate the results of this study. A standard LMS and the proposed method were applied to correct those signals and the energies of remaining artifacts were compared. With optimal parameterization, the proposed artifact reduction method achieved systematically better results than the standard LMS (90% of FIESTA artifacts were removed, against 63% with standard LMS, 92% of EPI artifacts were removed against 43% with standard LMS). This proves there is room for serious improvement on parameterization of least mean squares for intra-MRI ECG artifact reduction, which can be achieved by using the MR sequence settings. Further study will be lead to adapt the step size in real time during an MRI sequence.

S91

Temporary Cardiac Pacing Leads Safety in MRI

Qi Zeng, Qinyan Wang, Ji Chen

University of Houston
Houston, Texas

Temporary cardiac pacing leads are widely used to treat tachyarrhythmia until long-term therapy can be initiated. After or during the surgery, MRI exams are often required to evaluate the outcome of the surgery. However during the MRI procedure, the RF induced heating on these metallic medical leads can lead to very high temperature rises at the lead tip and lead to human tissue damage. Different from the fully implanted pacemaker leads, the temporary leads are partially implanted and the MRI safety study has not been full investigated.

In this study, temperature rises for temporary cardiac leads in different virtual family models and phantom models are evaluated using transfer function method. This method use an integration to relate the RF heating with the characteristics of pacing leads and the incident tangential electric field along different lead pathways inside human body. The transfer functions are the common mode current distribution along the lead when excited by unit current sources at tips and are independent of lead trajectory. By this approach, computational burdens induced by tremendous lead trajectories are resolved. Several experiment validations were used to validate the accuracy of this approach. Specifically, the RF induced heating can be calculated as:

$$Heating_{tip} \propto \left(\int E_{tan} \cdot TF dl \right)^2 \quad (1)$$

Results of some investigations

Model	Temperature rising
Adult-Male	0.30 °C
Boy	0.34 °C
ASTM phantom	0.33 °C

0.34 °C when average SAR normalized to 2 W/Kg for all the configurations studied here.

In this paper RF heating along temporary cardiac leads in three different body models: adult male model, boy model, and ASTM phantom are studied. The lead lengths are 40 cm and the maximum temperature rising is

Comparison of Measurement and Calculation of the Electric Field Transfer Function for an Active Implant Lead in Different Media

John Nyenhuis, John Jallal, Xiaoyi Min, Shiloh Sison*, Gabriel Mouchawar

St. Jude Medical
Sylmar, United States

Patients with active implantable medical devices (AIMD) may be at risk of harm from RF-induced heating during an MRI scan. The AIMD lead picks up RF energy which gives rise to a current along the lead body and electric fields at the electrodes resulting in increased temperature. The amount of RF-induced lead heating is mainly attributed to the electric field tangential (E_{tan}) to the lead path, which can be predicted by using an electrical field transfer function (TFE) associated in different media. ISO/IEC 10974 presents different media for testing of active implants. High conductivity media (HCM), with conductivity $\sigma = 0.47$

properties and low conductivity media (LCM), with $\sigma = 0.045$ S/m and $\epsilon = 11$ simulates fatty tissues. The objective of this report is to compare measured and calculated TFE in HCM and LCM on a model lead. The simulated test lead was a 22-gauge insulated wire with 60 cm length that was covered with an insulating cap at the proximal end and had 3 mm of insulation removed at the distal end to form the electrode. Calculations were made with ANSYS HFSS finite element analysis software. TFE was measured with a Bemcalc transfer function system in a phantom with dimension of 15 x 15 x 120 cm. Difference in TFE for HCM and LCM arise from the longer wavelength in LCM. TFE measured in a phantom will reproduce well the response of an implanted lead to the incident tangential electric field. Comparison of the calculated and measured TFE for a phantom can be used to assess uncertainty in RF-induced temperature rise arising from the transfer function measurement. TFE measurements can be used in the development of a lead model for the heterogeneous tissues that are present in the body.

S91

Lead Heating of a MRI Conditionally Safe Pacemaker System

Gabriel Moucharwar, Shiloh Sison*, Shawn Chen, Xiaoyi Min, Ji Chen, John Nyenhuis, Richard Williamson

St. Jude Medical, Inc
Sylmar, United States

We utilized the ISO/IEC JWG 10974 Tier 3 approach to evaluate lead heating under normal (2 W/kg) and 1st level control mode (4 W/kg) of the St. Jude Medical Accent Tendril MRI lead and Accent MRI pacemaker. Electric fields were simulated in five virtual human models with various lead pathways in commercial scanners. Electric fields were extracted at both normal operation mode and 1st level control mode. Clinically relevant lead states of various levels of fluid ingress were studied, and the lead transfer function (TF) with the highest ingress heating was selected. It was then integrated with the extracted electric fields to estimate in-vitro temperature rises. A validated thermal model scaled the in-vitro temperature estimates to in-vivo results. The thermal model simulated the worst case conditions using an extreme level of tissue encapsulation of the inductor with cardiac tissue. Uncertainties from measurements, TF, and in vivo simulations were assessed with the Monte Carlo (MC) method. Safety was assessed based upon the accepted 43 °C standard (Meshorer, 1983) for cardiac tissue interfacing with the lead tip helix electrode and lead MRI filter inductor. Over 400 different patient and MRI system permutations were simulated. When combined with exhaustive lead pathways, and MC analysis, over 14 million scans were simulated. Our results indicate that the risk associated with MRI scans of patients with an Tendril MRI/Accent MRI pacemaker system due to cardiac damage at the lead tip helix electrode or at the MRI lead MRI filter inductor is extremely low for 4 W/kg scans, and miniscule for 2 W/kg scans.

Furthermore, these results are based upon taking into account worst case considerations into every modeling step (worst case lead states, worst case lead systems, and worst case tissue encapsulation).

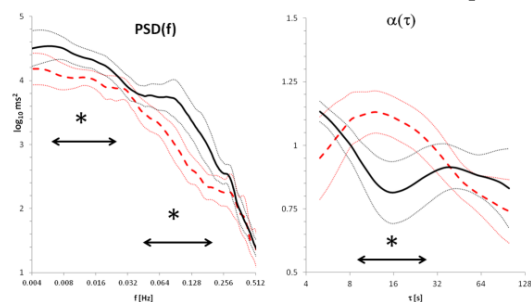
S91

Spectral and Fractal Structures of Heart Rate Variability in Coronary Artery Disease Patients without Myocardial Infarction

Paolo Castiglioni, Marco Di Rienzo, Alberto Radaelli

IRCCS Fondazione Don Carlo Gnocchi
Milan, Italy

Heart rate variability (HRV) analysis may allow risk stratification in coronary artery disease (CAD), but few studies evaluated HRV in CAD patients without myocardial infarction (MI) and with preserved ejection fraction. This evaluation is important because often sudden cardiac death occurs without previous cardiovascular events, like MI. Thus our aim is to describe spectral and fractal structures of HRV in these CAD patients. We recorded tacograms



Power spectra (*left*) and scale coefficients spectra (*right*) in CAD patients (dashed line) and controls: $m \pm \text{sem}$. Asterisks indicate bands where spectra differ at $p < 0.05$.

in 10 CAD supine patients without MI and 10 controls matched by age and ejection fraction, considering stable segments of 14' duration. We estimated log-transformed power spectra, PSD(f), with a broadband approach to optimize frequency resolution, between 0.004 and 0.500 Hz. We also estimated the recently

proposed temporal spectrum of self-similarity scale coefficients, $\alpha(\tau)$, with a broadband approach for $5 \leq \tau \leq 100$ s. Frequency- and temporal-spectra of the two groups were compared at each spectral line by unpaired t-test (figure).

The power spectrum was significantly lower ($p < 0.05$) in CAD patients over two separate bands: 0.047-0.240 Hz (range centered over the low frequency band) and 0.007-0.022 Hz (range of the slower components in the very low frequency band). The spectrum of scale coefficients was significantly higher in CAD patients over a single temporal band, between 9 and 25 s, corresponding to variability components in the low-frequency band.

Results suggest that in CAD patients, even with preserved ejection fraction and without MI, the low frequency peak is almost completely absent, and the lack of this specific oscillatory component not only decreases the low frequency power but also alters the heart rate fractal structure of this band. Results also indicate a reduction of the slower fluctuations that, in this case, is not associated with an altered fractal dynamics.

S92

On Modelling RR Tails in Heart Rate Variability Studies: An Extreme Value Analysis

Sónia Gouveia*, Manuel G Scotto

University of Aveiro
Portugal

Recently, large deviations from a Gaussian RR distribution have been proved to be an independent mortality predictor in chronic heart failure (CHF) patients. The RR distribution exhibits heavier tails than does the Gaussian and, thus, the probability of observing a long RR is higher than when assuming Gaussianity. Within this context, extreme value theory can be used to quantify the probability of a long RR occurrence provided that it exceeds a suitable (fixed) threshold, by means of the statistical characterization of the RR tail distribution. Here, tail characterization does not rely on the Gaussian assumption but by fitting the Generalized Pareto distribution (GPD) to the excesses above a high threshold, and through the analysis of its corresponding shape γ (tail index) and scale σ^* parameters. When $\gamma=0$, the underlying distribution belongs to the Gumbel domain of attraction (a class of distributions exhibiting exponential-type tails which includes the Gaussian), while $\gamma>0$ is indicative of a heavy-tailed distribution, i.e. with polynomial-type tails. The GPD parameters are estimated by Peak-over-Threshold (POT) procedure and standard errors are approximated by reproducing POT in bootstrap replicates of the original exceedance values. The new approach is illustrated with two 24-h RR recordings from PhysioBank: normal subject (nsr001) and CHF patient (chf201). Data was resampled at 2 Hz and wavelet analysis allowed to reconstruct one signal containing the RR power traditionally related to the respiratory rhythm (~ 0.25 Hz) and another to sympathetic baroreflex activity (~ 0.1 Hz). The fitted distributions for the normal subject exhibit $\gamma=0$ for both LF and HF (-0.01 ± 0.03 and 0.04 ± 0.02) while $\gamma>0$ for the CHF patient (0.12 ± 0.06 and 0.15 ± 0.03). Thus, the CHF distributions are heavy-tailed, indicating a non-negligible probability that a very long RR interval can occur. In a future study, it remains to assess the impact of these preliminary findings in CHF mortality prediction.

S92

Heart Rate Variability Analysis of Normal and Intrauterine Growth Restricted Children using Sample Entropy

Taher Biala*, J Alexandre Lobo M, Michael Wailoo, Fernando Schindwein

Higher Institute of Medical Technology, Misrata, Libya
Misrata, Libyan Arab Jamahiriya

It is well documented in literature that Heart Rate Variability (HRV) entropies for healthy subjects may present higher values of Sample Entropy (SampEn), a measure of system complexity, when compared with subjects with specific pathological conditions. Nevertheless, for new groups and conditions, nonlinear measures must be considered and discussed. This work proposes the use of SampEn to analyze 2 different groups of children during 24-hour ECG/HRV monitoring. The considered database consists of 20 children (age 9.18 ± 0.68), divided in two groups: 10 Normal (5 female) and 10 children (5 female) with medical history of intrauterine growth restricted (IUGR). Four different entropies calculations were considered: the complete 24 hours trace; before sleep time; during sleep and after sleep time. Statistic t-test was considered for intra and intergroup comparison. The results showed significant difference ($P < 0.0349$) during sleep time interval between normal group (SampEn= 1.2325 ± 0.094) and IUGR group (SampEn= 1.3517 ± 0.122). This result may indicate that IUGR children may develop higher levels of complexity during sleep time. The other intervals presented no significant difference in intergroup comparison. An intragroup analysis was also considered and both groups showed significant difference between before sleep and during sleep intervals. For the normal group ($P < 0.001$), before sleep (SampEn= 1.0237 ± 0.103) and during sleep (SampEn= 1.2325 ± 0.094). For the IUGR group ($P < 0.013$), before sleep (SampEn= 1.1173 ± 0.223) and during sleep (SampEn= 1.3517 ± 0.122). The results indicate that SampEn may be considered as a measure of HRV complexity to monitor normal and children with medical history of IUGR. Further studies with other nonlinear measures and with an expanded database are going to be considered.

S92

Instantaneous Bispectral Analysis of Heartbeat Dynamics for the Assessment of Major Depression

Ronald G Garcia*, Gaetano Valenza, Carlos Tomaz, Riccardo Barbieri

Massachusetts General Hospital, Harvard Medical School, Boston
Charlestown, United States

Introduction: Major depression (MD) diagnosis is based on clinical evaluations of self-reported symptomatology. Currently, there are neither specific physiological nor biochemical markers that can be taken into account to objectify MD. In this study, we investigate the link between instantaneous bispectral analysis of heartbeat dynamics and major depression in response to an emotion-eliciting task.

Methods: Forty-eight patients with MD (22.6 ± 4.7 years), and 48 gender- and age-matched healthy controls (HC) (23.5 ± 4.9 years) were exposed to an audio-visual task consisting on a set of eleven slides accompanied by a narrative with two different versions: one emotionally neutral (N) and the other emotionally arousing (E). Subjects from each group were randomly assigned to the N or E stimulus version of the story. Continuous ECG signal (lead II) was collected at 250 Hz. and point process analysis of heartbeat dynamics was performed to obtain instantaneous features derived from standard time-domain analysis, as well as linear (LF, HF, LF/HF) and bispectral (LL, LH, and HH) frequency-domain features. Mean values of all features were computed over the 30s segment of emotional elicitation session.

Results: No significant differences in time and frequency domain linear parameters were found between the groups. MD and HC subjects exposed to the N version of the story were also comparable in relation to point-process bispectral features. However in those subjects exposed to the E version of the story, HH measures, which are markers of parasympathetic activity, were able to discern between patients and HC (590.5 ± 459.8 vs 1820.4 ± 723.6 a.u., $p=0.02$).

Conclusions: Our results reveal that time-varying complex dynamics of parasympathetic activity are significantly reduced in MD compared to HC in response to emotional elicitation, therefore we conclude that instantaneous bispectral analysis could be a promising tool for differential diagnosis in mental health.

Autonomic Nervous System Assessment in Critically Ill Patients Undergoing a Cognitive Rehabilitation Therapy

David Hernando*, Marc Turon, Raquel Bailón, Sol Fernandez-Gonzalo, Jesús Lázaro, Gemma Gomà, Eduardo Gil, Jaume Montanyà, Josefina López, Candelaria De Haro, Pablo Laguna, Lluís Blanch

Spain

Recent clinical and electrophysiological studies reveal a high incidence of autonomic nervous system (ANS) dysfunction in patients treated in medical and surgical Intensive Care Units (ICUs). ANS disturbances may produce diverse and unexpected consequences. For instance, critically ill patients are at risk of neurocognitive impairments that may persist after hospital discharge, and ANS dysfunction leading cholinergic deficiency seems one of the most viable reasons to explain the development of long-term sequelae. Cognitive rehabilitation (CR) is a behavioral therapy that has proven to be effective improving cognitive deficits in clinical populations with abnormalities in brain activation patterns. A total of 17 critically ill patients received CR aimed to improve the ANS status, which was quantified in terms of HRV. The CR included cognitive exercises aimed to improve prefrontal activation. It was specifically designed for these patients by using Kinect technology. HRV was derived from the recorded ECG signal during pre-CR, CR and post-CR. Power in the specific frequency bands related to sympathetic and parasympathetic systems was computed (PLF and PHF for low and high frequency bands, respectively). PLF was computed within the classic band, while PHF was computed within a band centered at respiratory rate, hypothesizing it is especially important in ventilated patients. The ratio PLF/PHF was also computed. Changes in the HRV parameters from pre-CR to CR, and from pre-CR to post-CR were studied. Comparing with baseline values, 9 patients showed a decreased PLF in post-CR, while 8 patients presented a higher PLF. In 12 patients, PHF increased after the CR session, suggesting an increase of parasympathetic activity. These differences in the evolution of the HRV parameters among different patients may be due to their different pathologies and medication. Despite these differences, CR seems to increase parasympathetic activity after the session in the majority of the patients (12 out of 17).

S92

Heart Rate Variability Associated with Walking Zen Meditation Kinhin: towards 'Contemplatio Actione'

Masaki Hoshiyama*, Asagi Hoshiyama

Meisei University
Kamakura-shi, Japan

Zen is a traditional meditation method which utilizes unification of body, respiration and mind. Zen is spreading widely into western world today, realizing deeper meditation with minimum body movement and distraction. While heart rate variability (HRV) during sitting Zen (Zazen) has been studied in the past, there remains a lack of consensus whether heart rate during walking Zen (Kinhin) elicit consistent HRV differences for experienced Zen meditator and beginners. To better understand the effect of Zen experience on hemodynamic events elicited by deep Kinhin meditation, we studied heart rate in experienced Zen meditator and beginner. The study took place over 4 sets of Kinhin meditations in a quiet, Zen practice hall. Each set of Kinhin lasted at least for 25 minutes. The first sets were used for habituation, and the data obtained from the following three sets were used for analysis. Power spectrum analysis showed distinctive change in frequency components. Very low frequency (VLF) components decreased and high frequency (HF) components increased for experienced meditator ($p=0.05$). Most notably, detrended fluctuations analysis (DFA) of HRV were around 1/2 for experienced and 0.85 for beginner. During Kinhin practice, we put our both hands on a lower chest so that we can keep our center of balance in the lower abdomen (Tanden) with lower abdominal muscle contraction, practice Tanden breathing, and keep mind free from distraction. We attribute the decrease of VLF components, increase of HF components and decrease of DFA exponent in experienced meditator to the parasympathetic stimulation, and to the minimal use of antigravity muscles in the optimal walking posture generated by Tanden located center of balance, as contrasted with the active use of antigravity muscles in the unstable posture by beginners, hence to the effective regulation of mind during meditation toward the edge of sleep, but not quite over it.

S92

Impact of Mental Stress on Heart Rate Asymmetry

Saman Parvaneh*, Nima Toosizadeh, Sadaf Moharreri

Philips Research North America, Briarcliff Minor, USA
Rochester, United States

Background: Stress causes negative impacts on health of an individual. Objective assessment of stress through biological signals such as heart rate gained lots of attention recently. Previous studies have demonstrated that stress reduces heart rate variability (HRV), but less is known on the impact of stress on heart rate asymmetry (HRA), a new approach that quantifies increase or decrease of heart rate with respect to previous beat. Since HRA is corresponding to unequal contributions of accelerations and decelerations in heart rate, it is hypothesized that stress can affect HRA.

Method: ECG data of 10 individuals from a retrospective database from Physionet was employed. For each person, data was available during low, medium and high stress conditions. Three common HRA indices (Porta Index-PI, Guzik Index-GI and Slope Index-SI) were calculated within five minutes time windows across different stress levels. Conditions with different stress levels were compared using ANOVAs and post-hoc LSD ($p < 0.05$).

Results: Analysis of data revealed that HRA significantly reduced by stress level ($p < 0.05$). Specifically, lower HRA was observed in high stress (PI: 48.87 1.20, GI: 49.75 0.37, and SI: 49.73 0.41), compared to medium stress (PI: 47.42 2.33, GI: 50.04 0.44, and SI: 50.04 0.45) and low stress (PI: 49.59 0.62, GI: 50.74 0.44, and SI: 50.80 0.38). Further pairwise comparison revealed that PI was significantly different between low and medium stress ($p = 0.004$) as well as medium stress and high stress ($p = 0.047$). Also, GI and SI were an independent discriminator between low and medium stress ($p < 0.001$) as well as low and high stress ($p < 0.001$).

Discussion: This study suggests that assessment of heart rate asymmetry can discriminate different level of stress and can be used in conjunction with conventional HRV parameters. We speculate that reduction in HRA (having more heart rate acceleration compared to decelerations) may be linked to reduction in activity of parasympathetic nervous system in more stressful situations.

S93

Heart morphology differences induced by intrauterine growth restriction measured on the ECG in teenagers

Nuria Ortigosa¹, Fátima Crispi², Raquel Bailón^{3,4}, Mérida Rodríguez², Eduard Gratacós², Sebastián Savari⁵, Marta Sitges⁵, Bart Bijmens⁶, Pablo Laguna^{3,4}

¹ I.U. Matemática Pura y Aplicada, Universitat Politècnica de València, Spain

² Fetal i+D Medicine Research Center, BCNatal-Barcelona Center for Maternal-Fetal and Neonatal Medicine (Hospital Clínic and Hospital Sant Joan de Deu). IDIBAPS, University of Barcelona, (CIBER-ER).

³ Aragón Institute of Engineering Research (I3A), University of Zaragoza, Spain

⁴ CIBER-BBN, Spain

⁵ Dept. of Cardiology (Institut Clínic del Tòrax), Hospital Clínic - Institut d'Inv. Biomèdiques August Pi i Sunyer, Univ. Barcelona, Spain.

⁶ ICREA, Universitat Pompeu Fabra, Spain.

Aims: Teenagers who had suffered from intrauterine growth restriction (IUGR) during their mothers' pregnancy usually present more spherical hearts (smaller relation between base to apex measure and basal diameter), measured using echocardiograms, which has been associated with long-term cardiac dysfunction. This study aims to analyse these heart morphology changes by means of the surface ECG so as to have an early diagnostic tool of this pathology.

Methods: 59 teenagers conformed the study population. 18 suffered from IUGR inside the womb, and 41 that were used as control subjects. Once QRS and T-wave loops were obtained from the vectorcardiogram, the angle between the depolarization and repolarization dominant vectors in the three-dimensional space (θ_{RT}), and the absolute and relative angles between the dominant vectors and the three orthogonal planes were studied.

Results: The angle between the dominant vector of the QRS loop and XZ-plane (ϕ_{R-XZ}) showed larger values for teenagers who suffered from IUGR than for control subjects ($p < 0.002$). In addition, the difference between ϕ_{R-XZ} and the angle of the dominant vector of T-wave loop (ϕ_{T-XZ}) projected on XZ-plane was also larger for IUGR teenagers, being significantly different ($p < 0.002$).

Conclusion: The present study presents a novel approach of a ECG-based non-invasive estimator of heart morphology differences generated by IUGR in teenagers, opening the door for a much easier diagnosis and follow-up of potential candidates for this dysfunction.

Superiority of the Automated 5-Minute Summary ECG to Cardiologist Over-read Triplicate ECGs in Detection of QTc Change

Jay W Mason*, Shaun Szot, Brock Heinz

University of Utah
Reno, United States

Introduction: In thorough QT (TQT) studies placebo and moxifloxacin are administered to assess sensitivity of detecting increased QTc. This allows validation of ECG measurement methods. The best method will detect a smaller change over baseline during placebo treatment (dQTc) and will identify moxifloxacin-induced QT increase more accurately.

Methods: The 5-minute ECG is derived from 300 second continuous 12-lead ECG recordings at each time point. Representative beats calculated from all normal beats are used to construct a summary ECG. We analyzed data from a cross-over TQT study of 48 subjects. Using the summary ECG, QT was measured, and the RR interval was calculated from the average cycle length of all normal consecutive beats, using an automated algorithm based on CalECG v3. These measurements were compared to cardiologist over-reading in Escribe of 3 ECGs extracted from the 5-minute time point window in 3 ways: the variance from 0 of dQTcF in the placebo arm, a positive drug effect in the moxifloxacin arm, defined as an increase in dQTcF ≥ 5 msec by hour 4 and a decrease below Cmax by hour 9, and visual differentiation between the placebo and moxifloxacin curves in dQTcF vs time plots of each.

Results: (automated 5-minute ECG vs triplicate cardiologist over-read, respectively): Mean placebo dQTcF (msec): -2.03 vs. -2.16; numeric moxifloxacin criteria met 85 vs 80%; moxifloxacin and placebo graphically identified correctly: 81 vs 78%. The 5-minute ECG was superior in all three measures.

Conclusions: These results indicate that the automated 5-minute ECG is potentially more accurate than the triplicate over-reading method for determining presence and absence of drug-related QTc change. The automated method is much less costly and could reduce sample size requirements. An analysis of 8 additional TQT studies is underway.

S93

Predicting Mood Changes in Bipolar Disorder through Heartbeat Nonlinear Dynamics: a Preliminary Study

Gaetano Valenza*, Mimma Nardelli, Gilles Bertschy, Claudio Gentili, Antonio Lanata, Enzo Pasquale Scilingo

Italy

Bipolar disorder is characterized by swing mood alternating from depression (negative pole), to manic (positive), maybe including mixed states. Despite the high prevalence and high cost of treating, the clinical assessment and management of this condition is still ill-defined. Currently, the patient mood is typically assessed by clinician-administered rating scales and subjective evaluations exclusively. To this extent, in this study, we propose a methodology predicting mood changes using heartbeat nonlinear dynamics. Such changes are intended as transitioning between euthymic state (EUT), i.e., the good affective balance, and non-euthymic state. We analyzed Heart Rate Variability (HRV) series gathered from four bipolar patients (2 females, age: 27.5 ± 5.8 , range: 23-36) undergoing 24h ECG monitoring through textile-based wearable system. Each patient was monitored twice a week, for 14 weeks, being able to perform normal (unstructured) activities. From each acquisition the longest artifact-free segment of signal was selected through visual inspection (minimum length: 5.2h). Sub-segments of 5 minutes of this segment were used to calculate significant features, which were defined in the time and frequency domains, as well as from nonlinear analysis (entropy measures). The time evolution of each HRV feature was synthesized through detrended fluctuation analysis ($\alpha 1$ and $\alpha 2$). Finally, the actual prediction of the future mood state relied on nu-Support Vector Machines. Considering data from a current observation at t_0 , and related past observations, personalized prediction accuracies in forecasting the mood state (EUT/non-EUT) at time $t+1$ were 70.6%, 75%, 73.33%, 77.78%. Knowing in advance whether the patient is getting better or not effectively help clinicians to optimize the therapy and make changes if necessary, and to perform a more accurate clinical monitoring and plan a treatment at very early stage. This approach is intended to be a 'proof of concept' of the possibility of predicting mood states in bipolar patients through heartbeat nonlinear dynamics exclusively.

S93

Repolarization Parameters of Heart Transplant Subjects

Josef Halamek*, Pavel Jurak, Tereza Reichlova, Petr Vesely, Pavel Leinveber

Institute of Scientific Instruments of the Czech Academy of Sciences
Brno, Czech Republic

Introduction: Significant differences exist in heart rate and repolarization parameters between men and women. We analyzed these differences in heart transplant patients sorted according to the sex of recipient and donor. Six groups were measured: A) N=20; man/man (recipient/donor); B) N=21; woman/man; C) N=17; woman/woman; D) N=15; man/woman; E) N=23; healthy men; F) N=15; healthy women. Continuous ECG (40 min, 5 kHz, 24 bit) was measured over five postural changes: supine, sitting, supine, standing and supine. QTc was analyzed after QT hysteresis elimination and different QTc corrections (subject specific linear and nonlinear, Fridericia and general linear) were used. The heart rate changes were mostly narrow and the parameters of subject specific corrections were noisy.

Results: Known differences exist between groups E and F. Women have shorter RR (NS), longer QTc $P < 0.001$ and steeper QT slope (NS). Minimal RR and QT were in group D (RR=706±70 ms, QT=331±23 ms). QTc depends on used algorithm, general formulas as Fridericia or linear with slope 0.154 give similar results with significant differences among groups. Recipient men have significantly shorter QTc than recipient women (A*B, A*C $P < 0.01$). No dependency on sex of donor was found (B*C NS), the connected groups AB*CD have nearly equal QTc. Subject specific correction has lower significance due to narrow RR span, therefore AD*BC connected groups should be used to achieve significant results ($P < 0.01$). QT slope was noisy and no dependency could be determined at heart transplant patients.

Conclusions: The heart rate and RR variability depend before all on sex of donor; the reason may be the size of heart. The QTc depends significantly on sex of recipients, no dependency on sex of donors was found. Narrow span of RR in heart transplant subjects limits the subject specific analysis.

S93

Assessment of Joint Interactions between Respiration and Baroreflex Activity using Joint Symbolic Dynamics in Heart Failure Patients

Muammar Kabir*, Elyar Ghafoori, Larisa Tereshchenko

Oregon Health and Science University
Portland, United States

In this paper we employed a novel approach based on joint symbolic dynamics (JSD) to study interaction between respiratory phase and baroreflex activity. Electrocardiogram (ECG) and blood pressure recordings from six participants with history of heart failure were included in this study. First, the ECG R-peaks and systolic blood pressure indices were detected using parabolic fitting. Second, the respiratory signal was derived from Frank orthogonal ECG leads using QRS slopes and R-wave angles. Third, time series of R-R intervals and systolic blood pressure (SBP) were extracted, and respiratory phases were obtained using the Hilbert transform. Subsequently, each series was transformed into binary symbol vectors based on their successive changes and words of length '2' were formed. Baroreflex patterns were studied using word combinations representing baroreflex activity for specific changes in respiratory phases. Baroreflex activity was significantly higher for alternating low-high/high-low heart rate and SBP during inspiration as compared to continuous increase or decrease in heart rate and SBP (wiSBP=10,wiHR=01,wRP=11: $39.1 \pm 9.3\%$ vs. wiSBP=00,wiHR=11,wRP=11: $6.4 \pm 3.9\%$, $p < 0.0001$).

S93

Electrogram Coupling as a Measure of Local Conduction during Atrial Fibrillation

Stef Zeemering*, Piotr Podziemski, Arne van Hunnik, Bart Maesen, Pietro Bonizzi, Ulrich Schotten

Maastricht University
Maastricht, The Netherlands

Aims: Invasive high-density contact mapping of atrial fibrillation (AF) provides detailed information on complexity of electrical conduction patterns. The degree of similarity between electrogram morphology at adjacent sites during AF may contain information related to AF substrate complexity and serve as a surrogate parameter to characterize conduction patterns without the need for electrogram annotation.

Methods: Electrograms were recorded with a grid of 16×16 electrodes (1.5mm electrode distance) in 21 patients during cardiac surgery (12 paroxysmal AF (PAF), 9 persistent AF (persAF)). Signals were acquired for 10 seconds at 1kHz, from both the right atrial free wall and posterior left atrium. Coupling between electrograms was defined as $1 - \text{the relative root mean square error of the reconstruction of a central electrogram by a linear combination of surrounding electrograms at a certain distance}$. Coupling ranged from 1 (complete coupling) to 0 (no coupling), and was computed with nonnegative least squares using only complete, symmetric topologies. For each electrode, coupling c as a function of electrode distance x was modelled by an exponential decay function: $c(x) = e^{-\lambda x}$. Half-decay distance $c_{0.5}$ was defined as $\frac{\ln(2)}{\lambda}$ and compared to conventional conduction-related contact mapping parameters, i.e. conduction velocity (CV), number of waves per AF cycle (NW) and electrode dissociation (D).

Results: Electrogram coupling was weaker in persAF than in PAF ($c_{0.5}$ (median \pm MAD): $2.4 \pm 0.5\text{mm}$ vs. $3.2 \pm 1.2\text{mm}$, $p < 0.02$, Wilcoxon rank-sum test). High correlation (Spearman's) was found between mean $c_{0.5}$ and mean CV ($r = 0.85$, $p < 0.001$). Other parameters showed only moderate correlation (NW: $r = -0.51$, $p < 0.01$, D: $r = -0.51$, $p < 0.001$).

Conclusion: Differences in AF conduction velocity between patients can be accurately described using a surrogate parameter based on the degree of electrogram coupling. This technique can for instance be applied to high-density contact recordings to quickly assess the Class I effect of antiarrhythmic drugs, both in atrial and ventricular recordings.

Diagnosis of Atrial Fibrillation by means of Implantable Devices: The Role of Remote Monitoring

Eugenio Cervesato*, Eugenia Bruschetta, Denis Fantin, Francesca Loro, Delia Zadnik, Marco Brieda, Ermanno Dametto, Federica Del Bianco, Sara Zardo, Edda Pollesel, Catya Zorzi, Matteo Cassin

Cardiology Dept. - ARC, Pordenone, Italy
Pordenone, Italy

Background: Atrial fibrillation (AF) is responsible for most hospitalizations for arrhythmia and is an independent risk factor for stroke. The cardioembolic stroke is almost always related to the presence of AF in any form (paroxysmal, persistent, permanent) and is characterized by high mortality and high residual disability. The clinical history of patients implanted with PM / AICD is frequently complicated by new occurrence or the recurrence of AF. We evaluated the role of remote monitoring of implanted devices for accurate detection of symptomatic or silent AF especially when there is an atrial electrode.

Materials and methods: Out of the 3876 patients followed in our laboratory, 699 (18%) were managed through remote monitoring systems: 279 Medtronic (169 PM, 105 AICD, 5 REVEAL), 245 Biotronik (124 PM, 119 AICD, 2 REVEAL), 86 Boston (8 PM, 78 AICD), 79 St Jude (9 PM, 70 AICD), 10 Sorin (AICD).

Results: Automatic alerts of the remote monitoring systems were set to early detect and track episodes of AF by using algorithms capable of measuring the daily burden, the length and frequency of AF episodes and the ventricular response in some device models. The strategy adopted in our center include nurses in charge of evaluating transmissions (about 96,000/year), assessing the severity of the alarms, consulting the cardiologist when needed and collaborating with him for the communication with the patient and the management of the therapy. The workload of the staff was: nursing time 435, cardiologist time 87 hours/year. Ambulatory examinations were reduced by 9.9% (year 2014 vs 2013) and mean time resulted 6 vs 15 minutes/patient.

Conclusions: Remote monitoring can reduce the incidence of hospitalizations for stroke and arrhythmias thanks to the early recognition and management of the episodes of AF. It allows to reduce ambulatory examinations and staff time dedicated to each patient.

Assessment of QT-RR Intervals Relation in Patients with Atrial Fibrillation

Luca Iozzia*, Luca T Mainardi, Federico Lombardi, Valentina D A Corino

Politecnico di Milano
Milan, Italy

QT-RR relation has been deeply investigated during sinus rhythm. However there are not established methods for the evaluation of QT-RR relation in patients with atrial fibrillation (AF). The aim of the present study was to assess the relation between QT and preceding RR intervals in ECG signal of patients with AF using different methods. We analyzed data from 26 patients (age 64 ± 12 years, 60% men) that were included in the study for programmed electrical cardioversion (EC) for persistent AF. Two leads surface ECGs were recorded for 10 minutes before EC. Repolarization duration was defined as the interval between R apex and T apex, overcoming the difficulty in detection of Q onset and T offset in ECG signals during AF. Because of the presence of T waves with double peaks, a two-step procedure was applied: 1) coarse localization of T apex; 2) refinement of T apex position by fitting the T wave by a 4th polynomial curve. Seven methods were used to study RT-RR relation: each of them considers a different number of averaged preceding RR intervals (from 1 to 5) correlated to the RT segment. A linear regression was applied to compare the slopes of the different methods. The mean value of RT-RR(1) slope of the regression line was compared to the mean value of RT-RR slope of other methods. A slightly increased was observed when a larger number of preceding RR intervals was considered (RT-RR(1) 0.030 ± 0.013 , RT-RR(1-2) 0.028 ± 0.012 , n.s., RT-RR(1-3) 0.033 ± 0.012 , n.s., RT-RR(1-4) 0.035 ± 0.016 , $p < 0.0001$, RT-RR(1-5) 0.039 ± 0.018 , $p < 0.0001$, RT-RR(1-5)m 0.048 ± 0.022 , $p < 0.0001$, RT-RR(2) 0.000 ± 0.007 , $p < 0.0001$). The most significant variation was observed among the mean value of RT-RR(1) slope with the mean value of RT-RR(1-5)m slope: 0.030 ± 0.013 vs 0.048 ± 0.022 , $p < 0.0001$. Interestingly the RT-RR correlation was completely lost when only the second previous RR interval was related to the RT interval.

S94

A High-Density Activation Map Estimation During Atrial Fibrillation

Alejandro Alcaine*, Natasja M.S. de Groot, Maurits A. Allesie, Pablo Laguna, Juan Pablo Martínez, Richard P.M. Houben

BSICoS Group, I3A, IIS Aragón, Universidad de Zaragoza. Zaragoza, Spain.

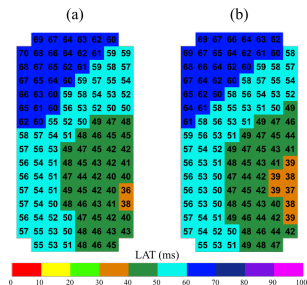
Aims: Creation of atrial fibrillation (AF) activation maps from unipolar electrograms (u-EGM) requires identification of local activation times (LAT) by determining the maximum negative slope of the signal, hence relying in the detector accuracy and generally requiring manual review. In general, LAT detection ignores spatiotemporal information embedded in the u-EGM signal morphology, which could be useful in high-density multi-electrode array (MEA) recordings. In this study, an approach to construct activation maps by simultaneous analysis of activation patterns is proposed.

Materials: Atrial intra-operative epicardial high-density recordings from one patient undergoing open chest surgery were used for this study. This data was recorded using a MEA sensor positioned over the right appendage of the atrium during AF. The MEA sensor has 124 circular electrodes spaced 2 mm and disposed in a 8×16 rectangular grid.

Methods: The complete MEA sensor is segmented in small electrode clusters and signals generated from an activation pattern model were fitted on the measured data by iterative optimization of the model parameters based on a cost function. Finally activation map reconstruction is performed by combining those single solutions.

Results: The accuracy was evaluated by comparing estimated LATs with those audited by expert electrophysiologists. The estimation error on a total of 236 beats (28369 LATs) was 0.29 ± 6.01 ms highly correlated ($\rho = 0.93$) with the reference. Figure shows an example of map estimation with the proposed method against the reference activation map.

Conclusions: Complex spatial activation patterns can be decomposed into local activation patterns derived from fitting an activation model, allowing the creation of high-density activation maps.



Activation maps: (a) Reference and (b) estimated. LATs are expressed in ms.

Automatic Detection of Atrial Fibrillation using MEMS accelerometer

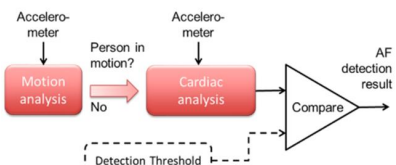
Tero Koivisto*, Mikko Pänkäälä, Tero Hurnanen, Tuija Vasankari, Tuomas Kiviniemi, Antti Saraste, Juhani Airaksinen

Technology Research Center, University of Turku, Finland

Atrial fibrillation (AF) is a very common cardiac arrhythmia, present in approximately two percent of the general population, approximately 140 million people worldwide. AF accounts for 20-40% of all strokes globally – up to 185,000 deaths per year in Europe alone. This study aimed to assess the applicability of SeismoCardioGraphy (SCG) for the automatic detection of Atrial Fibrillation (AF). The electrocardiogram (ECG) was used as a gold standard method for AF detection.

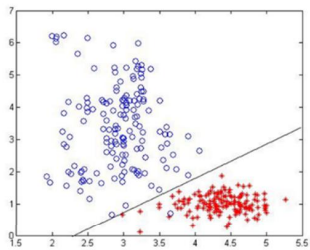
SCG was recorded in dorso-ventral direction while at rest in supine position simultaneously with the ECG assessment during both AF and sinus rhythm (after cardioversion) from 12 patients, so that the assessment time was approximately 10 minutes for each patient. ECG was measured with two electrodes attached to the skin, while SCG assembly (2 x 4 cm) was attached to the center of the anterior chest wall with an adhesive tape. ECG electrodes and SCG sensor (a tiny MEMS accelerometer) were connected to a battery powered main unit with wires. Measurement data was saved to a SD memory card and analyzed retrospectively in Matlab. An SCG-based AF-detection algorithm was developed and its performance tested with the acquired clinical data.

The algorithm is able to distinguish AF positive samples (asterisk) from AF negative samples (circles) with a sensitivity of 99% and specificity of 99%, when the length of the analyzed signal is only 70 seconds in total. Parts of signal having excessive motion artefacts are automatically rejected (see figure below).



Today ECG is the primary method for detecting arrhythmias in telemonitoring applications, but reliable analysis requires good electrode-to-patient contact and motion artifact elimination. Given the very small dimensions of modern MEMS accelerometers (2 x 2 mm), SCG based detection method may provide totally new venues especially for asymptomatic AF detection.

S94



The U Wave in Atrial Fibrillation

Philip Langley*, John Bourke, Alan Murray

University of Hull
Hull, United Kingdom

The prevalence and characteristics of the ECG U wave in atrial fibrillation (AF) have not previously been reported due to its measurement difficulty and U waves are often neglected in QRST cancellation for deriving the atrial fibrillatory wave. The aims of this study were to test the feasibility of measuring U waves in the presence of atrial fibrillatory waves using ventricular beat averaging and to establish the prevalence and amplitude of U waves in 12-lead ECGs of AF patients. 12-lead ECGs of 9 patients in AF were analysed. Ventricular beats were automatically detected and RR histograms (bin size 50ms) constructed. Only beats with similar RR intervals were averaged, specifically those with RR at the mode of the RR histogram. These beats were aligned to the R wave peak and averaged to generate an average ventricular beat in each lead of sufficient duration to include QRST and U waves. From the average beat U wave polarity (positive, negative, biphasic, flat) and amplitude in the 12 leads was measured. The ratio of amplitude of U wave to atrial fibrillatory wave in lead V1 was calculated. U waves were measureable in all patients. U waves were predominantly positive in leads I, II, V3, V4, V5 and V6, negative in leads aVR and V1, biphasic in lead III and flat in aVL. Mean absolute U wave amplitude across leads was 0.02 mV. In lead V1 the U wave amplitude was on average 0.17 (range 0.1 to 0.4) times the amplitude of the atrial fibrillatory wave. U waves can be measured by ventricular beat averaging in AF patients. In most patients U wave amplitude is small relative to atrial fibrillatory wave.

S94

STEMI classification in acute ischemia: dependence on the position of the ST deviation measurement relative to the J point

Sumche Man*, C. Cato Ter Haar, Arie C. Maan, Martin J. Schalij, Cees A. Swenne

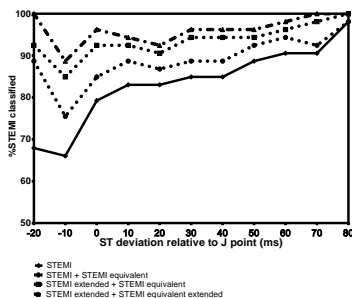
Cardiology Department, Leiden University Medical Center, Leiden, the Netherlands

INTRODUCTION: Currently, ST-elevation/ST-elevation equivalent (STEMI) or non-ST elevation (NSTEMI) classification of ECGs made in acute coronary syndrome (ACS) patients is essential to triage the patient for percutaneous coronary intervention (PCI). The guidelines dictate that STEMI classification is done by using ST-deviation measurements at the J point. However, the J-point amplitude can be obscured because of ischemia-induced conduction delays and/or ischemia-induced early repolarization. ST-deviation measurements at a fixed time-interval after the J point is one of the often-suggested solutions. However, the impact of the position of the ST-deviation measurement on STEMI classification is not known. In our current study, we investigate if STEMI classification of ACS ECGs depends on the position of ST-deviation measurement relative to the J point.

METHODS: We analyzed ECGs of 53 ACS patients scheduled for primary PCI and with an angiographically demonstrated completely occluded culprit artery. In each ECG, ST deviation was measured at the J point (last J point of all leads) and at 10 fixed time-intervals relative to the J point (-20, -10, +10, +20, +30, +40, +50, +60, +70 and +80 ms). ECGs were analyzed by using our custom-made LEADS program. Four STEMI classifications (STEMI; STEMI + STEMequivalent; STEMIextended + STEMIequivalent; STEMIextended + STEMIequivalentExtended) were done per ST deviation. Finally, the percentages STEMI-classified ECGs were computed per ST-deviation measurement.

RESULTS: The study group consisted of 13/40 female/male, mean±SD age 59.6±14.9 years. Percentages STEMI-classified ECGs per STEMI classification per ST deviation (83,88,90,96%, respectively, see Figure) were almost steady between J+10 to J+40 ms.

CONCLUSION: The impact of the position of the ST-deviation measurement on the STEMI classification is minimal when measured in the J+10 to J+40ms range, while early measurement bear the risk of underdiagnosis. Further investigation including ACS-negative ECGs is needed to corroborate these results.



SA1

Long Term Follow Up of the Early Repolarization Pattern in Participants in the West of Scotland Coronary Prevention Study

Elaine Clark, Ian Ford, Peter W. Macfarlane

University of Glasgow, Scotland

The West of Scotland Coronary Prevention Study was a primary prevention trial aimed at assessing the effects of pravastatin in males with hypercholesterolemia but no history of myocardial infarction. As part of that study, baseline 12 lead ECGs were recorded in digital form around 1990.

The aim of the present study was to analyse the baseline ECGs to look for the early repolarization (ER) pattern and to see if there was any adverse outcome associated with this ECG abnormality during 15 years of follow up.

At baseline, 6595 men aged 45-64 (mean age 55.2 ± 5.5) were recruited. All individuals were flagged with the Scottish Government Record Linkage System so that subsequent hospitalization and/or death would be recorded centrally. 12 lead ECGs were recorded using a Siemens Sicard 440 ECG machine and stored on a Mingocare system. 6575 ECGs were recently retrieved from the database and analysed with the 2014 development version of the University of Glasgow ECG Analysis Program, which incorporates criteria for the detection of the ER pattern. A census was taken 15 years after entry into the study. Analysis was undertaken to see if there was any difference in outcome over this period, irrespective of treatment, for those with versus those without the ER pattern.

At baseline, 1398 individuals had the ER pattern. Analysis of the 15 year outcomes data using Kaplan-Meier analysis showed that there was no significant difference between those with and without the ER pattern (Fig 1). This was true for the outcome of fatal or non fatal myocardial infarction and also for all cause mortality ($P=0.65$).

In this particular population, it has been shown that the early repolarization pattern is of no prognostic significance with respect to fatal or non fatal myocardial infarction or all cause mortality.

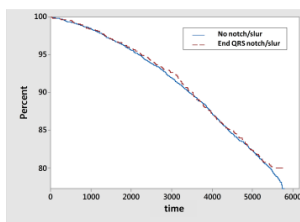


Fig 1. Survival plot for all cause mortality.

Circadian Modulation on T-wave Alternans Activity in Chronic Heart Failure Patients

Alba Martín-Yebra*, Enrico G Caiani, Pablo Laguna, Violeta Monasterio, Juan Pablo Martínez

Universidad de Zaragoza
Spain

Aim: Long-term average TWA activity has been shown to be an independent predictor of sudden cardiac death (SCD) in chronic heart failure (CHF) patients. However, the influence of circadian rhythms on TWA remains understudied. In this study we assessed circadian TWA changes in a CHF population and evaluated whether the prognostic value of TWA indices is sensitive to the circadian pattern.

Materials and Methods: Holter ECG recordings from 626 consecutive patients with mild-to-moderate CHF were analyzed (2 or 3 leads, sampling frequency 200 Hz). Among the initial population, 52 subjects had SCD. Index of average alternans (IAA) quantifying the average TWA level was measured in consecutive 6-hour intervals (00.00-06.00 h; 06.00-12.00 h; 12.00-18.00 h; 18.00-24.00 h) using a fully automated method based on periodic component analysis and the Laplacian likelihood ratio method. Survival analysis was performed considering SCD as an independent endpoint.

Results: IAA changed along the time of the day, with statistically significant lower values during the night than during daytime, being IAA maximal for the interval 12.00-18.00 h (mean \pm SD, IAA(00-06)=13.64 \pm 11.29 μ V, IAA(12-18)= 21.93 \pm 22.23 μ V, $p<0.001$). This pattern is similar to the one observed in the mean Heart Rate (HR(00-06)= 68 \pm 12.3beats/min, HR(12-18) = 77.2 \pm 14.4 beats/min, $p<0.0001$). However, a low correlation ($r=.109$) was found between IAA and HR and when computing IAA HR-restricted indices (IAAx, $x=\{70,80,90\}$, HR ranging from $x-10$ to x beats/min) the same oscillation pattern remains still visible. After dichotomization of patients based on the third quartile of IAA indices, only IAA(12-18) successfully predicted SCD (hazard ratio: 1.99 per μ V, IC: 1.12-3.53, $p=0.019$).

Conclusions: Circadian pattern modulates the IAA index, and time of the day should be considered for SCD risk prediction. Average TWA activity during the afternoon (from 12 to 18 h) is associated with the risk of SCD in CHF patients.

SA1

Validation of the Vessel-Specific Leads (VSLs) for Acute Ischemia Detection on a Dataset with Non-Ischemic ST-Segment Deviation

John Wang*, Olle Pahlm, Galen Wagner, James Warren, Milan Horacek

Philips Healthcare
Andover, United States

Introduction: Existing criteria recommended by ACC/ESC for identifying patients with ST elevation myocardial infarction (STEMI) from the 12-lead ECG perform with high specificity (SP), but low sensitivity (SE). In our previous studies, we found that the SE of acute ischemia detection can be markedly improved without any loss of SP by calculating, from the 12-lead ECG, ST deviation in 3 “optimal” vessel-specific leads (VSLs). To further validate the method, we evaluated the SP performance using a dataset with non-ischemic ST-segment changes.

Method: 12-lead ECGs of 100 patients (75 males/25 females, age range 12-83 years, average age 52 years) were retrieved from a centralized ECG management system at Skane University Hospital, Lund, Sweden. These ECGs were chosen to represent five subgroups with various causes of pathological ST-deviation, other than acute coronary occlusion: a) ventricular pre-excitation (n=12), b) acute pericarditis (n=26), c) "early repolarization syndrome" (ERS) (n=14), d) left ventricular hypertrophy (LVH) with “strain” (n=26), and e) left bundle branch block (LBBB) (n=22). ECGs with inadequate signal quality, heart rate exceeding 120 bpm and/or atrial flutter were not selected for this study population. Both STEMI criteria and VSLs method were tested. SP, calculated for each subgroup and combined, was used as the performance measure for comparison.

Results: SP test results using the STEMI criteria were 100%, 4%, 29%, 100%, and 64% for the five subgroups: pre-excitation, pericarditis, ERS, LVH, and LBBB, respectively. The corresponding results for the VSLs method were 92%, 85%, 100%, 77%, and 64%. For the whole group, SP results were 57% for the STEMI criteria and 81% for the VSLs method.

Conclusions: Based on these results we can conclude that the VSLs method not only is more sensitive in detecting acute ischemia but also more specific in rejecting patients with non-ischemic ST deviation than the existing STEMI criteria.

SA1

A Fundamental Relationship between Intraventricular Conduction and Heart Rate

Jay W Mason*, Robert L Lux, Benhur Aysin, Thomas E Moon, Martino Vaglio, Fabio Badilini, Brock Heinz

University of Utah
Reno, United States

Aims: A relationship between the electrocardiographic QRS interval duration, a measure of intraventricular conduction time, and the diurnally varying heart rate has not been recognized or characterized. The purpose of this study was to document and characterize the QRS-RR interval relationship.

Methods and Results: To evaluate the relationship between spontaneously varying heart rate and intraventricular conduction time in humans, we analyzed electrocardiographic data from 885 Holter recordings in 410 normal subjects participating in 5 clinical trials (the Holter group), and from 38,891 standard 10-second electrocardiogram recordings in 948 normal subjects participating in 9 clinical trials (the ECG population). The slope of the linear regression of QRS on RR was positive in 94% of subjects in the Holter group with an average slope of 0.0126, which indicates an increase in QRS duration of 1.26 msec for an increase in RR interval of 100 msec (the equivalent of a change in heart rate from 60 to 55 bpm). In the ECG population the QRS-RR regression slope was also positive (0.0171, $p < 0.0001$).

Conclusions: There is a robust, direct relationship between the spontaneously changing RR interval and intraventricular conduction time represented by the duration of the QRS interval. As heart rate increases, QRS duration decreases. This new observation has important physiological and clinical implications.

SA1

Engineering Issues in Clinical Electrocardiography

JW Mason*

This session will be completed with an open discussion led by JW Mason. Please plan to stay for this extended session.

SA1

***In Silico* Investigation of Short QT Syndrome-Linked Potassium Channel Mutations on Electro-Mechanical Function of Human Atrial Cells**

Dominic G Whittaker*, Michael A Colman, Jules C Hancox, Henggui Zhang

University of Manchester
Manchester, UK

Introduction: Atrial Fibrillation (AF) is a common clinical presentation of the short QT syndrome (SQTS). However, the link between gene mutations underlying the SQTS and increased susceptibility to AF remains unclear. This study aimed to investigate the functional impact of two gain-of-function potassium channel mutations on the electrical and mechanical activities of human atrial cells; namely the SQT1-related N588K and SQT2-related V307L mutations to channels encoded by the human *Ether-à-go-go-Related Gene (hERG)* and *KCNQ1* gene, respectively.

Methods: A contemporary human atrial action potential (AP) model was coupled to an established cardiac myofilament model. Markov formulations of the rapid and slow delayed rectifier currents, I_{Kr} and I_{Ks} , the α subunits of which are encoded by *hERG* and *KCNQ1*, respectively, were implemented in wild type (WT) and mutation conditions. The effects of the mutations on AP duration at 90% repolarisation (APD_{90}), peak current density, intracellular calcium transient, and contractile force were evaluated both with and without inclusion of a stretch-activated current, I_{SAC} .

Results: The N588K and V307L mutations were found to increase peak current density of I_{Kr} and I_{Ks} , respectively, in agreement with experimental observations. This served to (i) accelerate atrial repolarisation, reducing the APD_{90} by ~25%/~15% compared with WT for the N588K/V307L mutations at a stimulation frequency of 1 Hz; and (ii) stabilise re-entrant circuits in tissue, increasing the dominant frequency of re-entry from ~3.5 Hz in WT to ~4.5 Hz/~5 Hz for N588K/V307L. Secondary effects of the mutations resulted in decreased calcium transient amplitude, and a consequent reduction in the contractile force, by ~39%/~20% for N588K/V307L. Effects of including stretch-activated channels depended on the AP morphology.

Conclusion: The significant acceleration in atrial AP repolarisation and modest impairment in contractile function could have important implications in understanding the mechanisms behind which SQTS alters atrial function and increases vulnerability towards AF.

SA2

Uncertainty and Sensitivity Analysis of the Courtemanche-Ramirez-Nattel Human Atrial Cell mMdel using Gaussian Process Emulators

Eugene TY Chang*, Richard H Clayton

University of Sheffield
Sheffield, United Kingdom

Motivation: Models of cardiac cellular electrophysiology are highly detailed with many input parameters. However, the effect of input parameters on model outputs is often not well characterised. Uncertainty and sensitivity analysis using Monte Carlo techniques require large numbers of model runs. In this study we investigated Gaussian Process (GP) emulators, which provide a computationally cheap way to assess uncertainty and sensitivity analysis.

Methods: We constructed GP emulators for 6 metrics of action potential shape (max dV/dt , max voltage, dome voltage, action potential duration to 90% repolarisation (APD90), resting voltage and APD to 50% repolarization), as a function of maximal conductance. The emulators were fitted to design data obtained from 150 model runs where the input parameters varied within a range of $\pm 1/3$ of their default value, and where each point in parameter space was selected using Latin hypercube sampling. The emulators were then used to calculate variance based sensitivity indices.

Results: Variance based sensitivity indices describe the proportion of output variance that can be attribute to variance in an input. We found that action potential upstroke (max dV/dt) and maximum voltage were both highly sensitive to G_{Na} , with sensitivity indices of 0.75 and 0.89 respectively. Dome voltage was sensitive to G_{Kur} (0.2) and G_{CaL} (0.51), and G_{K1} had a strong effect on APD90 (0.35) and resting voltage (0.41). APD50 was most sensitive to G_{CaL} (0.35). These sensitivity indices were comparable to sensitivity determined from partial least squares regression.

Conclusions: GP emulators provide a computationally efficient way to undertake sensitivity analysis in cardiac cell models. Both parameters and outputs are treated explicitly as normal distributions, with means and variances. Thus it is possible to undertake uncertainty quantification as well as sensitivity analysis using this approach.

SA2

Sensitivity Analysis of Ectopic Electrical Activity in Pulmonary Vein Myocardium

Hitomi Sano*, Yuichiro Tanaka, Yasuhiro Naito, Masaru Tomita

Keio University
Fujisawa, Japan

The pulmonary vein contains a myocardial layer which is capable of generating spontaneous or triggered action potentials, which is considered to play a central role in the generation and maintenance of atrial fibrillation. The pulmonary vein myocardial layer is extending from the left atrium, but has less negative resting membrane potential due to a lower density of the inwardly rectifying $K(+)$ current ($I(K1)$). Although electrophysiological and pharmacological characteristics of the pulmonary vein myocardium are compiled in various literatures, a comprehensive understanding of the spontaneous action potentials generated in the myocardial layer is yet to be assessed. Here, we integrated electrophysiological properties of the pulmonary vein myocardial layer on the basis of the guinea pig ventricular cell model. Based on the preceding research which reported that approximately half of the isolated pulmonary vein myocardial layer exhibited spontaneous action potential and the remaining half was quiescent, we constructed various combinations of the pulmonary vein myocardial models in order to represent the variation of the action potential tracings. As a result, we predicted that the spontaneous action potentials, including burst-like action potentials, are observed when relative current densities of $Na(+)$ current, L-type $Ca(2+)$ current, $IK1$, rapid component of delayed rectifying $K(+)$ current, and ACh-activated $K(+)$ current were varied. We further modified the model to represent late component of $Na(+)$ current ($I(NaL)$) in order to predict antiarrhythmic effect of ranolazine, a selective $INaL$ blocker, on the predicted spontaneous action potentials.

SA2

Are Multi-electrode Arrays Able to Differentiate Anatomical from Functional Reentries in an Excitable Sheet?

Laura Martínez*, José Jalife, Omer Berenfeld, Javier Saiz

Universitat Politècnica de València
Valencia, Spain

Atrial fibrillation (AF) is the most common cardiac arrhythmia in clinical practice. Anatomical and functional reentries seem to be important in driving AF. Therefore, it is of great importance to identify and locate them. Multi-electrode array systems are increasingly being used to map the atrial electrical activity in humans. We use computer simulations of reentries during paroxysmal AF in three different 3D sheets of dimensions $4.98 \text{ cm} \times 4.98 \text{ cm} \times 0.03 \text{ cm}$, corresponding to left atrial tissue (Sim1), pulmonary veins tissue (Sim2) and mitral valve ring tissue (Sim3). The transmembrane potential (V_m) is obtained by solving the mono-domain reaction-diffusion equation with the finite elements method. Electrograms (EGM) are computed through the extracellular electrical potentials (ϕ_e), calculated by using V_m as input for the second bidomain model equation with the finite element method and Neumann boundary conditions. The EGM are interpolated to perform phase maps based on the Hilbert transform, detect the phase singularities (PS) and build dominant frequency (DF) maps, in order to study if the multi-electrode array systems can distinguish properly between anatomical and functional reentries. Our results show that although there is no difference between phase maps corresponding to anatomical and functional reentries (all they exhibit rotors and therefore, in all cases a trajectory is tracked through the PS detections), overlapping the trajectories with the DF maps obtained it is able to distinguish anatomical from functional reentries. DF ranged between 8.7-14.6 Hz for Sim1, 1-9 Hz for Sim2 and 1-6.8 Hz for Sim3. In Sim1 (functional reentry) the trajectory location coincides spatially with the region of highest DF, while in Sim2 and Sim3 (anatomical reentries) the trajectory is located in the region of lowest DF. We conclude that multi-electrode arrays are able to distinguish whether a reentry is anatomical or functional in an excitable sheet.

SA2

Simulation of the Pacemaker Created from the Cardiomyocytes by Reducing Inward-Rectifier K⁺ Current

Yue Zhang, Kuanquan Wang*, Henggui Zhang, Yongfeng Yuan

Harbin Institute of Technology
Harbin, China

Aims: This study aimed to develop a 2D model of human bio-pacemaker created from the ventricular endo-myocytes. We tested the stability of the pacemaker and investigated its driving capability, finding the ways and critical size of the pacemaker for robust pacing and driving.

Methods: First, the TNNP06 human ventricular model was used to investigate the automaticity of the created single pacing cell. Then the 2D model was developed by incorporating the automatic cells into the ventricular sheet in three different ways shown in Figure 1, (1) the first ten volumes of endo-myocytes were replaced by automatic cells, (2) the pacemaker tissue was connected with the ventricular sheet by a bridge consisted of endo-myocytes, (3) the bridge was consisted of Purkinje fiber cells. In the last two ways, the pacemaker was

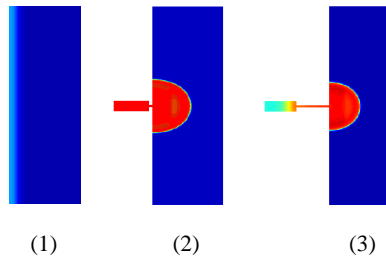


Figure1. Three different ways the pacemaker incorporated into.

set 50 cells in length and 20 cells in width. Simulation time for both single cell and 2D model was more than 600,000ms. The ventricular sheet was designed 100 cells in length and 400 cells in width.

Results: For single pacing cell, the action potentials were stable with the period around 852ms. For 2D tissue, the pacemaker in the first way could not drive the tissue at all, while the whole ventricular sheet could be driven in the other two ways. However, the period was around 910ms in the second way, while the pacemaker in the third way paced at the same rhythm to the single auto-cell, whose period was about 852ms.

Conclusion: The pacemaker connected with Purkinje fiber cells drove the ventricular tissue more easily with only 1,000 pacing cells; while the tissue couldn't be driven, though there were 4,000 pacing cells in the first way. This demonstrated that the driving force of pacemaker closely related to the conduction mode besides the size. This study could provide guidance and advice for the bio-experiments.

SA3

The Role of Purkinje Automaticity as an Arrhythmia Mechanism in Hyperkalaemia

Violeta Monasterio¹, Jesús Carro^{1,3}, Esther Pueyo^{2,3}, José F Rodríguez^{3,4}

¹ Universidad San Jorge, Villanueva de Gállego, Spain

² CIBER-BBN, Zaragoza, Spain

³ Universidad de Zaragoza, Zaragoza, Spain

⁴ Politecnico di Milano, Milano, Italy

Aims: Purkinje (PK) cells pacemaker activity is usually suppressed by the sino-atrial node. Under abnormal conditions, PK cells may produce ectopic focal activity leading to tachycardia and fibrillation. This computational modelling work illustrates the potential role of PK automaticity as an arrhythmia mechanism in hyperkalaemia.

Methods: First, the automaticity of isolated PK cells under hyperkalaemic conditions was investigated with the Stewart et al. 2009 model. $[K^+]_o$ was varied from 5.4 to 16.2 mM and the average cycle length (CL) of spontaneous action potentials (APs) was measured. Second, the effects of PK automaticity in hyperkalaemia were investigated in a 1-D model of the PK-ventricle subsystem composed of 3 cm of PK cells connected to 1 cm of endocardial cells (ten Tusscher and Panfilov 2006 model). The fibre was stimulated at CL = 1000 ms for 5 min while $[K^+]_o$ was increased to $[K^+]_o^{max}$ of 5.4, 6.3, 7.2 and 8.1 mM (Figure 1a).

Results: The autorhythmic period of PK cells was strongly influenced by hyperkalaemia, with average CLs varying from 1057 ms for $[K^+]_o = 5.4$ mM to 762 ms for $[K^+]_o = 8.1$ mM. On the contrary, AP-duration (APD) was found to increase with $[K^+]_o$ (Figure 1b). In the PK-ventricle model, no automaticity was observed in PK cells for $[K^+]_o^{max} = 5.4$ and 6.3 mM. For $[K^+]_o^{max} = 7.2$ and 8.1 mM, spontaneous APs appeared in zone 3, with the focal activity being propagated towards both fibre ends. Complex patterns of spontaneous and stimulation-driven APs were observed by the end of the 5-min period.

Conclusion: Altered PK automaticity under hyperkalaemia may play an important role in the generation of ventricular arrhythmias.

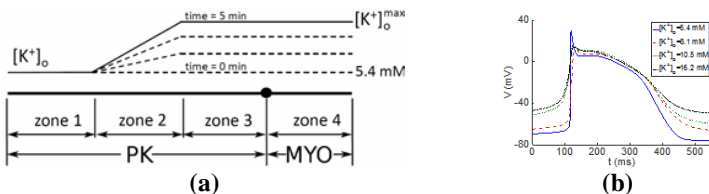


Figure 1. a) Purkinje-ventricle simulation setup; b) AP-duration vs. $[K^+]_o$.

A Novel Computational Model of the Human Sinoatrial Action Potential

Alan Fabbri*, Matteo Fantini, Ronald Wilders, Stefano Severi

University of Bologna
Cesena, Italy

Aims: This work aimed to formulate a human sinoatrial node (SAN) action potential (AP) computational model able to reproduce the available experimental data and to assess the effects of funny current (If) block on cycle length (CL).

Methods: The Severi-DiFrancesco rabbit SAN model was the starting point. Identification of currents, pumps and exchangers was led including experimental data from electrophysiology, gene expression and by tuning the parameters to reproduce as close as possible the experimental traces (AP morphology and calcium transient). In order to quantitatively assess the model performances we computed AP features (action potential amplitude (APA), maximum diastolic potential (MDP), maximum upstroke velocity (Vmax), action potential durations at 20, 50 and 90% of repolarization (APD20,50,90), overshoot (OS) and diastolic depolarization rate for the first 100 ms (DDR100)) and Cai transient features (minimum and maximum Ca²⁺ concentration, Ca²⁺ transient amplitude (TA) and transient amplitude at 20, 50 and 90% of the decay). The effects of If modulation on CL was evaluated by a progressive block of this current (30, 70, 90, 100%).

Results: The model showed a good accordance with experimental traces. Both AP features and Cai transient were close to the experimental values (i.e. Predicted by the model: CL=835 ms APD90=134.0 ms, DDR100= 43.5 mV/s; experimental CL=828 ± 15 ms, APD90=143.5 ± 34.9 ms, DDR100= 48.9 ± 18 mV/s) If block led to a significant CL increase (+20.7%), even if lower than those recorded in 2 mM Cs⁺ perfused cells (+26%).

Conclusions: AP waveforms and Ca²⁺ transient generated by the model are in good agreement with experimental data. Further investigations on the effects of single current modulations are needed, but this model is a first step to a reliable human SAN model.

SA3

Development of a Novel Markov Chain Model for Oxidative-dependent CaMKII δ Activation

Shanzhuo Zhang, Qince Li, Kuanquan Wang*, Henggui Zhang

United Kingdom

Introduction and aims: Dysfunction in the Calcium-calmodulin dependent kinase II (CaMKII) signaling can lead to several pathologies, such as heart failure and arrhythmia. Especially, the role of CaMKII signaling in oxidative stress-induced arrhythmias remains unclear. In previous studies, persistent kinase activity of CaMKII was linked to the activation pathway of autophosphorylation, but recently, a novel activation pathway involves oxidation was identified. In this study, we aimed to develop a new Markov chain model of CaMKII δ -isoform (CaMKII δ) that involves both the two activation pathways to better simulate CaMKII signaling under oxidative stress in cardiomyocytes.

Methods: CaMKII is activated by binding a fully Ca²⁺-bound calmodulin (Ca²⁺/CaM) to its autoinhibitory domain, which enables further CaMKII autophosphorylation or oxidation. Based on the four-state model developed by Chiba et al, we implemented two oxidized states including a Ca²⁺/CaM-bound state and a Ca²⁺/CaM-dissociated state, representing the new pathway of oxidation-dependent activation. Based on experimental data of the CaMKII δ autophosphorylation and oxidation, rate constants between states were fit by using the damped least-squares method.

Results: Using the model, we reproduced the CaM affinity to CaMKII δ , the dependence of autophosphorylation and CaMKII δ activation on CaM, which were observed in previous experimental studies. The frequency-dependent activation of CaMKII was simulated for both CaMKII α - and δ -isoforms, results of which matched to the experimental data measured in α -isoform. For the oxidation pathway, our simulation suggested that H₂O₂ increased the kinase activity in a dose-dependent manner, which also fitted to experimental data.

Conclusions: A novel Markov chain model has been developed to reproduce both autophosphorylation-dependent and oxidation-dependent CaMKII activation. As CaMKII δ is the most abundant in the heart, the developed model will be a powerful tool to examine the mechanism of arrhythmias caused by abnormal CaMKII signaling under oxidative stress when it is integrated into existing cardiac electrophysiological models.

SA3

Evaluating Exponential Integrators for Markov Chain Ion Channel Models

Tomas Stry*^{*}, Vadim Biktashev

United Kingdom

Aims: We evaluate accuracy and efficiency of exponential integrators applied to numerically stiff Markov chain (MC) models of cardiac ion channel. The aim is to allow increase of the time step without getting numerical instabilities.

Methods: Cardiac action potentials are simulated using cellular model (Faber et al. 2007) containing two MC ion channel models: Ryanodine receptor (RyR) and L-type calcium channel (ICaL). In the original code by Faber et al., the ionic concentrations, membrane potential and MC components were updated using forward Euler (FE) scheme. All gate type ionic channels were computed using exponential integration proposed by Rush and Larsen (1978). The time step was set to 1 microsecond. We adjusted the Matrix Rush-Larsen (MRL) method proposed previously (Stry and Biktashev, 2015) to the MC models of this specific cellular model. The method involves pre-computing and tabulation of the matrix exponentials via diagonalization. However, the transition rates in the present MCs depend on two dynamic variables, which makes tabulation problematic. We overcome this by exploiting special structures of the matrices of the transition rates.

Results: The FE method gives instability when time step increases. The maximal time step is 6.4, 37 and 190 microseconds for RyR, ICaL and ionic concentrations, respectively. The instabilities in MC models are quenched by using suggested exponential integration. If computed at same time step size as FE, the exponential integration increases the computational cost by 85%, 21% and 11% for RyR, ICaL and whole cell, respectively. However, it allows increase in the time step well above the instability threshold of explicit solvers.

Conclusions: Exponential solvers for the Markov chains in this model allow the increase of the time step by a factor of 30, resulting in reduction of computational time by a factor of 27.

SA3

Applying Novel Identification Protocols to Markov Models of INa

Michael Clerx*, Pieter Collins, Paul GA Volders

Netherlands

The kinetics of the cardiac fast sodium current INa can be accurately recreated by Markov models trained on whole-cell patch clamp data. Theoretical studies have indicated that well-designed whole-cell patch clamp experiments have the potential to find best fits that are locally unique. Since the rate equations for Markov models can be ad-hoc, this type of identifiability is a necessary (though not sufficient) condition for a meaningful interpretation of the estimated values. In this study we investigate the feasibility of applying theoretically tested identification protocols in a wet-lab setting and perform preliminary experiments. A model, a protocol and a test for local uniqueness were implemented. The protocol was then optimized to create a rapid sequence of voltage steps capable of uniquely identifying the model's parameters. Patch-clamp experiments were performed on CHO cells transfected with wild-type SCN5A and a model was trained on the resulting data. Based on these experiments, we updated our identifiability checking method to account for various sources of error. Noise was reduced by averaging multiple runs and capacitance artifacts were simply be cut from the signal. Membrane charging time was measured using a model cell and added to the model used for identification. With these restrictions in place we then showed how neither our protocol nor a sequence of established protocols could identify the used model, after which we removed the unidentifiable parts to create a new, identifiable model of human cardiac INa. Leak current in the measured data was estimated and found to be non-linear, making it difficult to separate it from remaining active components of INa. We suggest further experimentation using channel blockers to overcome this hurdle. We conclude novel identification protocols can be used to rapidly and uniquely identify INa Markov model parameters, provided that leak current is dealt with in an adequate way.

SA3

The Accuracy of Beat-Interval Based Algorithms for Detecting Atrial Fibrillation

Alan Kennedy*, Dewar Finlay, Daniel Guldenring, Raymond Bond, James McLaughlin

United Kingdom

Automated detection of Atrial Fibrillation (AF) from the surface electrocardiogram (ECG) remains a challenge. Some have suggested that a major source of false positives from beat interval AF algorithms are ectopic beats and/or other supraventricular arrhythmias. However, this has not been thoroughly investigated. This study aims to evaluate the accuracy of four commonly implemented beat-interval based AF algorithms (1) The coefficient of variance (CV), (2) Root Mean Square of the Successive Differences (RMSSD), (3) turning point ratio (TPR) and (4) Sample Entropy (SampEn). All four algorithms were tested on R-R interval data from patients in normal sinus rhythm, atrial fibrillation, ectopic beats and supraventricular tachycardia (SVT). The algorithms were first assessed based on dataset 1, which consisted of the Physionet AF database (AFDB). The algorithms were then reassessed on dataset 2 which consisted of the same AFDB along with data from non-AF patients experiencing ectopic beats (extracted from the MIT arrhythmia database) and the Physionet Supraventricular Arrhythmia database. Receiver operating characteristic (ROC) analysis was then used to determine the performance of each algorithm over different segment lengths (SL) ranging from 30 to 120 beats. On dataset 1 the CV had the greatest detection performance (AUC = 92.13% at SL = 60) when compared to RMSSD (AUC = 90.44% at SL=120), SampEn (AUC=86.82%, SL =120) and TPR (AUC = 76.14, SL = 120). On dataset 2 the CV also performed best (AUC = 89.20% at SL = 60), followed by RMSSD (AUC = 86.16%, SL = 90), SampEn (AUC = 83.50%, SL = 120) and TPR (AUC = 77.52 at SL = 60). When comparing algorithm results from both datasets, a clear reduction in algorithm performance was found in dataset 2 (AUC = 93% vs. 89%). This study demonstrates that R-R based algorithms have reduced accuracy when monitoring patients with ectopic beats and/or supraventricular tachycardia.

SA4

Analyzing the Atrial Depolarization Wavefront Triggered from Sinus Node and Coronary Sinus for Identification of the Arrhythmogenic Substrate.

Bhawna Verma*, Tobias Oesterlein, Armin Luik, Claus Schmitt, Olaf Dössel

Institute of Biomedical Engineering, Karlsruhe Institute of Technology, Karlsruhe, Germany

Abstract: Atrial arrhythmias are the most common cardiac arrhythmias. After drug therapy, the most commonly used procedure to cure arrhythmias is the catheter ablation procedure. The success rate of this procedure is moderate due to the constraints in precisely locating the arrhythmogenic substrate. In this work the identification of the arrhythmogenic substrate area was done in order to locate the region of interest for catheter ablation procedure.

Methods: The study has been done on two clinical cases. The left atrium was paced from the electrodes on the coronary sinus (CS) catheter, since it (CS catheter) remains stationary throughout the recording. The 400-350 ms protocol was used for pacing. The depolarization wavefront originating from the sinus node and the pacing points in CS were analyzed on the basis of the differences in the local activation time maps. The regions of slow and fast conduction were identified. The correlation coefficient between two depolarization wavefronts was also calculated in order to find the similarities in terms of propagation directions and morphology. The region having the differences in propagation pattern in the depolarization wavefront that originated from consecutive triggering at one location in the CS after 350 ms were marked as the region of interest. The activity duration has also been visualized over the atrium in order to find the region with maximum duration of the atrial activities.

Result: The local activation time visualization over the atrium, helped in better understanding of the depolarization wavefronts propagation pattern with respect to different triggering points. The regions marked on the basis of the differences on the depolarization wavefront propagations and large activity durations were the regions of interest, since these could potentially be the arrhythmogenic substrate.

Conclusion: Ablating in the region of interest could potentially help in removing the arrhythmogenic substrates and getting the normal rhythm back, thereby improving the success rate of the ablation procedure.

Atrial Fibrillation Detection Evaluation - Performance Measures

Sándor Hargittai*

Hungary

Aims: Atrial fibrillation is the most commonly sustained arrhythmia in clinical practice worldwide. It's essential that AF detection algorithms should be powerful. The appropriate measures are crucial for comparing the algorithms and measuring their discriminative properties and predictive abilities. This paper is addressed to study the proper performance metrics for evaluation.

Method: The current ANSI/AAMI standard recommends using two metrics – sensitivity and positive predictivity. We argue with this combination of indicators of diagnostic performance. Whilst the sensitivity is the intrinsic quality of the algorithms, the positive productivity is more characteristic of the predictive power at the different AF prevalence. We reviewed the potential metrics for evaluation applied in the different disciplines. The sensitivity and specificity are the best paired performance measures which are the inherent properties of algorithms and do not depend on the prevalence. However, using paired indicators can be a disadvantage in comparing the performance of detection algorithms, especially if one of them does not outperform the others on both indicators. This problem can be eliminated using one aggregated metric. The useful measures reveal the degree of association between predicted and observed presence of AF. F-measure, diagnostic odds ratio, accuracy, kappa agreement, regression and correlation coefficients were closely reviewed. Result: Some measures do not take into account the true negative case, others give the same value at very different sensitivities and specificities. The phi correlation coefficient and kappa coefficient are the best measures of association between predicted and observed presences of AF. However, they significantly depend on prevalence. This is reasonable because the algorithms behave differently at extreme values of prevalence. The solution is averaging these parameters over the prevalence.

Conclusions: We propose to utilize sensitivity, specificity, average phi correlation coefficient and kappa coefficient as performance measures of atrial fibrillation detection algorithms.

SA4

Improved detection of activation timings in endoatrial electrograms through a modified sinusoidal recomposition method.

M Valinoti, G V Lozupone, P Sabbatani, R Mantovan, S Severi, C Corsi

DEI, University of Bologna, Cesena, Italy

Introduction. Atrial fibrillation (AF) is the most common type of arrhythmia and the mechanisms that sustain it are not yet clearly identified. In this regard, many theories based on atrial electrical activation have been proposed to target AF mechanisms. Because the phase of the electrograms is less affected by noise than amplitude, the phase analysis is one of the most robust method for identifying and quantifying spatiotemporal organization of fibrillation. In this work, we propose an improved method for signal phase reconstruction and atrial activation timings (AATs) detection.

Methods. Six patients with paroxysmal AF were enrolled in the study and endocavitary atrial signals acquired using a 64-electrodes contact catheter. Electrograms were analyzed by applying the standard procedure based on the Hilbert transform (HT) and with sinusoidal wavelet recomposition (SR). In addition, a new technique based on the research of maximum negative derivative of the unipolar electrograms and a modified version of signal recomposition (NDSR) was tested. Detected atrial activation timings (AATs) were compared with manual annotation performed by an expert cardiologist.

Results Comparison between AATs detected on a segment basis in 461 signals in sinus rhythm (5252 AATs) applying the three techniques are reported in the table. Mean cycle length duration (MCLD) computed applying SR and NDSR showed an error of $5.1\% \pm 4.2\%$ and $3.2\% \pm 3.4\%$, respectively.

	AAT detected	TP	FP	FN	Se (SD)	PPV (SD)
HT	30491	3424	27067	1816	63.2 (19.8)	11.1 (2.5)
SR	5339	1577	3762	3663	29.3 (10.7)	28.5 (9.3)
NDSR	5207	4359	848	881	82.6 (8.9)	83.2 (8.5)

Table. TP: true positive; FP/FN: false positive/negative; Se: sensibility; PPV: positive predictive value

Conclusion. We implemented three different computational approaches to identify atrial activities in sinus rhythm and we are testing them in AF condition with promising results. Future developments include the construction of the phase map in sinus and AF rhythm to visualize atrial electrical patterns.

SA4

Causality in Atrial Fibrillation Determined by Transfer Entropy

Katarzyna Kořna*, Daniel Steven, Stephan Willems, Jan J Żebrowski, Paweł Kuklik

Poland

Background: Atrial fibrillation (AF) is the most common and the most complex sustained arrhythmia. The mechanisms of AF are not fully understood and the treatment is suboptimal. High level of complexity makes characterization of wave conduction during AF extremely difficult. Here, we aim to use statistical approach characterizing AF a system with determined information flow using a concept of transfer entropy.

Methods: Left and right atrial electrograms at different locations (high right atrium (HRA) and coronary sinus (CS)) were recorded for 1 min using conventional catheters in 40 patients undergoing catheter ablation of AF. The procedure ended in success (spontaneous termination of arrhythmia) in 20 patients and 20 underwent electrical cardioversion due to lack of response. To assess causality in atria transfer entropy (TE) was used. Due to the fact that TE is defined on binary data, we introduced 3 methods of signal transformation. Transfer entropy was calculated between electrograms recorded along each catheter. To further explore TE properties, artificial signals connected in a chain generated with predefined uni-directional coupling (with the center signal acting as the conductor influencing neighbours which are then coupled downwards to the ends of the chain).

Results: We found asymmetry in information flow along catheters. In HRA catheter, information flows from proximal to distal portion of the catheter (from bottom to top of the atria) and in CS from the distal towards the proximal portion (from left to right atria). TE diagrams calculated using artificial signals show clear direction of information flow from the center of the chain toward its ends.

Conclusions: Information flow in the heart is asymmetric and it is possible to determine the direction of the flow. Causality analysis may be a promising tool in identification of the location within the atria sustaining AF (the "conductor") enabling more efficient catheter ablation.

SA4

Extracting Atrial Activations from Intracardiac Signals during Atrial Fibrillation using Adaptive Mathematical Morphology

S. Yazdani¹, A. Buttu¹, E. Pruvot², J.-M. Vesin¹, P. Pascale²

¹EPFL, Swiss Federal Institute of Technology

²Department of Cardiology, University Hospital Center Vaudois CHUV Lausanne, Switzerland

Purpose: Intracardiac activation time detection algorithms can be used in atrial fibrillation (AF) electrogram analysis as a first step in estimating AF characteristics, such as the AF cycle length. The performance of these algorithms is limited due to the varying morphologies and amplitudes of atrial activations. Our study aims at robustly extracting atrial activations using mathematical morphology (MM) operations with an adaptive structuring element.

Methods: Three consecutive patients (63 ± 1 y) with chronic AF (sustained AF duration 17 ± 8 m) underwent catheter ablation (CA). Before CA, multipolar catheters were sequentially placed within the four pulmonary veins and the left atrial appendage for a duration of one minute. An adaptive MM algorithm was developed to extract the atrial activations from the recordings by computing the average of the top- and bottom-hat MM operations with a predefined structuring element for a limited time window. The structuring element was then updated using a learning coefficient for every activation and continuously adapted based on morphological characteristics of the previously detected activations. For performance evaluation, atrial activation times estimated by adaptive MM were compared with those of the ground truth (manual annotation by an expert), and an implemented state of the art approach.

Results: For a total of 5216 annotated atrial activations, our method achieved a 99.1% detection rate, 99.5% specificity and 99.5% positive prediction value (PPV), against a state of the art approach with respectively 93.6%, 94.6% and 98.9% of detection rate, specificity and PPV.

Conclusions: Our preliminary results suggest that the adaptive structuring element can efficiently estimate atrial activation times. Our method works on an “activation-to-activation” basis, avoids excessive use of arbitrary thresholds, and incorporates physiological constraints. It offers low computational complexity, which makes it suitable approach for real-time/online scenarios.

SA4

Novel Filter Technique to Improve R-Peak Detection for ECG Data with Motion Artefacts from Wearable Systems

Nadine Lang*, Erik Haßlmeyer, Daniel Tantinger, Matthias Brischwein, Axel Heinrich, Heike Leutheuser, Stefan Gradl, Christian Weigand, Bjoern Eskofier, Matthias Struck

Fraunhofer Institute for Integrated Circuits IIS, Erlangen, Germany
Erlangen, Germany

The electrocardiogram (ECG) is one of the most reliable information sources for assessing cardiovascular health and training success. Since the early 1990s, the heart rate variability (HRV), namely the variation from beat to beat, has become the focus of investigations as it provides insight into the complex interplay of body circulation and the influence of the autonomic nervous system on heartbeats. However, HRV parameters during physical activity are poorly understood, mostly due to the challenging signal processing in the presence of motion artefacts. To derive HRV parameters in time (heart rate (HR)) and frequency domains (high frequency (HF), low frequency (LF)), it is crucial to reliably detect the exact position of the R-peaks. We introduce a novel filtering technique that can cope with motion artefacts in ECG data originating from physical activity. We suggest an infinite impulse response (IIR) filter instead of the commonly used finite impulse response (FIR) filter. Its advantage is the requirement of less coefficients (IIR: 6, FIR: ~70) to reach comparable quality, which results in shorter runtime. A disadvantage, however, is its nonlinear phase response. Therefore, we added a backward filter after the signal is filtered in forward direction. The same filter coefficients are used for both directional passes. The combined forward/backward filtering allows for a subsequent R-Peak detection that is robust against motion artefacts. Our R-peak detection algorithm is based on a zero-crossing algorithm (Köhler et al., 2003) that was additionally improved with respect to its robustness against motion artefacts (Tantinger et al., 2012). In preliminary tests on mobile data sets from different persons and activities (from sitting, walking and running to cycling and rowing) our developed algorithm leverages the detection accuracy of R-Peaks to 99, 93 % with only 16 false positives on 4646 detected peaks.

PB1

Assessment of the Potential of Morphological ECG Features for Person Identification

I Jekova^{1*}, I Christov¹, V Krasteva¹, G Bortolan², M Matveev¹

¹Institute of Biophysics and Biomedical Engineering, Sofia, Bulgaria

²Institute of Neuroscience, Padova, Italy

Nowadays, research on automatic person identification is focused on internal body physiological biometric characteristics, robust to hacker attacks and falsification. This work investigates ECG intra-individual differences using morphological features to study their potential for person identification.

Recordings from 146 individuals without cardiac diseases from ECG-ILSA database (standard 12-lead ECG, 10s duration) are used. Four ECG leads forming quasi-orthogonal lead system (II,III,VI,V5) are processed for extraction of averaged P-QRS-T patterns over 10s, QRS-T delineation and calculation of 15 morphological pattern features per lead: QRS-width; offset and amplitude of both maximal positive and negative peaks; slope from QRS-onset to first peak; slope from first to second peak; QRS positive, negative and total area; QRS velocity total area; number of samples crossing 70% of the maximal peak amplitude; T-wave – width, amplitude, onset-to-peak time. We calculate coefficient of variation for each feature (x): $CV(x)=100*(Standard\ Deviation(x)/Mean(x))$, to score its potential for providing large distance between samples that is important for the person identification task where enhanced intra-individual differences are beneficial.

We find the most distinctive features relevant to heterogeneous population ($CV>100\%$):

Mi_II(210%), Ar_II(116%), Mi_III(167%), S2_III(100%), Ar_III(102%), Mi_VI(124%), Mi_V5(120%), where Mi, Ar, S2 denote negative peak amplitude, QRS total area, slope from first to second peak. S2_III is strongly correlated with Ar_III ($r=-0.97, p<0.05$), and is excluded from the feature set. We apply Factor analysis by Principal components extraction method on the outstanding six features to verify the population heterogeneity.

The following accumulated variation is measured: with 6 factors (100%), 5 factors (92%), 4 factors (81%), 3 factors (66%). The accumulated variance of 66% for the first 3 factors with eigenvalues>1 presents high potential for person identification. Fig.1 is a projection of 6 features in 1st vs. 3rd factor plane, with obvious large distances. Fig.2 reveals the population heterogeneity in 3-feature space.

Fig.1. Projection of the variables on the factor-plane (1x3)

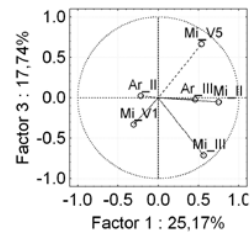
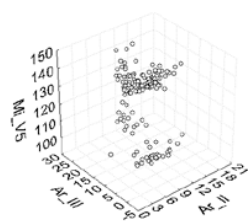


Fig.2. 3D Scatterplot Ar_II vs. Ar_III vs. Mi_V5



PB1

Adaptive frequency tracking for robust heart rate estimation using wrist-type photoplethysmographic signals during physical exercise

Sibylle Fallet*, Jean-Marc Vesin

Swiss Federal Institute of Technology
Lausanne, Switzerland

Purpose: In recent years, wearable photoplethysmographic (PPG) biosensors have appeared as very promising tools to monitor heart rate (HR) during physical exercise. However, PPG waveforms are easily corrupted by motion artifacts, rendering HR estimation difficult. To face this challenge, we developed a framework to estimate HR from PPG waveforms corrupted by motion artifacts and accelerometer (ACC) data. Our method comprises two main steps: adaptive noise cancellation and adaptive frequency tracking.

Methods: The database (2015 IEEE signal processing cup) is composed of two-channel PPG waveforms, three-axis ACC data and the ground-truth heart rates, recorded from 12 subjects running on a treadmill. In order to remove motion artifacts from the PPG waveforms, a Normalized Least Mean Squares (NLMS) algorithm was used with ACC data as reference noise inputs. Adaptive noise cancellation was applied to each PPG-ACC channel pair, resulting in six reconstructed PPG waveforms. In the second step, an adaptive band-pass filter was used to track the common frequency of the reconstructed PPG waveforms, i.e. HR. In this algorithm, the central frequency of the filter is updated every sample to track the instantaneous frequency. Each input signal contribution is weighted according to a signal-to-noise ratio parameter.

Results: Using our method, the averaged absolute error across the 12 subjects was 1.71 ± 0.49 beats-per-minute. The Person correlation coefficient was 0.994. Without NLMS, the error was 6.41 ± 6.13 beats-per-minute, highlighting the importance of motion artifacts cancellation. The results obtained demonstrate an improvement (error reduction of 27 %) compared to published results on the same database (error = 2.34 ± 0.83 beats-per-minute).

Conclusion: The proposed framework is accurate and can be implemented in almost real-time (averaged estimation delay of 1.5 seconds). Importantly, as all ACC-PPG combinations were used for motion artifacts cancellation, no assumption about individual ACC axis contribution was required.

Table 1: Summary of the results

Method	Average absolute error and standard deviation [BPM]
Adaptive frequency tracking only	6.41 ± 6.13
NLMS + Adaptive frequency tracking	1.71 ± 0.49
Published results on the same database	2.34 ± 0.83

PB1

Studying Heart Rate Variability from Ballistocardiography Acquired by Force Platform: Comparison with Conventional ECG

Alba Martín-Yebra*, Federica Landreani, Claudia Casellato, Esteban Pavan, Carlo Frigo, Pierre-François Migeotte, Enrico G Caiani

Politecnico di Milano
Italy

Aim: Ballistocardiography (BCG), measuring the heart beat-induced mass movements of the body generated by forces associated to heart contraction, has been recently reconsidered as a useful non-invasive technique to characterize cardiac performance, potentially offering a simple, efficient and affordable solution for home e-health cardiac monitoring. Our aim was to extract beat-to-beat heart rate variability series from BCG signal (B-HRV) acquired by a force platform, and to evaluate their correlation with ECG-HRV, both in time and spectral parameters.

Materials and Methods: BCG signals from 18 healthy volunteers (age range: 22-45 years) were acquired (sampling frequency 960Hz) by a capacitive 3D-force platform (Type 9286B, Kistler), simultaneously to the ECG signal, for 5 minutes in both standing (ST) and supine (SUP) positions. An algorithm to detect BCG systolic waves (H, I, J and K) in the longitudinal (head-foot) component has been developed, from which B-HRV series were computed and compared by correlation and Bland-Altman analyses against conventional HRV of RR series extracted from the ECG.

Results: All B-HRV series showed higher R^2 values and narrower confidence interval (CI, 2SD) for SUP compared to ST. For both postures, the JJ series showed the best performance (SUP: $R^2=0.998$, $CI=\pm 17ms$; ST: $R^2=0.968$, $CI=\pm 42ms$). Changes in mean RR between ST (25th-75th percentiles: 627-737ms) and SUP (792-989ms) were found in all B-HRV series, while higher normalized power at LF (PLFn) and lower PHFn in ST compared to SUP, found in HRV, was found in JJ series only, with best agreement for SUP position (PLFn: $R^2=0.92$, no bias and $CI(RR/JJ)=\pm 30\%$; PHFn: $R^2=0.89$, 21% bias(RR/JJ) and $CI(RR/JJ)=\pm 71\%$).

Conclusions: Posture affects accuracy of B-HRV time and frequency parameters compared to HRV, with the best performance obtained in SUP by the JJ series. This signal could be used as an alternative measurement of HRV in novel home e-health monitoring systems.

PB1

Cardiac Arrhythmia Recognition with Robust Discrete Wavelet-Based Feature Extraction via Classifier Synthesis of MLP-BP and PNN Neural Networks

Farhad Asadi¹, Mohammad Javad Mollakazemi¹, Seyyed Abbas Atyabi², Ali Ghaffari³

¹Young Researchers Club, Islamic Azad University, Science and Research Branch, Tehran, Iran

²Young Researchers Club, Islamic Azad University, South Tehran Branch, Tehran, Iran

³Cardiovascular Research Group (CVRG), Department of Mechanical Engineering at K.N.Toosi University of Technology, Tehran, Iran

Introduction: An ECG signal has important information that can help for reflecting cardiac activity of a patient and medical diagnosis. Consistent or periodical heart rhythm disorders can result cardiac arrhythmias. Therefore, classification algorithm for recognizing arrhythmias with satisfactory accuracy is necessary.

Aims: In this study, a robust wavelet based algorithm for detection and delineation of events in ECG signal is applied and then a new synthesis of MLP-BP and PNN neural networks for heart arrhythmia classification is described.

Methods: As a matter of fact any changes in the morphology of an ECG due to the arrhythmia were observed in time and frequency analysis so multi resolution analysis was applied for feature extraction. First, noise and artifacts were rejected by a discrete wavelet transform (DWT). Then, fiducial and J points of QRS complexes were obtained and corresponding DWT scales were segmented. Next, curve length and high order moment order based feature extraction were calculated for each excerpted segment and elements of feature vector for regulating the parameters of classifiers were obtained. After generation of feature source and segmentation, Multi-Layer Perceptron-Back Propagation (MLP-BP) neural networks and Probabilistic Neural Network (PNN) with different topologies were designed and tuned and their results were compared and also these classifier approaches were combined in parallel structure topology.

Results: The proposed algorithm was tested by all 48 record of the MIT-BIH arrhythmia database and also the proposed new topology of classifier was applied to five arrhythmias with names of Normal, RBBB, PVC, APB, VF belonging to 15 records of the MITDB. Finally, the average accuracy of 98.92% was obtained which was compared with similar studies in this subject.

PB1

Fusion Visualization for Cardiac Anatomical and Ischemic Models with Depth Weighted Optic Radiation Function

Fei Yang, Weigang Lu*, Lei Zhang, Wangmeng Zuo, Kuanquan Wang, Henggui Zhang

Ocean University of China, Qingdao, China
China

Despite the emerging of various innovations of visualization methods, highlighting and exploring the important functioning of interest of computational cardiac model still remain a challenging problem. Due to the complex and fine geometries of heart, the silhouette of the whole volume structure may be destroyed when there is a necessity to demonstrate cardiac electrophysiological behaviors. In this paper, we proposed a fusion visualization framework, which combines the electrophysiology pattern with the anatomy pattern through a novel multi-dimensional fusion transfer function and is great helpful for delineating the complicated relation between the tissue structure and its functions. Different from the intensity scalar value, those voxels with electrophysiological value in the human heart volume data represent propagation patterns of excitation waves of various tissues of the heart rather than those tissues themselves. Normal rendering model cannot explore functions of the heart at physiological or pathological conditions reliably. A depth weighted optic radiation model is thus presented in the framework to inspect the occluded cardiac ischemia information. According to the depth to the tissue boundary, the hidden ischemia region of pathological tissue can be revealed from complex overlapping features. Experiment results on the cardiac anatomy and electrophysiological simulation data verifies the effectiveness of the proposed method for intuitively exploring and inspecting electrophysiological activities with the preserved authentic context of anatomical structure, which is found to be useful in analyzing and explaining cardiac functioning phenomena.

PB1

Accuracy of Lead Removal Versus Linear Interpolation in Noninvasive Electrocardiographic Imaging (ECGI)

Laura Bear*, Mark Potse, Josselin Duchateau, Nejib Zemzemi, Rémi Dubois

France

Aims: ECGI reconstructs cardiac electrical activity from body surface potentials (BSPs). BSPs are typically recorded from upwards of 250 leads, with up to 50 unusable for various reasons. This study aims to determine the effect of this on inverse solutions, and to determine if linear interpolation of missing signals can regain information lost.

Methods: Two datasets were used: 1) synthetic data with epicardial (n=1607) and body surface potentials (n=252) for 6 pacing protocols, and 2) ex-vivo torso tank data with simultaneously recorded epicardial (n=247) and tank surface potentials (n=192) during right atrial pacing and 4 ischemic interventions. The tank data had 34 unusable BSPs, for the simulated data 40 different versions of 'broken' leads were defined: 31 small groups of 4-15 electrodes, and 9 different realistic patterns of 17-51 electrodes. Electrograms were reconstructed, using the method of fundamental solutions and Tikhonov regularization, from two sets of BSPs 1) after removing 'broken' signals (iEGM1), and 2) after replacing 'broken' signals with linearly interpolating (iEGM2). These were compared to potentials reconstructions using the full set of electrodes for synthetic data, and to directly recorded electrograms for the tank.

Results: For synthetic data, the majority of electrograms were reconstructed faithfully with iEGM1 (mean CC=0.99). For several versions of 'broken' leads, small regions of electrograms were reconstructed poorly (min CC=0.58, max RE=1.14), particularly when 'broken' electrodes were over the chest. Here, iEGM2 had lower CCs (min=-0.92) and higher REs (max=2.61) than iEGM1 (p-value<0.05). For other versions, there was no difference between iEGM1 and iEGM2 (p-values>0.05). For the tank, there was no difference between iEGM1 and iEGM2 for CCs (0.550 ± 0.309 and 0.549 ± 0.311) or REs (0.876 ± 0.182 and 0.873 ± 0.155) (p-values>0.05).

Conclusions: Missing BSPs can reduce inverse reconstruction accuracy depending on their location and number. Linear interpolation of missing BSPs does not improve, and can deteriorate reconstruction accuracy.

PB2

Exercise induced depolarization changes in BSPMs for assessment of ischemic heart disease

Michał Kania¹, Roman Maniewski¹, Rajmund Zaczek², Małgorzata Kobylecka³, Grzegorz Opolski², Leszek Królicki³

¹Nalecz Institute of Biocybernetics and Biomedical Engineering, Polish Academy of Sciences, Warsaw, Poland

²Chair and Department of Cardiology, Medical University of Warsaw, Warsaw, Poland

³Department of Nuclear Medicine, Medical University of Warsaw, Warsaw, Poland

The aim was to study the effect of exercise-induced ischemia on the distribution of heart potentials (BSPM) on the thorax surface within depolarization period. In particular the objective was to confirm effectiveness of some ECG depolarization markers in assessment of ischemic heart disease (IHD). The study group consisted of 90 patients and 33 healthy volunteers. The 67-lead high-resolution body surface potential maps were recorded before

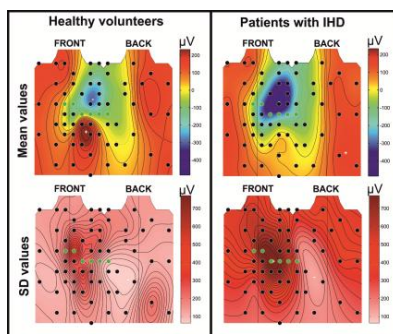


Fig. 1. Mean maps of QRS amplitude changes during exercise (Δ QRS) and corresponding standard deviation maps (SD).

and during exercise test carried out on supine ergometer. The distributions of ECG signals averaged in time at rest and at peak exercise were compared and nine ECG parameters describing exercise-induced changes in depolarization were calculated. The coronarography and SPECT results were used to verify the performance of tested parameters as IHD markers. It was observed that for patients with IHD, averaged decreases of QRS amplitude at peak exercise were higher ($-356 \mu\text{V}$) than in the group without IHD ($-163 \mu\text{V}$) and in the control group ($-127 \mu\text{V}$). Myocardial ischemia was associated also with enlargement of the area on the thorax surface, where the decrease in the amplitude and increase in shape changes of the QRS complex were observed. The effective ($p < 0.05$) parameters in the separation of patients with and without IHD were also shape parameters, like delta index determined using Distribution Function Method, and correlation coefficient. They may be used in the IHD diagnosis additionally to repolarization parameters. For IHD patients the changes in amplitude and ECG morphology were found in ECG electrodes located outside the area of precordial leads (Fig. 1). This may suggest that the standard ECG lead system is not the optimal for exercise assessment of IHD and could be improved.

Virtual Normal Bipolar and Laplacian Electrodes for Activation Map Construction in ECGi

Josselin Duchateau*, Yves Coudière, Mèlèze Hocini, Michel Haïssaguerre, Rémi Dubois

IHU LIRYC
Pessac, France

Introduction: ECGi computes pericardial potentials from high-density body surface recordings. Creation of local activation time (LAT) maps is an important post-processing requirement. The spatial and temporal low-pass effect of the torso propagation and the inverse problem resolution process, in the context of neighboring low and high amplitude sources make this task challenging. We sought to determine if heart surface laplacians and surface gradient – which can be derived from the computed potential field – would allow us to build more precise LAT maps.

Methods: Potential gradients along local surface normal vectors and surface laplacian of the potential were analytically derived from the inverse problem solution potential field. Two different datasets were used: 1) Synthetic data of epicardial and body surface potentials of 8 different simulated ventricular pacing maps. 2) In vivo clinical data from 7 different patients, with either paced (N=2) or spontaneous ventricular activation (N=5) with concomitant epicardial electro-anatomical mapping used as reference. LAT maps were calculated from either the reconstructed epicardial potentials, normal potential gradients or surface laplacians using a minimal dV/dT approach. Results On simulated data, maps derived from potentials, epicardial gradients and surface laplacians resulted in an average mean square error compared to reference (MSE) of 39.7 ± 8.3 , 36.9 ± 5.7 , 36.1 ± 5.6 ms, respectively. Differences between groups were non-significant. On clinical data, the different methods resulted in average MSE of 24.2 ± 9.1 , 20.9 ± 5.3 and 21.7 ± 6.6 ms respectively ($p=NS$). LAT enhancement was variable between subjects (Potential vs gradient MSE difference range $+5.3/-13.1$ ms; potential vs. laplacian MSE difference range $+4.5/-13.5$ ms), and maximal in paraseptal regions.

Conclusion: Normal gradients and surface laplacians could be used to create LAT maps. In simulations, and in clinical data, they resulted in a non-significant enhancement of LAT maps compared to a standard approach. They provided more local information, and were especially useful in paraseptal regions.

PB2

Generation of Combined-Modality Tetrahedral Meshes

Karli Gillette*, Jess Tate, Peter Van Dam, Eugene Kholmovski, Rob MacLeod

University of Utah
Salt Lake City, United States

Generating image based models for simulation is challenging due to the limitations of different image modalities. For example, magnetic resonance imaging (MRI) has high soft tissue contrast facilitating segmentation of the heart and other organs, whereas X-ray computed tomography (CT) scans have high bone contrast. Registering and combining components from different image modalities could accelerate geometric model generation. Quickly generated subject specific models would greatly advance applications of cardiac simulation and modeling, e.g., electrocardiographic forward and inverse problems.

In this study, we combined a pair of CT and MRI scans of a pig thorax to make a tetrahedral mesh and compared the following registration techniques: rigid, affine, thin plate spline morphing (TPSM), and iterative closest point (ICP), to superimpose the segmented bones from the CT scan on the soft tissues segmented from the MRI (background torso, heart, blood, and lung). We compared the registered CT bone segmentation to the ground truth bone from the MRI scan via the Dice coefficient and Hausdorff distance.

The Dice coefficients for TPSM, affine, rigid, and ICP were 0.23, 0.11, 0.07, and 0.10, and the Hausdorff distances were 165, 172, 118, and 150 mm, respectively. Despite relatively low Dice coefficients and high Hausdorff distances overall, the TPSM registered bones remained close to, but not overlapping, important soft tissue. Additionally, the spine followed its original curvature. The high qualitative agreement of the TPSM bone registration allows for the effective combining of segmentations from different modalities.

Generating meshes from the combined segmentations is a viable approach that could improve results in various simulated applications. Taking advantage of each modality's strength can reduce modeling building time that is critical for clinical use of patient specific modeling.

PB2

Evaluation of 2-norm versus Sparsity Regularization in Spline-Based Joint Reconstruction of Epicardial and Endocardial Potentials from Body-Surface Measurements

Jaume Coll-Font*, Jingjia Xu, Petr Stovicek, Dana H Brooks, Linwei Wang

Northeastern University
Boston, United States

Cardiac electrical imaging, reconstruction of cardiac electrical activity from body surface potentials, has gained increasing clinical interest as a noninvasive imaging modality for underlying electrophysiological phenomena. We have previously presented an approach using 1) a transmural regularization to improve the joint reconstruction of electrical potentials on both the inner and outer surface of the ventricles; and 2) a nonlinear low-order dynamic spline-based parameterization derived from the measured body surface signals to provide temporal regularization. This spline-based scheme also substantially reduces the temporal dimension, and thus the computation, required for reconstructing the complete potential sequence. This approach was tested for localizing endocardial pacing locations obtained from healthy hearts during catheter-based stimulation, using imprecise thorax geometry derived from limited computed tomographic scans. Results were promising, but the reconstructed solutions were overly smooth in space and time. Recently, L1-norm based spatial sparsity methods such as total-variation regularization have been reported to return more realistically sharp solutions in cardiac electrical imaging. In this paper, we compare and evaluate the performance of L2-norm based Tikhonov and L1-norm based total-variation regularization in conjunction with the spline parameterization. Numerical experiments were conducted on three subjects, each with multiple (~20) endocardial pacing sites. Activation isochrones and earliest sites of activation resulting from the two methods were compared, and evaluated against true pacing locations reported by the CARTO catheter mapping system. Variability was observed in the performance of the two methods across both pacing sites and subjects: while the L2 penalty provided a more accurate localization in some cases, total-variation regularization provided better solutions in others. This indicates the possibility that different norms are needed to obtain optimal solutions depending on the body-surface measurements. In our future work, we will investigate the approach of automatically inferring an optimal regularization norm from the data rather than fixing it a priori.

PB2

Method for Adult Cardiomyocytes Long-Term Viability Monitoring using Confocal Microscopy Techniques

Vratislav Cmiel*, Jan Odstřilík, Ondřej Svoboda, Larisa Baiazitova, Ivo Provazník

Brno University of Technology, Brno, Czech Republic
Brno, Czech Republic

Introduction: Enzymatically isolated cardiomyocytes are widely used in cardiovascular research as single models for their electrical and mechanical properties. Freshly isolated myocytes lose their viability and functionality very early, from single hours to single days. So their viability is usually tested before the experiments or monitored continuously in periodic time intervals. Observations using viability kits (e.g. LIVE / DEAD Cell Imaging Kit, Life Technologies) and fluorescent microscopy are often used for this purpose.

Methods: Advanced microscopy techniques together with automatic computer-based image analysis approaches were used to develop the method for long-term cardiomyocyte viability monitoring. The aim is to eliminate negative effects such as viability marker photobleaching and on the other hand, to point up different factors affecting viability. Experiments were performed on confocal laser scanning microscope equipped with gateable detectors. Adult rat cardiomyocytes were stained by Calcein that is suitable for non-toxic long time viability testing. High sensitive hybride detectors enabled time resolved and spectral study of Calcein fluorescence. We observed cell shape changes, Calcein fluorescence degradation together with its spectral properties, and fluorescence lifetime. All parameters were monitored in nine experiments including several tenths of cardiomyocytes. Time resolved and spectral image stacks were evaluated in MATLAB programming software using image analysis and reconstruction techniques. The relationship of each monitored parameters of the cardiomyocytes to viability were further evaluated statistically.

Results: The results show that there is significant decrease of Calcein fluorescence intensity in time as expected. The results show also a significant correlation between Calcein fluorescence lifetime and cardiomyocyte viability ($R > 0.9$). Adult cardiac cell shapes changes are apparent only at the last phase with ongoing necrosis - the cells change their shapes from cylindrical to circular, while Calcein fluorescence has no spectral shift. The proposed method has been shown as sufficient approach for long-term cardiomyocyte non-toxic viability monitoring.

Load-dependency in mechanical properties of sub-epicardial and sub-endocardial cardiomyocytes

Anastasia Khokhlova^{1,2}, Gentaro Iribe³, Olga Solovyova^{1,2}

¹Ural Federal University

²Institute of Immunology and Physiology Ural Branch of Russian Academy of Sciences, Yekaterinburg, Russia

³Okayama University, Graduate School of Medicine, Dentistry and Pharmaceutical Sciences, Okayama, Japan

Motivation: It is known that the mechanical properties of myocardium vary transmurally in the left ventricular wall and the heterogeneity may be associated with differences in excitation–contraction coupling in properties of cardiomyocyte from transmural regions. Although cardiomyocytes are exposed to dynamic changes in preload and afterload in intact heart, previous studies were limited in variety of applicable mechanical loading. Experimental and modeling study are used here to investigate mechanical function of sub-epicardial (EPI) and sub-endocardial (ENDO) cardiomyocytes in response to the applied load.

Methods: We investigate the differences in response to mechanical load between EPI and ENDO cells using our recently developed single cell stretch method. In this method, each cell end was held by a pair of carbon fibers to enable applying various types of physiological preload and afterload to the cells. We used our electromechanical EPI and ENDO models to simulate the responses of cardiomyocyte to the different contraction condition and to predict cellular mechanisms underlying the possible differences.

Results: No differences were observed between the EPI and ENDO cardiomyocytes in response to a change in afterload condition. Time to peak contraction (T_{\max}) was significantly longer in isotonic mode (low afterload) than in isometric mode (high afterload) while time constant of relaxation was significantly faster in isotonic mode of contraction in both cell subtypes.

Nevertheless increased preload leads EPI cells to show significantly greater delay in the T_{\max} compared with ENDO cells, resulting a decrease in transmural gradient in T_{\max} between the cells observed for low preload. Our models reproduce experimental results and suggest that differences in the kinetics of cross bridges and calcium-troponin C complexes assumed in ENDO and EPI models may essentially contribute to the differences in the preload-dependency between the cells.

Supported by The Russian Science Foundation (#14-35-00005) and JSPS KAKENHI 2628212.

PB3

Effects of Cardiac Structural Remodelling During Heart Failure on Cardiac Excitation – Insights from a Heterogeneous 3D Model of the Rabbit Atria

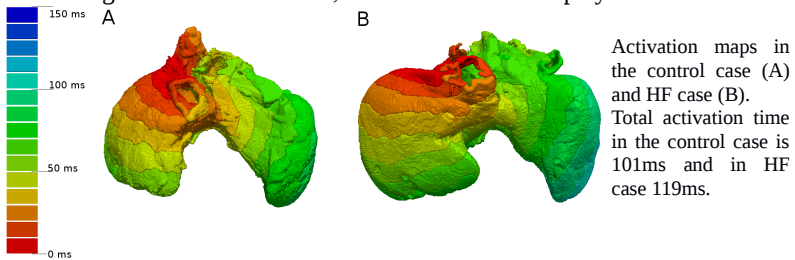
Petros Kottas, Michael A. Colman, Robert S. Stephenson, Simon J. Castro, Jonathan C. Jarvis, Mark Boyett, Henggui Zhang

Biological Physics Group, University of Manchester, Manchester, UK

Introduction: Clinical and animal model studies have shown that Heart Failure (HF) is associated with cardiac structural remodelling which includes cellular hypertrophy, tissue dilation, wall thinning and disruption of tissue fibre orientation. However, the functional impact of such structural remodelling on cardiac excitation conduction is unclear. The aim of this study is to investigate HF-induced structural remodelling on atrial excitation waves.

Methods: A multi-scale electrophysiologically detailed model of the rabbit atria was developed. The model was based on anatomical geometries of the rabbit atria, reconstructed from contrast enhanced micro-CT imaging in control and HF conditions. Using image-based analysis of the high-resolution datasets, the model was segmented into distinctive regions of the atria and tissue fibre orientation was extracted. Simulations were conducted in both anisotropic and isotropic conditions to assess the effect of fibre orientation on atrial activation.

Results: Atrial activation time was increased significantly from the control to the HF case in both anisotropic (by 19%) and isotropic (21%) conditions, due to the significantly increased tissue volume in HF. Consideration of fibre orientation in the models resulted in anisotropic conduction patterns with preferential conduction pathways in the atria, which showed that remodelling of tissue fibres in HF played little role in determining atrial activation time, whilst tissue dilation played a crucial role.



Conclusions: Atrial activation time is increased in HF as compared to the control condition due to remodeled anatomical structure (i.e. tissue size), rather than altered fibre orientation. Such an increased tissue substrate may facilitate re-entrant excitation waves in the atria.

Silicon Heart: An Easy to Use Interactive Real-Time Baroreflex Simulator

Michael Menzel*, Christopher Schölzel, Gernot Ernst, Andreas Dominik

THM University of Applied Sciences, KITE, Giessen, Germany

While the baroreflex loop is a well researched field of physiology, reliable prognosis and finding truly objective diagnostic criteria for baroreflex-related heart diseases are still difficult.

The required level of objectivity can probably only be achieved with the help of mathematical models. There are already numerous examples of such models in literature; however, to use them for diagnosis we must enable physicians to understand and use these models. Most existing models only allow to set parameters before execution while not providing any live feedback of the stimulus responses. This is not sufficient in order to analyse the dynamic behaviour of a living system.

Therefore we used extended equations of the well established Seidel-Herzel model of the baroreflex loop to build a simulator that runs in real time, and allows live monitoring and manipulation of physiological parameters.

The numerical value of important variables, such as neurotransmitter concentrations or breathing frequency, can easily be altered by turning the respective adjusting wheel. The resulting changes can immediately be observed in the measurement curves and frequency of the heartbeat flashing light.

In order to represent the physiological distribution of different components and their communication, the parts of the model are arranged on to physically separated devices. These run independently of each other, which results in a realistic asynchronous behaviour.

Our model allows to easily simulate disease conditions and medication effects, such as impaired parasympathetic function or administration of norepinephrine. It can be intuitively operated without knowledge of the implementation.

This makes the model a valuable tool to familiarise students and domain experts with the concepts of mathematical modelling.



PB3

Estimation of the Maximal Heart Rate to Improve Online Tonic-Clonic Seizure Detection using ECG

Thomas De Cooman*, Anouk Van de Vel, Berten Ceulemans, Lieven Lagae, Wim Van Paesschen, Bart Vanrumste, Sabine Van Huffel

KU Leuven
Heverlee, Belgium

Aims: Automated epileptic seizure detection using ECG is a big challenge when no patient-specific features are available. The main problem here is the high variability in the heart rate (HR) features amongst patients. When seizures last sufficiently long, a patient-specific maximum peak HR can be found. This maximum HR is a strong patient-specific feature which can increase the seizure detection performance as non-epileptic HR increases typically result in a lower peak HR. The aim here is to make an online estimation of this maximum achievable peak HR. From this estimation, we can compute a patient-independent lower boundary for the peak HR of strong HR increases, which can improve existing seizure detection algorithms using ECG.

Methods: An estimation of the maximum achievable HR is made by using LS-SVM regression. It is trained by using several pre-ictal HR features from tonic-clonic and complex partial seizures longer than 10s. Whenever a strong HR increase is detected, it is classified as an epileptic HR increase in case its peak HR exceeds the lower boundary of 90% of the estimated maximum peak HR. This algorithm is then combined with an existing algorithm using a classifier that uses both pre-ictal and ictal HR features to classify significant HR increases. Both algorithms are combined by using the AND-operator on the classification outputs.

Results: The estimation of the maximum peak HR follows the real fluctuations between the different patients very well. The combined seizure detection method was tested on more than 250 hours of nocturnal data from 7 pediatric epilepsy patients containing 24 tonic-clonic seizures. By adding the discussed procedure to an existing patient-independent seizure detector, the overall performance increased significantly: the number of false positives per hour decreased from 1.05 to 0.59, with only a limited negative effect on the sensitivity (from 22/24 to 21/24 seizures detected).

PB4

Entropy in Description of Vasovagal Syndrome Mechanism

Katarzyna Buszko*, Agnieszka Piątkowska, Edward Koźluk

Department of Theoretical Foundations of Bio-medical Science and Medical Informatics, Nicolaus Copernicus University in Toruń, Collegium Medicum in Bydgoszcz, Poland
Bydgoszcz, Poland

Entropy in description of vasovagal syndrome mechanism Katarzyna Buszko, Agnieszka Piątkowska, Edward Koźluk **Aims:** In our research we conducted nonlinear analysis of three signals: ECG, SBP (systolic blood pressure) and TPR (total peripheral resistance), which were measured simultaneously with the tilt table test. In the tilt test we examined patients recommended to diagnosis of vasovagal syncope (VVS). We used entropy of measured signals for description of the mechanism of VVS.

Methods: We examined 30 patients, that had the faint episode and were recommended to tilt table test. The tilt tests were performed with Task Force Monitor device. All examined patients fell in syncope in the supine test. For each patient the recorded values of RR, sBP, TPR were analyzed in moving windows of width of 100 points. We determined Approximate Entropy (ApEn) and Sample Entropy (SampEn) for each window. We also analyzed the value of entropy of recording signals 1-2 minutes before the faint and we compared it with the value of entropy of the signals measured in supine position. We also compared the values of the parameters: RRI[ms], HR[bpm], sBP[mmHg], dBP[mmHg], CO[l/min], SV[ml/m²] in vertical and supine position.

Results: We observed that, the values of ApEn and SampEn determined for TPR significantly decreased approximately from 0.9 to 0.4 and the decrease occurs 1,5-2 minutes before the syncope. In the supine position the mean values of: RRI=829, HR=73, dBP=70, CO=6.8, SV=93, TPR=998 differed significantly ($p<0.05$) from the mean values in vertical position: RRI=667, HR=93, dBP=80, CO=5.7, SV=60, TPR=1248

Conclusions: The changes of TPR are, apart from sBP and RRI, the predictor of VVS. In vertical position VVS is predicted by the decrease of the entropy of TPR. Entropy is useful tool for analyze RRI, sBP and TPR in diagnosis of VVS.

PB4

Is a Short Re-Feeding Program Effective in Reducing Adverse Cardiac Events in Eating Disorder Patients?

Herbert F Jelinek*, Mika P Tarvainen, David J Cornforth, Ian Spence, Jan Russell

Charles Sturt University
Australia

Patients who were admitted to the eating disorders program of the Northside Clinic, Sydney, Australia for a 6-week treatment program were assessed for improvement in both psychological and physiological health parameters. Eating disorder (ED) patients typically show improvements in weight following behavioural programs but sudden cardiac death remains a risk in those patients. Controls from a student cohort of the University of Sydney were age and gender matched with patients. The current study included recording of a 3-lead ECG for determination of heart rate in addition to clinical parameters at time of entry and completion of the program. Linear and nonlinear heart rate variability measures were determined using Kubios software available from the world-wide web from 20 minute, Lead 3 ECG recordings following a 5-minute rest period. Eighteen patients and thirty-one controls were included in the final analysis using nonparametric Signed rank analysis available on SPSS Version 20. Results comparing the change in HRV after the 6-week intervention for patients versus control are significant if $p < 0.05$ and reported as median values. No significant differences in HRV parameters were noted for the control group between Pre and Post recording periods.

For the ED group, mean RR interval length decreased significantly (Post-Pre mean RR = -64 ms, $p = 0.006$) and HF peak frequency increased (Post-Pre HF peak = 0.038 Hz, $p = 0.001$). High frequency (HF) peak indicates that the respiratory frequency has increased from Pre to Post measurement. RMSSD tended to decrease (Post-Pre RMSSD = -9 ms, $p = 0.047$) in the ED. The ED group is originally (Pre measurement) more parasympathetic during rest compared to controls, but they become more sympathetic after the intervention and thus approach the HRV measures of the controls.

PB4

Heart Rate Turbulence Modeling using Boosted Regression Trees

Óscar Barquero-Pérez, Rebeca Goya-Esteban, Arcadi García-Alberola, José Luis Rojo-Álvarez

Universidad Rey Juan Carlos
Fuenlabrada, Madrid, Spain

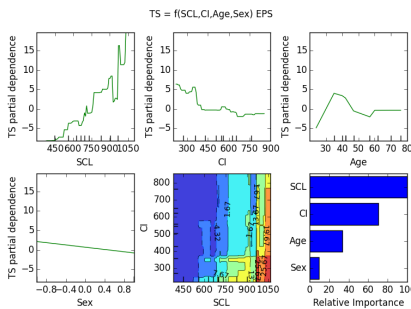
Background. Heart Rate Turbulence (HRT) is a relevant cardiac risk stratification criterion. It is accepted the baroreflex hypothesis as a source of the HRT. However, several studies showed different results about the relationship between coupling interval (CI) and HRT turbulence slope (TS) parameter.

Objective. Our aim was to propose a nonparametric model based on Boosted Regression Trees (BRT) of TS as a function of CI, heart rate (quantified by sinus cardiac length SCL in ms), Age and Sex.

Methods. We used a set of 11 patients with normal heart undergoing electrophysiological study (EPS) and 61 hollers from myocardial infarction (MI) patients (Hospital Arrixaca de Murcia). The MI set was split into: low-risk (MI-LR), and high-risk (MI-HR) according to HRT. We propose to model TS using BRT, which is an ensemble approach to build regression model using several trees.

Results. SCL was the explicative variable with the highest importance both in EPS and MI-LR. TS correlated nonlinearly with SCL, and negatively with CI both in EPS and MI-LR. The model was completely different for MI-HR. R^2 was higher for EPS (0.63) and MI-LR (0.38) than for MI-HR (0.28).

Conclusions. The model was in agreement with the baroreflex hypothesis, and the role of age and sex agrees with previous results for EPS and MI-LR. CI was the most important variable and positively correlated with TS in MI-HR.



TS partial dependence and variable importance.

PB4

Evaluation of Vital Parameter Response to Load Changes Using an Ergometer System in a Group of Healthy Subjects

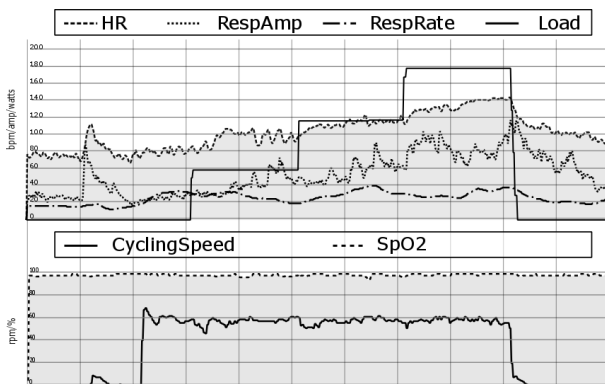
Alejandro Mendoza García, Ulrich Schreiber, Alois Knoll
Technical University Munich
Munich, Germany

Introduction: The response of the vital parameters on each person will be different depending on the physical condition. This paper describes a system that was created to evaluate these variations in order to do an estimation of the actual fitness of each individual and their improvement over time. The system consists of an ergometer with a programmable load, a Bioharness sensor to capture heart rate, ECG and respiration, a pulse oximeter for oxygen saturation and a wrist pressure sensor.

Methods: A fixed protocol was created consisting of an initial resting time of two minutes to obtain a baseline; afterwards the person was told to cycle for a comfortable speed of 55 rpm. The first minute was applied without a load, afterwards three load steps were given with an increase of 60 watts and a duration of 2 minutes between steps. Once the last step was finished the person is told to stop cycling and a cool down period of 2 minutes is recording, giving the heart enough time to recover.

Results: The graph shows the results of the session of one individual user. From this case we can observe that the heart rate started at approx. 75 bpm and reached 140 bpm when maximum load was applied. From all test subjects the resting heart rate ranged from 48 bpm to 80 bpm, and the maximum heart rate ranged from 128bpm to 181 bpm.

Conclusions: The proposed system and protocol enabled the study of reactions of the heart rate, respiration and pressure of different users, and from there obtain an estimation of their individual cardiovascular fitness.



PB4

Validation of Fetal Autonomic Brain Age Score

Dirk Hoyer*, Uwe Schneider, Dietrich Grönemeyer, Peter van Leeuwen

Germany

Aims: In connection with the evaluation of normal fetal functional maturation and developmental disturbances we have previously introduced the Fetal Autonomic Brain Age Score (fABAS). The score is based on heart rate pattern indices that are related to universal principles of developmental biology. fABAS was fitted to 30 min fetal magnetocardiographic (fMCG, Jena) recordings of 30 min duration as well as to 10 min subsets in active and quiet sleep. The present work aims at the validation of the fABAS methodology on 5 min recordings from an independent data base (fMCG, Bochum). Methods fABAS was adapted and cross-validated using previously described fMCG recordings from the Biomagnetic Center of the Jena University Hospital used as learn set and independent fMCG recordings from the Grönemeyer Institute for Microtherapy, University Witten/Herdecke used as validation set (5 min recordings, 510 of normal and 81 of fetuses with intra-uterine growth restriction (IUGR), aged 20-40 weeks of gestation). Results In spite of the higher level of snapshot like sampling of 5 min periods the fABAS methodology generally allows the assessment of the autonomic brain age maturation as well as of IUGR related changes. The results from both study centers are comparable. Conclusions fABAS obtained from fMCG recordings is a strong candidate for standardized assessment of functional maturation age and developmental disturbances. Even 5 min recordings seem to be valuable for screening for maturation problems. This is important with respect to the early identification of fetal developmental disorders that have implications for health problems in the later postnatal age and that cannot completely be compensated by later postnatal therapies.

PB4

Changes in Instantaneous Complex Dynamics during Exercise in Chronic Mountain Sickness

Gaetano Valenza*, Francesco Faita, Lorenza Pratali, Nicola Vanello, Antonio Lanata, Riccardo Barbieri, Enzo Pasquale Scilingo

Italy

Introduction: The combination of polycythemia and a variety of clinical symptoms (decreased physical performance, pulmonary hypertension, and an impairment in cerebral function) has been defined as chronic mountain sickness (CMS). The function of the autonomic nervous system in CMS remains to be defined. The nonlinear and complexity analysis of heartbeat dynamics has never been performed in dynamics protocol involving patients with CMS.

Aim: We hypothesize that tracking cardiovascular complexity of heartbeat dynamics can increase the knowledge on the CMS physio-pathology.

Materials and Methods: We studied heartbeat dynamics in 13 CMS males (age 52 ± 11) and 7 high altitude male dwellers as controls (C) (age 49 ± 10) during semi-supine bicycle exercise. All the data were acquired at 25W, 50W, and 100W along with a recovery session, and tested for statistical differences using Mann-Whitney non-parametric statistics. Instantaneous Dominant Lyapunov exponents (IDLE), as estimated through point-process nonlinear models with Laguerre and Volterra expansions, were evaluated from such series.

Results: Results showed that instantaneous heartbeat complex dynamics was significantly altered in CMS. Significant differences were found between CMS and C during the 25W ($p=0.00512$; IDLE C: -0.0768 ± 0.0378 ; IDLE CMS: -0.0037 ± 0.0591) and 50W ($p=0.0089$; IDLE C: -0.1283 ± 0.0081 ; IDLE CMS: 0.0075 ± 0.0794) sessions. Conversely, differences were not significant when analyzing the 100W session ($p=0.3402$; IDLE C: -0.1081 ± 0.0187 ; IDLE CMS: -0.0809 ± 0.0438).

Conclusions: Significant differences in IDLE were found during physical activity at 25W and 50W, with higher complexity level associated to CMS. Similar complexity changes between CMS and C were found during high intensity (100W) physical activity. Our results show for the first time that the time-varying complexity of the heartbeat is higher in CMS during exercise, both in low and medium degree of effort.

PB4

A Method to Measure Ventilation Rate during Cardiopulmonary Resuscitation using the Capnogram

Andoni Elola, Beatriz Chicote, Elisabete Aramendi, Erik Alonso, Unai Irusta, Mohamud Daya, James K Russell

University of the Basque Country (UPV/EHU), Bilbao, Spain

Hyperventilation, common both in- and out-of-hospital cardiac arrest, has been associated with worsened outcomes. Resuscitation guidelines emphasize the importance of good quality cardiopulmonary resuscitation (CPR), including ventilations at $8\text{-}10\text{ min}^{-1}$. The capnogram can be used to monitor ventilation, but chest compressions (CCs) introduce signal artifacts. There is limited information on automatic methods to guide ventilation during CPR.

Aim: Development of a method to detect ventilations in the capnogram, to give feedback on ventilation rate during CPR.

Materials: Twenty out-of-hospital cardiac arrest episodes were collected using the Philips HeartStart MRx monitor/defibrillator between 2006-2010 by Tualatin Valley FireRescue, Tigard, OR(USA). Each episode comprised: the capnogram, thoracic impedance, and compression depth signal(used to annotate intervals with CCs). In total, 848 min with 6307 ventilations were processed, 87% of time during CCs.

Methods: Ventilations were manually annotated observing the impedance and the capnography signals (gold standard). The capnogram was preprocessed, and the initial inspiration and expiration times of potential ventilations were automatically detected using the first difference. The algorithm identified real ventilations based on: duration of inspiration baseline, amplitudes of baseline/plateau intervals, and initial surface of expiratory plateau. The instantaneous ventilation rate was computed every 15 s using a sliding window of 1 min. Hyperventilation was defined as rates above 15 min^{-1} .

Results: The mean instantaneous ventilation rate from the gold standard was $14\pm 7.6\text{ min}^{-1}$, with 37% incidence of hyperventilation. The sensitivity(SE) and Positive Predictive Value (PPV) for the capnogram based ventilation detector were 96/96% (94/92% during ongoing CCs). The mean error in ventilation rate was $0.6\pm 1.2\text{ min}^{-1}$ and the SE/PPV for hyperventilation detection were 99/97%.

Conclusions: An algorithm is provided to detect ventilations in the capnogram during CPR, even in intervals artefacted by chest compressions.

PB4

Changes in Respiration During Emotional Stress

Alberto Hernando*, Jesús Lázaro, Adriana Arza, Jorge Mario Garzón, Eduardo Gil, Jordi Aguiló, Raquel Bailón

Spain

Although stress is a physiological response to a threatening situation, when it is prolonged or repetitive, it has been associated with psychic and somatic diseases. Thus, the importance of the objective measure and identification of stress. Respiration is one of the physiological variables affected by stress. In this work, we analyze changes in respiration during emotional stress induced by a modification of the Trier Social Stress Test in young healthy subjects. 23 volunteers (9 men) age 22.09 ± 3.2 y.o., participated in the study. The following stages in the test were analyzed: the prerelaxing stage (PR), the story telling stage (ST), where subjects are listening to stories that they must remember, the anticipation of stress (AS), where subjects are waiting for their evaluation, and the video exposition stage (VE), where a video showing the subject's performance is displayed in front of an audience. Respiration signal is recorded during the whole test using a thoracic band. Power spectral density (PSD) of respiration is computed in running windows of 2 minutes with 1 minute overlap using Welch periodogram. From each window, the respiratory frequency (RF) is estimated as the largest peak of the PSD. Then, the power around the peak is computed in a bandwidth of 0.04 Hz, and divided by the total power. This normalized respiratory peak power (RP) represents the concentration of power around the RF and is related to the variability of the RF within the interval. Respiratory parameters RF and RP from the 2-minute-windows are averaged in the analyzed stages. The median of mean RF for all subjects is significantly higher during stress stages than during relax, while the median of mean RP is lower (Table I). Results show that during stress stages respiratory frequency is higher and more variable than during relax (* $p < 0.05$ in Wilcoxon test).

Cost-efficient Accurate Monitoring of Respiration Rate Using ECG

Saeed Babaeizadeh

Advanced Algorithm Research Center, Philips Healthcare
Andover, MA, USA

Background: Respiration rate (RR) can be estimated from ECG which is useful when ECG, but not respiration, is monitored. Examples include wearables that monitor heart rate and rhythm, but not respiration except maybe through impedance. Measuring impedance, however, adds to the hardware cost and is prone to motion artifact. This study evaluates RR estimation using ECG beat-to-beat variations in either time intervals or QRS amplitude in one or two leads.

Method: PhysioNet/cebsdb database was used that contains two annotated channels of ECG and one channel of respiratory signal from a thoracic piezo-resistive band (RESP) on 20 presumed healthy volunteers. Three different techniques were used to derive the respiration waveform from ECG: 1) measure the peak to trough amplitude in each normal QRS in lead I or II (EDR_I and EDR_II); 2) use measurements in method 1 to get the mean heart axis (EDR_I&II); 3) measure peak-to-peak time variations due to respiratory sinus arrhythmia (EDR_RSA). RR was estimated as the oscillation frequency in a 30-second window sliding at 5-second steps. RESP was used as reference.

Results: A total of 9474 sets of RR values were analyzed. The rate from RESP was compared to that from other waveforms.

Compared to RESP	Mean±Std of Difference (bpm)	Correlation Coefficient
EDR_I	0.12 ± 1.12	0.95
EDR_II	0.08 ± 1.47	0.91
EDR_I&II	0.15 ± 1.16	0.94
EDR_RSA	0.94 ± 2.81	0.65

QRS amplitude performs better than RSA in these presumed healthy individuals. For cardiac patients with less pronounced RSA, this difference in accuracy may be even larger. Lead I is better than lead II or combination.

Conclusion: Respiration rate can be accurately estimated from a single lead of ECG. The huge advantage is no need for additional hardware for patients whose ECG is monitored. This estimation is more accurate by analyzing changes in QRS amplitude than in heart rate.

PB4

New Indices for Sleep Apnea Detection in Long-Time ECG Recordings

Agata Pietrzak, Gerard Cybulski*

Warsaw University of Technology
Warsaw, Poland

We used our computer program enabling detection of sleep apnea using long-time, one-channel ECG signal recordings. It allows the calculation of six commonly accepted heart rate variability (HRV) parameters in the time domain: the mean value of the RR interval, the standard deviation of the differences in duration between pairs of successive NN's ("successive differences"), the root mean square of successive differences, the number of successive difference exceeding 50 ms, the proportion of NN50 to the total number of NN's, and the standard deviation of the successive differences (SDSD). We also introduced an additional 34 indices which were created as combinations of some or all of the six basic HRV indices. For testing, we used 70 sample recordings from the Physionet database each containing single ECG signals 7 to 10 hours long. The analysis was performed on samples lasting 10000 seconds. The efficiency of the obstructive sleep apnea detection software was evaluated using the Receiver Operating Characteristic (ROC) method. For the six basic HRV indices, we found that the highest accuracy of discrimination was achieved for SDSD (88.5%). The area under the ROC curve was 0.89. The sensitivity and specificity were 96% and 70%, respectively. For one of the newly proposed indices, the average sum of squares of all six base indices, the accuracy was at the level of 90%. The area under the ROC curve was 0.90 and the sensitivity and specificity were 98% and 70%, respectively. It seems that further investigation of sleep apnea detection indices based on long-term ECG recordings is essential.

Accelerations versus Decelerations of the Heart Rhythm Differentiate Vasovagal Sensitive Humans

Danuta Makowiec, Wieslaw Miklaszewski, Beata Graff, Dorota Wejer, Zbigniew Struzik

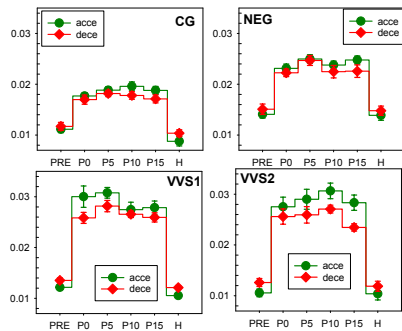
Institute of Theoretical Physics and Astrophysics, Gdańsk University
Gdańsk, Poland

Aims: Accelerations (driven by sympathetic branch of autonomic nervous system(ANS)) and decelerations (maintained by vagal activity), recorded during a head-up tilt (HUT) test, provide the information about the complex interplay between sympathetic and vagal responses to a rapid, though controlled, deregulation of homeostasis. We ask if the double exponential function which approximates the distributions of accelerations and deceleration can be used in assessing vasovagal pathophysiology evoked by the HUT test.

Methods: The HUT test was performed on 150 vasovagal patients. Each recording was divided into six five-minute windows: PRE, P0, P1, P2, P3, H. The PRE window represents the heart rhythm before tilting, windows P0–P3 in the up-right position, and H window back in the supine. The results are grouped accordingly to the HUT test result: negative (NEG, 50 subjects), syncope of mixed type (VVS1, 74 subjects), syncope of cardiodepressive type (VVS2, 26 subjects). The control group was established from the HUT test results obtained from 34 healthy individuals who did not faint during the test.

Results: Coefficients *acce* and *dece* change systematically in all groups considered. Their values increase in the up-right position. The size of the increase can be related to the strength of reflexes activated in response to the change in a body position.

A higher discrepancy between values of *acce* and *dece* observed in the groups VVS1 and VVS2 consisting of patients who fainted, than in the groups CG and NEG of people who did not faint, suggests that the difference between *acce* and *dece* measures the imbalanced ANS activation.



Coefficients *acce* and *dece* of the exponential $acce = e^{\Delta RR}$, $\Delta RR < 0$, and decelerations $dece = e^{-\Delta RR}$, $\Delta RR > 0$ in different time windows of the HUT test.

PB4

Visualization of Autonomic Drive on the Heart Rhythm by Network Representation of RR Increments

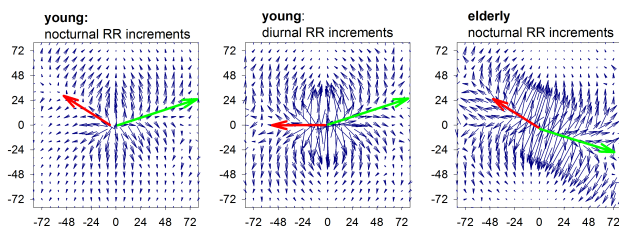
Danuta Makowiec, Zbigniew Struzik

Institute of Theoretical Physics and Astrophysics, Gdańsk University
Gdańsk, Poland

Introduction: The complex interplay between two branches of autonomic nervous system, sympathetic and vagal, in a healthy subject alternates due to the circadian cycle and aging. Beat-to-beat changes in RR intervals, called RR increments, when transformed into networks of transitions, provide a method for the attractive visualization of the alternations in dynamics of autonomic regulation caused by circadian cycle and aging.

Methods: At least 20 000 of subsequent RR increments, from diurnal and nocturnal parts of 24h Holter ECG recordings of healthy young (36 of age 19–29) and healthy elderly (18 of age: 80–89) subjects, are represented by transition networks. Each transition network describes conditional probability that a given RR increment will occur if some RR increment has occurred. Then the networks are pooled according to age and circadian cycle. Finally, the network structure is represented by gradient plots obtained from the network nearest-neighbors.

Results: Because of sympathetic domination during the day and vagal prevalence during the sleep, the interpretation to the intricate structure of the gradient graphs can be as follows. The



Gradient plots of transition networks for young and elderly subjects. Axis labels correspond to RR increments. The clocks hands are added to resemble the conclusion: a nine-past-ten for diurnal versus ten-past-ten for nocturnal rhythm in young people, and ten-past-twenty in case of nocturnal heart rhythm in elderly subjects.

left part of the plot reveals sympathetic activity, the right part displays vagal activity. If so, one can conclude that aging alternates the vagal regulation during the sleep from the persistent type in youth to the antipersistent one in the elderly.

Endurance Exercise Improves Heart Rate Complexity in the Presence of Vagal Withdrawal in Young Adults

Steven Perkins, Herbert Jelinek*, Beverlie de Jong, David Cornforth, Mika Tarvainen, Hayder Al-Aubaidy

Charles Sturt University, Albury, NSW, Australia
Australia

Sudden cardiac death (SCD) has been reported during and following physical activity. SCD may be due to vagal withdrawal and/or sympathetic dominance associated with the exercise occurring at any time during, immediately following, or up to several days after exercise. Heart rate variability (HRV) describes the influence of the autonomic nervous system on heart rate using time and frequency domain methods as well as nonlinear algorithms such as fractal and entropy-based analysis. Multiscale Renyi entropy is a nonlinear analysis option, which highlights the complexity of the heart rate at varying scales. In a pilot study we assessed the immediate post-exercise influence of endurance training on HRV in young adults. As expected, the linear domain parameter - root mean square of successive RR interval differences (RMSSD) showed vagal withdrawal (median; pre = 36.6 ms versus post = 24.6 ms) suggesting a possible increased risk of adverse cardiac events. However multiscale Renyi entropy indicated an increased complexity of the heart rate with entropy increasing following exercise in individuals participating in the training (median; pre = 1.146 versus post = 1.159). Despite decreased vagal influence, endurance training may be protective for some individuals that retain a higher heart rate complexity in the presence of vagal withdrawal.

PB5

Mental Stress Measurement- A Comparison Between HRV based and Respiration Based Technique

Shreyans Gandhi*, Maryam Shojaei Baghini, Soumyo Mukherji

Indian Institute of Technology Bombay
Mumbai, India

Background: There are many academically used methods based on Heart Rate Variability (HRV) for measurement of stress, yet the sensitivity of these methods for mental stress measurement is questioned in real life setting. Inhalation and exhalation during breathing is related to the sympathetic (SNS) and parasympathetic nervous system (PNS) balance. Stress being the disturbance of the SNS and PNS, changes the patterns of breathing. In this paper we present a novel respiration based method for stress measurement, tested on a population of 253 subjects using wearable sensors.

Method: Study was conducted on 253 subjects whose stress was measured in a carefully controlled setting via analysis of biomarkers collected by sensitive but readily available mobile sensors. Variation in detected stress for HRV based methods is discussed and same analysis is shown for respiration-based method. ECG sampled at 1kHz and respiration sampled at 20Hz was used for analysis. standard window size of 5 minute was used for calculation. Normal phase was of 40 min duration while stress was of 20 min. In normal phase, there is major frequency component present in power spectra of respiration signal. In stress phase, power spectra is distributed over larger frequency spectrum. There is no consistent dominant frequency of respiration. The rate and the amplitude varies, showing the non-rhythmic breathing. The disturbance is not consistent during the stress phase. The extent of disturbance changes with the acute stress instances. Spectral power with 1Hz band centered at dominant frequency peak gives a estimate of rhythmicity of respiration, which if used for detecting stress, gives better results than standard HRV methods ($p < 0.05$).

Conclusions: There is significant variation in sensitivities and artifact resilience across different HRV methods. Respiration can be used as a alternate method. Respiration if combined with existing methods may give more robust marker for mental stress measurement.

Evolution of the Heart Rate Variability Complexity during Kangchenjunga Climbing

Óscar Barquero-Pérez, Rebeca Goya-Esteban, Antonio Caamaño, Elena Sarabia Cachadiña, Carlos Martínez-García, José Luis Rojo-Álvarez

Universidad Rey Juan Carlos
Fuenlabrada, Madrid, Spain

Introduction. At high altitude there is a reduced oxygen pressure in the atmosphere which results in physiological changes. Heart Rate Variability (HRV) is a technique to quantify the autonomic nervous system regulation of the heart rate, allowing a noninvasive assessment in extreme environments.

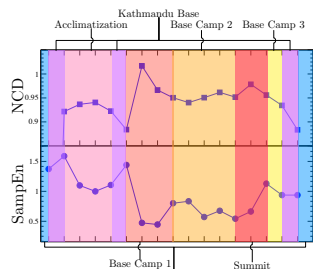
Aim. The aim of this work was to assess the evolution of the HRV complexity during Kangchenjunga (8.586 m) climbing.

Data. Three climbers recorded their RR-interval time series every day during the expedition. We divided the data in different stages: Spain Baseline, Kathmandu Baseline, Acclimation Trekking, Kathmandu After Acclimation, Base Camp, Camp 1, Camp 2, Summit, Camp 3, and Kathmandu after expedition.

Methods. We assessed the complexity of HRV using sample entropy (SampEn) and normalized compression distance (NCD), a measure coming from Information Theory, which compares two arbitrary sequences and outputs the dissimilarity between them. This measure exploits linear and nonlinear relations in the data and allows the comparison of sequences of different sizes. We estimated the dissimilarity of every stage in the climb against the first day using NCD.

Results. From the beginning and during acclimation dissimilarity (NCD) increased and then decreased once the climbers were acclimated. Dissimilarity jumped up in Base Camp stage. Then dissimilarity decreased from this point until the end of the expedition. SampEn showed an irregular behaviour without a clear pattern.

Conclusion. NCD provided a method to assess the dissimilarity of HRV between different stages in Kangchenjunga expedition climbing, and allowed to quantify the changes in HRV complexity.



NCD and SampEn evolution during the expedition for one climber.

PB5

Lower Instantaneous Entropy of Heartbeat Dynamics during Seizures in Untreated Temporal Lobe Epilepsy

Riccardo Barbieri*, Gaetano Valenza, Luca Citi, Fabio Placidi, Francesca Izzi, Maria Albanese, Maria Grazia Marciani, Maria Guerrisi, Andrea Romigi, Nicola Toschi

Massachusetts General Hospital - Harvard Medical School
United States

Introduction: Temporal lobe epilepsy (TLE) is associated with dysfunction of the autonomic nervous system, and cardiac events and/or central hypoventilation have been suggested as possible contributing factors in sudden unexpected death in epilepsy patients (SUDEP). While it is known that heart rate variability (HRV) changes in epilepsy comprise both ictal and interictal autonomic cardiac effects, the mechanisms leading to these alterations are not well understood. In this paper we investigate the alterations in instantaneous autonomic complexity during the ictal phase in untreated TLE.

Methods: Bipolar ECG recordings (sampling frequency: 256 Hz) were collected from 10 patients (age: 40.4 ± 17 years) with at least one seizure originating from temporal regions as recorded by video-EEG monitoring. For each patient, we selected a) a 2-minute long artifact-free interictal period (INT) and b) a 2-minute long artifact-free period containing a seizure (CRI) occurring at rest and during wakefulness in supine state. We computed mean values (over each recording period) of traditional HRV indexes, as well as novel instantaneous point-process Approximate and Sample Entropy (ipApEn and ipSampEn, respectively), and tested for significant effects (INT vs. CRI) using nonparametric statistics.

Results: Traditional ipApEn was significantly lower ($p < 0.02$) and ipSampEn was lower ($p < 0.065$) in CRI vs. INT (ipApEn: 0.1674 ± 0.0100 vs. 0.3035 ± 0.0268 ; ipSampEn: 0.1126 ± 0.0150 vs. 0.1993 ± 0.0220). The variability (median absolute deviation - MAD) of ipApEn was also significantly lower ($p < 0.03$) in CRI vs INT (0.0189 ± 0.0027 vs. 0.0233 ± 0.0023). No other significant differences were detected.

Conclusions: Our results suggest that ictal events in untreated TLE are associated with a decrease in heartbeat complexity and variability over time, possibly pointing toward subtle autonomic changes which may accompany or precede seizures and can only be detected using an instantaneous, time resolved approach to quantifying autonomic complexity.

Early Prediction of Ventricular Tachyarrhythmias based on Heart Rate Variability Analysis

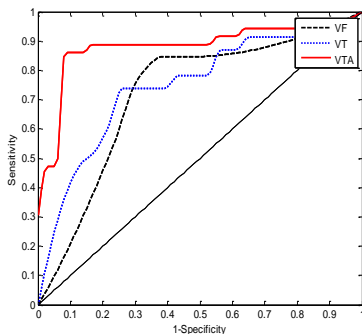
Hyojeong Lee, Myeongsook Seo, Segyeong Joo

Asan Medical Center, University of Ulsan College of Medicine
Seoul, Korea

Ventricular tachyarrhythmias (VTAs) are fatal events and it is obvious that early prediction of VTAs could help in reducing mortality rate due to sudden cardiac death (SCD). Heart rate variability (HRV) reflects all symptoms associated with autonomic nervous system as well as heart disease. Our group already developed a predictor for VTAs before 10s ahead of the events. To improve the performance of this predictor, in this study, we tried to predict VTAs earlier than 1-hour using parameters from HRV analysis and artificial neural network (ANN).

To collect electrocardiograms (ECGs) from patients, we developed a system for retrieving ECGs in real-time from 15 patient monitors in an intensive care unit (ICU) at Asan medical center (AMC) after obtaining approval from institutional reviewer board (IRB). ECGs from patients with implantable cardioverter defibrillator (ICD) and pacemaker were excluded and every ECGs of VTA events were reviewed by an experienced physician. RR intervals of 5 minutes before 1-hour from every VTA event were collected and for the control dataset, RR intervals of 5 minutes from the same patient were extracted when there was no events for at least 1 day after the collection period. Total VTA events collected were 110 (71 ventricular tachycardia (VT) and 39 ventricular fibrillation (VF) events). Therefore, total database used in this study contains 110 VTA data and 110 control data. For each data, 11 parameters of HRV analysis were calculated as in the previous research.

Three Classifiers with ANN were developed to predict VT, VF, and VTA (VT+VF). Randomly selected 2/3 of data were used in training ANNs and the remaining 1/3 of data were used for performance evaluation of the trained ANN. The performance of the predictors are shown in the figure. Area under the curve for predictors for VT, VF, and VTA are 0.74, 0.74, and 0.88, respectively. Although there are several limitations, the result is quite encouraging and these predictors can be adopted in many health-care devices with a little more improvement.



ROC curves for predictors for VT, VF, and VTA

PB5

The Development of LF/HF Ratio and its Dependence on the Mean Heart Rate in Children and Adolescents

Eva Zavodna*, Jana Hruskova, Ksenia Budinskaya, Zuzana Novakova, Hana Hrstkova, Ludmila Brazdova, Natasa Honzikova

St. Anne's University Hospital Brno
Brno, Czech Republic

In our previous study (Zavodna CJPP 2006; 84(12):1275-83), we shown how the dependency of the baroreflex sensitivity on the inter-beat intervals (IBI) can influence the results of a study and cover up the developmental changes. Therefore we decided to analyze another parameter – LF/HF ratio that assesses sympatho-vagal balance. We examined 424 healthy children and adolescents aged 11 to 20 years by the continuous noninvasive blood pressure monitoring for 5 minutes at rest with breathing regulated on 0.33Hz. IBI [ms] and heart rate (HR) [Hz] were measured beat-to-beat from the 3 min artefact-free recordings. Mean IBI and HR were calculated for each recording and their power spectra were calculated. LF/HF ratios of IBI and HR spectra were determined. The statistic was done for a whole group, and for subgroups of older children (11-15 years), adolescents (16-20 years), and for 10 particular age-subgroups. In the whole group and the subgroup of adolescents, we shown significant relationship between age and mean IBI or HR, but LF/HFIBI or LF/HFHR were age-independent. The analysis of the subgroup of children shown, that not only IBI and HR but also LF/HFIBI or LF/HFHR were significantly age-dependent. The further analysis showed a negative significant correlation of IBI vs. LF/HFIBI and a positive correlation of HR vs. LF/HFHR in the whole group and in children or adolescents. Significant relationship IBI vs. LF/HFIBI and HR vs. LF/HFHR was in particular age-subgroups from 11 to 14 years, but it was insignificant in subgroups from 15 to 20 years. Our analysis showed the increase of LF/HF ratio up to the age of 15 years. when the development of sympatho-vagal balance seems to be finished. Strong relationship between IBI or HR and LF/HF ratios could covered the development changes. Supported by European Regional Development Found (No.CZ.1.05/1.1.00/02.0123).

PB5

The Effect of Voltage-Sensitive Dye di-4-ANEPPS on Heart Rate Variability in Langendorff-Perfused Isolated Rabbit Heart

Oto Janoušek*, Marina Ronzhina, Jakub Hejč, Veronika Olejníčková, Tibor Stračina, Kateřina Fialová, Marie Nováková, Ivo Provazník, Jana Kolářová

Brno University of Technology
Brno, Czech Republic

Aims: It is known that di-4-ANEPPS causes prolongation of action potential duration in isolated cells, although this phenomenon has not been observed in the whole organ. In order to reveal any di-4-ANEPPS-induced changes in the system controlling heart rate, the effects of di-4-ANEPPS on heart rate variability during staining and washout were investigated.

Methods: Time domain, frequency domain and non-linear HRV parameters (21 in total) were evaluated on tachograms from five New Zealand White rabbit isolated hearts perfused on Langendorff apparatus with Krebs-Henseleit solution (1.25 mM Ca²⁺, 37°C, 85 mmHg). Diluted di-4-ANEPPS (stock solution 2 mM diluted in perfusion solution up to final concentration of 2 μ M) was administered (25 minutes) into the cardiac tissue via coronary system. The same period was used for washout and control. Experiment were performed in dark to avoid photobleaching.

Results: The effect of di-4-ANEPPS was quantified by Wilcoxon rank-sum test for two pairs of experimental conditions: (1) control – loading and (2) loading – washout. There are no statistically significant ($\alpha = 0.05$) differences in HRV parameters in both control-loading and loading-washout pairs of experimental phases. However, remarkable trends appear in some HRV parameters: (a) RR interval duration prolongs in the first three minutes of loading; (b) the short-time variation of tachograms increases after 15 minutes of loading; (c) the complexity of the tachogram rapidly increases due to di-4-ANEPPS loading and effect of di-4-ANEPPS on the system controlling the heart rate is irreversible.

Conclusions: The presence of di-4-ANEPPS molecules in the heart tissue affects heart rhythm, but the degree of di-4-ANEPPS influence on heart rhythm is insignificant. It can be concluded that di-4-ANEPPS may be used in cardiac experiments combining optical mapping with heart rhythm analysis, however the RR interval prolongation due to di-4-ANEPPS loading should be considered.

PB5

Changes in Heart Rate Circadian Rhythm following Exercise in Middle-Aged Men

Herbert F Jelinek*, Chandan Karmakar, Antti M Kiviniemi, Mikko P Tulppo, Timo H Mäkikallio, Arto J Hautala, Heikki V Huikuri, Ahsan H Khandoker, Marimuthu Palaniswami

Australia

Exercise have been associated with improved cardiovascular health. Health effects of exercise may be associated with the circadian rhythm of the heart and may specifically reduced the risk of heart attacks during high-risk periods over the 24 hours. Linear and nonlinear heart rate variability (HRV) measures indicate the degree of heart rate modulation by the autonomic nervous system. Twenty-one sedentary middle-aged men underwent an 8-week moderate-volume exercise program and 24-hour heart rate recordings were obtained prior and following the exercise period. Temporal dynamic changes over the 24-hour period were calculated using the complex correlation measure (CCM) derived from the Poincaré Plot and analyzed in 1-hour intervals. The maximum significant differences between pre and post moderate-volume exercise were between the morning hours of 8.30 to 9.30 AM ($p=0.011$) and in the afternoon between 4.00 and 5.00 PM ($p=0.021$). In the morning the temporal dynamics (mean \pm sd) increased from 0.1 ± 0.02 to 0.15 ± 0.06 . In the afternoon period the increase was from 0.11 ± 0.04 to 0.14 ± 0.05 . An increase in CCM indicates a more complex temporal dynamics of the heart rate and an improved parasympathetic influence.

Evaluating Valence level of Pictures Stimuli in Heart Rate Variability Respons

Shahab Rezaei*, Sadaf Moharreri, Nader Jafarnia Dabanloo

Islamic Azad University, Khomeini Shahr Branch, Isfahan, Iran
Iran (Islamic Republic of)

Valence, as used in psychology of emotions, means the attractiveness (positive valence) or aversiveness (negative valence) of an event, object, or situation which is also used to characterize and categorize specific emotions. Heart Rate Variability, the variation over time of the period between consecutive heartbeats, is thought to reflect the heart's ability to adopt to changing circumstances by detecting and quickly responding to unpredictable stimuli. In this paper, we try to use heart response to stimulation with two groups of pictures that are labeled as positive valence which are pleasant for the subjects and negative valence which are unpleasant to them. For this purpose, we used valence part of the Self-Assessment Manikin Test to measure and determine the effects of pictures on subjects which were used as a visual stimulus while the lead II of ECG was recorded from 20 boys as subjects during the stimuli. Time, frequency and nonlinear parameters of the signals have been extracted. The results show that the heart rate increase in response to the positive pictures while it had a decrease in response to negative pictures. The frequency power in LF and HF bands increase in positive and negative mode, respectively. After evaluating the results, we used Kruskal-Wallis test which is a nonparametric version of ANOVA analysis distribution to define the level of significance of each feature for different groups of subjects to demonstrate and distinguish the effects of positive and negative valence in heart rate. The results show that, for instance, the features are able to discriminate this two groups by $p < E-4$ for frequency features; $p < E-3$ for Poincare plot features (SD1 and SD2) and $p < E-2$ for nonlinear features such as Sample Entropy.

Reduced Variability in Pulse Wave Velocity and Heart Rate in Depressed Patients with Suicidal Ideation

Ahsan Habib Khandoker*, Veena Luthra, Yousef Abou Allaban, Raqibul Mostafa, Nayeefa Chowdhury, Khawza I Ahmed, Simanto Saha, Herbert Jelinek

Khalifa University
Abu Dhabi, United Arab Emirates

Major depressive disorder (MDD) is emerging as an independent cardiovascular disease risk factor. Globally, suicidal behaviour is the third most common cause of death among depressed patients (fifteen percent of depressed patients die by suicide). However, its treatments, employing medication and psychological interventions are only partially effective, as the biological understandings of the phenomena remain ill-defined. The aim of this study was to investigate if Heart Rate Variability (HRV) and Pulse Wave Velocity (PWV) are different in MDD patients with suicidal ideation and healthy volunteers. 22 unmedicated MDD patients with a history of suicidal ideations (Age: 33.2 ± 14.5 years) and 46 healthy volunteers (Age: 31.5 ± 10) were recruited for a case-control analysis at a psychiatric clinic in the UAE. We used the Hamilton Depression Rating Scale and the Beck Depression Inventory to assess depression severity. Cardiac autonomic function was evaluated by the measurement of HRV parameters. Frequency-domain indices of HRV were obtained. PWV was estimated from ratio of half of the height and Pulse Transit Time which is defined as the time delay between the R-wave of the ECG and the arrival of the pulse wave in the index finger. MDD Patients were found to have reduced cardiac vagal control [High frequency power of HRV ; 764.3 ± 110 vs 2341.2 ± 378 ms²; $p < 0.01$] and reduced variance in PWV [0.059 ± 0.044 vs 0.102 ± 0.108 (cm/ms)²; $p < 0.01$] compared to healthy volunteers, and depression severity was negatively correlated ($r = -0.74$; $p < 0.01$) with cardiac vagal control positively ($r = 0.86$; $p < 0.01$) with standard deviation of PWV. No difference in average PWV were found in the two groups of participants. Reduced heart rate variability and reduced pulse wave velocity variability in MDD patients with suicidal ideation may lead to arterial stiffness and higher risk of future cardiovascular diseases. Treatment modalities should consider restoring autonomic function of MDD patients with suicidal ideation.

PB5

Discovering Prototypical Vital Signs Dynamic Behaviors within a Patient Cohort for Physiological Monitoring

Li-Wei Lehman*, Roger Mark

MIT
Cambridge, United States

Background The cardiovascular system can exhibit a remarkable temporal range of vital sign dynamic behaviors. We present a Gaussian Mixture Model based approach to discover prototypical time series patterns with similar trends and dynamical structures shared across a patient cohort. The premise of our approach is that dynamic patterns of vital signs, common among patients with similar disease progressions, may have prognostic values. Our goal is to identify prototypical temporal structures in vital signs time series that can be used to alert clinicians to patients at high risk of physiological deterioration.

Methodology We used Gaussian Mixture Models (GMMs) to jointly model multiple physiological time series from a patient cohort to discover a collection of prototypical dynamic behaviors shared across the entire cohort. Each such dynamic behavior was captured as a Gaussian component or a "cluster" of time series segments with similar transient dynamics, abrupt changes, and trends at multiple time-scales. The Expectation-Maximization algorithm was performed to find the maximum-likelihood set of model parameters as well as the cluster assignment of each segment. Logistic regression analysis was used to identify Gaussian components that were significantly associated with adverse outcomes.

Experiments/Results We applied our technique to minute-by-minute heart rate and blood pressure time series of MIMIC II adult patients to identify prototypical hemodynamic responses from vasopressor withdrawals. Among a total of 322 patients with pressor weaning episodes, 207 were unstable (pressor restarted within [2,24] hours), and 115 were stable (pressor not restarted). A GMM with 16 components (determined using the Bayesian Information Criterion) was built. Our approach was able to identify patterns from Gaussian mixture components with statistically significant ($p=0.026$) associations with the unstable event. These results suggest promising applications of the proposed approach in treatment decision support and in identifying vital signs temporal patterns associated with impending hemodynamic instability.

PB6

Patient Prognosis from Vital Sign Time Series: Combining Convolutional Neural Networks with a Dynamical Systems Approach

Li-Wei Lehman*, Mohammad Ghassemi, Jasper Snoek, Shamim Nemati

MIT
Cambridge, United States

Background: Subtle dynamical patterns in physiological time-series, often difficult to observe by naked eyes, may contain important information about the pathophysiological state of patients and their long-term outcomes. We present an approach to physiological time-series analysis that simultaneously models the underlying dynamical systems using a switching state-space model, and the high-level transition patterns among the states using Convolutional Neural Networks (CNNs). CNNs have been shown recently to produce state-of-the-art performance in image classification tasks. This success is largely attributed to their ability to exploit hierarchical structures for feature learning. However, direct application of CNNs to physiological time-series have been limited due to presence of underlying physiological control systems, capable of exhibiting rich dynamical patterns at multiple time-scales.

Methods: To address this limitation, we propose a stacked switching vector-autoregressive (SVAR)-CNN architecture. The SVAR-layer extracts dynamical features (or modes) from the time-series, which are then fed into the CNN-layer to extract higher-level features representative of transition patterns among the dynamical modes. We evaluate our approach using 8-hours of minute-by-minute mean arterial blood pressure (BP) from over 450 patients in the MIMIC-II database, resulting in 480 BP time-series observations per patient. We modeled the time-series using a third-order SVAR process with 20 modes, resulting in first-level dynamical features of size 20×480 per patient. A fully connected CNN is then used to learn hierarchical features from these inputs, and to predict hospital mortality.

Results: The combined CNN/SVAR approach using BP time-series achieved a median and interquartile-range AUC of 0.74[0.69, 0.75], significantly outperforming CNN-alone (0.54[0.46, 0.59]), and SVAR-alone with logistic regression (0.69[0.65, 0.72]). As a baseline comparison, an existing acuity metric SAPS-I, using 14 different physiological/lab measurements gave an AUC of 0.65[0.59, 0.71]. Our results indicate that including an SVAR layer improves the ability of CNNs to classify nonlinear and nonstationary time-series.

PB6

Comparison of Repeatability of Blood Pressure Measurements between Oscillometric and Auscultatory Methods

Chengyu Liu^{1,2}, Dingchang Zheng¹, Clive Griffiths¹, Alan Murray¹

¹ Institute of Cellular Medicine, Newcastle University, Newcastle upon Tyne, UK

² School of Control Science and Engineering, Shandong University, Jinan, China

Non-invasive blood pressure (NIBP) measurement plays a crucial role in routine examinations and monitoring. The auscultatory method is considered the gold standard measurement. The oscillometric method is used by the majority of automatic NIBP measurement devices. The comparison of repeatability between the two methods is usually based on three repeat measurements. However, there is currently little information available on the comparison of repeatability when performing more than three repeat measurements. This study aimed to provide this information.

Oscillometric cuff pressure waveforms and Korotkoff sound signals were synchronously recorded digitally from 20 normotensive subjects during standard BP measurement at slow linear deflation rates of 2-3 mmHg/s. Eight repeat measurements were performed for each subject. For the oscillometric method, the pressure in the cuff corresponding to the maximum oscillometric pulse peak (A_{\max}) determined the mean arterial pressure (MAP), and corresponding to 50% of A_{\max} in the high pressure range and 70% of A_{\max} in the low pressure range during cuff deflation determined the SBP and DBP respectively. For the auscultatory method, SBP and DBP were determined by replaying the Korotkoff sound signals to a trained listener. MAP was determined using the typical formula: $MAP = DBP + (SBP - DBP) / 3$.

The standard deviation of eight SBP, MAP and DBP measurements for each subject was calculated as the index of repeatability (SBP_{SD} , MAP_{SD} and DBP_{SD} respectively). The results showed that all three indices from the oscillometric method were significant higher than those from the auscultatory method (all $P < 0.01$). Specifically, indices were all greater for oscillometric measurement by 2.31 mmHg for SBP_{SD} (mean \pm SD: 5.26 \pm 1.27 vs 2.95 \pm 0.89 mmHg), by 1.23 mmHg for MAP_{SD} (3.55 \pm 1.12 vs 2.32 \pm 0.88 mmHg), and by 1.24 mmHg for DBP_{SD} (3.83 \pm 1.43 vs 2.59 \pm 1.04 mmHg).

The repeatability differences from the multiple repeat measurements suggest that the widely used oscillometric method can not replace the auscultation method in clinical applications.

PB6

Aging Changes in the Regularity of Hemodynamic Parameters during Six-Minute Walk Test

Marcos Hortelano, Richard Reilly, Raquel Cervigón*

UCLM
Cuenca, Spain

This study is focused on examining the hemodynamic profile in different age groups undergoing an active stand to investigate the influence of aging on the regularity of hemodynamic patterns during exercise. The database included 57 participants, 28 were young aged $30,83 \pm 3,90$, 11 were females and 17 males. The rest of patients were over 60 years ($69,78 \pm 6,36$) of whom 15 (65,22%) were women. The participants underwent the six-minute walk test with non-invasive beat-to-beat blood pressure monitoring. Hemodynamic parameters were registered during three phases: a pre-exercise stand lasting 3 minutes (phase 1), a six minutes walking phase (phase 2) and a post-exercise stand lasting 3 minutes (phase 3). Different hemodynamic parameters such as, HR (pulse rate derived from the pulse interval), systolic blood pressure (SBP), diastolic blood pressure (DBP) and cardiac output (CO) were extracted at each phase. Shannon entropy was applied to the hemodynamic parameters time series belong to both groups of population. In phase 1 DBP Shannon entropy showed differences between the younger group ($3,08 \pm 0,24$) and the older group ($2,71 \pm 0,44$) with a statistical significance of $p < 0,001$. The same trend was observed in phase 3 with a statistical signification of $p = 0,009$. In addition, HR entropy showed differences between phases and between stages in both groups: in phase 1 values went from $3,15 \pm 0,32$ for the younger group to $2,21 \pm 0,52$ for the older group ($p < 0,001$), and in the rest of the phases the differences between groups followed the same trend with statistical significant differences, as well as CO entropy values with differences along the phases in both groups. Hemodynamic parameters regularity during the exercise shows differences between groups as a result of the age, especially HR showed higher irregularity in the younger group. This index can be useful to provide information on the hemodynamic changes that occur as a result of age during exercise.

PB6

A Novel Method for Arterial Blood Pressure Pulse Detection Based on a New Coupling Strategy and Discrete Wavelet Transform

Farhad Asadi, Mohammad Javad Mollakazemi, S Ali Akbar Moosavian

Department of Mechanical Engineering, K.N.Toosi University of Technology, Tehran, Iran

In this study, a new method is presented for detection of arterial blood pressure pulses (ABP). The algorithm employs discrete wavelet transform (dwt) decomposition to extract ABP waveform features. In the proposed method, two strategies are used. In the first strategy, the algorithm uses only the dwt coefficients of ABP. The second strategy which is introduced for the first time in this paper, the coupled dwt coefficients of ABP and electrocardiogram (ECG) are used. When dwt coefficients of ECG and ABP are coupled the detection of ABP pulses is easier and more accurate in noisy parts of the signal. Furthermore, this coupling strategy is useful for the detection of ECG R-peaks since the ABP pulses make the ECG R-peaks detectable when ECG is noisy. To meet this end, adaptive thresholding and different dwt functions were employed and fitted because of different morphologies of ABP and ECG signals. Also, the ABP-ECG delay time is studied and measured in different recordings and set for 254 milliseconds.

For evaluation, 170 accessible recordings of the multimodal training set of PhysioNet/Computing in Cardiology Challenge 2014 which contained both ECG and ABP waveforms were used. The first and second strategy obtained average accuracy of 87.56% and 88.53%, respectively.

Investigation of the Pro-arrhythmic Effects of Domperidone by a Simulation Study

Jing Zhou, Yongfeng Yuan, Qince Li, Kuanquan Wang*, Zhili Li, Henggui Zhang

School of Computer Science and Technology, Harbin Institute of Technology, Harbin, China

Domperidone, an alternative to cisapride, is commonly used to treat gastrointestinal disorders. However, it was reported that similar to cisapride, domperidone might be associated with a high risk of sudden cardiac death (SCD). In a recent epidemiological study, the odds ratio for SCD with domperidone was reported to be 3.72, which increased to 11.4 for daily doses > 30 mg. This paper investigated the pro-arrhythmic effects of domperidone by a multi-scale biophysically detailed computational model of the heart.

The ten Tusscher et al. model of human ventricular cells was implemented. Dose-dependent blocks of I_{Kr} by domperidone (10, 30, 100 300 and 1000nmol/L) were based on experimental data of Benoit Drolet et al.. At cellular level, action potentials (APs) of cellular models were evoked with a basic cycle length (BCL) of 1000ms, from which effects of domperidone on action potential duration (APD) and APD_{90} restitution curves were calculated. At tissue level, effects of domperidone on conduction velocity (CV) of electrical excitation waves, pseudo electrocardiograms (pseudo-ECG) and vulnerable window (VW) were quantified.

Our simulation results showed that domperidone prolonged APD and QT interval significantly and dose-dependently. At 100nmol/L, domperidone prolonged APD by 5.7% and QT interval by 6.8%, which increased to 10.3% and 12.8% respectively at 300nmol/L. With the increase of drug concentration, the slope of APD_{90} restitution curves increased towards shorter diastolic intervals, indicating increasing incidence of generating action potential alternans. In 1-D strand simulations, domperidone slowed down CV and augmented VW to generate unidirectional conduction in response to a premature stimulus. The measured VW increased by 7.9% and 18.6% for 100 and 300nmol/L compared to the control condition.

In conclusion, domperidone has profound and dose-dependent effects on cardiac electrophysiological properties at cellular and tissue level. It increases APD and QT interval, augments tissue's vulnerability for genesis of unidirectional conduction, which are all pro-arrhythmic.

PB7

Model-based Analysis of the Effects of Thioridazine Enantiomers on the Rabbit Papillary Action Potential.

Ask S Jensen, Cristian P Pennisi, Cristian Sevcencu, Jørn B Christensen, Jette E Kristiansen, Johannes J Struijk

Aalborg University
Aalborg, Denmark

Aims: The aim of this study was to investigate mechanisms underlying the effects of the thioridazine enantiomers on the rabbit papillary action potential duration (AP, APD).

Methods: An adapted computational model of the rabbit ventricular action potential was used to carry out a model-based analysis of experimental data. The data consisted of transmembrane AP recordings from isolated right ventricular papillary muscles from 21 rabbits in four groups: control, (-)-thioridazine, (+)-thioridazine, and the racemate. Drug effects were determined using two different methods; an inverse method based on literature values of thioridazine racemate induced I_{Kr} inhibition and a forward method based on our data alone. Drug effects were modeled by inhibition of the I_{Kr} and I_{CaL} currents.

Results: Simultaneous inhibition of I_{Kr} and I_{CaL} resulted in a more accurate description of the observed drug effects than could I_{Kr} inhibition alone. The forward method resulted in the following values of I_{Kr} inhibition at 10 mg L⁻¹: Racemate = 45%, (-)-thioridazine = 0%, and (+)-thioridazine = 85%. For the inverse method, a level of 78.8% inhibition due to the racemate was obtained from the literature. The following levels of I_{Kr} inhibition were determined: (-)-thioridazine = 35%, (+)-thioridazine = 80%.

Conclusion: I_{Kr} inhibition accurately described the observed APD prolongation, and the identified levels of I_{Kr} inhibition were plausible when compared to literature data for the racemate. Both methods found (-)-thioridazine to cause considerably less I_{Kr} inhibition than (+)-thioridazine or the racemate. These results indicate that the prolonging effects observed in the experiment may be primarily due to I_{Kr} inhibition.

PB7

Effects of Amiodarone on Ventricular Excitation Associated with the KCNJ2-Linked Short QT Syndrome: Insights from a Modelling Study

Cunjin Luo*, Kuanquan Wang, Ming Yuan, Zhili Li, Qingjie Wang, Yongfeng Yuan, Henggui Zhang

China

Introduction: Short QT syndrome (SQT3) is associated with ventricular arrhythmias that may lead to cardiac sudden death. However, effective pharmacological treatment for SQT3 remains unclear. Amiodarone has emerged as the leading antiarrhythmic therapy for termination and prevention of ventricular arrhythmia in different clinical settings because of its proven efficacy and safety. The aim of this study was to investigate the effects of amiodarone on cardiac excitation of the KCNJ2-linked short QT syndrome (SQT3).

Methods and Results: Effects of Kir2.1 D172N mutation-induced changes in Ik1 were incorporated into human ventricular cell and tissue models that considered the intrinsic electrical heterogeneity in the left ventricle. Actions of amiodarone were simulated by implementing a simple block pore theory to simulate the drug's effects on ICaL and IKr block for low dose (57% and 15% blocking of Gkr and GCaL respectively) and high dose (85% and 34% blocking of Gkr and GCaL respectively). In cellular simulations, we computed current traces of Ik1 and action potential duration (APD) of endomyocardial (ENDO), middle (M) and epicardium (EPI) cells both in control, mutant, and amiodarone-in-action conditions. In tissue simulations, the pharmacological effects of amiodarone on the characteristics of ECG were computed. It was shown that under the mutant conditions, the magnitude of Ik1 was increased and APD was abbreviated, QT interval in pseudo-ECG was abbreviated dramatically as compared to WT condition. Such changes under the D172N condition were more remarkable than those under the WT-D172N condition. As compared to WT condition, amiodarone prolonged action potential, and the QT interval of ECG significantly under WT-D172N condition at high dose, but insignificant at low dose; it produced almost the same effect on QT interval both at high dose and low dose under D172N condition. In both mutant conditions, amiodarone did not show noticeable effects on the T-wave amplitude.

Conclusions: Our simulation data suggests that amiodarone is an effective and safe, anti-arrhythmic drug for treatment of the KCNJ2-linked short QT syndrome. This study provides new insights into the pharmacokinetics of amiodarone for treatment of SQT3 under WT-D172N and D172N conditions.

PB7

Modeling and Simulation of Developmental Changes in Contractile Apparatus of Ventricular Cells

Mao Takiguchi*, Tamami Toki, Hitomi Sano, Yasuhiro Naito, Masaru Tomita

Inst. Adv. Biosci. Keio Univ
Fujiwara, Japan

The heart develops and acquires new functions, all while continuously pumping blood. Meanwhile, heart abnormalities that develop early in this process progress to congenital heart malformations. Accordingly, the developmental program of the heart, including expression of genes encoding ion channels, is likely to be tightly regulated. We previously modeled developmental changes in action potentials (AP) in rodent ventricular cells by integration of quantitative changes in ionic components of the cellular membrane and sarcoplasmic reticulum (SR) throughout the course of development using the Kyoto model, a comprehensive model of guinea pig ventricular cells. We then incorporated a glycolysis model to represent developmental changes in contribution of glycolysis and mitochondrial oxidative phosphorylation to ATP production in ventricular cells. Here, we further modified the model to represent developmental changes in contractile apparatus of ventricular cells. During the course of development, the ventricular cells utilize different isoforms of both myosin heavy chain and troponinI; the differences in isoforms affect Ca^{2+} sensitivity, ATPase activity, and velocity of contraction. In order to consider the differences in isoforms, we integrated a new contraction model to the Kyoto model; briefly, the new model considered tropomyosin which inhibits formation of cross-bridge by actin and myosin filaments. We varied the level of Ca^{2+} sensitivity in order to obtain similar traces for contractile force between the original Kyoto model and the modified model. We also modified the new contraction model to consider ATP consumption by myosin-ATPase in order to simulate the changes in ATPase activity caused by the difference in MHC isoforms. The modified model enabled us to compare the contribution of developmental changes in the ATP consumption via contraction to excitation-contraction coupling, which is regulated differently between fetal and adult guinea pigs.

PB7

Investigation of The Mechanisms Underlying Cardiac Alternans – insights from a Computational Study

Wei Wang*, Haibo Ni, Henggui Zhang

United Kingdom

Introduction: Cardiac alternans, manifested as cyclical oscillations in action potential duration (APD) and Ca^{2+} transient (CaT), is a risk factor for cardiac arrhythmia. Electrical and CaT alternans are believed to be strongly correlated. However, the primary mechanisms underlying the occurrence of cardiac alternans are unclear. The aim of this study was to determine the causes of cardiac alternans by computational modelling.

Method: The O'Hara-Rudy model of human ventricular cells was implemented to simulate cardiac action potential (AP) alternans. Parameters of intracellular Ca^{2+} handling were changed to elucidate the impacts of intracellular Ca^{2+} dynamics on genesis of alternans. In simulations, AP alternans were evoked by decreasing the pacing cycle length from 600 to 230ms. During the time courses of AP alternans, ICaL and the sarcoplasmic reticulum (SR) content were analysed. Correlation between electrical and CaT alternans was elucidated by AP-clamp utilizing large and small morphology of APs.

Results: AP-clamp simulation showed that CaT alternans were generated at fast pacing rates, but absent at slow rates irrespective of AP alternans. Presence of CaT alternans in the absence of AP alternans suggested that CaT alternans preceded before AP alternans. By inhibiting the intracellular Ca^{2+} release from the SR, CaT alternans were abolished, demonstrating a crucial role of the intracellular Ca^{2+} handling dynamics in genesis of cardiac alternans. In addition, CaT alternans were observed without apparent association with alternating ICaL, but closely related to the alteration of the SR content.

Conclusions: Our simulation data suggests that the leading cause of cardiac alternans in the human ventricle is CaT alternans, whereas AP alternans are the secondary result. These simulation findings are consistent with a recent experimental study in rabbit atrial and ventricular cells, adding a theoretical basis for understanding the mechanism of cardiac alternans.

PB7

Simulation of Effects of Inward-Rectifier K^+ Current on the Automaticity of Human Ventricular Tissue

Yue Zhang, Kuanquan Wang^{*}, Henggui Zhang, Yongfeng Yuan

Harbin Institute of Technology
Harbin, China

Aims: The aim of the study is to investigate the effects of inward-rectifier K^+ current (I_{K1}) on the 2D human ventricular tissue when automaticity generates.

Methods: First, the TNNP06 human ventricular model was used to investigate the stability and periods of automaticity when I_{K1} was depressed in different degree. Then an idealized 2D human ventricular tissue was developed, which was 100 cells in length and 400 cells in width. We simulated the effects of I_{K1} on the tissue in two cases. Case 1: the left three volumes of endocardial cells were stimulated for 1ms per 800ms. Case 2: the same cells were only stimulated once for 1ms at 10ms. At the same time, the pseudo ECGs were recorded.

Results: The automatic periods elongated with the increase of G_{K1} . The period was about 750ms for $G_{K1}=0$ nS/pF, 780ms for $G_{K1}=0.1$ nS/pF, and 826ms for $G_{K1}=0.2$ nS/pF. For the 2D tissue, when $G_{K1}=0.1$ nS/pF, the conduction of electrical excitation in case 1 was almost the same to that in case 2 when $t > 1880$ ms, though the tissue was stimulated per 800ms. The ECGs were also the same except the very little tips generating in case 1 because of the stimulations. When $G_{K1}=0.2$ nS/pF, the excitation propagation and the ECGs were totally different in the two cases. The tissue was controlled by the regular stimulations in case 1 while it was regulated by the automaticity in case 2 with only once stimulation. ECGs for $G_{K1}=0.2$ nS/pF were shown in Figure 1.

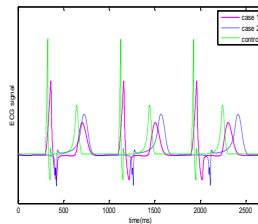


Figure 1. Pseudo ECG when $G_{K1} = 0.2$ nS/pF.

Conclusion: The autorhythmicity increased with the decreasing of I_{K1} . The lower the I_{K1} was, the stronger the automaticity acted. The tissue was under automatic rhythm when I_{K1} was small enough while stimulations regained to control the tissue with the increasing of I_{K1} .

PB7

Calcium Leak Induced Sinus Bradycardia

Qingjie Wang*, Sanjay Kharche, Gareth Jones, Cunjin Luo,
Chengchun Tang, Henggui Zhang

School of Physics and Astronomy
United Kingdom

Introduction: Catecholaminergic polymorphic ventricular tachycardia (CPVT) is a debilitating condition that often results in sudden cardiac death. Spontaneous calcium leak from sarcoplasmic reticulum is responsible for CPVT-related arrhythmias. CPVT patients as well as CPVT mouse models exhibit resting sinus bradycardia, which in turn increases the risk for ventricular arrhythmia. In this computational study, we determined the effects of sarcoplasmic reticulum calcium leak on the functions of sinoatrial node cells.

Methods: A sarcoplasmic reticulum calcium leak current, I_{leak} , was increased in models of mouse sino-atrial node cells. The I_{leak} current is determined by v_2 , the calcium leak rate constant from the net sarcoplasmic reticulum. Action potentials in sino-atrial node cell model were simulated with changing v_2 in a range of values.

Results: Our simulation results showed that increasing v_2 from 0 to $2 \times 10^{-5} \text{ ms}^{-1}$ resulted in a slightly shorter cycle length. The pacing cycle length increased steadily till v_2 values became $3.1 \times 10^{-5} \text{ ms}^{-1}$. Further increases of v_2 gave rise to long-short, big amplitude-small amplitude oscillations and pacemaking arrest. Increase in calcium leak resulted in decreases in subspace calcium concentration and L-type calcium and $\text{Na}^+/\text{Ca}^{2+}$ exchanger current amplitude. A reduction in maximum upstroke velocity of the membrane potential was also observed.

Conclusions: The results showed the significance of calcium leak as a major mechanism of sinoatrial node dysfunctions, which underlies the mechanisms of bradycardia in CPVT patients.

Estimation of extent damage tissue by multi-resolution analysis of the electrocardiogram and Arterial Blood Pressure

Seyyed Abbas Atyabi¹, M Javad Mollakazemi², Farhad Asadi², Hamid Ebrahimi Orimi³, Ali Ghaffari³

¹Young Researchers Club, Islamic Azad University, South Tehran Branch, Tehran, Iran

²Young Researchers Club, Islamic Azad University, Science and Research Branch, Tehran, Iran

³Cardiovascular Research Group (CVRG), Department of Mechanical Engineering at K.N.Toosi University of Technology, Tehran, Iran

Introduction: Coronary artery congestion is a common heart disease which causes a lack of oxygen and nutrients in the heart muscle that is felt as chest pain (ischemia disease). This misbalance can continue until the first cell is destroyed which is called myocardial infarction.

Aim: In this paper we aim to determine the amount of tissue damage by simulating myocardial infarction in laboratory rats.

Method: the synchronic electromechanical signals of 50 wistar rats including the electrocardiogram (ECG) and atrial blood pressure (ABP) signals were used for extent estimation of damage tissue. The signals were recorded at 30 minutes in normal state and 30 minutes in myocardial infarction (MI) and ischemia state which was resulted by artificial complete blocking of left anterior descending coronary artery (LAD). In another case, the vasopressin (AVP) in various doses was injected to 40 rats. In each case, images of the heart sections were extracted. Afterwards, the wavelet packet transform (WPT) was applied to the recorded ECG and ABP signals for decomposing them into dyadic scales. Then, 50 proper scales which were more informative for discrimination of different ischemia phases from each other and from healthy phase were chosen and the entropy of corresponding wavelet coefficients was considered as the feature vector. Furthermore, the amount of damage tissue of rat heart was measured by image processing techniques. Finally, the amount of damage tissue was measured using artificial neural networks (ANN) based techniques.

Results: The extent of the damage tissue was estimated based on the ANN and multi-resolution analysis of the synchronic electromechanical signals with the average error of the 3.32% for the normal and ischemia tissue in all the AVP doses.

Time-Course of T-wave Flattening and P-R Prolongation under β -Adrenergic Challenge are Associated with Short-Term Biphasic Poincaré Shift in Mice

Conrado J Calvo*, David Filgueiras, Francisco J Chorro, José Millet
Spain

Introduction: β -adrenergic challenge is commonly used to exacerbate electrical conduction abnormalities in transgenic mice models with specific genotype affecting cardiovascular function in humans. Quantification of T-wave morphological alterations is of interest to assess ventricular repolarization abnormalities. PR and QTc intervals play also an important role assessing atrio-ventricular and ventricular conduction abnormalities under drug testing or autonomous challenge. Automatic characterization of the time-course of isoproterenol effects on these parameters in Mice has not been described in detail.

Methods: Offline weekly short-term (up to 25 min) sequential ECG analysis was carried out from anesthetized mice littermates (n=5) using subcutaneous limb ECG electrodes at 2KHz sample rate. After robust QRS detection, heart rate variability (HRV) was assessed using poincaré surface identity line profiles (PLP) and correlated to P-R/QTc and morphological T-wave variability. ECG intervals and measurements were assessed in baseline and after challenge with isoproterenol until complete recovery. T-wave alterations were quantified using a derived flattening score (FS) adapted for mice to include geometrical and peakedness modifications.

Results: Weekly isoproterenol conduction disturbances were observed during the time course of isoproterenol, mainly, PR (79.25 ± 4.24 ms vs 25.37 ± 2.07 ms, baseline vs follow-up recovery, $p < 0.05$) and QRS prolongation (14.41 ± 1.03 ms vs 10.8 ± 0.25 ms, $p < 0.05$). QTc intervals were significantly prolonged in the initial week (37.6 ± 5.37 vs 25.37 ± 2.07 ms), yet preserved after follow-up. Morphological short-term remodeling was observed as a transient flattening on T-wave assessed by the FS ($12.02 \pm 1.7\%$ to $23.4 \pm 5.4\%$) and sudden reduction in T-wave area. In turn, a non-significant trend was observed as measured from signal averaged ECGs after recovery. A biphasic effect on PLP shift upon isoproterenol challenge was associated and observed depending upon initial rhythm which accelerated during follow-up.

Conclusions: Conduction and repolarization beat-to-beat modifications induced after isoproterenol challenge were accurately tracked. The morphological flattening score derived for Mice electrophysiology was useful to assess changes on T-wave morphology, yet further validation is mandatory.

PB8

A Comparison Study Between Fainter and Non-fainter Subjects During Head-Up Tilt Test using Reconstructed Phase Space

Nadine Khodor*, Guy Carrault, David Matelot, Nathalie Ville, François Carre, Alfredo Hernandez

Université de Rennes 1
France

Introduction: The analysis of cardiac dynamics based on time series extracted from cardiovascular signals (e.g. electrocardiogram, blood pressure) is relevant for differentiating between normal and pathological cases with feasible functions in the diagnosis and risk estimation. In this study, the dynamic behavior of cardiovascular time series is analyzed using reconstructed phase space to identify differences between subjects who developed syncope during head-up tilt test (fainters) and others who did not (non-fainters).

Method: Electrocardiogram and arterial blood pressure were recorded from 29 non-fainter and 28 fainter subjects. RR-interval, Amplitude of Systolic blood pressure (AmpS), peak amplitude of the first derivative of blood pressure (dPdt_max) and Pulse Transit Time (PTT) were extracted. Different features, such as the phase space density and indices derived from the recurrence quantification analysis, were computed from the phase space area of the above cited time series. In order to identify fainter and non-fainter groups, we selected the most pertinent parameters using Relief method to be used for further classification by K-nearest neighbor.

Results: The results show that by applying a cross-validation procedure repeated 10 times, using half of the population in the training step, the performance of the classification is approximately the same in all these time series with sensitivity (Se) near to 66.5% and specificity (Sp) around 62% during the first 5min of supine position. These values increase in the first 15min of tilted position to Se= 67% and Sp= 73%. By looking for the best combination and using an optimal fusion node, we demonstrate that the joint analysis of RR and dPdt_max provides a sensibility around 95% and a specificity of 87%.

Conclusions: Although the individual performance of each time series (RR, AmpS, PTT, dPdt_max) are not very high, this analysis suggests that a multivariate analysis enhances the classification performance, and predicts the outcome of the HUTT.

PB8

The Effect of Heart Orientation on High Frequency QRS Components in Multiple Bandwidths

Jakub Hejč*, Marina Ronzhina, Oto Janoušek, Veronika Olejníčková, Marie Nováková, Jana Kolářová

Czech Republic

Aims: Reduced power of high frequency oscillations inside the QRS complex reflects ischemic pathology in the heart. In order to show spatial and frequency dependencies, we examined the effect of heart orientation on power of high frequency components under normal and ischemia condition within various frequency bands.

Methods: Root mean square of the signal in QRS region within frequency bands from 150 Hz to 700 Hz (with bandwidth 100 Hz and step size 50 Hz) and heart rotation around longitudinal axes (10° intervals within the range between $0-90^\circ$) were computed from four New Zealand rabbit isolated hearts according to Langendorff perfused by Krebs-Henseleit solution (1.25 mM Ca^{2+} ; 37°C ; 85 mmHg). Orthogonal lead system were used to record electrograms. Experimental protocol included control, ischemia and reperfusion phase.

Results: In this pilot study, the circular contour map and normalized RMS was used to interpret spatial and frequency dependency under normal, ischemia and reperfusion condition with lower frequencies placed in the center of the contour map. Under normal condition, isolines creates ellipsoidal structures with semi-major axis oriented mostly parallel to the ventricular septum. Highest RMS values at lower frequencies are distributed around semi-major axis. Under ischemia condition, isolines passes to the circular or irregular structures with RMS level uniformly distributed over all angles and returns back to the original shape after reperfusion.

Conclusions: Presented method shows specific changes in shape of multidimensional RMS level distribution under normal and ischemia condition using frequency and spatial dimension. RMS level of high frequency signal in non-ischemic isolated heart differs within lead orientation and its maximum lies in a small region around specific angle. Reduction of RMS level during ischemia is largest in this region which leads to the circular structure in the contour map.

Ischemic ST Deviation Episodes Recognition via ECG using Extreme Learning Machine and Kernel Density Estimation

Dena Mafie*, Seyyed Abbas Atyabi, Ali Ghaffari

Tehran, Iran (Islamic Republic of)

Introduction: Accurate diagnosis of myocardial ischemia plays an important role in prevention of subsequent fatal complications such as myocardial infarction and ischemia induced sudden cardiac death. In the past several years, many methods have been proposed to detect ischemia based on ST segment deviation. Due to presence of noise and error in calculations, correct diagnosis between ischemic ST episodes and normal beats and thus exact detection of myocardial ischemia still remains unsolved. **Aims:** This study aims to develop a new, robust method to distinguish ischemic ST episodes from normal beats using extreme learning machine and kernel density estimation classifiers. This method is developed and evaluated using ECG signals of European ST-T database.

Methods: In this study, first a method based on wavelet transform is implemented for pre-processing and baseline wandering removal. Then a discrete wavelet based method detects exact locations of QRS complexes. After that, for each heartbeat five features are extracted for better differentiating of ischemic episodes from normal ones, which are summarized as follow: Slope from QRS onset to offset point, length multiplied by area curve (LAC) of the region between QRS offset and T-peak point, normalized and signed sum of QRS offset to isoelectric level, slope from T-wave onset to offset point and normalized and signed sum of T-wave offset to isoelectric level. Finally, Extreme learning machine (EML) and kernel density estimation (KDE) are applied as classifiers to detect ischemic episodes from normal beats.

Results: Using European ST-T database for train and test, the algorithm is evaluated by EML and KDE classifiers. Sensitivity and specificity for KDE were 0.93 and 0.91, respectively. Sensitivity and specificity for EML classifier were 0.945 and 0.927, respectively. The obtained results clearly confirm that the presented method is noise robust and EML is superior to traditional KDE classifier.

PB8

Characterisation of Cells Migration Through Cardiac Tissue using Advanced Microscopy Techniques and Matlab Simulation

Larisa Baiazitova*, Josef Skopalík, Vratislav Čmiel, Ondřej Svoboda, Ivo Provazník, Zdenka Fohlerová, Jaromír Hubálek

Department of Biomedical Engineering, FEEC, Brno University of Technology, Brno, Czech Republic
Brno, Czech Republic

Introduction: Mesenchymal stromal cells (MSC) and neutrophils (NP) migration are important factors of the infarcted hearts remodeling. These both types of the cells can migrate through cardiac extracellular matrix to the central ischemic region. Massive invasivity of NP cause serious problem of ventricular remodeling, on the other hand high speed of the MSC migration brings benefits, MSC can interact with ischemic myocytes and reduce myocytes apoptosis and left ventricular remodeling. The quantitative description of MSC and NP migration through collagen matrix is important aim of modern biomedicine.

Methods: NP and MSC migration through peri-infarct zone was simulated in special chambers (bottom area is 10 x 20 mm) connected by collagen channel (1 x 1 x 2 mm). Bottom of the system was constructed from glass plane, compatible with confocal microscopy. System was hold under 37°C and 5-21% O₂. First chamber was starting point of migrating MSC and NP. Second chamber included living or hypoxic myocytes (model of ischemic compartment). Collagen tunnel was donated by fixed cardiomyocyte for better simulation of real tissue. Monitoring of migrating cells was performed on the confocal laser scanning microscope Leica TCS SP8 X equipped with the picosecond White Light Laser (WLL). NP and MSC were stained by fluorescence nanoparticles, cardiomyocytes were stained by calcein, and thus separate monitoring of migrating cells was implemented.

Results: In this work chemotaxis movement of MSC through collagen tunnel between two chambers was studied. The average speed of migration was about 15 µm/hour for MSC and about 80 µm/hour for NP. Speed was significantly modulated by collagen type, collagen concentration, collagen fiber orientation and also by cardiomyocyte viability (gradient of chemoattractants). These results were adopted into the mathematical diffusion model created in Matlab software.

PB8

Changes in the Electrocardiogram Induced by Coronary Artery Bypass Grafting

Dimiter Simov, Ivaylo Christov*, Giovanni Bortolan, Mikhail Matveev, Ivo Petrov, Vessela Krasteva

Institute of Biophysics and Biomedical Engineering – Bulgarian Academy of Sciences, Sofia, Bulgaria

Objectives: The goal of this research is to investigate the ECG changes provoked by coronary artery bypass grafting (CABG) surgery.

Materials and Methods: ECG recordings of patients undergone CABG surgery have been collected: number of patients 20 (men 95%, age 64.4±8.4), records duration 10-15 minutes. The number of bypasses for each individual is from 1 to 4 (40% of the patients are with 4). The ECG recordings are pre- and post-surgery, from 2 to 10 days after the intervention. In order to avoid accidental events or noise in the ECG, the QRS-complex, the ST elevation and T-wave parameters' measurements are performed on an average P-QRS-T interval. The method of Bortolan and Christov, approved at the PhysioNet/Computing in Cardiology Challenge, 2008, Bologna has been used for the detection of episodes of T-wave alternans (TWA).

Results: Pre- and post-surgery measurements and Means ± Standard Deviations are presented in the Table.

TWA [numb]		HR [bpm]		QRS ampl [mV]		T ampl [mV]		ST elev [mV]		QRS-T ang [degr]	
pre	post	pre	post	pre	post	pre	post	pre	post	pre	post
2.5	3.8	68.1	82.1	1.12	1.07	0.34	0.24	0.05	0.06	83.7	52.2
±	±	±	±	±	±	±	±	±	±	±	±
2.8	3.4	9.2	10.5	0.51	0.59	0.28	0.24	0.06	0.09	53.8	54.0
p = 0.080		p = 0.0010		n.s.		n.s.		n.s.		p = 0.070	

Discussions: The QRS amplitude, the T-wave amplitude and the ST elevation did not change in the pre- and post-stages. The TWA showed a clear upward trend (p=0.080) in the post-stage, and the QRS-T angle in the frontal plane showed a clear downward trend (p=0.070) in the post-stage, although both have no statistical significance. Significant increase (p=0.0010) in the post-stage was obtained for the HR. Four patients had the risk factor of negative T waves in lead V2, which is highly correlated with the number of TWA episodes (5 ± 2.4 episodes in the negative T-waves, vs. 2.9 ± 3.2 episodes in the positive T-waves).

Conclusion: The ECG changes caused by CABG are indicating a light increased cardiac risk in the 2-10 post-operative days of the study.

PB8

Hemodialysis-Induced ST-Segment Deviation

Iana Simova, Ivaylo Christov*, Giovanni Bortolan, Roger Abächerli, Liliana Kambova, Irena Jekova

Institute of Biophysics and Biomedical Engineering – Bulgarian Academy of Sciences, Sofia, Bulgaria

Objectives: Hemodialysis (HD) is often associated with ECG changes, the significance of which is not fully understood. The goal of this research is to investigate the ST-segment changes provoked by HD.

Materials and Methods: We recorded ECGs of 58 patients undergoing HD (52% males, age 59 ± 13 years, renal disease duration 9.7 ± 6.7 years, haemodialysis duration 5.2 ± 4.4 years). Serum electrolytes (potassium-K, sodium-Na, phosphorus-Ph and calcium-Ca), urea and creatinine levels were evaluated before and after haemodialysis. All parameters were measured on an average P-QRS-T interval in order to avoid accidental events or noise.

Results: Pre- and post-HD ECG measurements (mean \pm standard deviations) were:

ST-dev_pre: 0.10 ± 0.09 mV; ST-dev_post: 0.12 ± 0.12 mV; $p = 0.0018$

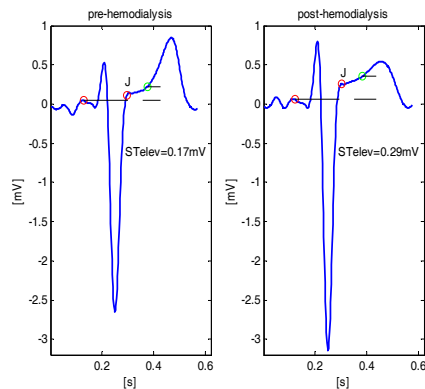
QRS-ampl_pre: 1.34 ± 0.64 mV; QRS-ampl_post: 1.55 ± 0.79 mV; $p < 0.001$

T-ampl_pre: 0.43 ± 0.31 mV; T-ampl_post: 0.36 ± 0.28 mV; $p = 0.0012$

An example of pre- and post-HD average P-QRS-T interval is shown in the figure. There was an increase of the QRS amplitude and the ST-deviation, and a decrease of T-wave amplitude in the post-HD ECG, compared to the pre-HD one.

Discussions: HD leads to a significant change in the QRS and T-wave amplitude and a considerable shift in the ST-segment. The decrease of the T-wave amplitude and the upward shift of the ST-segment could be explained by potassium decrease during HD. Baseline ST-segment shift, however, was with mean positive deviation, while typical for mild hyperkalaemia is ST depression. This suggested that there could be other possible mechanisms. QRS amplitude increase could be explained by the decrease of the extracellular fluid and blood volume and hence a decrease of the cardiac preload, rather than a decrease of the thorax impedance.

Conclusion: HD induces ECG changes, which could not be entirely explained by alteration in haemodynamic and electrolyte shift.



Classification of Ventricular Premature and Ischemic Beats in Animal Electrograms

Marina Ronzhina*, Lucie Maršánová, Radovan Smíšek, Veronika Olejníčková, Oto Janoušek, Petr Veselý, Jana Kolářová, Marie Nováková, Ivo Provazník

Brno University of Technology
Brno, Czech Republic

Introduction: There are many approaches for automatic classification of different pathological events including ventricular premature beats (VPBs) in human ECG. In most cases, VPBs are distinguished from normal beats. In experimental data, VPBs may appear as a result of some changes in experimental condition, such as pharmacological intervention or ischemia induction. In last case, VPBs detection may be complicated due to the similarity between morphology of VPBs and ischemic beats. In this work, classification of four types of heart beats is presented.

Methods: Two horizontal orthogonal electrograms recorded from isolated hearts of ten rabbits during experiments with global ischemia (20 min long stabilization and three repetitions of 10 min long ischemia and reperfusion) were used. After detection of QRS and manual delineation of selected QRS-T segments (normal, VPBs, middle and extreme ischemic beats selected from data recorded during stabilization and ischemic periods), 71 morphological features (7 joint for both leads and 32 for each lead separately) were calculated from the segments including durations, amplitudes, and areas under various parts of QRS-T. Feature set was then reduced using results of Kruskal-Wallis test accompanied with multicomparison Tukey-Kramer test and also principal component analysis (PCA). Four classification models such as discriminant function analysis, k-Nearest Neighbours (k-NN), support vector machine (SVM), and Naive Bayes were then trained and tested using 10-fold cross-validation.

Results: Three sets with 4 (joint for leads), 10 (lead I), and 12 (lead II) features were chosen with statistical test. 10 principal components explaining 93% of the whole data variance were selected using PCA. The highest total classification accuracy (ACC) was obtained with k-NN (ACC=0,96) and SVM (ACC=0,92) models trained on all feature sets together. Using of PCA-reduced set allows reaching of similar results with all models. As expected, reduced ACC mainly related to misclassifications between extreme ischemic beats and VPBs.

PB8

The Frequency Changes in Electrograms During Ischemia Experiments – Analysis by Matching Pursuit Decomposition

Jana Kolářová*, Petr Doležal, Marie Nováková, Ivo Provazník

Brno University of Technology
Brno, Czech Republic

Aims: The aim of this study is to analyse frequency components in electrograms (EGs) recorded from surface of isolated guinea pig hearts perfused by Langendorff. The frequency components change markable during global ischemia experiments.

Methods: The eight guinea pig hearts was used in this study. After the heart isolation, the heart was fixed to perfusion setup by the stump of aorta and then placed into thermostat-controlled bath (37°C) filled with Krebs-Henseleit (K-H) solution. The solution was continuously oxygenated with 95% O₂ and 5% CO₂. The heart was then perfused with the same solution at the constant perfusion pressure for 25-30 minutes (control period). After that, global ischemia was induced for 15 minutes and then, perfusion was restored for next 15 minutes. During all periods (control, ischemia, reperfusion) simultaneous touch-free recordings of the electrogram were performed. The EG signals were analysed by Matching Pursuit (MP) decomposition. This method decomposes a signal into an optimal linear expansion of waveforms, which are functions previously defined in a dictionary, and thus extends capability of traditional tools. The MP method is applied to study changes of energy of EG signal frequency components during three experimental periods. The histograms of the relative frequency of waveforms resulting from MP were computed to show frequency details for each experimental period.

Results: The study shows significant shifts of majority energy frequency components during ischemia and their recovery after reperfusion. Further, MP confirmed subtle frequency changes within QRS complexes during the experiment. MP offers information about frequency components which are not so perceptible in the results from the wavelet transform which is used more often.

Magnetocardiography did not Uncover Electrically Silent Ischemia in an In-Silico Study Case

Danila Potyagaylo, Gunnar Seemann, Walther HW Schulze, Olaf Dössel

Institute of Biomedical Engineering, Karlsruhe Institute of Technology
Karlsruhe, Germany

Introduction: Over the last decades, the information content which could be derived from cardiac electric and magnetic field measurements was debated. Our co-workers Wilhelms *et al.* investigated electrically silent acute ischemias in human ventricles caused by occlusion of a coronary artery. In the present work, we extend the previous study by calculating associated magnetic fields.

Methods: In this study we simulated the magnetic fields produced by early stage acute ischemia with varying transmural extent. Multiscale computational simulations are performed for calculations of body surface potential maps (BSPM) and magnetic fields on a magnetometer sensor matrix situated above the anterior chest wall. Depending on the ischemia size, the ST-segments of simulated electrocardiograms (ECG) experienced depression for subendocardial cases and elevation for transmural ischemias. One intermediate extent resulted in a zero ST-segment in BSPM which makes it diagnostically indistinguishable from a healthy case.

Results: Magnetic field calculations for this electrically silent ischemia also revealed no difference compared to the control case. For other cases, both ECG and MCG signals during ST-segments showed either depression or elevation from zero line.

Conclusion: In this specific case MCG did not deliver additional information to uncover electrically silent ischemia. For a general conclusion, further in-silico investigations with different ischemia shapes, sizes and positions should be performed and clinical studies with recording of both ECG and MCG signals must be conducted.

PB8

Detection of Electrode Interchange in Right Precordial and Posterior ECG Leads

I Jekova^{1*}, V Krasteva¹, R Leber², R Schmid², R Abächerli^{2,3}

¹Institute of Biophysics and Biomedical Engineering, Sofia, Bulgaria

²Schiller AG, Baar, Switzerland

³CRIB, University Hospital Basel, Switzerland

Lead reversal has been reported to occur in 0.4-4% of all standard 12-lead ECGs. This proportion might be much higher for 16-lead ECGs, including the uncommon right-sided precordial and posterior leads. Considering that the supplementary electrodes are placed for specific diagnostic purposes (improved study of right ventricle pathologies, scanning for presence of posterior myocardial infarction), their incorrect placement can simulate/mask ECG abnormalities and might lead to wrong therapy decisions.

This study presents a method for automated detection of misplaced right precordial (V3R,V4R) and posterior (V8,V9) leads, based on assessment of the correlation between QRS-T patterns in lead pairs. The incorrect placement of V3R,V4R is detected by analysis of MatrixR (4x4), including the correlation coefficients between QRS-T waveforms in V4R,V3R,V3,V4. Analyzing rows and columns in MatrixR, any deviation from the trend for gradual increase of correlation coefficients towards the cell where a lead is compared to itself, is considered as lead reversal. Similarly, the misplacement of V8,V9 is detected by analyzing MatrixR (5x5), with correlation coefficients between V4,V5,V6,V8,V9.

Both methods are tested with an ECG database, including 1333 16-lead recordings (standard 12 leads + V3R,V4R,V8,V9) collected from chest pain patients at the Emergency Department of University Hospital, Basel via the Schiller CS-200 Excellence (1kHz sampling, 1 μ V resolution). The device does not give any feedback to the user with respect to lead reversal so that correct electrode placement during ECG acquisition is assumed. We simulated particular reversal sets, including: (i) leads involved in MatrixR (V3,V4,V3R,V4R and V4,V5,V6,V8,V9); (ii) additional leads for which interchange is quite possible (V8,V9,V3R,V4R). The specificity (Sp=83.4%) for the correct electrode placement and the sensitivity (Se=93.4 to 96.5%) for the simulated reversals are presented in Table 1. The limited Sp could be partially due to true interchanges during ECG acquisition, considering the lack of experience for placement of V3R,V4R,V8,V9.

Table 1.

Leads	Number of electrode positions	Sp	Se (mean \pm std)
V3,V4,V3R,V4R	23 reversals + 1 correct placement	83.4 %	(93.4 \pm 4.5) %
V4,V5,V6,V8,V9	119 reversals + 1 correct placement	83.4 %	(96.5 \pm 4.3) %
V8,V9,V3R,V4R	23 reversals + 1 correct placement	83.4 %	(94.0 \pm 4.6) %

Distribution Entropy for short-term QT Interval Variability Analysis: A Comparison between the Heart Failure and Normal Control Groups

Yang Li¹, Peng Li¹, Chandan Karmakar^{2,3}, Changchun Liu¹

¹School of Control Science and Engineering, Shandong University, Jinan, P. R. China

²Electrical & Electronic Engineering Department, University of Melbourne, Melbourne, Australia

³Centre of Pattern Recognition and Data Analytics (PRaDA), Deakin University, Geelong, Australia

QT interval is physiologically related to the ventricular depolarization and repolarization. Previous studies have proved the beat to beat QT interval variability (QTV) helpful for evaluating the cardiac mortality and severity of illness in patients with cardiac dysfunction. Currently, a common method for quantifying QTV is the QT variability index (QTVI). Owing to the nonlinear nature of QTV data, recent studies have also applied advanced entropy methods, such as the approximate entropy (ApEn) and sample entropy (SampEn). Most recently, a novel distribution entropy (DistEn) has been reported to have superior performance compared with conventional methods for especially short length data. We thus aimed, in the present study, to investigate the short-term QTV data in heart failure (HF) patients by this novel DistEn.

Thirty-three HF patients and 34 healthy subjects were studied, and between the two groups, no statistical significance in age and gender was found. Electrocardiography (ECG) data with a standard limb-II configuration was recorded at a sampling frequency of 1,000 Hz for at least 5 min. A template compressing-stretching approach was applied to automatically extract the beat-to-beat QT intervals. DistEn, as well as traditional SampEn, fuzzy entropy (FuzzyEn), and QTVI, were performed for each QTV series.

Results demonstrated a statistically significantly increased DistEn of QTV in HF group compared with the normal control group ($p < 0.001$). No significant difference was found in both SampEn and FuzzyEn between the two groups. In addition, results also suggested a significantly increased QTVI in HF group ($p < 0.01$). Pearson correlation analysis showed that DistEn was significantly related to QTVI in HF group ($p < 0.05$), whereas no significant relation was found between them in healthy control group. The results indicated that the DistEn analysis of QTV data may provide a valuable additional feature for evaluating the cardiac functioning in HF patients.

PB8

A Novel Technique for Analysing Beat-to-Beat Dynamical Changes of QT-RR Distribution for Arrhythmia Prediction

Mohammad Hasan Imam, Chandan Karmakar*, Ahsan Khandoker, Marimuthu Palaniswami

Deakin University
Australia

Ventricular tachycardia (VT) leading to ventricular fibrillation (VF) is the major cause of sudden cardiac death (SCD) with subjects with or without any history of cardiac disease. Prediction of the initiation of ventricular fibrillation is crucial for both successful preventive measure and effective defibrillation therapy. A lot of studies have been done based on electrocardiogram (ECG) waveform analysis for VF detection but this field still needs more perfection. Both HRV and QTV related parameters were reported to be analysed for VT/VF detection and prediction with inconsistent results in different populations. In this study, we propose a novel time domain measurement tool to detect the pattern of dynamical changes of both RR and QT intervals in subjects having sustained VT/VF episodes from VFDB and AHA database (www.physionet.org). We also analyse the same pattern in some healthy subjects from Fantasia database and compare the distribution of patterns between healthy and VT/VF subjects. Our findings showed that the distribution of QT-RR dynamics are statistically significantly different ($p < 0.05$) in healthy subjects from VT/VF in particular before the start of VF episode. Therefore, distribution of change in QT-RR dynamics may provide insight of the underlying instability before VF events and can be used for better prediction of arrhythmogenesis.

The Effects of Electrode Placement on an Automated Algorithm for Detecting ST Segment Changes on the 12-Lead ECG

Dewar Finlay*, Raymond Bond, Alan Kennedy, Daniel Guldenring, James McLaughlin

Belfast, United Kingdom

It is known that variations in electrode placement can result in significant variability in recorded ECG waveforms. In this study we investigate the effect that variations in precordial electrode placement can have on the detection of ST segment changes associated with coronary artery occlusion. Our experiments were based on analysis of data from 45 subjects who had 120 lead BSPMs recorded during percutaneous transluminal coronary angioplasty (PTCA). A total of 90 BSPMs were studied representing the 45 subjects at baseline and the same 45 subjects during peak balloon inflation (15 left anterior descending, 15 left circumflex and 15 right coronary artery). Twenty-one 12-lead ECGs were extracted from each BSPM. This included a 12-lead ECG extracted corresponding with correct precordial electrode positioning and further 12 lead ECGs corresponding with uniform vertical movement of all of the precordial leads in 5mm increments up to +/-50mm away from the correct position. To facilitate analysis a computer algorithm, based on the current ESC/ACCF/AHA/WHF guidelines for the detection of STEMI and Non-STEMI, using MATLAB. This algorithm was applied to all of the extracted 12-lead ECGs. Median sensitivity and specificity, based upon all baseline versus all peak balloon inflation cases, were calculated for results generated at each electrode position. With the precordial leads positioned correctly sensitivity and specificity were 62.2% and 80.0% respectively. When all precordial leads were placed 50mm superior to their correct position sensitivity and specificity increased to 71.1% and 82.2% respectively. At 50mm inferior to the correct position the sensitivity and specificity were 60.0% and 77.8% respectively. The results show a variation of more than 10% in sensitivity when the electrodes are moved 100mm vertically. Specificity shows less variability under the same conditions.

PB8

Reduction of False Cardiac Arrhythmia Alarms Through the Use of Machine Learning Techniques

Miguel Caballero, Grace Mirsky*

Benedictine University
United States

Due to the so-called “crying wolf” effect, frequent false cardiac arrhythmia alarms have been shown to diminish staff attentiveness and thus reduce the quality of care patients receive in the ICU. The PhysioNet/Computing in Cardiology 2015 Challenge seeks to improve patient care by decreasing the number of these false cardiac arrhythmia alarms. Using a training set of 750 multi-parameter recordings organized by type of arrhythmia alarm, we developed a decision tree for each arrhythmia category. We derived the features utilized in the decision tree from the arterial blood pressure (ABP) waveform, the photoplethysmogram (PPG), and the electrocardiogram (ECG). We achieved the following results for the training set (average scores for all five arrhythmia types): true positives = 36.0%, false positives = 11.4%, false negatives = 5.1% and true negatives = 46.3%. The test set is comprised of 500 records that are hidden from the participants for the duration of the challenge. For Phase I, our score for the real-time test set = 57.64 and retrospective test set = 61.15, resulting in an overall score of 59.39. For Phase II, we plan to further investigate additional machine learning techniques.

Signal Quality-Based Approach to False Arrhythmia Alarms Reduction

Adam Mahdi*, Dragana Nikolic

University of Oxford
Oxford, United Kingdom

Motivation: Frequent incidences of false alarms in the Intensive Care Unit (ICU) have been recognized as a challenging problem for several reasons. They can affect the desensitization of warnings, decrease of response times of the medical staff and ultimately decrease the quality of care. In relation with the PhysioNet/CinC 2015 challenge the current study aimed at developing a computational method to reduce the ICU false alarms associated with five life-threatening arrhythmias: asystole, extreme bradycardia and tachycardia, ventricular tachycardia and ventricular flutter/fibrillation.

Methods: The organizers provided 750 multimodal recordings (two ECG leads together with arterial blood pressure (ABP) and/or photoplethysmogram (PPG)) for testing the false arrhythmia alarms reduction algorithms. Initially, only a combination of signal quality indices of ABP (sqiABP) and PPG (sqiPPG) together with the provided definitions of the five alarms have been used to accept or suppress the alarm. Subsequently, a QRS detector of the ECG signals was incorporated and used for the final decision (all alarms except ventricular fibrillation).

Results: The preliminary algorithm, which incorporates the QRS complex detector, showed an improvement of the reduction rate of the false alarms under consideration except for ventricular tachycardia with the 84% and 55% real-time true positive (TP) and true negative (TN), respectively; 86% and 60% retrospective TP and TN, respectively and the overall score of 55.37.

Conclusions: The analysis of sqiABP and sqiPPG showed limited correlation with TP and TN, especially for ventricular tachycardia. This suggests a need for assessing and using the signal quality index of ECG (sqiECG) for reconstructing the corrupted parts of the signal and the final decision. Thus, an extended Kalman filter with the modified McSharry ECG generator is being developed to filter the corrupted portions of the data; and sqiECG based on the Belanger's estimation of the covariance matrix is currently being incorporated.

PB9

Reducing False Arrhythmia Alarms in the ICU

Nadi Sadr*, Doan Trang Nguyen, Chandan Kalra, Alistair McEwan,
Philip de Chazal

Sydney, Australia

In this study, we develop algorithms that reduce the arrhythmia false alarms in the ICU by processing the four signals of PPG, ABP, ECG Lead II, Augmented right arm ECG. Our algorithms detect five arrhythmias including asystole, extreme bradycardia, extreme tachycardia, and ventricular flutter and fibrillation. Both real time and retrospective algorithms are provided. Our processing proceeded as follows. Firstly, preprocessing was applied to the ECG signals by two median filters in order to remove the noise. Then a Hilbert-transform based QRS detector algorithm was used to detect R waves from the ECG signals. Following this, RR intervals were calculated from the two ECG signals. These RR intervals were combined with the RR intervals detected from PPG and ABP signal calculated using the algorithms provided by the competition organisers. The combined RR intervals were smoothed with a 5 point moving average filter and thresholded at the clinically important values for the 5 arrhythmias. To further assist the detection ventricular fibrillation we calculated the power spectral density (PSD) of ECG signals and identified frequency components suggesting ventricular fibrillation. Our first phase overall result was a 82% True Positive Rate, 51% True Negative Rate with score of 49.84.

False Alarm Reduction in ICU by Fusion of Neuro-SVM Classifiers and Heartbeat Detection from Multimodal Data: Geometrical and Multi-resolution Analysis

Mohammad Javad Mollakazemi, Seyyed Abbas Atyabi, Farhad Asadi, Ali Ghaffari

Cardiovascular Research Group (CVRG), Department of Mechanical Engineering at K.N.Toosi University of Technology, Tehran, Iran

Background: Online-monitoring systems in Intensive Care Unit (ICU) are affected by high rate of irrelevant alarms which are caused by fluctuations, noise and outliers in the measured time series data. False alarms can affect care process adversely and impact both patients and clinical staff.

Aim: This study aims to propose an algorithm to reduce false arrhythmia alarms in ICU.

Methods: In this approach, two analyses were used for arrhythmia detection. The first analysis was time-frequency domain analysis and the other one was time domain analysis. In time-frequency analysis the major processed waveform was electrocardiogram signal (ECG). Firstly, the signal was pre-processed to remove impulsive artefacts, power line interference and baseline wandering. The non-value data was eliminated and then was estimated based on nearest-neighbor method. Then, wavelet packet transform was applied to the resulted ECG with function of 'syms6' at level 8. The energy of the nodes of the wavelet packet transform was used as the feature vector. Afterward, with analysis of the ROC curve for feature discrimination, fifty proper nodes were selected. After feature selection, two classifiers of artificial neural network (ANN) and support vector machine (SVM) was implemented. In time domain analysis, ECG, arterial blood pressure (ABP) and photoplethysmogram signal (PPG) were used. The heart rate was derived by fusing these waveforms. If the extracted heart rate was outside the variable range specified by the alarm, then the alarm was suppressed. Finally, after getting the results from ANN, SVM and time domain analysis the final decision was made based on the majority voting.

Results: This method was tested by 500 recordings of the PhysioNet/CinC Challenge 2015 test dataset and the real-time, retrospective and overall scores of 44.81%, 47.84% and 46.35% were obtained, respectively.

PB9

Reducing False Arrhythmia Alarms in the ICU

Soo-Kng Teo, Jian Cheng Wong, Bo Yang, Feng Yang, Tian You Zhang, Ling Feng, Toon Wei Lim, Yi Su*

Institute of High Performance Computing, A*STAR, Singapore
Singapore

Aims: This study assessed the feasibility of using multimodal data, namely ECG, ABP and PLETH for reducing the incidence of false alarms in the Intensive Care Unit (ICU) for the PhysioNet/Computing in Cardiology Challenge.

Methods: Our approach relies on the detection of heartbeats using both the ECG and ABP/PLETH signals. The intervals between heartbeats are then used to determine if the triggered alarm is a true or false alarm. The detailed steps for this alarm classification is as described: (i) Perform quality check for the individual signals during the last 30 sec-onds window. Detection of heart-beats will be performed using only signals that pass this quality check. (ii) The `gqrs` and `wabp` routines in the WFDB toolbox are used to identify the ECG peaks and ABP/PLETH peaks from the respective signals. An in-house algorithm (adapted from last year's challenge) is used to cross validate the peaks from both set of signals. The delay between the ECG peaks and ABP/PLETH peaks are computed using a moving average approach and this delay is used to identify the ECG peaks when the ECG signal is noisy. (iii) If ABP/PLETH signal is noisy, an error-correction is implemented in our algorithm to check the computed delay. The error-correction ensures that within any sampled interval, if either the ECG or ABP/PLETH signal is NOT noisy, the locations of the heartbeat are uniquely identified. (iv) The time intervals between heartbeats in the last 16 seconds and the corresponding heartbeat per minutes (bpm) are computed. The bpm is then used as a criterion to determine if a triggered alarm is classified as a true or false alarm.

Results: (Unofficial Phase): TPR TNR Score Overall 63%
84% 52.73

PB9

Multi-modal Integrated Approach towards Reducing False Arrhythmia Alarms During Continuous Patient Monitoring; PhysioNet/Computing in Cardiology Challenge 2015

Sardar Ansari*, Ashwin Belle, Kayvan Najarian

University of Michigan
Ann arbor, United States

Introduction: Physiologic alarms during continuous monitoring of patients have become an imperative aspect of modern healthcare; however such alarms continue to remain unreliable. Our aim in this project is to build a robust and reliable physiological alarm verification mechanism.

Methods: The proposed algorithm computes and combines bio-markers from prevailing physiologic waveforms such as electrocardiogram (ECG), arterial blood pressure (ABP) and photoplethysmogram (PPG) to verify ICU alarms. Customized peak detection is one of the most crucial steps in alarm verification. The authors have designed a robust peak detection algorithm using the information from multimodal data, e.g., ECG, ABP and/or PPG signals. The peak detection algorithm is sophisticated enough to accurately mark the abnormal ECG peaks such as the ones associated with ventricular tachycardia. The identified peaks are then used to extract features from the signal, such as normalized power and maximum duration of the peaks. Then, the features are fed into a support vector machine to classify the true and false alarms.

Results: The proposed algorithm increases the accuracy for Asystole, Extreme Bradycardia, Extreme Tachycardia, Ventricular Tachycardia and Ventricular Flutter/Fibrillation alarm verification to 0.918, 0.877, 0.971, 0.845, 0.733 and 0.869 in the training dataset, respectively (using 10-fold cross-validation). This translates into a 23.9% improvement from the original algorithm provided by PhysioNet. The results of applying the full algorithm to the test dataset were not acquired due to a server error. However, an earlier version of the algorithm focused on Asystole alarms increased the true positive and true negative rates from 0.75 and 0.47 to 0.92 and 0.80 on the test dataset, respectively. That resulted in an increase in the overall score from 47.57 to 53.10.

Conclusions: These results indicate that a combination of filtering, robust peak detection, feature extraction and machine learning can greatly improve the accuracy of alarm verification.

PB9

Reliability of Clinical Alarm Detection in Intensive Care Units

Charalampos Tsimenidis, Alan Murray*

Newcastle University
Newcastle upon Tyne, United Kingdom

In hospital environments advanced medical devices are vital for both monitoring and therapy. Many have alarms, especially in intensive care areas. To ensure that important and unwanted clinical events are not missed, there is a tendency for devices to react to noise and artefact in the physiological waveforms, with many resulting false alarms. PhysioNet along with Computing in Cardiology have made available clinical alarm data, to allow improved algorithms for alarm detection to be developed. We present our results. Our analysis steps included: high pass filtering to remove baseline instability, scaling to normalise waveform amplitudes, detection of noisy including flat waveforms, differentiation to accentuate sharp waveform edges, beat detection, timing between beats preceding alarm onset, and detection of alarm conditions. When the waveforms were assessed as noisy they were labelled as false alarms. When noise-free and alarm conditions were met they were labelled as true alarms. The original PhysioNet analysis algorithm analysed blood pressure (BP) and photoplethysmograph (PPG) waveform data, resulting in true alarm detection sensitivity of 89% and 88%, and specificity of 38% and 38%, for the learning and test (score 46) data sets respectively, indicating a similar range of data in both sets. We investigated the use of ECG data alone with the learning data, and this resulted in overall gross sensitivity and specificity for the first ECG channel of 89% and 68%, and for the second, 87% and 68% respectively. When BP and PPG were analysed following detection of noise in the ECG the results were 92% and 56%, and 90% and 54% respectively. We have shown that analysis of the ECG alone can obtain average sensitivity of 88%, with little difference in results between two simultaneous ECG channels. Use of additional physiological data improved sensitivity by 3% points, but decreased specificity by 13% points.

PB9

Reducing False Arrhythmia Alarms in the ICU using Novel Signal Quality Indices Assessment Method

Runnan He*, Henggui Zhang, Kuanquan Wang, Yongfeng Yuan, Qince Li, Jiabin Pan, Zhiqiang Sheng, Na Zhao

United Kingdom

The physiological signals such as the electrocardiogram (ECG) and arterial blood pressure (ABP) in the ICU are often severely corrupted by noise, artifact and missing data, which lead to large errors in the estimation of the signals values. Frequent false alarms due to data corruption will lead not only to sleep deprivation for patients and stress for patients and staff, but also to wasted time, resources, and to a desensitization of clinical staff to real alarms and a consequent drop in the overall level of care. We started with the signal quality assessment of vital signs in intensive care patients, derived the signal quality index (SQI) to reveal the degree of signal quality. Based on the SQI, the vital signs were estimated in the presence of high levels of noise and artifact. And then the arrhythmia false alarm reduction algorithm in ICU monitors was accomplished. The method is based upon the concept of fusing multiple SQIs and HR estimates derived from multiple ECG leads and an invasive ABP waveform recorded from ICU patients. Physiological SQIs were obtained by analyzing the statistical characteristics of each waveform and their relationships to each other. The SQI of ECG signals was obtained by combining four analysis methods: the comparison of multiple beat detection algorithms, and the SQI of ABP signals was obtained by a combination of two algorithms: a beat-by-beat fuzzy logic-based assessment of features in the ABP waveform and heuristic constraints of each ABP pulse to determine normality. HR estimates from the ECG and ABP are tracked with separate Kalman filters, which use three methods of calculation HR. Results show that the overall TPR and TNR are respectively 63 and 79 percent, and the overall score for the challenge in phase I is 50.41.

PB9

Reducing False Arrhythmia Alarms by Means of Beat Clustering

Tilo Himmelsbach*

Germany

The aim of reducing false alarms in ICU-units can only be reached if arrhythmia-detecting algorithms become more sophisticated and adaptive to individual characteristics of patients. In order to discriminate normal sinus-rhythm from artifacts or arrhythmia it is firstly necessary to define a simple but decent description of the normal (patient individual) qrs-shape. Therefore all qrs-complexes prior to the potentially arrhythmic event are taken to form such a description. Firstly, the given signals are filtered and qrs-complexes are detected. Features are extracted from each detected qrs-complex in order to get a low-dimensional description of their patterns. By the use of those features a clustering of all detected qrs-complexes is done. There is no assumption for a single normal qrs-shape, so there can be multiple clusters describing different normal qrs-shapes. In order to classify clusters as “normal” they must contain a certain minimum amount of consecutive qrs-complexes. In the last seconds of each measurement, where the arrhythmia is expected to occur, potential qrs-complexes are assigned to clusters by means of minimizing a distance measure. If this minimal distance is higher than a certain threshold the shape is classified as an artifact. The classification of different arrhythmia-types is then done by concerning the qrs-shapes as well as the resulting heart-rate. Solely the arrhythmia of ventricular fibrillation states an exception from this frame-work for not having qrs-complexes. Ventricular fibrillation is instead detected by the use of features from the frequency domain. The algorithm realizing the above described idea could not get to run properly before the end of the unofficial phase, so an overall score of only 43.02 was reached.

Identification of ECG Signal Pattern Changes to Reduce the Incidence of Ventricular Tachycardia False Alarms

Vytautas Abromavičius*, Artūras Serackis, Andrius Gudiškis

Vilnius Gediminas Technical University
Vilnius, Lithuania

The aim of this study is to propose an algorithm for real-time analysis of two simultaneously recorded ECG signals in order to identify the ventricular tachycardia (VT) incidence. The VT alarms are usually initiated by 5 or more ventricular beats observed with heart rate higher than 100 bpm. Visual analysis of the ECG signal shape recorded during true VT incident lead to the hypothesis that these incidents are followed by noticeable changes of the QRS complex shape and evenly spaced heart beat annotations. The quality of the heart rate estimation highly depends on the quality of the monitored signals. The accidental distortions of the monitored signals shape may trigger the false alarm. The proposed algorithm compares ECG signal shape parameters with historical data, collected for the same patient and uses threshold function to make a decision between acceptable and non-acceptable ECG signal quality for initiation of alarm. Two proposed algorithm modifications were analysed in this study. 1st modification uses 1 minute length historical data to estimate the mean magnitude of the ECG signal and compare with mean values of currently received ECG data in real time. The 2nd modification uses continuous monitoring of the RR intervals in ECG signal. Standard deviation of the signal is estimated. The decision to initiate VT incident is made by comparing the heart rate estimated from 5 consecutive beats (taking the mean value) with 100 bpm threshold together with estimation of the standard deviation of the RR intervals in the same analysis frame. A subset of data of the Physionet/CinC Challenge 2015 is used to test both algorithm modifications. The test set of 500 hidden records produced overall score of 51.04 (32.37 for VT), with 88% TPR, 45% TNR for the 1st modification and 45.4 (34.82 for VT), with 76% TPR, 52% TNR for 2nd.

PB9

Reducing False Arrhythmia Alarm by Quality Assessment of Multimodal Physiological Signals using Cepstrum Analysis

Yongwei Zhu*

Institute for Infocomm Research
Singapore, Singapore

Reducing false arrhythmia alarm by quality assessment of multimodal physiological signals using cepstrum analysis This study aimed for reducing false arrhythmia alarm by quality assessment of the multimodal physiological signals, including ECG, ABP and PPG, by using cepstrum-based analysis. Our cepstrum analysis method could assess the quality of pulsatile signals and estimate beat-to-beat interval in the signals as the same time. A novel step of windowing of the logarithm spectrum in the calculation of cepstrum was introduced. A dominant cepstral peak would present if two beat patterns repeated in the time analysis window, regardless of the morphology of the waveform pattern. The cepstral peak can serve as an indicator of the correctness of detected beats and the soundness of two heart beats repeating. The quality of a signal is classified by using threshold values, which is different for different modalities. In addition, the quality of two more synchronized signals can also be verified if the beat-to-beat intervals detected agree to each other. For reducing the false arrhythmia alarm by quality assessment, some simple rules were used. For instance, when the quality of signals of any modality of the alarm window is good and the detected heart rate is not within alarming range, then the alarm is classified as false alarm. Morphological features of specific modality have not been used at current stage, as such this method has some limitation on detecting false alarm when quality of all signal modality is bad. Based on the results on the test data, the method works best for Tachycardia. The true positive rate is 88% and true negative rate is 80%. We would apply more morphological features and use classifiers for better performance in the next stage.

PB9

Case-Based Reasoning and Multimodal Data Classification using Exponential Similarity and Signal Quality Indices

Haiyan Yu*, Jiang Shen, Man Xu

Chongqing University of Posts and Telecommunications
Chongqing, China

All bedside monitors are prone to heterogeneity and missing data, yet each multimodal sample data contains different sets of multi-dimensional attributes. To reduce the incidence of false alarms in the Intensive Care Unit (ICU), a new automated algorithm was proposed. The algorithm was based on both novel and previously published signal quality metrics. Kurtosis-based signal quality index (kSQI) was presented to abstract complex features from the ECG waveforms, as well as the jsQI and ppgSQI. The annotations were obtained with the wabp function from the target signal, after being preprocessed. Signal quality indices were used as the inputs to a case-based reasoning classifier with an exponential similarity. This classifier was trained with the posted 750 records of the PhysioNet/CinC 2015 Challenge to estimate the quality of query segments of ECG waveforms. Compared with the algorithms with decision rules based on the thresholds, the performance of our proposed algorithm improves the interpretability without sacrificing performance. Evaluated with the hidden test dataset, both real-time and retrospective, the results of this method show that the overall score is 46.19 with true positive rate 83% and true negative rate 43%. This algorithm offers a fresh perspective on reducing the maximum number of false alarms while avoiding the suppression of true alarms, and a new way of thinking about the balance of accuracy and interpretability in predictive modeling.

PB9

Algorithm for Life-Threatening Arrhythmias Detection with Reduced False Alarms Ratio

Iga Grzegorzczuk*, Kamil Ciuchciński, Jan Gierałtowski, Katarzyna Kośna, Piotr Podziemski, Mateusz Soliński

Warsaw University of Technology
Warsaw, Poland

With the increasing quality and costs of health services a lot of stress is put to provide excellent care on the ICU, where patients are in the most demanding condition and need reliable monitoring. However, the amount of false alarms of cardiac episodes still outnumbers the true ones significantly. These situations might result from the poor quality or loss of the signals and prevent proper analysis. The advanced analysis of multiple signals such as ECG, BP and PLETH registered by monitoring system might enable reduction of the false alarms and improve its performance. We analyzed 750 multi-channel recordings with the sampling rate of 250 Hz from the PhysioNet Challenge 2015 training set, which contains 2 types of signals: real-time with the length of 5 minutes recorded before the alarm and retrospective with additional 30 s after alarm. Each alarm was labeled either 'true' or 'false'. Our task was to reduce number of false alarms, while avoiding the suppression of true ones. Each recording contained two ECG leads and at least one additional pulsatile waveform (e.g. blood pressure, photoplethysmogram). Our algorithm focuses on detecting the most prominent part of a QRS complex i.e. RS slope to find location of R peaks from ECG signal. Similar slope detection method is performed for other channels provided. Basing on obtained annotations algorithm verifies whether the alarm was true or false for following arrhythmic events: Asystole, Bradycardia and Tachycardia, using criteria given in the Challenge. In case of signals recorded during Ventricular Flutter and Fibrillation, where it is not possible to detect QRS complexes direct signal morphology assessment is used. Work on the implementation of neural networks for these diseases is in progress. The preliminary test score of the PhysioNet Challenge was 45.85 for Real-time event and 50.78 for Retrospective event, giving overall score 48.24.

PB9

T-Wave Alternans Hysteresis on Heart Rate

Laura Burattini*, Sumche Man, Sandro Fioretti, Francesco Di Nardo, Cees A Swenne

Università Politecnica delle Marche
Ancona, Italy

Microvolt T-wave alternans (TWA), a subtle every-other-beat fluctuation of the electrocardiographic (ECG) T-wave amplitude, is a promising risk index for the occurrence of malignant ventricular arrhythmias and sudden cardiac death. It is well-known that TWA tends to increase with heart rate (HR). Consequently, TWA is usually analyzed at accelerated HRs often reached through exercise. Since TWA during recovery is usually not analyzed, it is not clear yet if TWA and HR are linked by an one-to-one correspondence, or if it does exist a TWA hysteresis on HR. To investigate such issue our HR adaptive match filter based method for automatic TWA identification was applied to ECG recordings of 266 patients with implanted cardio-defibrillator. The ECGs were acquired during a bicycle ergometer test which included a HR-increasing exercise phase and a HR-decreasing recovery phase. Both phases were characterized by a HR ranging from 80 bpm to 125 bpm. Results indicate that in both phases TWA has a positive association with HR but, at each HR, exercise TWA is typically different from recovery TWA. Specifically, TWA increases exponentially during exercise (fitting-exponential-curve correlation: $\rho=0.99$, $P<10^{-7}$) while decreases linearly during recovery (fitting-line correlation: $\rho=0.94$, $P<10^{-4}$). Fitting exercise-exponential-curve and recovery-line cross at about 110 bpm, so that for lower HRs (80-105 bpm) exercise TWA is significantly lower than recovery TWA (median values: 19 μV vs. 26 μV ; $P<10^{-8}$), while for higher HRs (115-125 bpm) exercise TWA is significantly higher than recovery TWA (median values: 40 μV vs. 27 μV ; $P<10^{-8}$). Thus, it can be concluded that it does exist a TWA hysteresis on HR since TWA does not depend only on the actual value of HR but also on such value being reached during exercise or recovery.

Three-Dimensional Echocardiography Based Evaluation of Right Ventricular Remodeling in Patients with Pressure Overload

Francesco Maffessanti*, Karima Addetia, Megan Yamat, Lynn Weinert, Roberto Lang, Victor Mor-Avi

United States

Although 3D echocardiography (3DE) allows imaging of right ventricular (RV) morphology, regional RV remodeling has not been evaluated using 3DE. We developed a technique to quantify regional RV shape and tested its ability to characterize RV shape in normal subjects and in patients with RV pressure overload. Transthoracic 3DE images were acquired in 54 subjects (39 patients with pulmonary artery hypertension, PAH, and 15 normal controls, NL). 3D RV surfaces were reconstructed at end-diastole and end-systole (ED, ES) and analyzed using custom software to calculate 3D mean curvature of the inflow and outflow tracts, apex and body (both divided into free-wall and septum). Septal segments in NLs were characterized by concavity (curvature <0) in ED and slight convexity (curvature >0) in ES. Conversely, the septum remained convex throughout the cardiac cycle in PAH. In the NL group, the body free-wall transitioned from a convex surface to a more flattened surface during contraction, while the convexity of the apex free-wall increased. In contrast, in PAH, both RV free-wall segments remained equally convex throughout the cardiac cycle. Curvature analysis using 3DE allows quantitative evaluation of RV remodeling, which could be used to track differential changes in regional RV shape, as a way to assess disease progression or regression.

A Study of Early Afterdepolarizations in Human Ventricular Tissue

Nele Vandersickel, Alexander V Panfilov*

Gent University
Gent, Belgium

Sudden cardiac death is often caused by cardiac arrhythmias. Recently, special attention has been given to a certain arrhythmogenic condition, the long-QT syndrome, which occurs as a result of genetic mutations or drug toxicity. The underlying mechanisms of arrhythmias, caused by the long-QT syndrome, are not fully understood. However, arrhythmias are often connected to special excitations of cardiac cells, called early afterdepolarizations (EADs), which are depolarizations during the repolarizing phase of the action potential. So far, EADs have been studied mainly in isolated cardiac cells. However, the question on how EADs at the single-cell level can result in fibrillation at the tissue level and whole heart level especially in human cell models, remains underinvestigated. In this study, we investigate how EADs at the single cell level can give rise to arrhythmias at tissue level and in the anatomically accurate model of human ventricles. We use a TenTusscherPanfilov06 model for human ventricular cells and induce EADs by modeling experimental conditions which have been shown to evoke EADs at a single-cell level, i.e. by reducing the repolarization reserve (RR). We find that three types of abnormal wave patterns emerge. The first type is fibrillation consisting of Na-mediated and Ca-mediated waves, which has also been found in experiments by Chang et al. and is called bi-stable wave propagation. Reducing the RR further results in the emerging of a second type of fibrillation consisting of solely Ca-mediated spiral waves. Finally, further reduction of the RR results in the formation of Ca phase-waves. We characterize the observed patterns in terms of numbers and type of phase similarities and study dynamics of 2D rotors and the three dimensional filaments in the whole heart model and relate it to arrhythmias which can occur under such conditions, including the Torsade de Pointes.

Computer Simulations of Three-dimensional Coronary Blood Flow After CABG and Simulated PCI Procedures

Jun-Mei Zhang*, Tong Luo, Jia Lin Soon, Ning Kang, Kenny Yoong Kong Sin, Swee Yaw Tan, Teing Ee Tan, Chong Hee Lim, Mathew Jose Chakaramakkil, Adrian Seng Wae Ooi, Aileen Mae Lomarda, Ru San Tan, Liang Zhong

National Heart Centre Singapore
Singapore, Singapore

Aims: Percutaneous coronary intervention (PCI) and coronary artery bypass grafting (CABG) are treatment procedures for patients with coronary artery disease. Despite many trials comparing their clinical outcomes, there are few quantitative comparisons of their relative effects on coronary blood flow (CBF) post procedure. We aim to develop a tool to mimic both PCI and CABG, and to perform CBF analyses before and after the procedures.

Methods: A patient with triple-vessel coronary artery stenoses was recruited. He received CABG with three grafts: left internal mammary artery (LIMA) to left anterior descending artery (LAD); saphenous vein graft (SVG) to obtuse marginal (OM); and SVG to posterior descending artery (PDA). Computed tomography angiography (CTA) images were acquired after surgery, from which a post-CABG model was reconstructed using our customized tool. A baseline pre-procedural model was simulated by removing the three grafts. A PCI model was built by simulated dilatation of the native coronary stenoses with virtual stents (Figure). A total of 1.6, 1.8 and 2.1 million cells were generated for the baseline, PCI and CABG models, respectively. Blood was assumed to be a non-Newtonian fluid with Carreau model. Through solving Navies-Stokes equations, CBF distribution was determined in all models.

Results: In the pre-procedural model, CBF downstream of LAD, OM and PDA were 22.4ml/min, 10.3ml/min and 12.9ml/min, respectively. In the PCI model, the CBF increased to 29.0ml/min, 10.5ml/min and 15.0ml/min, respectively. In the CABG model, the CBF increased to 39.6ml/min, 12.6ml/min and 16.5ml/min, respectively. More than the simulated PCI procedure, CABG improved CBF downstream of the respective stenoses in the pre-procedural model.

Conclusions: This patient-specific simulation of three-dimensional CBF will enable clinicians and scientists to feasibly quantitate the effects of PCI and CABG on patients with coronary artery disease. This holds potential for individualized treatment planning, and may ultimately lead to improved patient care.

Author Index

Aarts, Ronald M,	82	Ariga, Rina,	3
Abächerli, Roger,	308, 312	aruscotti, Mirko,	1
Abaecherli, Roger,	201	Arza, Adriana,	274
Abboud, Shimon,	101	Asadi, Farhad, ...	255, 293, 301, 319
Abou Allaban, Yousef,	288	Atienza, David,	31, 41
Addetia, Karima,	330	Attarodi, Gholamreza,	198
Adeniran, Ismail,	124	Atyabi, Seyyed Abbas,	255, 301, 305, 319
Agostinelli, Angela,	56, 179	Augustyniak, Piotr,	55
Aguiló, Jordi,	274	Aysin, Benhur,	233
Ahmed, Khawza I,	288	Babaeizadeh, Saeed,	72, 275
Airaksinen, Juhani,	227	Babic, Aleksandar,	47
Akhbardeh, Alireza,	17	Badilini, Fabio,	233
Aktas, Mehmet,	181	Bai, Jieyun,	192
Akulov, Sergey,	163	Bai, Xiangyun,	38
Akulova, Anna,	163	Baiazitova, Larisa,	122, 262, 306
Alamdari, Nasim,	17	Baig, Tariq,	176
Al-Aubaidy, Hayder,	279	Bailón, Raquel,	215, 218, 274
Albanese, Maria,	282	Barbieri, Riccardo, ...	162, 214, 272, 282
Alberto, Alex C,	185	Bargiotas, Ioannis,	196
Alcaine, Alejandro,	226	Barquero-Ñirez, Uscar, 34,	269, 281
Alcaraz, Raul,	12, 13, 132, 133	Bartolucci, Chiara,	1
Aletras, Anthony,	94, 95, 127	Baumert, Mathias,	57
Almeida, Rute,	187	Bear, Laura,	62, 64, 257
Almeida, Tiago,	74, 141	Béhar, Nathalie,	67
Almeida, Tiago P,	14, 15, 16	Bellanger, Jean-Jacques,	98
Alonso, Daniel,	150	Belle, Ashwin,	321
Alonso, Erik,	273	Beltrón-Molina, Ferney A,	22
Alonso-Atienza, Felipe,	63	Benchimol-Barbosa, Paulo Roberto,	54, 138
Alueva, Yulia,	97	Benson, Alan P,	174
Álvarez, Diego,	63	Berenfeld, Omer,	238
Alvarez-Lacalle, Enrique,	91	Berg, Sebastian,	176
Amblard, Amel,	88	Berjano, Enrique,	19
Amoore, John,	5	Bertschy, Gilles,	220
Angel, Fabielle,	149	Betancur, Julian,	98
Angeletti, Rachele,	24	Bevan, Graham H,	117
Ansari, Sardar,	321	Bhatia, Kanwal K,	73
Aquilina, Michele,	46	Biala, Taher,	213
Arad, Marina,	101		
Aramendi, Elisabete,	150, 273		
Arentz, Thomas,	131		

Bidar, Elham,.....	134	Caballero, Miguel,	316
Bijnens, Bart,.....	218	Cabasson, Aline,	59
Biktashev, Vadim,	243	Caiani, Enrico,.....	4, 194
Binczak, Stéphane,.....	178	Caiani, Enrico G, ...	25, 27, 231, 254
Bissell, Malenka,	194	Cairns, Andrew,	53
Blaber, Andrew,	7, 102, 126	Callaghan, Fraser M,.....	2
Black, Pauline,.....	114	Calvo, Conrado J, 42, 142, 190, 302	
Blanch, Lluís,	215	Calvo, Mireia,	67
Blasi, Claudio,.....	183	Cano, Óscar,	11
Bleda, Andres,.....	108	Cantalapiedra, Inma R,.....	118
Bleda, Andres L,	112	Cantalapiedra, Inmaculada R, ...	91
Boccia, Edda,.....	191	Cantwell, Chris D,	130
Bollache, Emilie,.....	23, 193, 196	Carminati, M Chiara,	25, 27
Bond, Raymond, .	43, 53, 111, 114, 245, 315	Carrasco-Sosa, Salvador,	6, 9
Boniotti, Cinzia,.....	25	Carrault, Guy,	303
Bonizzi, Pietro,	61, 86, 223	Carre, François,.....	303
Bonnemains, Laurent,.....	207	Carro, Jesús,	240
Bortolan, Giovanni,..	252, 307, 308	Carvalho, Paulo,	186
Bourke, John,	228	Casaleggio, Aldo,	188
Boyett, Mark,	264	Casellato, Claudia,	254
Bragard, Jean,	118	Cassin, Matteo,.....	224
Branagh, David,.....	110	Castells, Francisco,	42, 137
Brazdova, Ludmila,	284	Castiglioni, Paolo,	211
Breen, Cathal,	53	Castro, Simon,	264
Brieda, Marco,	224	Catherwood, Philip A,.....	110
Brinkmeyer, Christoph,.....	186	Cebrian, Antonio,	190
Brischwein, Matthias,	251	Cebrián, Antonio,	142
Brooks, Dana H,	60, 65, 261	Ceruti, Alessandro,	195
Brotos, Daniel,	109	Cervesato, Eugenio,.....	224
Brugada, Josep,.....	153	Cervigón, Raquel,	292
Bruschetta, Eugenia,.....	224	Cervigyn, Raquel,.....	137
Bucchi, Annalisa,.....	1	Ceulemans, Berten,	266
Budinskaya, Ksenia,	284	Chakaramakkil, Mathew Jose,.	332
Bulatovic, Ivana,.....	47	Chalin, Abdullah,	50
Burattini, Laura,	56, 179, 329	Chang, Eugene TY,	73, 119, 236
Buszko, Katarzyna,.....	267	Chapelle, Dominique,.....	126
Buttu, Andrea,	250	Chen, Gang,	173
Bұһm, Anna,	184	Chen, Ji,	208, 210
Caamaño, Antonio,	34, 281	Chen, Shawn,.....	210
		Chicote, Beatriz, 144, 150, 151, 273	

Child, Nick,	168	Coury Pedrosa, Roberto,	54, 138
Chorro, Francisco J, ...	42, 142, 190, 302	Couto, Paula,	204
Chowdhury, Nayeefa,	288	Crispi, Fátima,	218
Christensen, Jørn Bolstad,	116, 295	Cudière, Yves,	63
Christofle-Boulard, Sylvain,	88	Currie, Jonathan,	114
Christov, Ivaylo,	252, 307, 308	Cybulski, Gerard,	276
Chronaki, Catherine,	50	da Fonseca, Henrique,	96
Chu, Gavin,	74	Dallet, Corentin,	62, 64
Chu, Gavin S,	14, 15, 16	Daluwatte, Chathuri,	83, 203
Chumarnaya, Tatiana,	97	Dametto, Ermanno,	224
Chóvez, Carlos E,	63	Dastagir, Nawshin,	15, 16
Citi, Luca,	162, 282	Davidovic, Andjela,	115
Ciuchciński, Kamil,	328	Davis, Jordan,	173
Clark, Elaine,	230	Daya, Mohamud,	273
Clayton, Richard H,	73, 119, 236	De Cesare, Alain,	2, 196
Clément-Guinaudeau, Stéphanie,	23	de Chazal, Philip,	84, 318
Clerx, Michael,	244	De Cooman, Thomas,	266
Clifford, Gari,	77, 199	de Freitas, Nando,	3
Cluitmans, Matthijs,	61	de Groot, Natasja MS,	226
Cluzel, Philippe,	2	De Haro, Candelaria,	215
Cmiel, Vratislav,	122, 262	de Jong, Beverlie,	279
Čmiel, Vratislav,	306	de Jong, Monique,	61
Coll-Font, Jaume,	60, 65, 261	de Jongh, Marjolein C,	146
Collins, Pieter,	244	De Marchi, Luca,	195
Colman, Michael,	264	De Wel, Ofelie,	154
Colman, Michael A,	124, 235	Defrance, Carine,	2
Colman, Michael Alan,	90, 139	Del Bianco, Federica,	224
Colombo, Andrea,	27	Deliire, Quentin,	87
Corcuera, Carlos,	150	Della Corte, Alessandro,	194
Corino, Valentina D A,	225	Desplantez, Thomas,	115
Corino, Valentina DA,	128	Di Bella, Gianluca,	93
Cornforth, David,	279	Di Nardo, Francesco, ..	56, 179, 329
Cornforth, David J,	268	Di Rienzo, Marco,	32, 69, 211
Corsi, Cristiana,	24, 28, 195, 248	Díaz-Valencia, Raquel,	99
Cosmi, Erich,	197	Didon, Jean-Philippe,	149
Couceiro, Ricardo,	186	Diebold, Benoit,	23
Couderc, Jean-Philippe, ...	117, 181	DiFrancesco, Dario,	1
Coudiere, Yves,	115	Doessel, Olaf,	65
Coudière, Yves,	62, 64, 259	Dokuchaev, Arseniy,	89
		Doležal, Petr,	310

Dominik, Andreas,	265	Félix, Paulo,	58
Dössel, Olaf,	182, 246, 311	Feng, Ling,	320
Dovancescu, Silviu,	72	Fenton, Flavio,	125
Du, XiaoWei,	30	Ferdeghini, Ezio-Maria,	93
Dubois, Remi,	64	Fernández, Carmen,	11
Dubois, Rémi,	62, 178, 257, 259	Fernandez-Gonzalo, Sol,	215
Duchateau, Josselin, ...	62, 64, 257, 259	Ferrero, Jose M,	175
Eatock, Julie,	73	Feuerstein, Delphine,	88
Ebrahimi Orimi, Hamid,	301	Fialova, Katerina,	123
Echebarria, Blas,	91, 118	Fialová, Kateřina,	140, 285
Eerikđinen, Linda M,	82	Filgueiras, David,	302
Eftestul, Trygve,	206	Filgueiras-Rama, David,	42
Eichhorn, Stefan,	21	Finlay, Dewar, 43, 53, 111, 114, 245, 315
Eickholt, Christian,	186	Finlay, Dewar D,	110
Eindhoven, Daniëlle,	172	Finlay, Malcom,	183
El-Hamad, Fatima,	57	Fioretti, Sandro,	56, 179, 329
Elola, Andoni,	273	Florez Pacheco, Edward,	96
Elorza, Jorge,	118	Fohlerová, Zdenka,	306
Elvira, Victor,	157	Foolad, Faezeh,	198
Endo, Miyuki,	100	Ford, Ian,	230
Egan, Kjersti,	206	Forkan, Abdur Rahim Mohammad,	52
Ernst, Gernot,	265	Freitas, Eduardo,	141
Escalona, Omar,	75	Frigo, Carlo,	254
Eskofier, Bjoern,	113, 251	Funtova, Irina,	87
Evin, Morgane,	2, 45	Gaffney, Robert,	53
Fabbri, Alan,	241	Galbis, Antonio,	11
Fabbri, Claudio,	28	Galeotti, Lorian,	203
Facila, Lorenzo,	132	Gall, David,	87
Faes, Luca,	166, 169	Galla, Tobias,	73
Faita, Francesco,	272	Galluzzo, Francesca,	195
Fallet, Sibylle,	78, 253	Gan, Zizhao,	139
Fantin, Denis,	224	Gandhi, Shreyans,	280
Fantini, Matteo,	241	Garcia, Ronald G,	214
Fasano, Antonio,	155	García-Alberola, Arcadi, 51, 180, 269
Fatemizadeh, Emad,	198	García-Alberola, Arcadio,	48, 99
Fayn, Jocelyne,	49	Garg, Amanmeet,	102
Fazel-Rezai, Reza,	10, 17, 102	Garreau, Mireille,	98
Felblinger, Jacques,	207		
Felix, Jorge,	12, 13		

Garzón, Jorge Mario,	274	Guerra, Jose M,	19
Gatsori, Efrosini,	66	Guerrero, Gustavo,.....	88
Gentili, Claudio,	220	Guerrisi, Maria,.....	282
Gény, Bernard,.....	149	Guill, Antonio,.....	190
Gerardo-Giorda, Luca,	19	Guillem, Maria S,	74
Ghaffari, Ali,	255, 301, 305, 319	Guillén-Mandujano, Alejandra, 6, 9	
Ghafoori, Elyar,	18, 222	Guillou, Andrĳ,	207
Ghassemi, Mohammad,.....	290	Guizani, Nachoua,	49
Ghassemi, Mohammad Mahdi, 170		Guldenring, Daniel,.....	43, 53, 111, 245, 315
Gierałtowski, Jan,.....	160, 328	Gurev, Slava,.....	92
Giesecke, Anders,	47	Gurev, Viatcheslav,.....	117
Gil, Eduardo,	215, 274	Haïssaguerre, Michel,.....	259
Gill, Jaswinder S,	168	Halamek, Josef, 20, 70, 79, 143, 221	
Gillette, Karli,	260	Halámek, Josef,	140
Giuliani, Corrado,.....	56, 179	Hamilton, Emily F,	35
Goldoozian, Layli S,.....	167	Hancox, Jules C,	235
Gomà, Gemma,.....	215	Hanson, Ben,	168, 183
Gomis, Pedro,	67	Hargittai, Sándor,	247
Gonzalez Salvador, Alberto,.....	36	Haris, Kostas,	94
Gonzalez-Fernandez, Rene Ivan,	106, 107	Haritopoulos, Michel,.....	33
González-Otero, Digna M,	151	Haßlmeyer, Erik,	251
González-Otero, Digna M,	144	Hautala, Arto J,	286
González-Suñrez, Ana,.....	19	Hawks, Claudia,	118
Goovaerts, Griet,	154, 158	Hayes-Gill, Barrie,.....	174
Goroso, Gustavo,	74	He, Runnan,.....	323
Gouveia, Synia,	212	Heinrich, Axel,	251
Goya-Esteban, Rebeca, 34, 269, 281		Heinz, Brock,.....	219, 233
Gradl, Stefan,	251	Hejč, Jakub,.....	285, 304
Graff, Beata,.....	166	Henn, Patrick,	53
Graindorge, Laurence,	88	Henriksson, Mikael,	128
Gratacós, Eduard,	218	Henriques, Jorge,.....	186
Grieve, Stuart M,	2	Hernandes, Alfredo,	88
Griffiths, Clive,	291	Hernandez, Alfredo,	303
Grisan, Enrico,.....	197	Hernández, Alfredo,	67
Grönemeyer, Dietrich,.....	271	Hernando, Alberto,.....	274
Grzegorzczuk, Iga,.....	328	Hernando, David,	215
Gu, Linxia,	71	Hidalgo-Muñoz, Antonio R, 136, 167	
Guan, Kaomei,	40	Himmelsbach, Tilo,.....	324
Guerra, Francisco,.....	33	Hocini, Méléze,.....	259

Hofmann, Christian,.....	108, 112	Jimenez-Serrano, Santiago,.....	42
Holden, Arun V,	174	Jin, Qinghui,.....	30
Holmer, Mattias,.....	8	Johannesen, Lars,	203
Honzikova, Natasa,	284	Jones, Gareth,.....	300
Hoog Antink, Christoph,	80, 184	Jones, Gareth M,	124
Horacek, Milan,.....	232	Joo, Segyeong,.....	283
Hornero, Fernando,	132	Jost, Daniel,	149
Hortelano, Marcos,.....	292	Jover, Carlos,	150
Hoshiyama, Asagi,.....	216	Jurak, Pavel,....	20, 70, 79, 143, 221
Hoshiyama, Masaki,.....	216	Jurakova, Katerina,.....	20
Houben, Richard PM,.....	226	Kabir, Muammar,	18, 222
Hoyer, Dirk,.....	271	Kachenoura, Nadjia, 2, 23, 45, 193,	196
Hrstkova, Hana,	284	Kalidas, Vignesh,.....	200
Hruskova, Jana,.....	105, 284	Kalra, Chandan,	318
Hu, Weichih,	152	Kambova, Liliana,	308
Hubálek, Jaromír,.....	306	Kamphuis, Vivian P,	146
Huikuri, Heikki V,	286	Kang, Ning,	332
Hurnanen, Tero,.....	227	Kania, Michal,	59
Hyttinen, Jari,.....	37	Kania, Michał,.....	258
Ibrahim, Abdullah,	71	Kantasis, George,.....	94, 127
Illanes, Alfredo,.....	33	Kańtoch, Eliaz,.....	29
Imam, Mohammad Hasan, 103, 314		Karel, Joel,	86
Imperial, Sébastien,	126	Karel, Joël,	61
Iozzia, Luca,.....	225	Karmakar, Chandan,.....	
Iribe, Gentaro,	263	103, 104, 286, 313, 314
Irusta, Unai,	150, 273	Katsnelson, Leonid,	120, 148
Izzi, Francesca,	282	Katsnelson, Leonid B,	89
Jacquemet, Vincent,	13, 121	Kella, Danesh,.....	77, 199
Jacquir, Sabir,.....	178	Kelm, Malte,	186
Jadidi, Amir,	131	Kennedy, Alan,	43, 245, 315
Jafarnia Dabanloo, Nader, 198, 287		Khalil, Ibrahim,	52
Jalife, José,	238	Khandoker, Ahsan,	314
Jallal, John,.....	209	Khandoker, Ahsan H,.....	100, 286
Janousek, Oto,	123	Khandoker, Ahsan Habib,	288
Janoušek, Oto,	285, 304, 309	Kharche, Sanjay,	300
Jarvis, Jonathan,.....	264	Kheirati Roonizi, Ebadollah,	159
Jekova, Irena, ...	201, 252, 308, 312	Khodor, Nadine,	303
Jelinek, Herbert,.....	279, 288	Khokhlova, Anastasia,	120, 263
Jelinek, Herbert F,.....	268, 286	Kholmovski, Eugene,	260
Jensen, Ask Schou,.....	116, 295		

Lin, Chun-Cheng,.....	152	Maestre, Rafael,	108, 112
Lin, Yen Ting,.....	73	Maffessanti, Francesco,	330
Lin, Yu-Wei,.....	152	Mafi, Dena,	255, 293, 319
Lipoldova, Jolana,	20, 143	Mafie, Dena,	301, 305
Liu, Changchun,	104, 313	Maglaveras, Nicos,	94
Liu, Chengyu,	5, 104, 202, 291	Mahdi, Adam,	317
Liu, Hongduoer,	165	Mainardi, Luca,.....	183
Lobo M, J Alexandre,	213	Mainardi, Luca T,	159, 225
Loeliger, Hans-Andrea,	171	Mäkikallio, Timo H,.....	286
Loiodice, Corinne,	88	Makowiec, Danuta, ..	166, 277, 278
Lomarda, Aileen Mae,.....	332	Man, Sumche,...	146, 179, 229, 329
Lombardi, Federico,.....	225	Maniewski, Roman,.....	258
Lombardi, Massimo,	194	Manis, George,	66
Lombardi, Prospero,	32, 69	Manoharan, Ganesh,.....	75
Lopes, Coeli M,	117	Mantilla, Juan,	98
Lopez Reyez, Alejandro,.....	106	Mantovan, Roberto,.....	248
López, Josefina,.....	215	Maqueda, Магна,.....	109
Lopez-Cardona, Juan Dayron, .	106,	Marciani, Maria Grazia,	282
107		Marinazzo, Daniele,.....	169
Lopez-Creagh, Rolando Emilio,	106	Mark, Roger, .	50, 77, 170, 199, 289
Lopez-Rodriguez, Rolando,	106, 107	Markhasin, Vladimir,	148
Lorenzini, Cinzia,	46	Markhasin, Vladimir S,	97
Loro, Francesca,	224	Maršánová, Lucie,	309
Lozupone, Graziano Vito,.....	248	Martín-Caballero, Carlos,	34
Lu, Weigang,	256	Martinez, Arturo,.....	133
Luca, Adrian,	121	Martínez, Juan Pablo,.....	226, 231
Luchitskaya, Elena,.....	87	Martinez, Luis J,.....	22
Luengo, David,	157	Martínez-García, Carlos,.....	281
Luik, Armin,.....	246	Martinez, Laura,	238
Luo, Cunjin,	189, 296, 300	Martyn-Yebra, Alba,.....	231, 254
Luo, Tong,	332	Marzbanrad, Faezeh,.....	100
Luther, Stefan,	176, 177, 191	Mason, Jay W,	219, 233
Luthra, Veena,	288	Mason, JW,	234
Lux, Robert L,	233	Matejkova, Magdalena,	70
Lyon, Aurore,	3	Matelot, David,.....	303
Maan, Arie C,	146, 229	Matos Molina, Danelia,	158
Mabo, Philippe,.....	67	Matthews, Rosa,.....	174
Macfarlane, Peter,	230	Matveev, Mikhail,.....	252, 307
MacLeod, Rob,	260	McCullagh, Paul,.....	114
Maesen, Bart,	223	McEaney, David,.....	75

McEwan, Alistair,	318	Mor-Avi, Victor,	193, 330
McLaughlin, James,	43, 245, 315	Moreno, Javier,	137
McLaughlin, James AD,	110	Moreno-González, Rafael,	180
Meijer van Putten, Rosalie ME, .	40	Moss, Arthur,	181
Meillet, Valentin,	62	Mostafa, Raqibul,	288
Mejía-Rodríguez, Aldo R,	6	Moucharwar, Gabriel,	210
Melcher, Vivien,	108, 112	Mouchawar, Gabriel,	209
Mena-Tobar, Andres,	175	Moudr, Jiri,	105
Mendoza Garcia, Alejandro, 21,	270	Mousseaux, Elie,	23, 45, 196
Ménétré, Sarah,	149, 207	Muehlsteff, Jens,	186
Mengarelli, Isabella,	40	Mukherji, Soumyo,	280
Menzel, Michael,	265	Mulet-Cartaya, Margarita, 106,	107
Meo, Marianna,	39, 136	Murali, Srinivasan,	31, 41
Meste, Olivier,	39, 59, 136	Murray, Alan,	5, 228, 291, 322
Meyer, Christian,	186	Nacenta, Jose M,	112
Mieke, Stephan,	5	Nadal, Jurandir,	54, 138, 185
Migeotte, Pierre-François, .	87, 254	Naito, Yasuhiro,	237, 297
Migliore, Michele,	188	Najarian, Kayvan,	321
Mikhailov, Sergey P,	97	Nardelli, Mimma,	220
Miklaszewski, Wieslaw,	277	Nasario-Junior, Olivassé,	138
Millet, Jose,	190	Nasario-Junior, Olivassý,	54
Millet, José,	42, 137, 142, 302	Naz, Aneela,	174
Min, Xiaoyi,	209, 210	Nemati, Shamim,	170, 290
Mincholé, Ana,	3	Nesteruk, Igor,	194
Mirmohamadsadeghi, Leila,	156	Neubauer, Stefan,	3
Mirsky, Grace,	316	Neyton, Clément,	149
Moharreri, Sadaf,	217, 287	Ng, Fu Siong,	130
Moireau, Philippe,	126	Ng, G André,	14, 15, 16, 74
Mollakazemi, Mohammad Javad, ...	255, 293, 301, 319	Nguyen, Doan Trang,	318
Monasterio, Violeta,	231, 240	Ni, Haibo,	139, 145, 235, 298
Monserrat-García-de-Pablo, María,	180	Nikitina, Larisa,	89
Montanyà, Jaume,	215	Nikolic, Dragana,	317
Moody, Benjamin,	77, 199	Nollo, Giandomenico,	169
Moon, Thomas E,	233	Nordenfur, Tim,	47
Moosavian, Seyyed Ali Akbar, .	293	Novak, Miroslav,	20, 143
Mora Jiménez, Inmaculada,	180	Novakova, Marie,	123
Mora-Jiménez, Inmaculada, 48, 51,	99	Nováková, Marie,	140, 285, 304, 309, 310
		Novakova, Zuzana,	284
		Nyenhuis, John,	209, 210

Odstrcilik, Jan,.....	122, 262	Perera, Alexandre,.....	109
Oesterlein, Tobias,.....	182, 246	Perez Alday, Erick Andres,.....	
Olariu, Claudia,	162	90, 139, 145
Olde, Bo,	8	Perkins, Steven,.....	279
Olejnickova, Veronika,.....	123	Perry, Diane,.....	77, 199
Olejníčková, Veronika,	285, 304, 309	Pertutti, Simone,	28
Oliveira, Henrique,.....	141	Pervolaraki, Eleftheria,.....	174
Omer, Noam,	101	Pesl, Martin,	122
Ooi, Adrian Seng Wae,.....	332	Peters, Nicholas S,	130
Opolski, Grzegorz,.....	258	Petitmangin, Grégory,	207
Orini, Michele,	147, 168, 183	Petrov, Ivo,	307
Ørn, Stein,.....	206	Piątkowska, Agnieszka,.....	267
Ortigosa, Nuria,.....	11, 218	Piatti, Filippo,	194
Otani, Niels,	177	Piazzese, Concetta,.....	27
Paci, Michelangelo,.....	37	Pietrzak, Agata,	276
Page, Stephen,.....	174	Pingitore, Alessandro,	93
Pahlm, Olle,.....	232	Pirola, Selene,.....	194
Paiva, Rui Pedro,.....	186	Placidi, Fabio,	282
Palaniswami, Marimuthu,.....		Plaza, Sandra,	144
.....	100, 103, 286, 314	Plesinger, Filip,	20, 70, 79, 143
Pan, Jiabin,	323	Podziemski, Piotr,.....	
Panfilov, Alexander V,.....	331	134, 135, 223, 328
Pänkäälä, Mikko,.....	227	Poignard, Clair,	115
Paredes, José Luis,	98	Pollesel, Edda,	224
Parra-Rojas, César,.....	90	Polski, Marcin,	21
Parvaneh, Saman,	217	Positano, Vincenzo,	93
Pascale, Patrizio,	250	Potse, Mark,	27, 62, 64, 257
Patel, Amit,	193	Potyagaylo, Danila,.....	65, 311
Pavan, Esteban,.....	254	Pratali, Lorenza,.....	272
Peace, Aaron,.....	53	Presedo, Jesús,	58
Peeters, Ralf,.....	61, 86	Pribyl, Jan,	122
Pellicer, Soledad,	112	Provaznik, Ivo,	122, 123, 262
Penaranda, Angelina,.....	118	Provazník, Ivo, ..	285, 306, 309, 310
Peñaranda, Angelina,.....	91	Pruvot, Etienne,.....	250
Peng, Yi,	165	Pueyo, Esther,	240
Pennisi, Cristian Pablo,	116, 295	Qureshi, Norman A,.....	130
Pepi, Mauro,	4, 25, 27	Radaelli, Alberto,.....	211
Pepin, Jean-Louis,	88	Ramalho, Ruben,	204
Perdrix, Ludivine,	23	Ramos, Pablo,.....	153
		Ravagli, Enrico,	1

Redaelli, Alberto,	194	Ruiz de Gauna, Sofía,	144
Redheuil, Alban,	2, 23, 45, 196	Ruiz de Gauna, Sofya,	151
Reichlova, Tereza,	20, 143, 221	Ruiz, Jesús,	144, 151
Reilly, Richard,	292	Russell, James K,	273
Requena-Carrión, Jesús,	22	Russell, Jan,	268
Rezaei, Shahab,	287	Ruwald, Anne-Christine,	181
Ribas Ripoll, Vicent J,	153	Ruwald, Martin,	181
Rice, Jeremy,	92	Sabbatani, Paolo,	248
Rice, John J,	117	Sadr, Nadi,	84, 318
Rieta, Jose J,	12, 13	Saha, Simanto,	288
Rieta, Jose Joaquin,	132, 133	Saiz, Javier,	238
Rincon, Francisco,	31	Salgado, Lizet C,	22
Rincón, Francisco,	41	Salinet, João,	15, 141
Rios-Muñoz, Gonzalo,	157	Salinet, João L,	14, 16
Ripsweden, Jonaz,	47	Salinet, Joro,	74
Rivolta, Massimo W,	117, 159	Samset, Eigil,	47
Rix, Hervý,	59	Sánchez-Caro, Alfonso,	51
Robles, Felipe,	33	Sandberg, Frida,	8, 128, 129
Roca, Emma,	109	Sano, Hitomi,	237, 297
Rocha, Ana Paula,	187	Sanromán-Junquera, Margarita, ...	48, 99
Rodrigues, Rui,	204	Santa, Guadalupe,	112
Rodríguez, Blanca,	3	Saoudi, N,	76
Rodríguez, José Félix,	240	Saoudi, Nadir,	136
Rodríguez, Mérida,	218	Sarabia-Cachadiña, Elena,	281
Rodríguez-Matas, Jose F,	175	Saraste, Antti,	227
Rojo Álvarez, José Luis,	180	Sarmiento Alvarez, Luis Omar, ..	36
Rojo-Álvarez, José Luis, .	34, 48, 51, 99, 269, 281	Sassi, Roberto,	159, 183
Romero, Daniel,	67	Savari, Sebastián,	218
Romigi, Andrea,	282	Schalij, Martin J,	172, 229
Roney, Caroline H,	130	Scharinger, Josef,	26
Ronzhina, Marina, ...	122, 123, 140, 285, 304, 309	Schlegel, Todd T,	161
Rooijackers, Michael J,	82	Sch lindwein, Fernando,	74, 213
Roses, Eduardo J,	190	Sch lindwein, Fernando S, 14, 15, 16	
Rossi, Paolo,	188	Schmid, Ramun,	201, 312
Rota, Marcello,	39	Schmitt, Claus,	246
Rottmann, Markus,	131	Schmitz, Björn,	112
Rovai, Daniele,	93	Schmitz, Björn,	108
Rudolph, Dan-Timon,	182	Schneider, Uwe,	271
		Schnell, Frédéric,	98

Schölzel, Christopher,	265	Sotaquira, Miguel,	4
Schotten, Ulrich,	134, 223	Soukup, Ladislav,	70
Schreiber, Ulrich,	270	Soulat, Gilles,	45
Schulze, Walther,	65, 311	Sousa, Paulo,	187
Scilingo, Enzo Pasquale, ...	220, 272	Spence, Ian,	268
Scotto, Manuel G,	212	Srinivasan, Neil,	147
Scully, Christopher G,	83, 203	Stafford, Peter J,	14, 15, 16
Seemann, Gunnar,	131, 311	Starc, Vito,	161
Seo, Myeongsook,	283	Stary, Tomas,	243
Sevcencu, Cristian,	116, 295	Steinwender, Clemens,	26
Severi, Stefano,	1, 37, 241, 248	Stephenson, Robert,	264
Shahin, Abdullah,	77, 199	Steven, Daniel,	135, 249
Shajahan, T K,	176	Stovicek, Petr,	60, 261
Shen, Jiang,	327	Stračina, Tibor,	285
Sheng, Zhiqiang,	323	Strauss, David G,	83, 203
Sherwin, Spencer J,	130	Stroh, Annemarie,	21
Shiferaw, Yohannes,	91	Struck, Matthias,	113, 251
Shiguemi Furuie, Sergio,	96	Struijk, Johannes Jan,	116, 295
Shikhaleva, Elena,	89	Struzik, Zbigniew,	277
Shojaei Baghini, Maryam,	280	Struzik, Zbigniew R,	278
Shoucri, Rachad,	68	Sturla, Francesco,	194
Signore, Sergio,	39	Su, Yi,	205, 320
Silva, Ikaro,	77, 199	Such, Luis,	190
Silva, Marta João,	187	Such-Miquel, Luis,	190
Simov, Dimiter,	307	Sulman, Tatiana,	89
Simova, Iana,	308	Surrel, Grÿgoire,	41
Sin, Kenny Yoong Kong,	332	Suárez Leyn, Alexander Alexeis, 158	
Singsaas, Erlend,	206	Svoboda, Ondrej,	262
Sison, Shiloh,	209, 210	Svoboda, Ondřej,	306
Sitges, Marta,	218	Swenne, Cees A, 146, 179, 229, 329	
Skopalík, Josef,	306	Swoboda, Roland,	26
Smíšek, Radovan,	309	Szepietowska, Barbara,	181
Snoek, Jasper,	290	Szot, Shaun,	219
Soguero-Ruiz, Cristina,	51	Taggart, Peter,	147, 168
Solem, Kristian,	8	Takiguchi, Mao,	297
Soliński, Mateusz,	328	Tamborini, Gloria,	4, 27
Solovyova, Olga, 97, 120, 148, 263		Tamil, Lakshman,	200
Soon, Jia Lin,	332	Tan, May-Ling,	205
Soria, J Manuel,	109	Tan, Ru San,	332
Sörnmo, Leif,	8, 128	Tan, Ru-San,	205

Tan, Swee Yaw,	332	Vaglio, Martino,.....	233
Tan, Teing Ee,.....	332	Vaini, Emanuele,.....	32, 69
Tanaka, Yuichiro,	237	Valenza, Gaetano, ...	214, 220, 272, 282
Tang, Chengchun,	300	Valinoti, Maddalena,	248
Tang, Hong,.....	202	van Dam, Eelco,.....	111
Tank, Jens,.....	87	van Dam, Peter,.....	111
Tantinger, Daniel,	113, 251	Van Dam, Peter,	260
Tao, Ruojie,.....	30	van Dam, Peter M,	60
Tarroni, Giacomo,	197	Van de Borne, Philippe,.....	87
Tarvainen, Mika,	279	Van de Vel, Anouk,	266
Tarvainen, Mika P,	268	Van Duijvenboden, Stefan,.....	168
Tatar, Aziz,	88	van Gent, Jos,	108
Tate, Jess,.....	260	van Ginneken, Antoni CG,	40
Tavakolian, Kouhyar, 7, 10, 17, 85, 102, 126		Van Huffel, Sabine,	44, 154, 158, 266
Tayebjee, Muzahir,	174	van Hunnik, Arne,.....	134, 223
Teichmann, Daniel,	184	van Leeuwen, Peter,.....	271
Teijeiro, Tomás,	58	Van Paesschen, Wim,	266
Teixidó-Roman, Miguel,.....	153	Vandenberk, Bert,	154
Teo, Soo-Kng,.....	205, 320	Vandeput, Steven,	158
Ter Haar, C Cato,.....	229	Vandersickel, Nele,.....	331
Tereshchenko, Larisa,	18, 222	Vanello, Nicola,.....	272
Thomsen, Poul Erik Bloch,	181	Vanheusden, Frederique J,..	14, 15, 16
Tobola, Andreas,.....	108	Vanrumste, Bart,	266
Toki, Tamami,	297	Vanschoren, Joaquin,	82
Tomasi, Corrado,	24	Varon, Carolina,.....	44
Tomaz, Carlos,	214	Vasankari, Tuija,	227
Tomita, Masaru,.....	237, 297	Vázquez Seisdedos, Carlos,	158
Toosizadeh, Nima,	217	Velde, Enno van der,	172
Tormos, Alvaro,	190	Venkatesh, Bharath Ambale,...	196
Toschi, Nicola,.....	282	Verkerk, Arie O,	40
Treskes, Roderick,.....	172	Verma, Ajay,	10, 102
Tsimenidis, Charalampos,.....	322	Verma, Bhawna,	246
Tuan, Jiun H,	14	Vesely, Petr,.....	221
Tulppo, Mikko P,	286	Veselý, Petr,.....	309
Turon, Marc,.....	215	Veselə, Petr,.....	140
Tzortzis, Konstantinos N,	130	Vesin, Jean-Marc, 78, 121, 156, 250, 253	
Ugoeke, Nene,	181		
Unger, Laura,	131		
Uzelac, Ilija,.....	125		

Vicente, Jose,	203	Williamson, Richard,.....	210
Vidales, Noelia,	151	Winter, Reidar,	47
Vijayakumar, Vani,	96	Woie, Leik,	206
Vikulova, Nathalie,.....	120	Wojdeł, Anna,.....	153
Villani, Valeria,	155	Wong, Jian Cheng,	320
Ville, Nathalie,.....	303	Xanthis, Christos,.....	95, 127
Virag, Nathalie,	121	Xia, Xiaojuan,	181
Viscor, Ivo,	70	Xu, Binbin,	178
Visentin, Silvia,.....	197	Xu, Jingjia,.....	261
Vliegen, Hubert W,	146	Xu, Kevin,.....	173
Volders, Paul,.....	61	Xu, Man,	327
Volders, Paul GA,	244	Yagbe-Mayans, Jaime,	142
Vollmer, Marcus,	164	Yahai, Hussein,	178
Vondra, Vlastimil,	70	Yamat, Megan,	330
Votta, Emiliano,	194	Yang, Bo,.....	320
Vullings, Rik,.....	82	Yang, Fei,	256
Wadehn, Federico,	171	Yang, Feng,	320
Wagner, Galen,	232	Yang, Jian,.....	30
Wailoo, Michael,.....	213	Yang, Xinhui,.....	173
Wallman, Mikael,.....	129	Yazdani, Sasan,	78, 250
Walsh, Philip,	75	Yu, Haiyan,.....	327
Wang, John,	232	Yu, Wen-Chung,.....	196
Wang, Kuanquan, 38, 189, 192, 239, 242, 256, 294, 296, 299, 323		Yuan, Ming,	189, 296
Wang, Linwei,	261	Yuan, Yongfeng, 38, 189, 239, 294, 296, 299, 323	
Wang, Qingjie,	189, 296, 300	Zaczek, Rajmund,	258
Wang, Qinyan,	208	Zadnik, Delia,.....	224
Wang, Wei,	145, 298	Zahedi, Edmond,	167
Wang, Zhigang,	165	Zakeri, Vahid,.....	85
Warren, James,	232	Zardo, Sara,	224
Warrick, Philip A,	35	Zareba, Wojciech,.....	181
Watkins, Hugh,	3	Zarzoso, Manuel,	190
Weigand, Christian,	113, 251	Zarzoso, Vicente,	136, 167
Weinert, Lynn,	27, 330	Zavodna, Eva,	105, 284
Wejer, Dorota,	166	Żebrowski, Jan,	160
Westra, Ronald,	61	Żebrowski, Jan J,.....	135, 249
Whittaker, Dominic G,	235	Zeemering, Stef,	86, 134, 223
Wilders, Ronald,.....	40, 241	Zegers, Jan G,	40
Willems, Rik,	154	Zemzemi, Nejib,.....	62, 63, 64, 257
Willems, Stephan,.....	135, 249	Zeng, Qi,	208

Zhan, Ping,	165
Zhang, Chen,	139
Zhang, Henggui, 38, 124, 139, 145, 189, 192, 235, 239, 242, 256, 264, 294, 296, 298, 299, 300, 323	
Zhang, Huanqian,	30
Zhang, Jun-Mei,	332
Zhang, Lei,	256
Zhang, Shanzhuo,	242
Zhang, Shulin,	30
Zhang, Tian You,	320
Zhang, Yue,	239, 299
Zhao, Jianlong,	30
Zhao, Lina,	202
Zhao, Na,	38, 323
Zhao, Shijia,	71
Zhao, Yue,	171
Zheng, Dingchang,	5, 291
Zhong, Liang,	205, 332
Zhou, Jing,	294
Zhu, Yongwei,	326
Zimmitti, Matteo,	24
Zong, Wei,	81
Zorzi, Catya,	224
Zrenner, Markus,	113
Zuo, Wangmeng,	256

